20. SITE 688[1]

Shipboard Scientific Party[2]

HOLE 688A

Date occupied: 1715 L, 4 December 1986

Date departed: 0230 L, 7 December 1986

Time on hole: 57 hr 15 min

Position: 11°32.26'S, 78°56.57'W

Water depth (sea level; corrected m, echo-sounding): 3819.8

Water depth (rig floor; corrected m, echo-sounding): 3830.3

Bottom felt (m, drill pipe): 3828.5

Penetration (m): 350.3

Number of cores: 37

Total length of cored section (m): 350.3

Total core recovered (m): 245.29

Core recovery (%): 70.0%

Oldest sediment cored
  Depth (mbsf): 350.3
  Nature: Diatomaceous mudstone
  Age: Pliocene(?)

HOLE 688B

Date occupied: 0230 L, 7 December 1986

Date departed: 0330 L, 8 December 1986

Time on hole: 25 hr

Position: 11°32.26'S, 78°56.57'W

Water depth (sea level; corrected m, echo-sounding): 3819.8

Water depth (rig floor; corrected m, echo-sounding): 3830.3

Bottom felt (m, drill pipe): 3828.5

Penetration (m): 360.0

Number of cores: 0

Total length of cored section (m): 0

Total core recovered (m): 0

Core recovery (%): 0

Oldest sediment cored N/A

HOLE 688C

Date occupied: 0330 L, 8 December 1986

Date departed: 1800 L, 9 December 1986

Time on hole: 38 hr 30 min

Position: 11°32.26'S, 78°56.57'W

Water depth (sea level; corrected m, echo-sounding): 3819.8

Water depth (rig floor; corrected m, echo-sounding): 3830.3

Bottom felt (m, drill pipe): 3836.3

Penetration (m): 359.8

Number of cores: 1

Total length of cored section (m): 9.5

Total core recovered (m): 1.19

Core recovery (%): 12.5

Oldest sediment cored
  Depth (mbsf): 359.8
  Nature: Diatomaceous mud
  Age: Quaternary

HOLE 688D

Date occupied: 1800 L, 9 December 1986

Date departed: 2315 L, 10 December 1986

Time on hole: 29 hr 15 min

Position: 11°32.26'S, 78°56.57'W

Water depth (sea level; corrected m, echo-sounding): 3825.8

Water depth (rig floor; corrected m, echo-sounding): 3836.3

Bottom felt (m, drill pipe): 3836.3

Penetration (m): 345.0

Number of cores: 0

Total length of cored section (m): 0

---

[1] Suess, E., von Huene, R., et al., 1988. *Proc. ODP, Init. Repts.*, 112: College Station, TX (Ocean Drilling Program).

[2] Erwin Suess (Co-Chief Scientist), Oregon State University, College of Oceanography, Corvallis, OR 97331; Roland von Huene (Co-Chief Scientist), U.S. Geological Survey, Branch of Pacific Marine Geology, 345 Middlefield Rd. M/S 999, Menlo Park, CA 94025; Kay-Christian Emeis (ODP Staff Scientist), Ocean Drilling Program, Texas A&M University, College Station, TX 77843; Jacques Bourgois, Département de Géotectonique, Université Pierre et Marie Curie, 4 Place Jussieu, 75230 Paris Cedex 05, France; José del C. Cruzado Castañeda, Petroleos del Peru S. A., Paseo de la Republica 3361, San Isidro, Lima, Peru; Patrick De Wever, CNRS, Laboratoire de Stratigraphie, Université Pierre et Marie Curie, 4 Place Jussieu, 75230 Paris Cedex 05, France; Geoffrey Eglinton, University of Bristol, School of Chemistry, Cantock's Close, Bristol BS8 1TS, England; Robert Garrison, University of California, Earth Sciences, Applied Sciences Building, Santa Cruz, CA 95064; Matt Greenberg, Lamont-Doherty Geological Observatory, Columbia University, Palisades, NY 10964; Elard Herrera Paz, Petroleos del Peru, S. A., Paseo de la Republica 3361, San Isidro, Lima, Peru; Phillip Hill, Atlantic Geoscience Centre, Bedford Institute of Oceanography, Box 1006, Dartmouth, Nova Scotia B2Y 4A2, Canada; Masako Ibaraki, Geoscience Institute, Faculty of Science, Shizuoka University, Shizuoka 422, Japan; Miriam Kastner, Scripps Institution of Oceanography, SVH, A-102, La Jolla, CA 92093; Alan E. S. Kemp, Department of Oceanography, The University, Southampton SO9 5NH, England; Keith Kvenvolden, U.S. Geological Survey, Branch of Pacific Marine Geology, 345 Middlefield Rd., M/S 999, Menlo Park, CA 94025; Robert Langridge, Department of Geological Sciences, Queen's University at Kingston, Ontario K7L 3A2, Canada; Nancy Lindsley-Griffin, University of Nebraska, Department of Geology, 214 Bessey Hall, Lincoln, NE 68588-0340; Janice Marsters, Department of Oceanography, Dalhousie University, Halifax, Nova Scotia B3H 4J1, Canada; Erlend Martini, Geologisch-Paläontologisches Institut der Universität Frankfurt, Senckenberg-Anlage 32-34, D-6000, Frankfurt/Main, Federal Republic of Germany; Robert McCabe, Department of Geophysics, Texas A&M University, College Station, TX 77843; Leonidas Ocola, Laboratorio Central, Instituto Geofisico del Peru, Lima, Peru; Johanna Resig, Department of Geology and Geophysics, University of Hawaii, Honolulu, HI 96822; Agapito Wilfredo Sanchez Fernandez, Instituto Geologico Minero y Metalurgico, Pablo Bermudez 211, Lima, Peru; Hans-Joachim Schrader, College of Oceanography, Oregon State University, Corvallis, OR 97331 (currently at Department of Geology, University of Bergen, N-5000 Bergen, Norway); Todd Thornburg, College of Oceanography, Oregon State University, Corvallis, OR 97331; Gerold Wefer, Universität Bremen, Fachbereich Geowissenschaften, Postfach 330 440, D-2800 Bremen 33, Federal Republic of Germany; Makoto Yamano, Earthquake Research Institute, University of Tokyo, Bunkyo-ku, Tokyo 113, Japan.

Total core recovered (m): 0

Core recovery (%): 0

Oldest sediment cored N/A

HOLE 688E

Date occupied: 2315 L, 10 December 1986

Date departed: 0900 L, 18 December 1986

Time on hole: 177 hr 45 min

Position: 11°32.28′S, 78°56.65′W

Water depth (sea level; corrected m, echo-sounding): 3825.8

Water depth (rig floor; corrected m, echo-sounding): 3836.3

Bottom felt (m, drill pipe): 3836.3

Penetration (m): 779.0

Number of cores: 46

Total length of cored section (m): 429.0

Total core recovered (m): 151.98

Core recovery (%): 35.43

Oldest sediment cored
Depth (mbsf): 419.5
Nature: Calcareous silty mudstone
Age: early Eocene
Measured velocity (km/s): 2.7

Principal results: The three distinct tectono-sedimentary environments encountered in the 779 m penetrated at Site 688 record progressively deeper water sedimentation from early Eocene to Quaternary time. The first sequence penetrated in Hole 688A and washed in Hole 688E consists of 339 m of bioturbated Quaternary diatomaceous muds. Common terrigenous turbidites in the top 66 m are evidence of an influx of reworked sediment. Within the diatomaceous muds, benthic foraminifer assemblages are representative of present water depths. From 75 to 312 mbsf, the sediment has a uniform black coloration that is associated with a significant content of pyrite and iron monosulfide. Biostratigraphic data indicate sedimentation rates of around 300 m/m.y. for the Quaternary section. An incipient fissility is developed in the Quaternary section below 100 mbsf.

The second major sedimentary unit is composed of diatomaceous to diatom-bearing muds of early Miocene to Pliocene–Quaternary age between 339 and 592 mbsf. Fissility is better developed below 339 mbsf. A biostratigraphic hiatus separating the Quaternary and Pliocene is recorded between 341 and 350 mbsf in Hole 688A and between 350 and 356 mbsf in Hole 688E. Finely laminated sediment of alternating diatomite and mudstone with associated minor phosphorite is present in the lower Miocene and Pliocene–Miocene sequence, signifying substantially shallower water (500–1500 m) than the present depths at Site 688 (3820 m). Throughout the Pliocene–Miocene sequence, pervasive soft sediment deformation was evident. Sedimentation rates for the Pliocene–Miocene section are approximately 23 m/m.y.

A marked lithological break to diatom-free calcareous sediment rich in terrigenous clastic detritus occurs at 593 mbsf. This coincides with a hiatus that spans the Eocene to the earliest Miocene, a period of approximately 21.5 m.y. Where recovered, the sediments retrieved from 593 to 659 mbsf are predominantly greenish-gray to dark greenish-gray, poorly sorted quartzo-litho-feldspathic sandstones, cemented by carbonate and interbedded with sandy siltstones and black mudstones. Benthic foraminifer assemblages for this section indicate a mid- and upper-bathyal (150–500 m) range of water depths. The early Eocene sequence from 678 to 745 mbsf includes abundant transported plant matter, coarse pebbly layers, and bioclastic material. Toward the base of this unit, calcareous mudstones and sandstones and silty, bioclastic limestones contain well-preserved mollusks. Some of these are still articulated and indicate little transportation before deposition. Benthic foraminifer and nannofossil assemblages indicate shelf depths for the deposition of this sequence. The oldest sediments recovered from 764 to 769.5 mbsf are composed of interbedded sandstones, siltstones, and mudstones having abundant plant material and foraminifer assemblages indicating shelf depths. A chert pebble at this level contains a planktonic foraminifer fauna of Cenomanian age identical to faunas of Albian to Cenomanian limestones and cherts of the Central Andes and the onshore Talara Basin. Sedimentation rates for the Eocene section are approximately 12 m/m.y. and are consistent with assumed breaks between pulses of sedimentation.

Site 688 provided the most extreme geochemical gradients of Leg 112. Maximum values of alkalinity, ammonia, and phosphate exceeded previous records for DSDP or ODP sites. Scientists predicted that the methane generated in these sediments would be present in the gas-hydrate phase, and Site 688 provided one of the best-documented occurrences of gas hydrates to date. The hiatus at 350 mbsf marks the boundary between two very different bodies of interstitial water. Best seen in the chloride profile, a distinct freshening may indicate dilution by water originating at depth from dewatering of subducted sediments.

BACKGROUND AND SCIENTIFIC OBJECTIVES

The objectives at Site 688 were much the same as those for Site 682. Because of the fractured condition of the rocks and the poor seismic imaging at Site 682, another site was selected from a reprocessed version of multichannel seismic-reflection record CDP-1. This record was not available at the time sites were proposed for Leg 112.

CDP-1 was shot for the Nazca Plate Project in 1973 and was stacked at 1200% during the initial processing (Hussong and Wipperman, 1981). Just before Leg 112, CDP-1 was stacked at 2400% and migrated (von Huene and Miller, this volume), which improved the seismic imaging to show numerous faults in areas considered chaotic in previous versions (Thornburg, 1985). This revealed an area where strata appeared less affected by major faults and where the basement could be reached with the drilling capabilities of the *Resolution*.

Site 688 is on the lower slope of the Peru Trench about 30 km landward of the trench axis (Fig. 1); the site is located about 32 km south-southeast, parallel to the regional trend from Site 682. A major objective was to establish the continental or oceanic origin of the crystalline basement in a location near the trench. Other objectives were (1) to establish the history of vertical tectonism, (2) to sample the stratigraphy of explosive volcanism, and (3) to sample distal and transported reworked material from coastal upwelling on the continental shelf.

The thick sediment-filling forearc basins off Peru are much younger than previous studies indicated. Thus, the most promising area for recovering Eocene sediment and basement are on the lower slope rather than in the midslope area. However, the fractured Eocene rock above the basement at Sites 682 and 683 could not contain the fluid pressures required for drilling. Fracturing was suspected from the character of the reflections in reprocessed CDP-2, which motivated us to find alternate sites after the initial site selection and just before Leg 112. Drilling established the validity of that concern and showed us that the unmigrated seismic data for Site 682 was inadequate for showing the basement, much less for fracturing. In reprocessed record CDP-1, we found an area with relatively little fracturing, where the Eocene section is thick and within drilling depths.

This Eocene section contains an important record of subsidence of the Peruvian margin. At the very least, the sediment section was expected to indicate whether the crust at this site was attached to the continent before the Andean orogeny or whether it was part of the oceanic crust attached at the Andean subduction zone. From studies based on geophysical data, we believe that the front of the margin consists of subsided continental crust. If this hypothesis is correct, the Andean subduction zone was dominated by tectonic processes and resulted in subcrustal erosion before the present tectonic regime, which is accretionary.

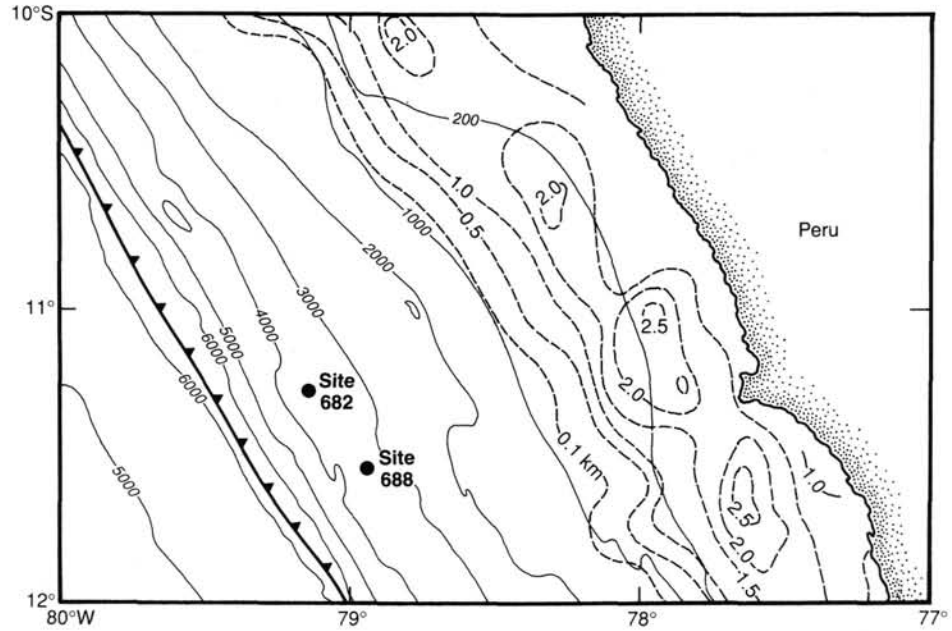

Figure 1. Bathymetry and sediment isopachs along the Peru continental margin at 11°S; intervals are in increments of 1000 m, beginning at a water depth of 200 m. Sediment isopachs are in increments of 0.5 km, beginning at 0.1 km; for an overview of all sites, see Site Chapter 679, Figure 1. Site 688 is located on the lower slope of the Peru Trench about 30 km landward of the trench axis. See "Introduction" (this volume) for regional location map of Leg 112 sites.

OPERATIONS

JOIDES Resolution departed Site 687 and headed for a point about 6 nmi east of Site 688, where we deployed the geophysical equipment for the approach to the site (Fig. 2). Navigation was during global positioning system (GPS) coverage, which helped establish the position of the ship, the bathymetry, and the identification of a fault, as predicted from the seismic record used to select the site. We dropped a beacon on the initial pass, and when the ship was steady over this beacon, we found our position was correct. The drill string was lowered shortly after 1800 L (local), 4 December 1986; the first core was brought on deck at about 0200 hr, 5 December. Coring continued normally until 2300 hr on 6 December 1986 (Table 1). At 350 mbsf, the sleeve at the top of the pore-water sampler parted while pulling a tension of only 20,000–30,000 lb on the drill string; subsequent fishing operations failed to bring up the instrument. Therefore, Hole 688B was washed to 350 mbsf, but when retrieving the first core, we found that the center bit had stuck. When all efforts to retrieve the center bit failed, we were forced to raise the drill string on board. We found that a piece of the pore-water sampler was jammed into the bit, had remained in the bit during the subsequent 350 m of drilling, and had prevented seating of the center bit. A new bottom-hole assembly (BHA) was rigged with a rotary bit and lowered. After washing down to 350 m (again in Hole 688C), our first coring attempt also re-

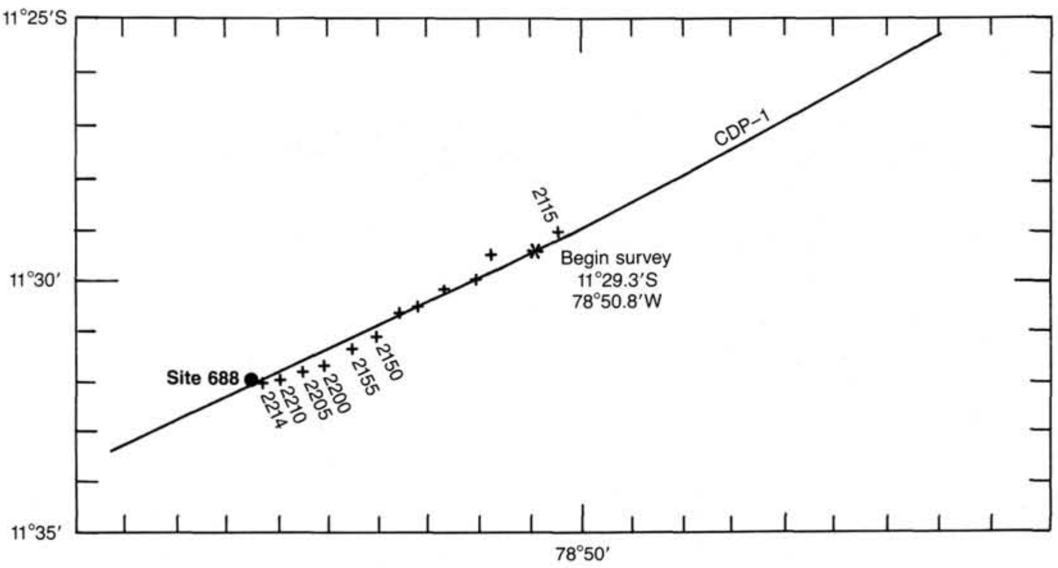

Figure 2. Track chart of approach to Site 688.

Table 1. Coring summary for Site 688.

Core/ Section	Date (Dec. 1986)	Time (UTC)	Depth (mbsf)	Length cored (m)	Length recovered (m)	Recovery (%)
112-688A-1H	5	0200	0–8.3	8.3	8.35	100.0
2H	5	0245	8.3–17.8	9.5	9.80	103.0
3H	5	0330	17.8–27.3	9.5	9.97	105.0
4H	5	0435	27.3–36.8	9.5	9.94	104.0
5H	5	0530	36.8–46.3	9.5	9.80	103.0
6H	5	0800	46.3–55.8	9.5	10.12	106.5
7H	5	0850	55.8–65.3	9.5	10.15	106.8
8X	5	0950	65.3–74.8	9.5	3.52	37.0
9X	5	1030	74.8–84.3	9.5	9.58	101.0
10X	5	1120	84.3–93.8	9.5	4.03	42.4
11X	5	1215	93.8–103.3	9.5	12.33	129.8
12X	5	1310	103.3–112.8	9.5	2.45	25.8
13X	5	1410	112.8–122.3	9.5	9.56	100.0
14X	5	1515	122.3–131.8	9.5	11.94	125.7
15X	5	1610	131.8–141.3	9.5	9.51	100.0
16X	5	1705	141.3–150.8	9.5	11.74	123.6
17X	5	1801	150.8–160.3	9.5	8.67	91.2
18X	5	2115	160.3–169.8	9.5	1.64	17.2
19X	5	2210	169.8–179.3	9.5	7.15	75.2
20X	5	2315	179.3–188.8	9.5	0.69	7.3
21X	6	0015	188.8–198.3	9.5	4.41	46.4
22X	6	0125	198.3–207.8	9.5	0.45	4.7
23X	6	0220	207.8–217.3	9 5	1.01	10.6
24X	6	0330	217.3–226.8	9.5	1.20	12.6
25X	6	0430	226.8–236.3	9.5	2.61	27.5
26X	6	0530	236.3–245.8	9.5	0.80	8.4
27X	6	0625	245.8–255.3	9.5	7.78	81.9
28X	6	0900	255.3–264.8	9.5	1.84	19.3
29X	6	1015	264.8–274.3	9.5	9.70	102.0
30X	6	1110	274.3–283.8	9.5	1.44	15.1
31X	6	1215	283.8–293.3	9.5	0.96	10.1
32X	6	1325	293.3–302.8	9.5	11.58	121.9
33X	6	1445	302.8–312.3	9.5	8.11	85.3
34X	6	1810	312.3–321.8	9.5	9.63	101.0
35X	6	1915	321.8–331.3	9.5	9.72	102.0
36X	6	2020	331.3–340.8	0.5	10.33	108.7
37X	6	2130	340.8–350.3	9.5	2.78	29.2
112-688C-1R	9	1400	350.3–359.8	9.5	1.19	12.5
112-688E-1R	11	2335	350.0–355.5	5.5	3.15	57.3
2R	12	0125	355.5–365.0	9.5	0.70	7.4
3R	12	0245	365.0–374.5	9.5	6.13	64.5
4R	12	0350	374.5–384.0	9.5	5.71	60.1
5R	12	0500	384.0–393.5	9.5	9.15	96.3
6R	12	0630	393.5–403.0	9.5	9.59	101.0
7R	12	0815	403.0–412.5	9.5	9.69	102.0
8R	12	0950	412.5–422.0	9.5	9.45	99.5
9R	12	1120	422.0–431.5	9.5	8.67	91.2
10R	12	1300	431.5–441.0	9.5	7.22	76.0
11R	12	1440	441.0–450.5	9.5	0.17	1.8
12R	12	1615	450.5–460.0	9.5	3.07	32.3
13R	12	1815	460.0–469.5	9.5	0.35	3.7
14R	12	2020	469.5–479.0	9.5	4.93	51.9
15R	13	0050	479.0–488.5	9.5	3.17	33.3
16R	13	0245	488.5–498.0	9.5	1.44	15.1
17R	13	0440	498.0–507.5	9.5	0.06	0.6
18R	13	0625	507.5–517.0	9.5	0.05	0.5
19R	13	0810	517.0–526.5	9.5	5.02	52.8
20R	13	0945	526.5–536.0	9.5	2.01	21.1
21R	13	1130	536.0–545.5	9.5	0.03	0.3
22R	13	1320	545.5–555.0	9.5	0.43	4.5
23R	13	1920	555.0–564.5	9.5	4.64	48.8
24R	13	2215	564.5–574.0	9.5	3.15	33.1
25R	14	0040	574.0–583.5	9.5	2.84	29.9
26R	13	0225	583.5–593.0	9.5	1.31	13.8
27R	14	0445	593.0–602.5	9.5	2.84	29.9
28R	14	0703	602.5–612.0	9.5	0.00	0.0
29R	14	0915	612.0–621.5	9.5	0.05	0.5
30R	14	1210	621.5–631.0	9.5	1.92	20.2
31R	14	1520	631.0–640.5	9.5	0.12	1.3
32R	14	1740	640.5–650.0	9.5	2.15	22.6
33R	14	2045	650.0–659.5	9.5	3.41	35.9
34R	14	2320	659.5–669.0	9.5	2.61	27.5
35R	15	0205	669.0–678.5	9.5	1.68	17.7
36R	15	0530	678.5–688.0	9.5	5.31	55.9
37R	15	0840	688.0–697.5	9.5	3.34	35.1
38R	15	1810	697.5–707.0	9.5	5.55	58.4
39R	15	2215	707.0–716.5	9.5	4.00	42.1
40R	16	0315	716.5–726.0	9.5	0.14	1.5
41R	16	1005	726.0–735.5	9.5	2.07	21.8
42R	16	1605	735.5–745.0	9.5	2.12	22.3
43R	16	1840	745.0–754.5	9.5	5.87	61.8
44R	16	2215	754.5–764.0	9.5	2.67	28.1
45R	17	0155	764.0–769.5	5.5	4.00	72.7
46R	18	0850	769.5–779.0	9.5	0.00	0.0

H = hydraulic; X = extended-core barrel; R = rotary.

sulted in a core barrel that could not be retrieved. The drill string was again raised; we found that the problem was that parts did not match. After correcting this problem, we lowered the drill string for the third time on 10 December 1986, and after washing to 350 mbsf in Hole 688D, the center bit again could not be retrieved. Somehow the center bit had unscrewed from the core barrel. Despite engaging the bottom 2 ft of the barrel with a fishing tool, the bit could not be dislodged. After four trips with the sand line failed, we pulled the drill string. We believe that because of wedging of the tool, nothing could pass through the BHA. Finally, we washed Hole 688E down to 350 mbsf and recovered the first core at 2330 hr, 11 December 1986. We continued coring from 12 December through about 0300 hr, 17 December 1986, taking time only to unplug the bit four times by sending a deplugging tool down the drill pipe. Again, the core barrel containing Core 112-688E-46R could not be retrieved after six tries, and the hole was abandoned without logging. We did not have enough time before the end of the leg to continue a program at Site 688 or to return to the shallow Site 679 to finish that hole to its target depth.

LITHOSTRATIGRAPHY

Lithologic Units

Sediments recovered at Site 688 were divided into three lithologic units on the basis of visual core descriptions, smear slides, and biostratigraphy (Fig. 3, Table 2). Lithologic Unit I is further subdivided into three subunits, and Unit II is subdivided into six subunits.

Lithologic Unit I

Cores 112-688A-1H through 112-688A-36X-6; depth, 0–338.5 mbsf; age, Quaternary.

Unit I is divided into three subunits (Fig. 3). Subunit IA consists of Quaternary diatomaceous muds and extends down to a depth of 66.5 mbsf. Subunit IB extends from 66.5 to 131.8 mbsf. It is in gradational contact with a more terrigeneous lithology above and with a less calcareous diatomaceous mud at its base. The top of Subunit IC is marked by a decrease in both foraminifers and nannofossils. Subunit IC consists of Quaternary diatomaceous mud marked by a strong black color, which we believe is the result of the presence of iron monosulfides of diagenetic origin. These iron monosulfides extend upsection into Subunit IB. The base of Subunit IC is at 338.5 mbsf.

Subunit IA

Cores 112-688A-1H through 112-688A-8H-1; depth, 0–66.5 mbsf.

Subunit IA consists of diatomaceous mud, predominantly dark olive gray or dark greenish-gray to greenish-gray and olive gray. Color changes are subtle and occur at intervals ranging from 10 to 100 cm. There is common evidence of moderate to extensive bioturbation. Diatom content ranges from 5%–15% up to 50%, averages 10%–20% and generally decreases downhole.

A significant enrichment in biogenic carbonate (foraminifers: 2% to 20%; nannofossils: 2% to 10%) occurs in Section 112-688A-2H-4. The biogenic carbonate content increases downhole up to a value of 40% in Core 112-688A-5H. The main lithological feature of Subunit IA is the occurrence of a substantial amount of detrital material that averages 7% and occurs as two distinctive sediment types:

1. Brownish-gray, coarse-grained, foraminifer terrigenous sands exhibit sharply defined basal contacts (Fig. 4) and graded bedding. Some of these sands (e.g., Sample 112-688A-2H-2, 73

cm) contain up to 40% benthic foraminifers of shallow-water origin. This suggests that foraminifers originated from the shelf.

2. Distinctive dark gray, micaceous, thinly bedded, quartzo-feldspathic sands also occur in Subunit IA. These sands are well sorted and ungraded (Fig. 5).

Authigenic pyrite is present throughout Subunit IA in amounts ranging from traces to 15%-20%. Small patches of black color are present throughout as well. The black color was inferred to indicate the presence of iron monosulfides. Peloidal accumulations of sponge spicules and collapsed sponges are common, particularly in Core 112-688A-6H, where these are scattered throughout. The sponges are flattened rings and range in size from about 0.5 cm in diameter to a maximum of 2.5 cm.

Subunit IB

Cores 112-688A-8H-2 through 112-688A-14X, CC; depth, 66.5-131.8 mbsf.

Subunit IB is a foraminifer- and nannofossil-bearing diatomaceous mud having a significant biogenic carbonate content. The foraminifer and nannofossil content is 10% to 40% and averages 25%. Great variation in relative calcareous fossil contents exists. Individually, these make up from 0% to 40% of the sediment; however, the total amount of biogenic carbonate is generally constant. Diatom content is 15% to 40% and averages 25%. The total biogenic contribution typically ranges from 30% to 70%, estimated from smear slide, and averages 40% to 55% throughout Subunit IB, with a general decrease of biogenic influx from top to bottom.

The boundary between Subunits IA and IB is not marked by a strong lithologic change. Subunit IB begins at Sample 112-688A-8H-1, 100 cm, where the first turbidite occurs. The boundary between Subunits IB and IC is marked by the appearance of biogenic carbonate, which occurs in Section 112-688A-14X, CC.

The sediment in Subunit IB is olive gray to dark olive gray from the top of the unit down to Section 112-688A-9X-5, where the gradational color changes to black. Section 112-688A-10X-1 is recorded as a massive black mud. The black color persists through Core 112-688A-36X.

Authigenic pyrite is present throughout Subunit IB and varies from 3%-4% to 15%. This authigenic pyrite is associated with iron monosulfide patches that are scattered throughout the sediment from the top of the unit down to Section 112-688A-10X-1. Below this, the iron monosulfides are not concentrated in small patches but are dispersed in the sediment, giving it a black color that is pervasive down to Section 112-688A-36X-6. After the cores were split and exposed, the black color progressively faded, probably because of oxidation of the unstable iron monosulfides (see "Diagenesis" section, this chapter). The color changes from black to olive black and olive gray during a short period ranging from 1 to 4 or 5 hr. As the black disappears, the sediment revealed moderate to extensive bioturbation, indicating that Subunit IB was deposited in an environment of oxygenated bottom waters.

Subunit IC

Cores 112-688A-15X through 112-688A-36X-6; depth, 131.8-338.5 mbsf.

Subunit IC consists of diatomaceous muds that exhibit a deep black color related to the presence of iron monosulfides, as mentioned previously. The boundary between Subunits IB and IC is marked by the appearance of biogenic carbonate (20%) at the base of Subunit IB and the occurrence of gas hydrates throughout the top core of Subunit IC (Core 112-688A-15X).

As the cores were exposed to air, this black mud oxidized to olive black, and the sedimentary structures of the recovered sediment became clearly visible, revealing moderate to extensive burrowing throughout (Fig. 6).

Sedimentary pyrite (FeS_2) occurs in the black mud as disseminated silt to clay-sized grains, with pyrite ranging from 1%-2% to 15% and an average of 5%-6% occuring together with iron monosulfides.

Lithologic Unit II

Cores 112-688A-36X to 112-688A-37X, 112-688C-1R, and 112-688E-1R to 112-688E-26R; depths: Hole 688A, 338.5-350.3 mbsf; Hole 688C, 350.3-359.8 mbsf; Hole 688E, 350.3-593.0 mbsf; age, Quaternary to early Miocene.

Subunit IIA extends from 338.5 to 350.3 mbsf in Hole 688A, from 350.3 to 359.8 mbsf in Hole 688C, and from 350.3 to 390.15 mbsf (112-688E-5R-5, 15 cm) in Hole 688E. The subunit ranges from Quaternary to Pliocene in age. Subunit IIA consists of predominantly very dark gray diatomaceous mudstone (Fig. 7). In Hole 688A, there is evidence of bioturbation throughout. Burrows are filled with coarse-grained sandy silt and large clasts (0.5 to 1 mm). In Holes 688C and 688E, no evidence for bioturbation exists, which suggests that no overlapping occurs between Hole 688A and Hole 688E. Thus, the cored thickness of Subunit IIA, roughly 50 m, is a minimum thickness (Figs. 8 and 9). The diatom content is 40% to 60% from smear-slide estimations. The quartz-feldspar content is very low (3%-10%), and the clay content ranges from 35% to 50%.

Subunit IIB extends from 390.15 mbsf (Sample 112-688E-5R-5, 15 cm) to 404 mbsf (Section 112-688E-7R, CC). A sharp change in color from olive gray to black marks the boundary between Subunits IIA and IIB. This change also is sharply recorded in the diatom content, which is 50% in Subunit IIA and less than 10% in Subunit IIB. The black mudstone of Subunit IIB is mainly massive.

A finely laminated section occurs from Samples 112-688E-6R-3, 92 cm, to 112-688E-7R-4, 85 cm (Fig. 10). Laminae exhibit variable spacing with thicknesses ranging from 2 to 6 cm. These laminae have three components: (1) pale-colored diatomite having diatom contents ranging from 75% to 95% (as the diatom content increases, the color becomes paler), (2) gray diatomaceous mudstone, and (3) dark olive gray diatomaceous silty mud. This laminated sequence is similar to sediments of the onshore Pisco Formation and is probably of the same Miocene to Pliocene age.

A zone of decollement marks the upper and lower boundary of the thick laminated sequence (Cores 112-688E-6R and 112-688E-7R), which has been extensively deformed by slumping (Fig. 11; see "Structure" section, this chapter).

Subunit IIC extends from 404 (Core 112-688E-8R) to 450 mbsf (Sample 112-688E-12R-1, 50 cm), is 46 m thick, and consists mainly of olive gray to black, diatom-bearing, silty mudstones (Fig. 12) that are predominantly, though not exclusively, massive. These mudstones contain 10% to 25% diatom frustules and are enriched in sand- and silt-sized terrigenous grains (between 25% and 50%), relative to lithologic Subunits IIB and IID. A 60-cm-thick bed of siltstone cemented by calcitic dolomite makes up a minor lithology. The sediment of Subunit IIC contains 1% to 10% authigenic calcite and/or dolomite, and most of the mudstones are strongly cemented.

Subunit IID extends from 450 mbsf (Sample 112-688E-12R-1, 55 cm) down to a zone of poor recovery in Sections 112-688E-17R, CC and 112-688E-18R, CC. Subunit IID is 50 to 60 m thick and consists of nannofossil- and foraminifer-bearing diatomaceous mudstone, generally dark olive gray to black. The upper boundary with Subunit IIC is marked by a sharp change in color from dark greenish-gray to dark olive. This sequence is moderately to extensively burrowed. Diatom content ranges from 10% to 40% and averages 20%-25%. Clay content is 10% to

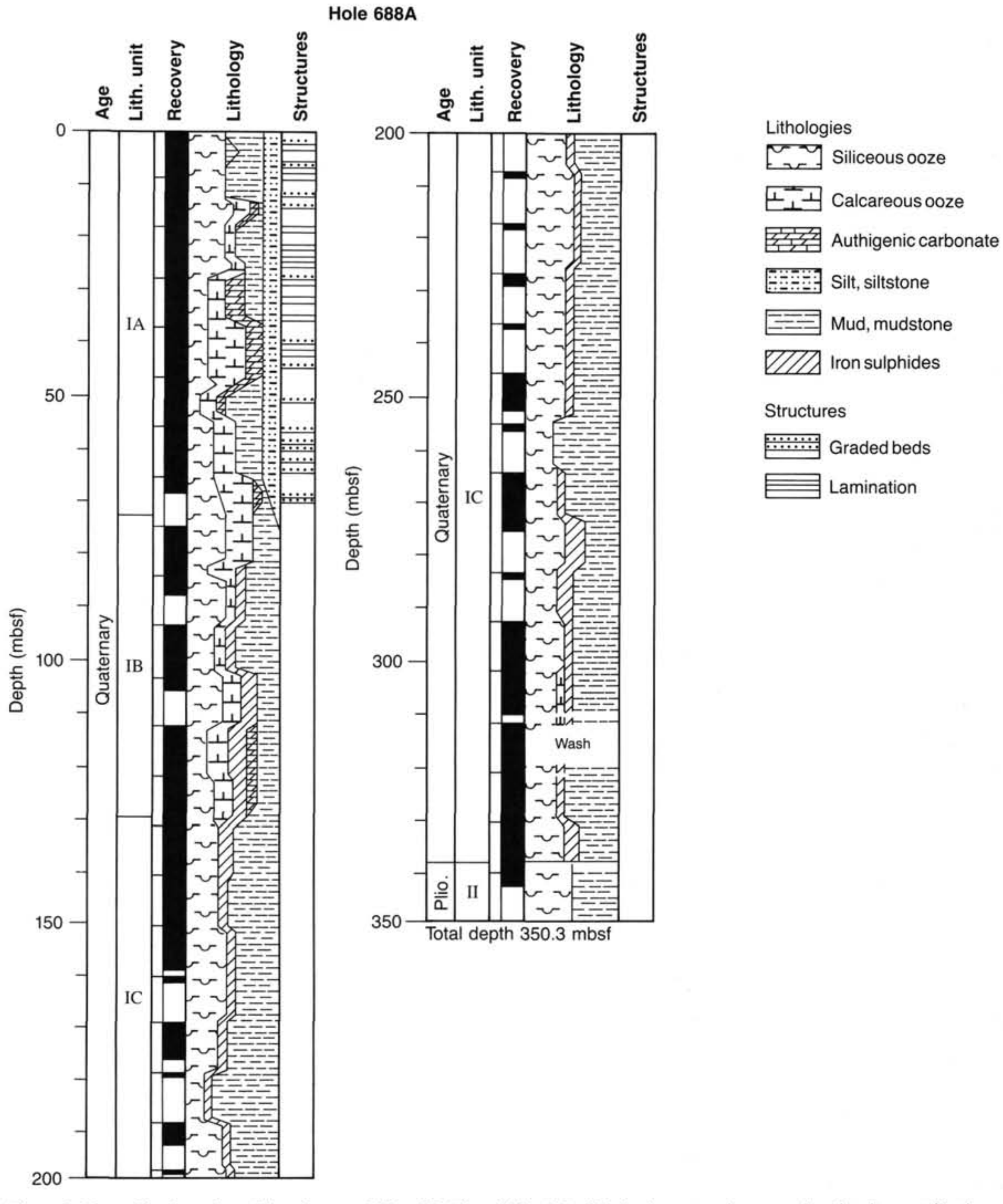

Figure 3. Generalized stratigraphic columns of Site 688. The width of the lithologic pattern is proportional to its contribution as estimated from smear-slide analysis. Core recovery and depth in meters are plotted at left; structural symbols are indicated at right.

60% and averages 40%. The sediment has 5% to 10% of silt-sized terrigenous grains that distinguishes it from Subunit IIC. Biogenic calcareous content averages 10%, and volcanic ash occurs as a minor lithology.

Subunit IID ranges in age from middle to late Miocene. The boundary between Subunits IID and IIC corresponds to the second hiatus, defined from diatom floral component studies (see "Biostratigraphy" section, this chapter).

Subunit IIE extends from 517 mbsf (Section 112-688E-19R-1) to 555 mbsf (Section 112-688E-22R, CC). The subunit is composed of a diatomaceous mudstone enriched in authigenic carbonates (5% to 10%–12%). The sediment is dark olive gray to black and moderately bioturbated. Five beds of dolomicrite occur in Core 112-688E-19R. These beds are olive gray and typically range from 3 to 25 cm thick. Dolomitization has occurred in the more porous beds, which were originally silty sand or diatom-rich layers. The dolomicritic beds that occur in Section 112-688E-19R-3 grade down into darker mudstone (Fig. 13). The upper contact of the dolomicritic bed located in Sample 112-688E-19R-3, 93–97 cm, is offset along cross faults (Fig. 14).

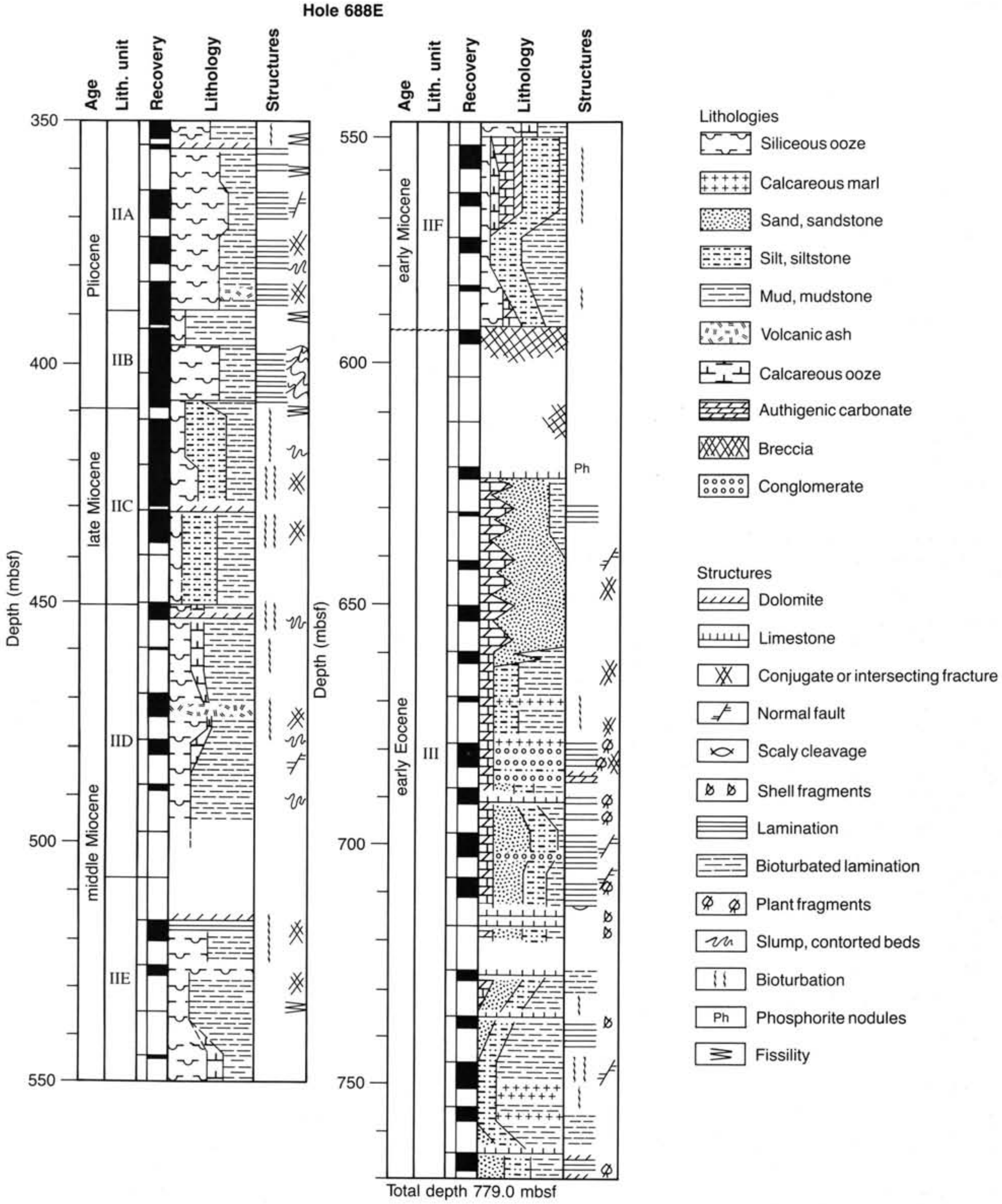

Figure 3 (continued).

Where these faults extend into the dolomicrite bed, no offset was observed (Fig. 13), indicating that deformation clearly precedes dolomitization.

Sample 112-688E-20R-1, 0-35 cm, contains interbedded olive diatomaceous ooze and diatomaceous mud that is extensively deformed by normal faults and associated plastic stretching of laminae. The dominant fault set inclines at 25° to the horizontal and offsets laminae that dip from 45° to 60° to the horizontal. Laminae also show necking and plastic flow along the displacement (Fig. 15). Thus, Subunit IIE exhibits further evidence of extensive deformations and disruption consistent with gravitational processes operating on the slope.

Subunit IIF extends from 555 mbsf (Section 112-688E-23R-1) to 593 mbsf (Section 112-688E-26R, CC) and is 38 m thick.

Table 2. Lithologic units for Site 688.

Lithologic unit	Lithology	Core/ section	Depth (mbsf)
I	----------------------------------	112-688A-1H-1—36X-6	0–338.5
IA	Nannofossil-bearing, diatomaceous muds with frequent sand interbeds.	112-688A-1H-1—8H-1	0–66.5
IB	Foraminifer- and nannofossil-bearing diatomaceous muds.	112-688A-8H-2—14X, CC	66.5–131.8
IC	Iron sulfide-bearing diatomaceous muds.	112-688A-15X-1—36X-6	131.8–338.5
II	----------------------------------	112-688A-36X, CC—37X, CC	338.5–350.3
		112-688C-1R	350.3–359.8
		112-688E-1R-1—26R, CC	350.3–593.0
IIA	Diatomaceous mudstones.	112-688A-36X, CC—37X, CC	338.5–350.3
		112-688C-1R	350.3–359.8
		112-688E-1R-1—5R-5	350.3–390.15
IIB	Diatomaceous and diatom-bearing mudstones.	112-688E-5R-5—7R, CC	390.15–404.0
IIC	Diatom-bearing mudstones.	112-688E-8R-1—12R-1	404.0–450.0
IID	Nannofossil- and foraminifer-bearing diatomaceous mudstones.	112-688E-12R-1—18R, CC	450.0–517.0
IIE	Diatomaceous mudstone.	112-688E-19R-1—22R, CC	517.0–555.0
IIF	Sandy siltstone.	112-688E-23R-1—26R, CC	555.0–593.0
	Zone of cataclastic breccia and poor recovery.	112-688E-27R-1—29R	593.0–621.5
III	Calcareous sandstones, siltstones, and mudstones with conglomerate beds.	112-688E-30R-1—45R, CC	621.5–769.5

Subunit IIF is late Miocene in age, according to our nannofossil and diatom flora studies (see "Biostratigraphy" section, this chapter).

Subunit IIF is composed mainly of sandy siltstone that ranges from dark olive gray to very dark gray. Diatom frustules range from 2% to 10% and generally increase downhole. Moderate bioturbation persists throughout the subunit but generally decreases downhole. The biogenic carbonate content is low and ranges from 2% to 5% in Cores 112-688E-23R and 112-688E-24R.

Rhombohedral, inclusion-free, dolomite crystals are common. However, much of the carbonate appears as fine-grained anhedral micrite or dolomite dispersed in the sediment. The total amount of authigenic carbonate ranges from 15% to 33% in Cores 112-688E-23R and 112-688E-24R and decreases down to 2%–5% in Core 112-688E-26R. The authigenic carbonate cements the siltstone and is hard to drill. Pyrite, glauconite, and phosphate are also components of the sediment and range from 15% to 20% of the total amount of carbonate in Core 112-688A-23R.

Zone of Cataclastic Breccia and Poor Recovery

Core 112-688E-27R shows three well-exposed intervals of cataclastic breccia (Figs. 16 through 18). These breccias are separated by unbrecciated sections, 30 to 60 cm thick, made up of dark gray calcareous siltstone, dark gray mudstone, dolomite-cemented sandstone, and blue gray sand interbedded with dark gray silty mud. These blocks are probably coherent blocks within the cataclastic breccia.

Core 112-688E-28R was void, and Core 112-688E-29R recovered only one sediment piece 5 cm long, consisting of a tectonic breccia (Fig. 19) that includes angular blocks of chert, siliceous mudstone, and phosphatic material.

Lithologic Unit III

Cores 112-688E-30R to 112-688E-45R, CC; depth, 621.5–769.5 mbsf; age, middle to early Eocene.

Lithologic Unit III is marked by a strong lithologic change. The unit is distinguished by an absence of diatoms and by a sharp increase in sand-sized terrigenous grains, especially quartz, feldspar, and rock fragments, which range from 20%–40% to 70%–75% and average 55%. Authigenic carbonate occurs throughout Unit III and shows a general decrease downhole from 40% or 45% to 0%. Although principally calcite, in places a few percent of dolomite rhombs are present. The values of carbonate content locally show large variations that suggest fluid circulation along beds with a higher porosity.

From 612 mbsf (Core 112-688E-30R) to 650 mbsf (Section 112-688E-33R, CC) Unit III is composed mainly of greenish-gray to dark greenish-gray, poorly sorted sandstone. This sandstone is interbedded with sandy siltstone (Fig. 20) and black mudstone (Fig. 21). The sandstone and siltstone are extensively cemented by calcitic dolomite. Carbonate content ranges from 10% to 25%–40%. Components of the sandstone are quartz, feldspar, and rock fragments in various proportions. Quartz content averages between 10% to 40%, and feldspar content varies from 5% to 25%. Rock fragments, including some metamorphic rock, range between 5% and 30%. Sands vary from fine-grained to very coarse-grained, and large fragments (Fig. 20) are angular to subangular. This suggests a nearby source for the detrital material. Disruption of the beds and syn-diagenetic faults (Fig. 20) indicate an unstable environment.

From 650 mbsf (Section 112-688E-33R, CC) to 714.5 mbsf (Sample 112-688E-39R-3, 88 cm) the sand content decreases, which parallels an increase of silt. In Section 112-688E-34R-1, massive to mottled black mudstone (30 cm thick) is interbedded with sandstone.

A 19-cm-thick bed of nannofossil ooze, a 75-cm-thick bed of nannofossil marl, and a 110-cm-thick bed of silty nannofossil marl occur in Cores 112-688E-35R and 112-688E-36R, which indicates the influence of an open-marine environment.

Dark gray, coarse-grained sandstone and pebbly sandstone occur in Samples 112-688E-36R-2, 1–15 cm; 112-688E-36R-2, 105–125 cm; 112-688E-36R-4, 20–45 cm; 112-688E-37R-1, 1–50 cm; 112-688E-37R-2, 135–150 cm; and 112-688E-37R-3, 1–5 cm. Pebbles are subangular to rounded (Figs. 22 and 23), and some grading is present; however, the material is generally poorly sorted (Fig. 23). Clasts are typically of quartz, sedimentary rocks, mud rip-ups, and volcanics. Clasts of chert, milky quartz, micritic limestone, and metamorphic rocks (micaschist) are also common.

The poorly sorted, pebbly sandstone, which is interbedded in mudstone or sandstone, exhibits a disorganized matrix (Fig. 23).

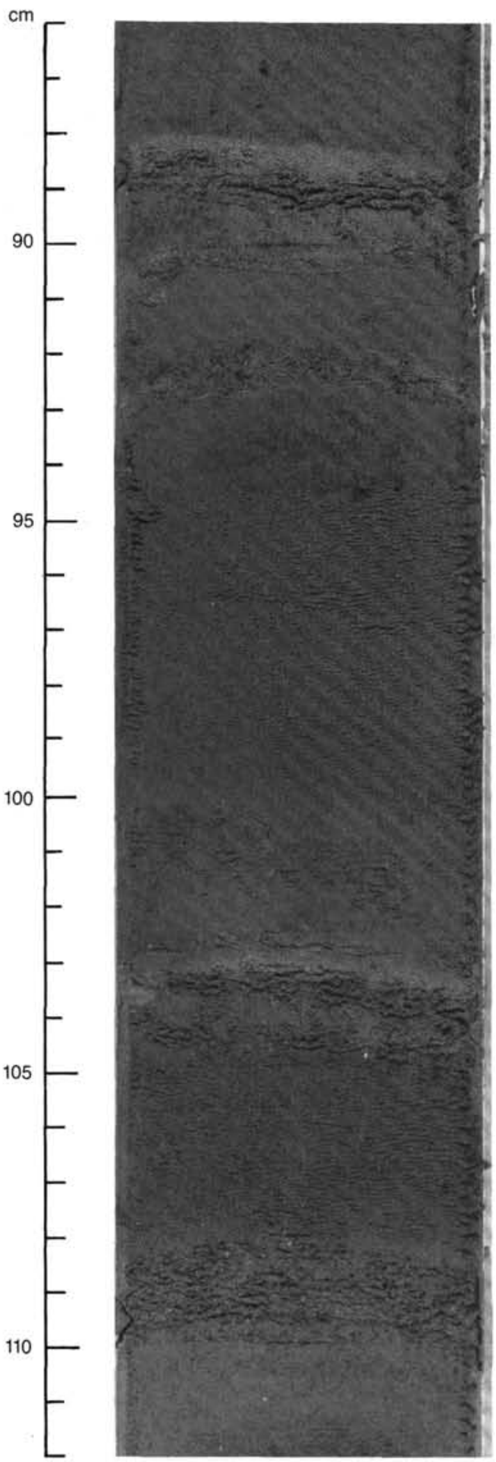

Figure 4. Turbidite bed of lithologic Subunit IA (Sample 112-688A-2H-4, 86–112 cm).

This is probably caused by periodic rapid wasting at the source of the detrital material from pulses in tectonic uplift of the source area.

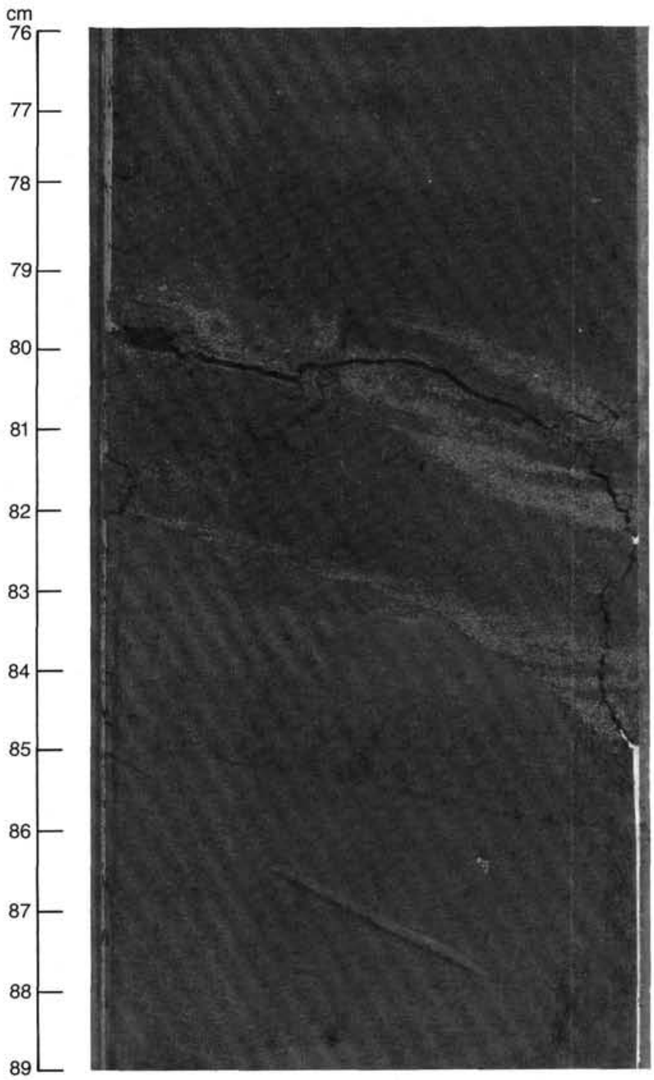

Figure 5. Ungraded clastic sediments and flame structure of Subunit IA. Note the onlapping on the erosional surface (Sample 112-688A-4H-5, 76–89 cm).

Bioclastic calcareous sandstone occurs in Sections 112-688E-39R, CC and 112-688E-40R, CC. Bioclasts include well-preserved oysters, the first nontransported evidence of a very shallow environment (Fig. 24). This shallow-water facies is associated with (1) dark gray quartz arenite that is slightly calcareous, faintly laminated, and moderately burrowed; (2) black to dark gray sandy mudstone and siltstone; (3) dark olive gray mudstone with thin to very thin interbeds of sandy mudstone; and (4) dark gray fine- to medium-grained sandstone.

Dark olive mudstone extends through Cores 112-688E-43R and 112-688E-44R. Bioturbation ranges from moderate to pervasive. Nannofossil content ranges from 10% to 20%; clay mineral content is high, and the detrital component is small and made up of fines.

The last core recovered at Hole 688E is made up of dark silty mudstone and very fine sandstone having abundant plant debris and calcareous silt as local laminae.

Diagenesis

Phosphate

Phosphatic materials are rare at Site 688. Phosphatic peloids, along with glauconite, occur only sporadically and in small amounts in all units at Site 688. Subunit IIC contains small amounts of F (friable) phosphate lenses in dolomitic diatomaceous mudstone (Cores 112-688E-7R and 112-688E-8R) and a layer of D (dense) phosphate nodules (Sample 112-688E-8R-4, 38–39 cm). D-phosphate nodules or layers occur at the uncon-

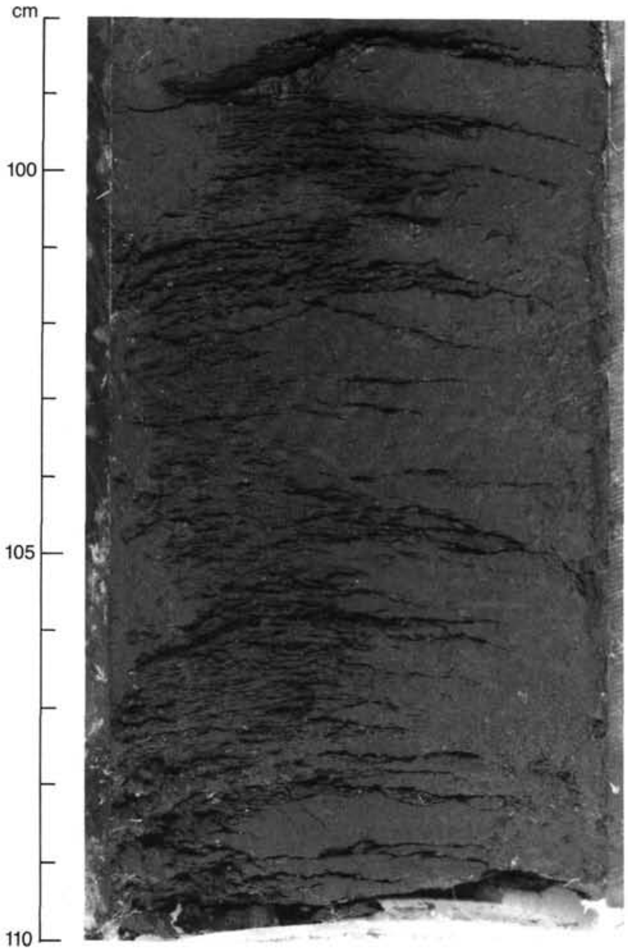

Figure 6. Well-developed fissility in mudstone of lithologic Subunit IC (Sample 112-688A-21X-3, 98–110 cm).

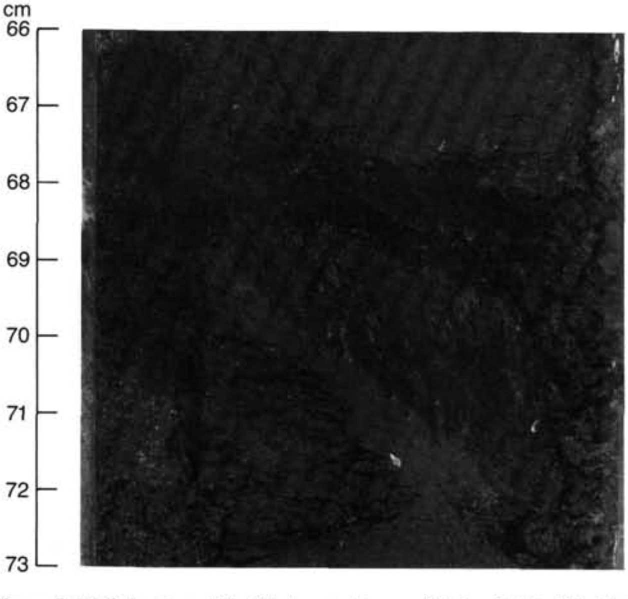

Figure 7. Well-developed fissility in mudstone of Subunit IIA. The fault in the center of the figure is analyzed in the "Structure" section (this chapter; Sample 112-688A-37X-2, 66–73 cm).

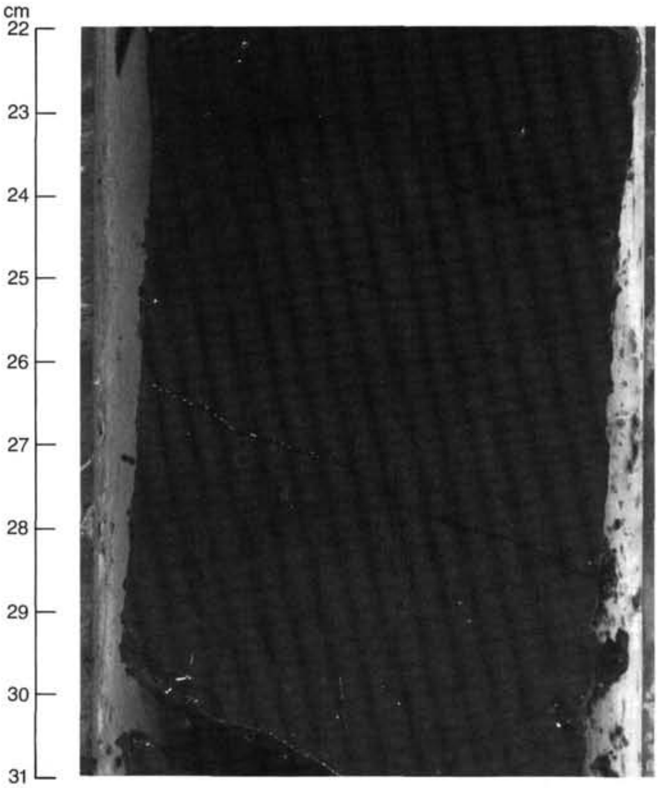

Figure 8. Pervasive anastomosing fabric in mudstone of Subunit IIA (Sample 112-688E-4R-1, 22–31 cm).

formable contact between lithologic Units II and III (Section 112-688E-29R, CC and Sample 112-688E-30R-1, 0–10 cm). These nodules are tectonically brecciated, and the resulting fractures are filled with coarse authigenic quartz crystals. Phosphatization in the sandstones of Unit III is discussed next.

Carbonate Diagenesis

Both calcite and dolomite are present as authigenic phases at Site 688, and calcite uniquely occurs as a replacement in the bottom part of the cored section. The upper 75 m of the section at Site 688 (lithologic Unit I to the top of Subunit IB; Cores 112-688A-1H through 112-688A-8X) is a zone of authigenic carbonate precipitation. Calcite is the main phase present, but at least small amounts of dolomite rhombs also invariably occur. Total authigenic carbonates in the diatomaceous muds of this upper zone range between 5% and 40%. Pore waters in this zone show decreasing calcium concentrations, which is consistent with calcite precipitation (see "Inorganic Geochemistry" section, this chapter).

Between depths of 75 and 422 mbsf (Cores 112-688A-9X through 112-688E-8R), both authigenic calcite and dolomite are present, but in smaller amounts than in the upper zone. The first lithified carbonate, a small dolomite nodule, occurs within this interval at 140.9 mbsf (Sample 112-688A-15X-7, 14 cm).

Lithified carbonates first become common in Subunit IIC at a depth of about 422 mbsf (Core 112-688E-9R). Dolomite is the main authigenic carbonate phase between 422 and 660 mbsf (Cores 112-688E-9R through 112-688E-33R), encompassing Subunits IIC to the top part of IIIA. The Mg^{2+}/Ca^{2+} ratio shows a marked decrease in this zone, which is compatible with dolomitization (see "Inorganic Geochemistry" section, this chapter). A distinctive, brecciated dolomite bed having dolomite-filled veins

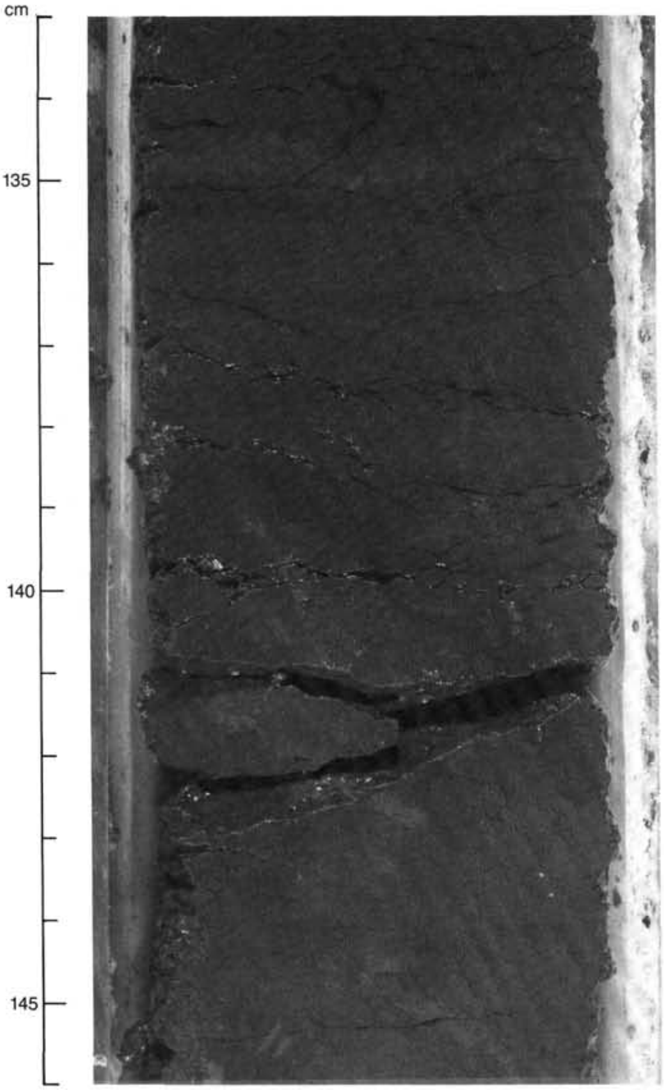

Figure 9. Pervasive anastomosing fabric in mudstone of Subunit IIA (Sample 112-688E-5R-1, 133–146 cm).

occurs at the top of Core 112-688E-10R. Core 112-688E-33R contains unusual greenish-gray veins having dolomite rhombs, including distinctive euhedral, twinned crystals in a chlorite matrix. The bottom part of the interval (422–660 mbsf) contains calcitized sandstones, which are described for the underlying zone where they are common.

From 660 to 779 mbsf (Cores 112-688E-34R through 112-688E-46R; lithologic Unit III) the main authigenic carbonate phase is calcite, although some lithified dolomitic beds are present. Much of the calcite occurs as cements in sandstones and siltstones. Examination of thin sections of sandstones from Cores 112-688E-32R, 112-688E-39R, and 112-688E-40R shows complete replacement of bioclasts, siliceous and phosphatic cements, and detrital sand grains by coarsely crystalline sparry calcite. Calcite-filled veins are also common in this zone. This calcitization is consistent with the large quantities of calcium in pore waters within this zone, probably the result of influxes of interstitial waters from tectonized zones below (see "Inorganic Geochemistry" section, this chapter). Relatively late-stage phosphatization apparently occurred in two of the samples examined in thin section. Sample 112-688E-40R, CC (9–10 cm) has a partly phosphatic cement and Sample 112-688E-41R-1, 45–48 cm, is a micritic limestone that is partly phosphatized; in both cases, a coarse calcitic spar cuts across the earlier phosphatized parts of the limestone. This phosphatization can be accounted for by the high values of both calcium and phosphate in the pore waters of this zone (see "Inorganic Geochemistry" section, this chapter).

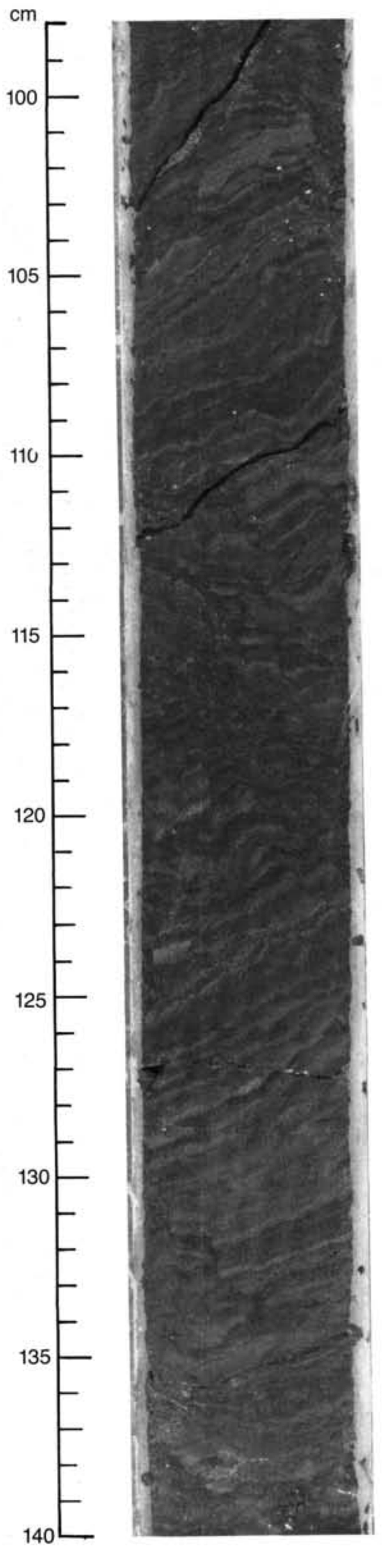

Figure 10. Finely laminated mudstone in a sliding mass of Subunit IIB (Sample 112-688E-6R-5, 98–140 cm).

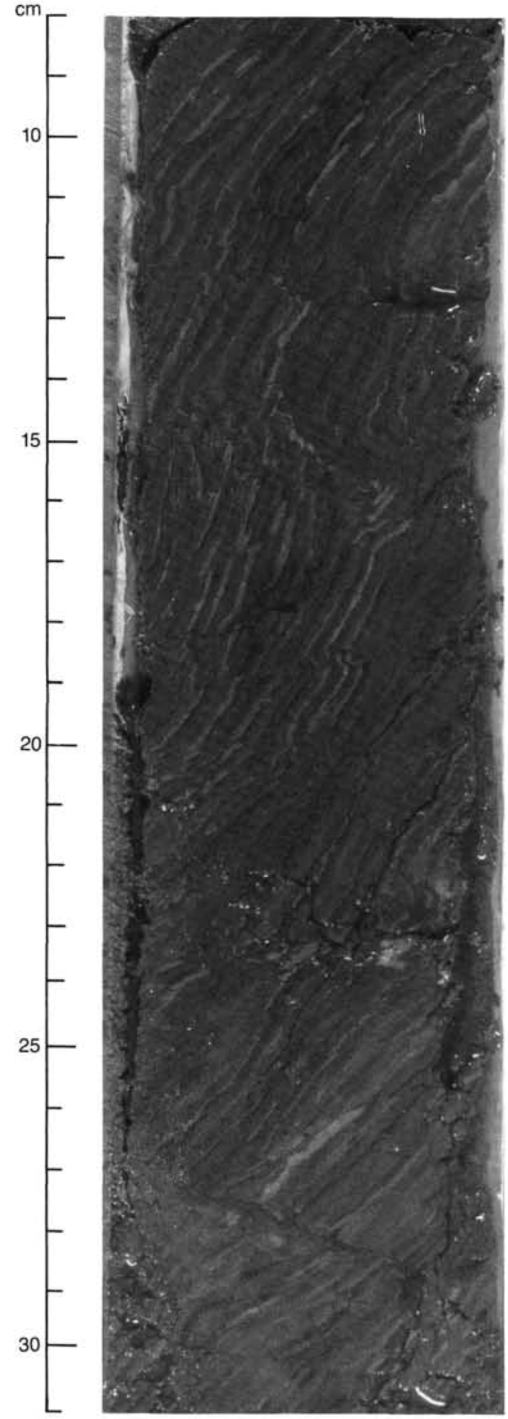

Figure 11. Slump structure in the finely laminated mudstone of the sliding mass of Subunit IIB (Sample 112-688E-6R-7, 8-31 cm).

Data from carbonate analyses are given in Tables 3 and 4 and in Figure 25.

Iron Sulfides

Nearly every smear slide of sediments from Site 688 contains pyrite framboids in abundances ranging from less than 5% to more than 15%. As at most other sites during Leg 112, many terrigenous rock fragments in the sands and sandstones are partly to completely replaced by pyrite. Small pyrite veins and water-escape structures occur in Cores 112-688A-5H through 112-688A-10X.

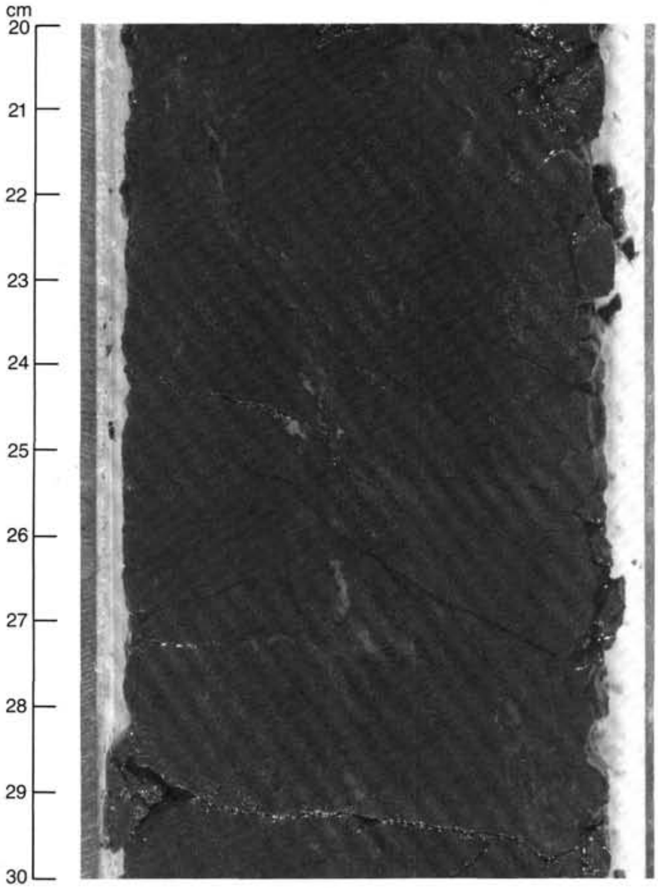

Figure 12. Vertical dip and associated vein structure in mudstone of Subunit IIC (Sample 112-688E-9R-3, 20-30 cm).

Like Site 685, parts of the section at Site 688 contain black, sooty, clay-sized opaque grains that may be iron monosulfides, possibly greigite or mackinawite. However, in contrast to Site 685, where the zone of sooty material is only 62 m thick (Cores 112-685A-4H through 112-685A-20X), sooty material occurs nearly continuously in a zone about 238 m thick at Site 688. This material first occurs sporadically at a depth of 27 mbsf (Core 112-688A-4H), becomes abundant at 75 mbsf (Core 112-688A-9H) and, with two exceptions noted below, occurs in every core through Core 112-688A-33X to a depth of 312 mbsf. Pyrite framboids co-occur with the sooty material, but only pyrite is present below Core 112-688A-33X.

In smear slides the sooty material has the appearance of very fine-grained, submicrometer-sized "dust" particles; these constitute up to 15% of some samples. This is apparently a metastable phase. When first split open, the core sections of the sooty sediment are black (2.5Y 2/0 to N1), but after exposure to air for about one-half hour, these begin to acquire olive gray colors (5Y 3/1 to 3/2). After several hours of exposure, the entire exposed surface of the split core becomes covered with an oxidized, olive gray veneer that coats black, unoxidized sediment below. In smear slides warmed on a hot plate for more than a few minutes, this opaque dust disappears and is replaced by a fine brown material that resembles iron oxides in appearance.

Magnetic measurements at Site 688 suggest that this sooty material may be greigite, a magnetic iron monosulfide mineral. Unlike all other sites during Leg 112, a strong magnetic signal persists to a depth of more than 300 mbsf at Site 688, coinciding with the distribution of the sooty material (see "Paleomagnet-

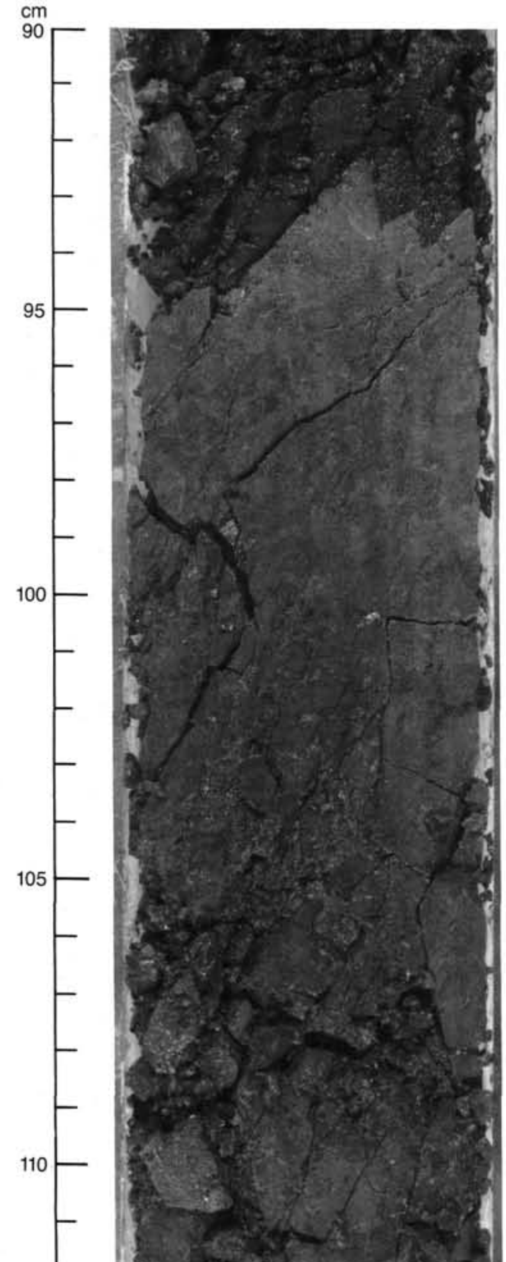

Figure 13. Dolomicritic bed grading down into darker mudstone (Subunit IIE; Sample 112-688E-4R-3, 90–115 cm).

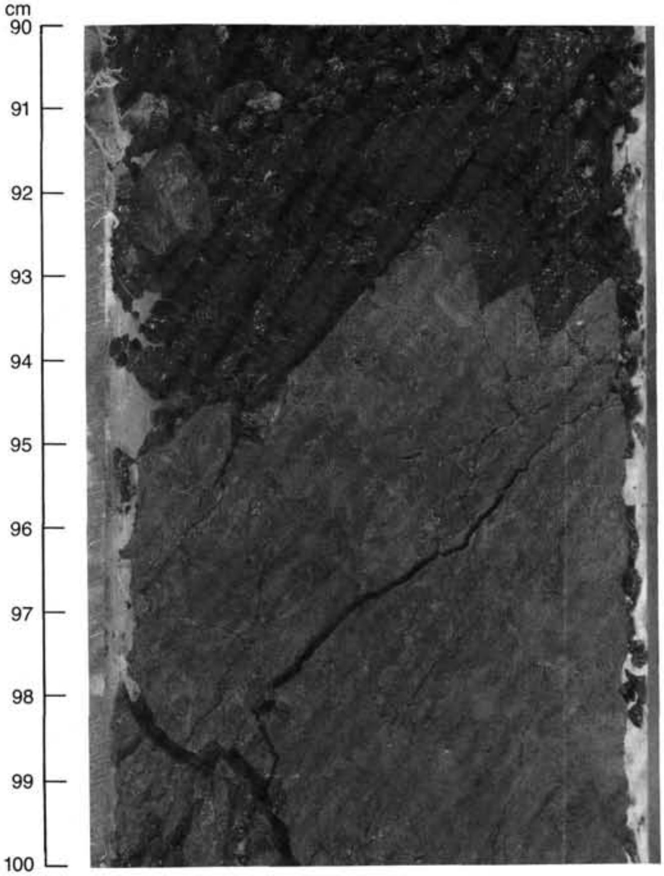

Figure 14. Cross faults offsetting the upper contact of a dolomicritic bed (Subunit IIE). Faulting precedes dolomitization (Sample 112-688E-19R-3, 90–100 cm).

ics" section, this chapter). Circumstantial evidence suggests that this magnetization was acquired during burial diagenesis (rather than at the time of sedimentation), perhaps at the time the iron monosulfide phase formed. Below a depth of about 95 mbsf, the section has normal polarity with the exception of Cores 112-688A-27X and 112-688A-28X, which are reversed. These are the only two cores between Cores 112-688A-8H and 112-688A-34X that do not contain abundant sooty material; hence, these may record a primary magnetic signal rather than one acquired by the precipitation of iron monosulfide during burial diagenesis.

The black iron monosulfides are thermodynamically unstable relative to pyrite, and normally are converted to pyrite by the addition of elemental sulfur during early diagenesis. The persistence of the black iron monosulfides, mentioned by Berner (1974) in the Pleistocene sediment of the deep Black Sea sediments, probably results from an insufficient amount of elemental sulfur to convert them entirely to pyrite. Berner (1974) proposed that the lack of sulfur is caused by the oxidation of H_2S from the sediment pore water after complete bacterial reduction of the limited quantity of dissolved sulfate. The limited sulfate in the Black Sea was caused by a higher rate of deposition and a lower sulfate concentration during the last Pleistocene glaciation. The main limiting factor off Peru may be a very high rate of deposition.

Silicate Diagenesis

Starting with Core 112-688E-23R (545.5 mbsf), secondary overgrowths on quartz and feldspar grains, along with euhedral authigenic feldspars, become common in sandy beds. Below this level, some sandstones have microcrystalline quartz cements along with phosphatic cements. These observations agree with the high values of silica in the pore waters at Site 688 (see "Inorganic Geochemistry" section, this chapter). As noted before, however, all of these earlier phases are replaced by calcite toward the bottom of the section.

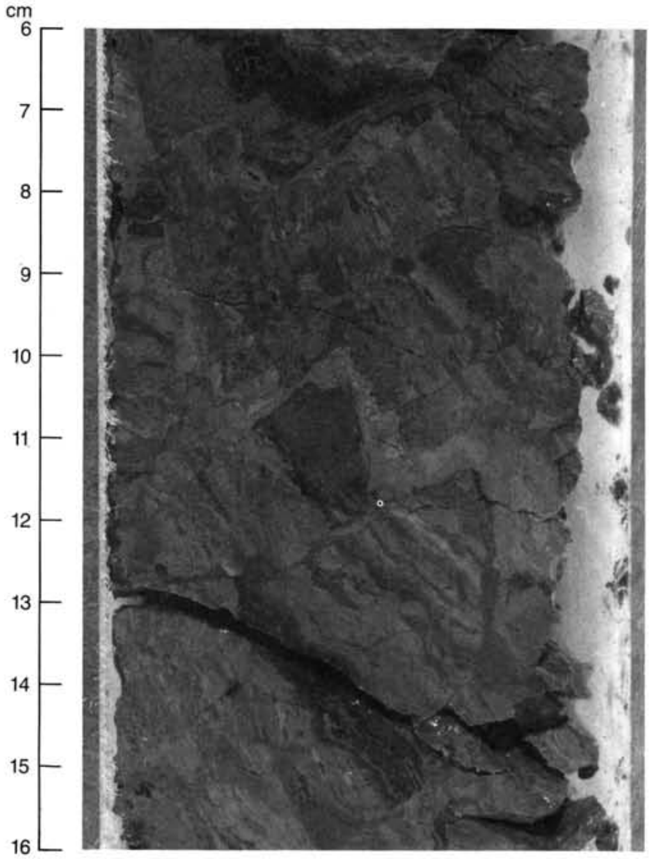

Figure 15. Extensive deformation by normal faulting associated with plastic stretching of laminae (Subunit IIE; Sample 112-688E-20R-1, 6–16 cm).

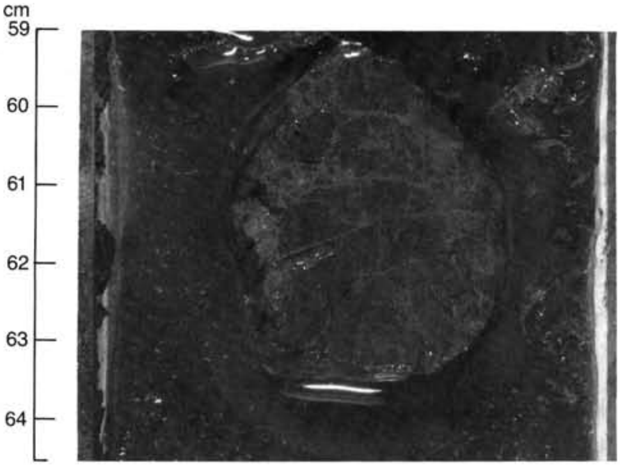

Figure 16. Cataclastic breccia of Sample 112-688E-27R-1, 59–64 cm.

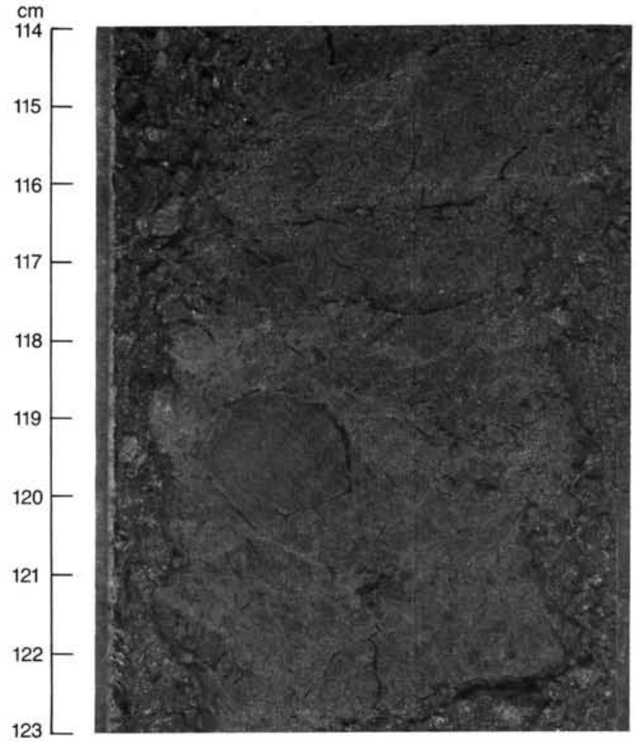

Figure 17. Cataclastic breccia of Sample 112-688E-27R-1, 114–123 cm.

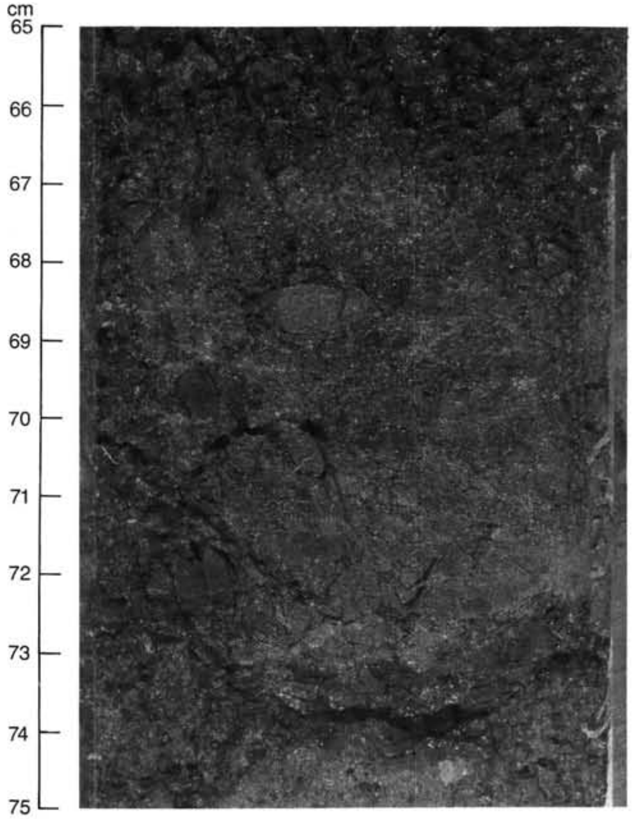

Figure 18. Cataclastic breccia of Sample 112-688E-27R-2, 65–75 cm.

Environments of Deposition

Three distinct sedimentary environments encountered in the 770 m penetrated at Site 688 record progressively deeper water sedimentation from early Eocene to Quaternary time. Lithologic Unit I represents a substantial (339 m) accumulation of bioturbated Quaternary diatomaceous muds. Biostratigraphic data indicate unusually high sedimentation rates of around 300 m/m.y. for this section. The uppermost 132 m is made up of dark olive gray to greenish-gray nannofossil- and foraminifer-bearing diatomaceous muds. Common foraminifer, terrigenous turbidites in the top 66 m indicate shelf-derived sediment influx. Within the diatomaceous muds, benthic foraminifer assemblages are representative of present water depths (see "Biostratigraphy"

Figure 19. Tectonic breccia recovered in Section 112-688E-29R, CC. Note the angular block of chert.

section, this chapter). The remainder of the Quaternary sequence is a diatomaceous mud having a low carbonate content. From 75 to 312 mbsf, the sediment has a uniform black coloration that is associated with significant pyrite and iron monosulfide contents. This represents a substantially thicker black section than that encountered at Site 685 (90 m). The black color and enrichment in monosulfide and pyrite are thought to be characteristic of high sedimentation rates.

Lithologic Unit II (339-593 mbsf) is composed of diatomaceous and diatom-bearing muds of early Miocene to Pliocene-Pleistocene age. A biostratigraphic hiatus separating the Pleistocene from the Pliocene is recorded between 341 and 350 mbsf in Hole 688A and between 350 and 356 mbsf in Hole 688E.

Dolomite occurs as a disseminated authigenic phase throughout lithologic Unit II, and discrete dolomite zones are developed at several intervals. A particularly dolomite-rich section occurs in the lower Miocene at 446 to 565 mbsf. Finely laminated sediment of alternating diatomite and mudstone with associated minor phosphorite is present in the upper Miocene and lower Pliocene. This facies association is similar to that of the contemporaneous sediments of the onshore Pisco Basin. Intervals of terrigenous sedimentation with reduced diatom content occur in the lower Miocene and in the lower Pliocene as well. Upper-to-middle bathyal, benthic foraminifer faunas indicate deposition of the Pliocene sequence in substantially shallower water (500-1500 m) than today's depths.

A marked lithological break to diatom-free calcareous sediment rich in terrigenous clastic detritus occurs at 593 mbsf. This coincides with a hiatus that spans the mid-Eocene to the earliest Miocene, a period of approximately 21.5 m.y. The sediments recovered from 621 to 659 mbsf are predominantly greenish-gray to dark greenish-gray, poorly sorted, quartzo-litho-feldspathic sandstones interbedded with sandy siltstones and black mudstones. These sandstones have a variable and dominantly calcitic cement. The sediments show evidence for syngenetic deformation. Beneath the sandstones from 659 to 678 mbsf, a siltier sequence contains nannofossil chalks and marls representing a more quiescent marine-influenced sedimentation. Reworked Cretaceous calcareous nannoplankton are recorded from the highest levels of the middle Eocene. Benthic foraminifer assemblages for this section indicate a mid- to upper-bathyal (150-500 m) range of water depths.

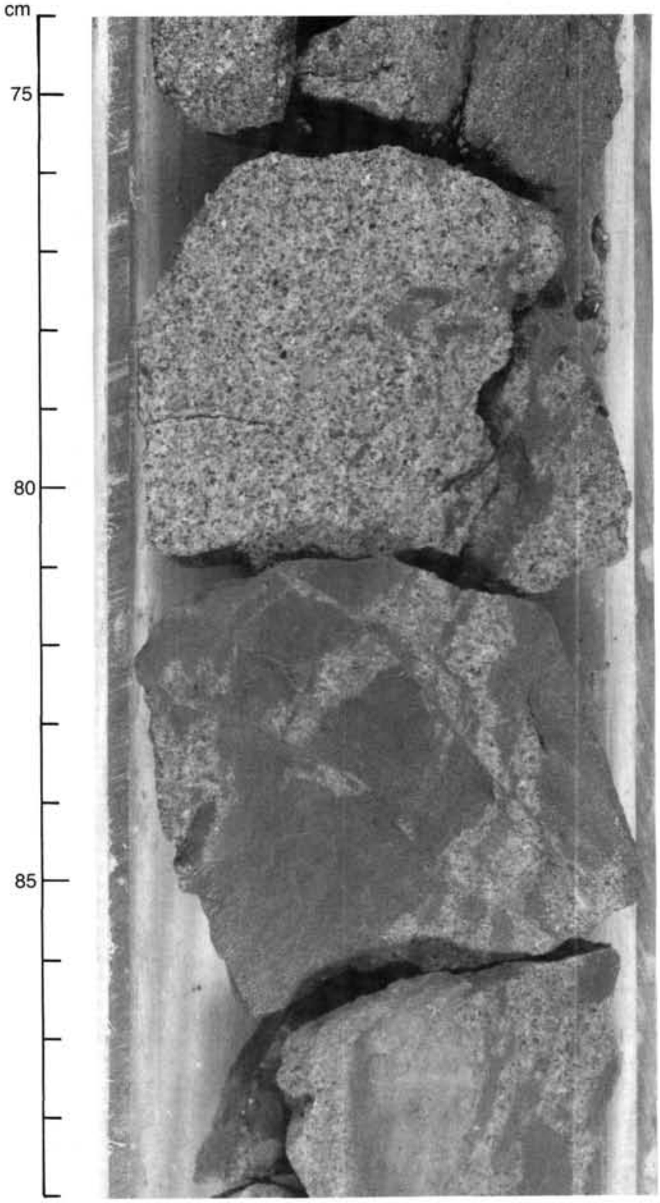

Figure 20. Poorly sorted sandstone and sandy siltstone of lithologic Unit III. Disruption of beds and syngenetic faults are also indicated (Sample 112-688E-32R-1, 74-89 cm).

A hiatus from early to mid-Eocene occurs at 678 mbsf. The lower Eocene sequence from 745 to 678 mbsf includes abundant transported plant matter, coarse pebbly layers, and bioclastic material. Toward the base of this unit, calcareous mudstones and sandstones and silty, bioclastic limestones contain well-preserved mollusks, some of which are still articulated. This indicates little transportation before deposition. Bioclastic material greatly decreases uphole in more sandstone intervals, pebbly sandstone, and conglomeratic zones containing clasts of milky quartz, metamorphic rocks, volcanics, micritic limestone, and chert. Benthic foraminifer and nannofossil assemblages indicate

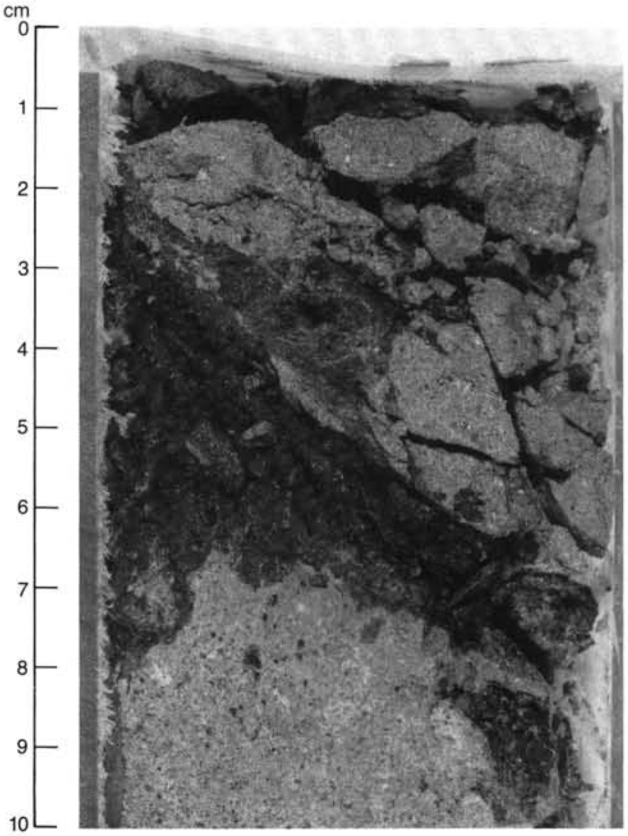

Figure 21. Angular rock fragments in the poorly sorted sandstone of Unit III (Sample 112-688E-32R-2, 0–10 cm).

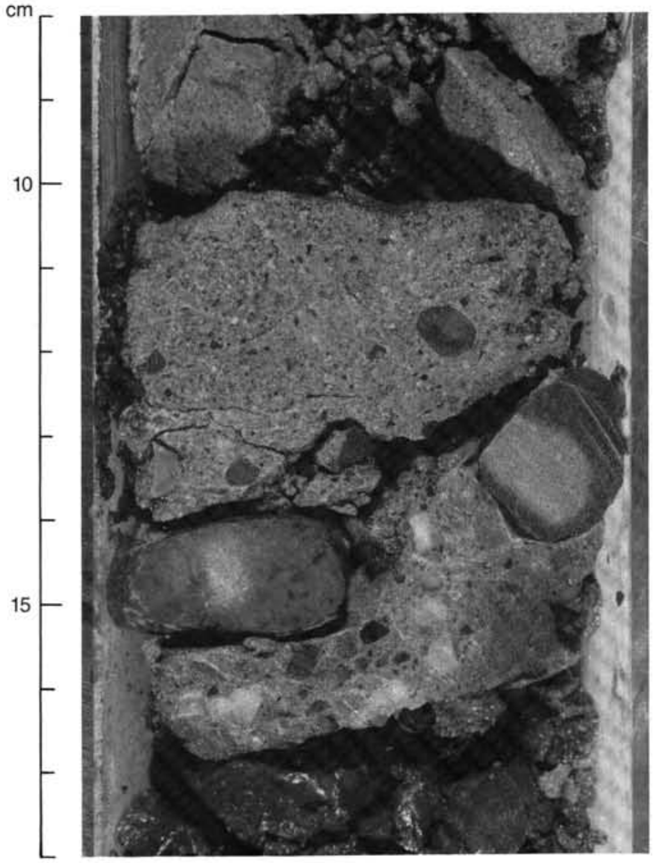

Figure 22. Rounded pebbles in pebbly sandstone of Unit III (Sample 112-688E-36R-2, 8–18 cm).

shelf depths for the deposition of this sequence. The interval from 745 to 764 mbsf contains predominantly dark olive gray mudstones, with minor siltstones and interbedded nannofossil chalks and marls and foraminifer faunas indicating depths of 150 to 500 m. The last sediments recovered from 764 to 769.5 mbsf are made up of interbedded sandstones, siltstones, and mudstones, with abundant plant material and foraminifer assemblages indicating shelf depths. A chert pebble at this level contains a planktonic foraminifer fauna of Cenomanian age identical to faunas of Albian to Cenomanian limestones and cherts of the Central Andes and the onshore Talara Basin. Planktonic and benthic foraminifer faunas throughout the Eocene sequence show close affinities with those of the coastal basins of Peru. Sedimentation rates for the Eocene section are approximately 12 m/m.y. and are consistent with breaks between the pulses of sedimentation.

Structure

The mudstones of Subunit IIA become more indurated and begin to develop an incipient fissility parallel to bedding. At Site 688, fissility first appears in Section 112-688A-11X-4 at a depth of 100 mbsf. This is significantly deeper than upslope in Hole 683A, where fissility develops at a depth of 42 mbsf (Section 112-683A-6H-7), but is almost at the same depth as in Hole 685A (Section 112-685A-14X-2), where it appears at 120 mbsf. The significantly higher sedimentation rate at Sites 685 and 688 may explain the greater depth of the first occurrence of fissility at these sites.

The boundary between lithologic Units I and II is marked by an increase in induration. The mudstones of Subunit IIA show a markedly stronger fissility than that developed in lithologic Unit I.

The first two cores of Hole 688E exhibit a fissility that is well developed in Cores 112-688A-36X, 112-688A-37X, and 112-688C-1R. From Section 112-688E-3R-1, normal microfaults indicate pervasive extension of the sequence. This style of deformation is developed more or less extensively throughout the entire Unit II. Thick, diatom-rich layers are dissected by networks of extensional faults. Interlayered diatomite and mudstone layers show combinations of extensional microfaults and more ductile boudinage. Compressional features are also locally developed.

The black mudstone of Subunit IIB exhibits the same pervasive anastomosing fabric described in Subunit IIA. The 11-m-thick laminated section is extensively deformed by microfaults and slump folds. Microboudinage, both normal and reverse microfaults, and advanced stages of stratal disruption, as in Sample 112-688E-6R-4, 30–120 cm, provide strong evidence for sliding. Zones of discordant beds, inclined at various angles relative to the surrounding beds, also suggest sliding. The upper contact of the laminated sequence is marked by a disaggregated zone (Sample 112-688E-6R-3, 81–92 cm). The lower contact is a fault surface that sharply truncates the laminated material. Below the laminated sediments, a very dark gray diatom-bearing silty mudstone also exhibits slump structures.

The interval from Cores 112-688E-9R-1 to 112-688E-9R-6 shows evidence of extensive deformation. The bedding orientations measured are variable and include vertical dips (Sample 112-688E-9R-3, 20–30 cm; Fig. 12), which suggests folding.

Discontinuous lenticular bedding was observed, with numerous sigmoidal dewatering veins roughly perpendicular to the bedding. We believe these dewatering features were formed during a first phase of compaction before folding. This is substantiated by a second phase of cross-cutting dewatering veins that

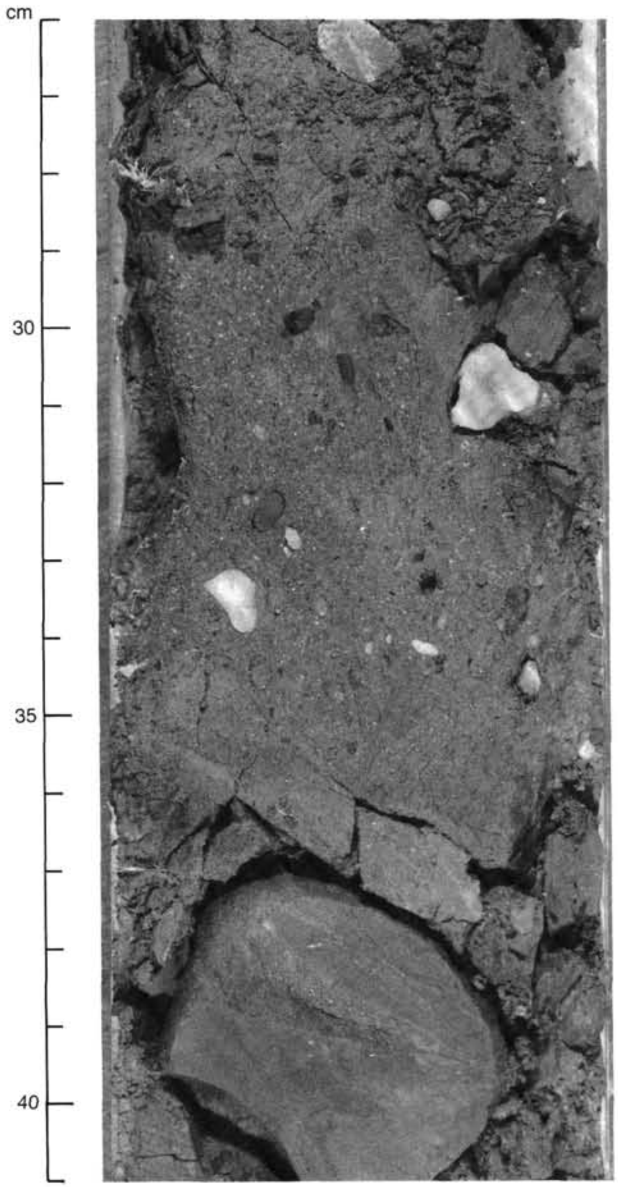

Figure 23. Disorganized matrix in pebbly sandstone of Unit III (Sample 112-688E-36R-4, 26–41 cm).

Figure 24. Shells and shell debris in bioclastic calcareous sandstone of Unit III (Sample 112-688E-40R, CC).

offset the veins of the first phase. The second-phase veins roughly parallel bedding, which suggests dewatering after folding. The pore-water content must have been high during deformation, which favors a slump origin for the fold.

Disruption of the sediment related to slump features and sliding occurs in various places throughout Subunit IID. The best example is in Core 112-688E-16R.

A more coherent deformation characterizes Subunit IIF, compared with Subunits IIA through IIE. Rare dewatering fractures and a variable (15°–60°) but persistent dip are the more prominent tectonic features of this interval.

We believe that Cores 112-688E-27R to 112-688E-29R (zone of cataclastic breccia and poor recovery) represent a thick zone of deformation induced by tectonic processes that included pulverization and brecciation at various scales. This zone of extensive and penetrative deformation has a minimum thickness of 3 m (recovered length) and may be as thick as 28.5 m.

The sediments of lithologic Unit III display numerous extensional microfaults. Although moderate dips are most common, some steep dips (Fig. 26) suggest the development of folding. These sandstones are frequently veined with carbonate, and vein-filled fractures are strongly developed in places. A scaly fabric similar to that observed at the base of Site 682 is locally developed in the mudstones.

A Reverse Fault: Analysis and Orientation

The Pliocene mudstone of lithologic Unit II (Sample 112-688A-37X-2, 66–73 cm; Fig. 9) exhibits a well-preserved fault surface. This fault surface has a classical polish and striated slickensides parallel to the direction of motion. The fault surface also exhibits little steps developed as the upper side block pulled apart during this movement. As these steps (Figs. 27 and 7) do not develop any penetrative deformation perpendicular to the main fault surface, we were able to infer the direction of movement on the fault.

Reconstruction of the local shortening orientation and determination of the paleostress field in which the fault formed have the following requirements:

Table 3. Carbonate in Hole 688A.

Core/section interval (cm)	Depth (mbsf)	Carbonate (%)
112-688A-1H-1, 82–83	0.82	7.0
1H-3, 82–83	3.82	5.92
1H-4, 145–150	5.95	1.00
1H-5, 82–83	6.82	1.33
2H-1, 44–45	8.74	1.00
2H-3, 44–45	11.74	1.33
2H-5, 44–45	14.74	1.75
2H-7, 44–45	17.74	10.34
3H-2, 42–43	19.72	10.68
3H-4, 145–150	23.75	17.60
4H-1, 44–45	27.74	12.59
4H-3, 44–45	30.74	6.51
5H-1, 64–65	37.44	7.67
5H-3, 64–65	40.44	49.87
6H-2, 65–66	48.45	13.76
6H-3, 140–150	50.70	8.75
6H-5, 63–4	52.93	1.58
7H-3, 71–72	59.51	9.26
8X-1, 57–58	65.87	21.35
9X-5, 110–111	81.90	9.17
9X-5, 140–150	82.20	8.58
9X-6, 110–111	83.40	1.50
10X-2, 32–33	86.12	8.76
11X-2, 28–29	95.58	8.09
12X-1, 55–56	103.85	8.59
12X-1, 140-150	104.70	7.83
13X-2, 66–67	114.96	5.34
13X-6, 66–67	120.96	11.84
14X-2, 85–86	124.65	8.84
14X-6, 85–86	130.65	4.34
17X-1, 58–59	151.38	3.50
16X-2, 11-12	142.91	0.32
16X-4, 140–150	147.20	2.25
16X-6, 12–13	148.92	2.50
17X-6, 58–59	158.88	2.75
18X-1, 133–134	161.63	4.17
19X-1, 58–59	170.38	8.59
19X-3, 140–150	174.20	5.33
19X-5, 58–59	176.38	7.26
21X-1, 63–64	189.43	14.68
21X-3, 63–64	192.43	8.17
21X-3, 108–118	192.88	2.75
22X-1, 20–21	198.50	9.67
23X-1, 69–70	208.49	2.92
24X-1, 50–51	217.80	2.00
25X-1, 62-63	227.42	1.83
25X-1, 140–150	228.20	2.42
26X-1, 33–34	236.63	1.42
28X-1, 55–56	255.85	1.92
27X-1, 25–26	246.05	1.08
27X-4, 140–150	251.70	1.42
30X-1, 115–125	275.45	1.75
32X-4, 37–38	297.04	23.10
33X-1, 86–87	303.66	3.59
33X-3, 140–150	307.20	5.33
34X-1, 68–69	312.98	1.75
34X-6, 68–69	320.48	1.83
36X-1, 85–86	332.15	1.75
36X-7, 85–86	340.85	1.17
36X-6, 140–150	339.90	0.92
37X-2, 59–60	342.89	1.00

Table 4. Carbonate in Hole 688E.

Core/section interval (cm)	Depth (mbsf)	Carbonate (%)
112-688E-8R-6, 71–73	420.71	2.34
9R-5, 102–104	429.02	1.92
12R-2, 51–54	452.51	3.67
12R-2, 113–114	453.13	8.59
14R-1, 141–142	470.91	15.93
14R-2, 42–45	471.42	6.92
16R-1, 42–43	488.92	3.67
19R-2, 16–17	518.66	0.75
20R-1, 53–54	527.03	0.58
23R-3, 79–80	558.79	12.68
24R-2, 94–95	566.94	6.92
25R-2, 45–46	575.95	1.67
26R-1, 51–52	584.01	0.83
27R-1, 10–12	593.10	0.83
27R-1, 66–67	593.66	2.92
27R-1, 85–86	593.85	5.67
35R-1, 19–20	669.19	2.84
35R-1, 121–122	670.21	3.42
36R-1, 54–55	679.04	9.67
36R-3, 54–55	682.04	1.42
36R-3, 95–96	682.45	2.00
37R-1, 103–104	689.03	2.67
39R-1, 115–116	708.15	6.84

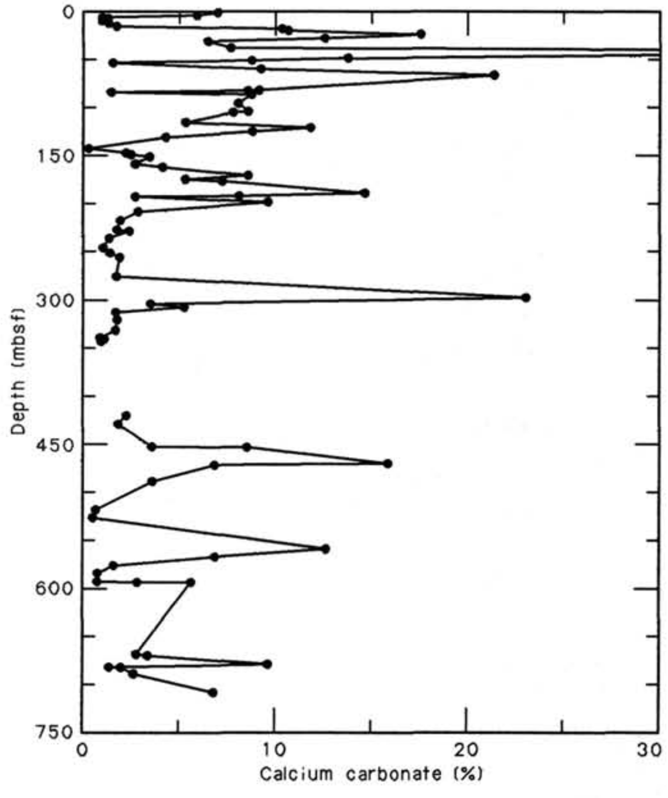

Figure 25. Carbonate measurements from Site 688.

1. Orientation of tectonic elements that characterize the fault as it was observed in the core. The fault plane is determined by its trace on the split core surface (*X*, *Y* is 45° relative to the core axis; Fig. 27) and its dip that is 60° relative to the split core surface. The pitch of the striated slickenside is 30° to the dip of the fault plane.

2. Orientation of the core from paleomagnetic measurements. These indicate that the fault strikes roughly 297° (see "Paleomagnetics" section, this chapter).

This allows us to infer the orientation of the stress field in which the fault worked. The maximum principal stress axis (σ_1) lies between 20° and 80°, with an average of almost 50° (Fig. 28).

The CDP-1 MCS record (Fig. 29), which was used to select Hole 688A for drilling, also reveals normal faults that dip seaward. This is in agreement with the tensional tectonics documented to the north (Bourgois et al., 1986) during the Seaperc cruise of the *Jean Charcot*. One of the normal faults located between Hole 688A and the scarp at the middle-slope/lower-slope boundary has a morphological signature, indicating tectonic activity at the present time. This fault cuts the thick Quaternary sequence of lithologic Unit I, the Pliocene–Quaternary bound-

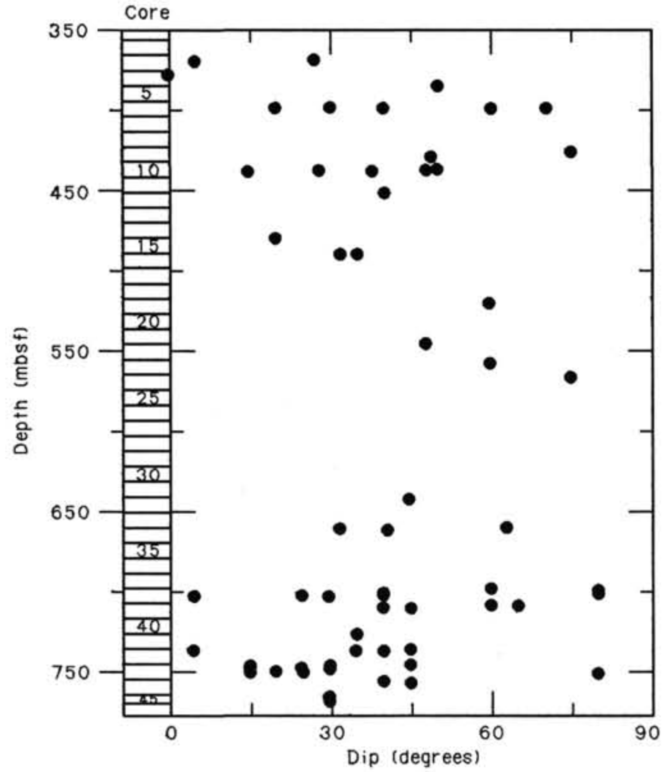

Figure 26. Bedding-plane dip measurements obtained from Hole 688E.

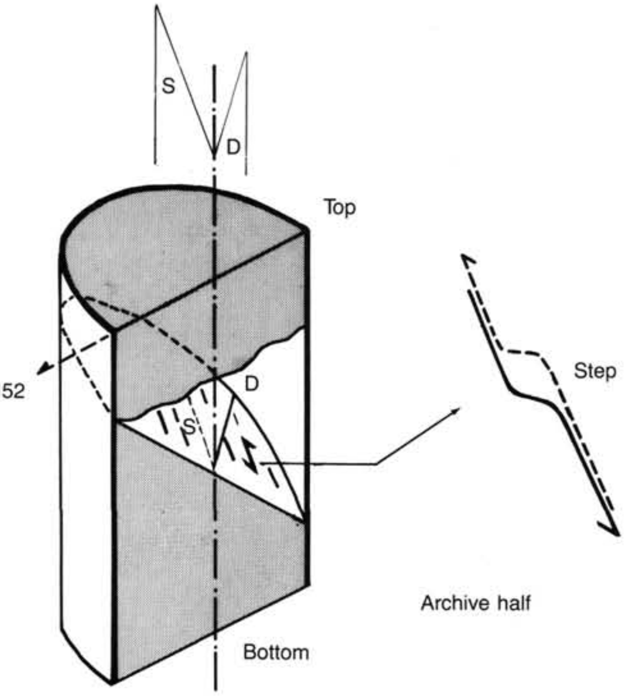

Figure 27. Orientation of the fault encountered in Sample 112-688A-37X-2, 66–73 cm.

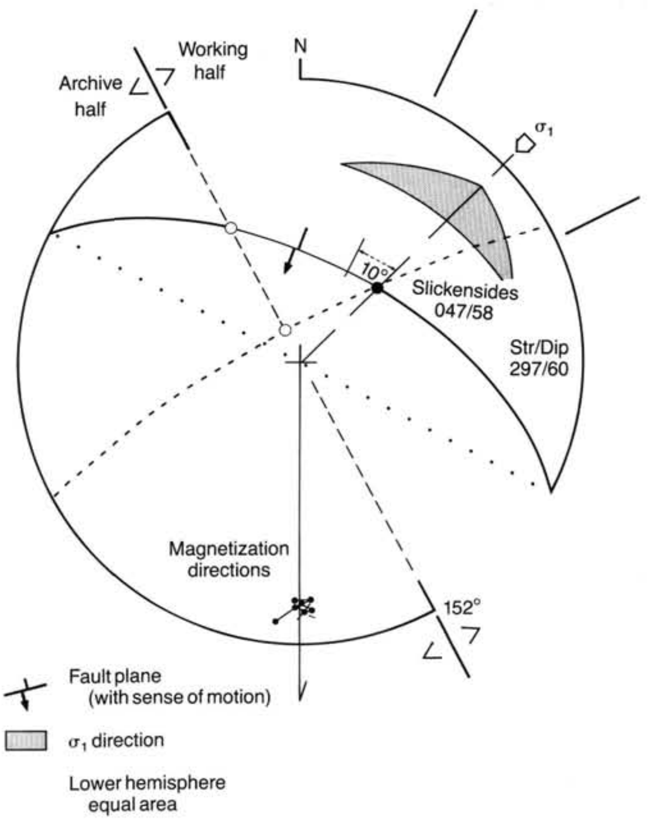

Figure 28. Equal-area stereographic projection showing the fault encountered in Sample 112-688A-37X-2, 66–73 cm. The direction of magnetization in the sample was measured and used to orient the fault. The orientation of the slickensides on the fault plane and some construction lines are also shown.

ary, and the Pliocene down to a strong reflector. Thus, tensional and compressional features occur together in Subunit IIA.

BIOSTRATIGRAPHY

Five holes were drilled in a water depth of 3820 m at Site 688, but cores were recovered from only three holes. Hole 688A penetrated 350.3 m of mostly Quaternary hemipelagic sediments. The lowermost sample at 343.4 mbsf may be of late Pliocene age. One core of Quaternary diatomaceous mud was recovered at 359.8 mbsf in Hole 688C. Hole 688E penetrated 779.0 m of Quaternary to Eocene sediments.

Siliceous microfossils (diatoms, silicoflagellates, and radiolarians) were abundant in Holes 688A and 688E (0–600 mbsf); radiolarians were rare and recrystallized below 600 to 767.8 mbsf; calcareous microfossils were commonly found in the upper part of the cored section (0–141.1 mbsf), but these also occurred sporadically in the lower part (141.3–767.7 mbsf).

Based on diatom biostratigraphy, four hiatuses were found (1) at 353 mbsf at the Pleistocene/Pliocene boundary, (2) at 368 mbsf at the Pliocene/late Miocene boundary, (3) at 453 mbsf in the middle Miocene, and (4) at 590 mbsf in the early Miocene. We recognized another hiatus using calcareous nannoplankton and radiolarian datums between the early Miocene and the Eocene, i.e., Sections 112-688E-26R, CC (584.6 mbsf) and 112-688E-27R, CC (595.7 mbsf).

Diatom assemblages are characteristic of the Humboldt Current system, with occasionally reworked coastal upwelling facies. Planktonic foraminifers occur in mixed assemblages (warm to temperate). Benthic foraminifers indicate a lower-bathyal environment throughout Hole 688A and a shelf-to-bathyal environment in the Eocene part of the section.

Based on diatom biostratigraphy, sedimentation rates are around 300 m/m.y. for the interval 40 to 320 mbsf, 23 m/m.y. for the interval 370 to 450 mbsf, and 12 m/m.y. for the interval 460 to 580 mbsf (Figs. 30 and 31).

Sedimentation rates at Site 688 (Fig. 32) are based on calcareous nannoplankton and silicoflagellates and increase down-

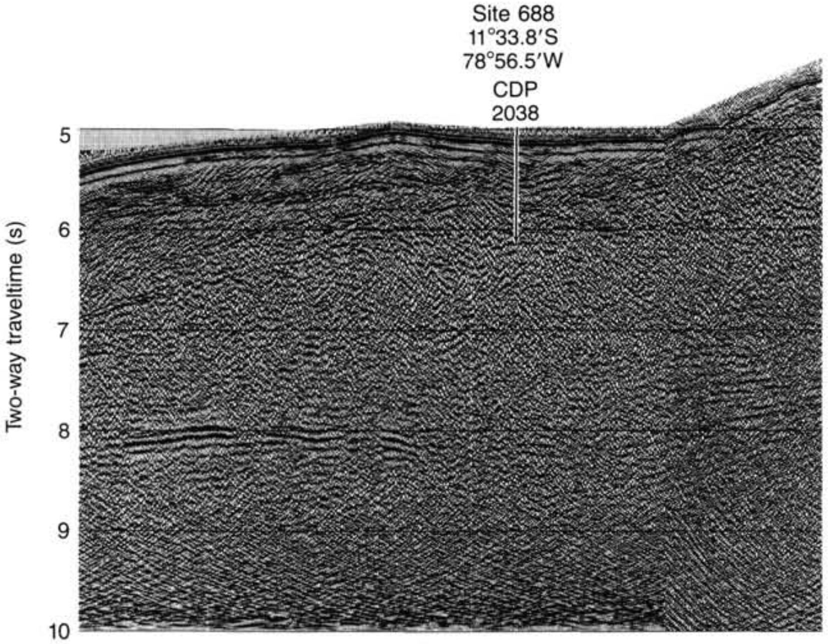

Figure 29. CDP-1 multichannel seismic record on the basis of which Hole 688E was drilled. Note the normal fault between the scarp and the drill hole.

ward from approximately 100 m/m.y. in the late Quaternary (0–46 mbsf) to approximately 135 m/m.y. in the late early Quaternary (46–179 mbsf), and to approximately 350 m/m.y. in the earliest Quaternary (179–340 mbsf).

Diatoms

Hole 688A

Marine planktonic diatoms are abundant and well to moderately well preserved in all acid-treated, core-catcher samples from Hole 688A. The flora consists of four different assemblages (types 1, 2, 3, and 4; see Fig. 30). All assemblages are characteristic of the Humboldt Current system. Reworking of Pliocene to Miocene specimens occurred sporadically throughout the section, with occasional Eocene admixtures. The lowest sample investigated, Section 112-688A-37, CC (343.4 mbsf) may be of early Quaternary or late Pliocene age.

The *Pseudoeunotia doliolus* Zone was found in Sections 112-688A-1H, CC through 112-688A-4H, CC (0–36.8 mbsf); the *Nitzschia reinholdii* Zone covered Sections 112-688A-5H, CC through 112-688A-37X, CC (46.3–343.4 mbsf). The subzone A/B boundary within the *Nitzschia reinholdii* Zone was placed between Sections 112-688A-34X, CC and 112-688A-35X, CC (321.7–331.2 mbsf).

We observed the following diatom and silicoflagellate datums: *Nitzschia reinholdii* last appearance datum (LAD) in Section 112-688A-5H, CC (46.3 mbsf), *Mesocena quadrangula* LAD in Section 112-688A-8X, CC (68.5 mbsf), *Rhizosolenia matuyama* LAD in Section 112-688A-15X, CC (152.7 mbsf), *Mesocena quadrangula* first appearance datum (FAD) in Section 112-688A-31X, CC (284.5 mbsf), *Rhizosolenia matuyama* FAD in Section 112-688A-31X, CC (284.5 mbsf), *Pseudoeunotia doliolus* FAD in Section 112-688A-35X, CC (331.2 mbsf), and *Rhizosolenia praebergonii* LAD in Section 112-688A-37X, CC (343.4 mbsf).

Based on the first occurrence of *Pseudoeunotia doliolus* in Section 112-688A-36X, CC (341.2 mbsf), the Quaternary/Pliocene boundary was placed between Sections 112-688A-36X, CC and 112-688A-37X, CC (341.28–343.4 mbsf). The first occurrence of *Pseudoeunotia doliolus* defines the base of the *Nitzschia reinholdii* Zone at 1.8 Ma (Barron, 1985). Koizumi (1986) reported FADs for *Pseudoeunotia doliolus* in a north-south transect in the North Pacific that ranged from 1.89 (equatorial Pacific) to 1.9 Ma at a latitude of 40°N. Burckle (1977) proposed a subdivision of the *Nitzschia reinholdii* Zone into A and B, based on the LAD of *Rhizosolenia praebergonii* at 1.55 Ma. The occurrence of *Nitzschia* species that are very close to *Nitzschia jouseae*, but differ in their finer areolation, may indicate that Section 112-688A-37X, CC (343.4 mbsf) is near the LAD of *Nitzschia jouseae*, which is around 2.5 Ma, and does not seem to be time transgressive in the North Pacific (Koizumi, 1986).

Sancetta (1982) reported that the extinction level of *Mesocena quadrangula* is reliable and occurs just above the Jaramillo Magnetic Chron, as reported by Burckle (1977), but the lower boundary is ill defined. She also reported that the "cold-water" form, *Rhizosolenia matuyama*, has a very short range just below and within the Jaramillo Chron (Burckle et al., 1982). These previously reported ranges seem to concur with our findings offshore Peru.

Reworking is common throughout the section. The interval from Sections 112-688A-1H, CC to 112-688A-7H, CC (0–65.7 mbsf) with rare *Rossiella tatsunokuchiensis*, *Rossiella praepaleacea*, *Pyxilla reticulata*, *Rouxia diploneides*, *Rhizosolenia barboi*, *Denticulopsis hustedtii*, and *Goniothecium odontella*; Section 112-688A-11X, CC (105.7 mbsf) with *Rossiella tatsunokuchiensis*, Section 112-688A-13X, CC (122.1 mbsf) with *Denticulopsis hustedtii*, Section 112-688A-20X, CC (179.8 mbsf) with *Rossiella tatsunokuchiensis*, Section 112-688A-30X, CC (275.5 mbsf) with *Rossiella tatsunokuchiensis*, Section 112-688A-36X, CC (341.2 mbsf) with *Goniothecium tenue*, *Thalassiosira praeconvexa*, *Asterolampra acutiloba*, and Section 112-688A-37X, CC (343.4 mbsf) with *Denticulopsis hustedtii.*

Based solely on the assumption that the LADs of *Rhizosolenia matuyama*, *Nitzschia reinholdii*, and *Rhizosolenia praebergonii* are correctly dated and *in situ* in Hole 688A, a sedimentation rate of 300 m/m.y. can be calculated. Based on the assumption that the FAD of *Pseudoeunotia doliolus* is correct and *in situ* and that Holocene sediments are found at the top of the recovered section, the resulting sedimentation rate is 280 m/m.y. The occurrence of *Rhizosolenia curvirostris* in sponge samples

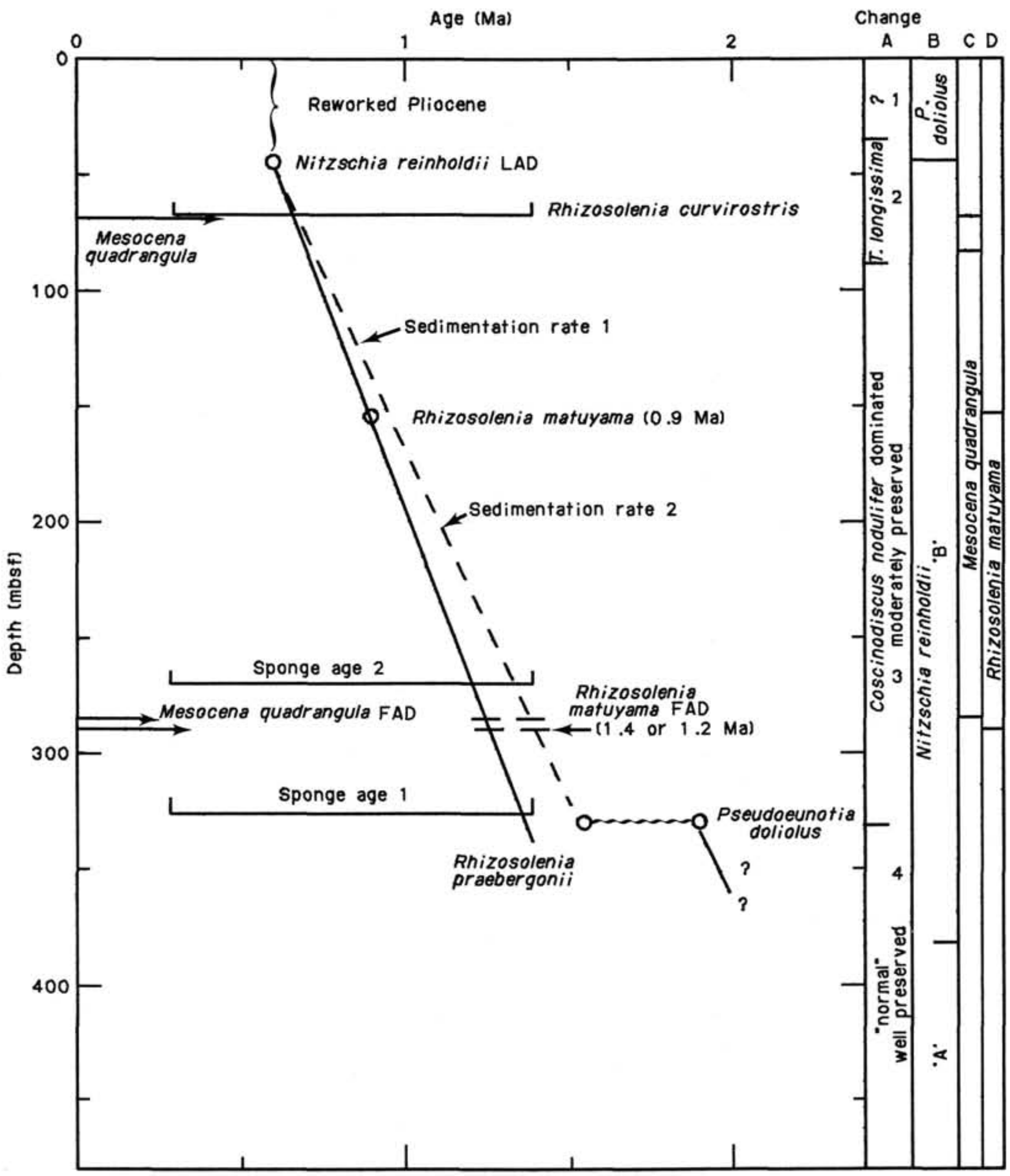

Figure 30. Age vs. depth plot of Hole 688A samples, based on diatom biostratigraphy. Hiatus H-4 occurs at 330 mbsf. Column A depicts diatom floral changes, column B is the general biostratigraphy of Barron (1985), column C brackets the occurrence of the silicoflagellate *Mesocena quadrangula*, and column D illustrates the range of *Rhizosolenia matuyama*.

from Core 112-688A-35X (321.8–331.2 mbsf) places an age bracket of 0.3 to 1.4 Ma (maximum ranges as determined from the North Pacific; Koizumi, 1986) for this entire core. A possible short hiatus thus may occur at 331.2 mbsf, removing part of the lower *Nitzschia reinholdii* Zone. Another hiatus, or a substantial decrease in sediment accumulation, should also be placed at the floral boundary of 36.8 mbsf.

The paucity of displaced marine benthic diatoms throughout the section was unexpected, as was the negligible admixture of displaced coastal-upwelling floral elements. No freshwater diatoms were observed.

Floral changes from a flora that is dominated by *Thalassionema nitzschioides*, *Thalassiothrix longissima*, *Thalassiosira eccentrica*, and *T. oestrupii* were found in Section 112-688A-4H, CC (36.8 mbsf). Below this boundary to Section 112-688A-10X, CC (88.0 mbsf), the assemblage is dominated by *Thalassiothrix longissima*, and preservation is moderate. The moderately well-preserved assemblage below this boundary to Section 112-688A-36X, CC (341.2 mbsf) is dominated by *Coscinodiscus nodulifer*, and preservation and diversity increase in Sections 112-688A-36X, CC (341.2 mbsf) to the basal Section 112-688A-37X, CC (343.4 mbsf). Detailed studies of the size variations of *Coscinodiscus nodulifer* may permit direct correlation to the oxygen-isotope stratigraphy in the Quaternary.

"Assemblage 1" (Fig. 30, column A) is a result of normal fertilization of the Humboldt Current system with temperate oceanic admixtures; "Assemblage 2" is a result of more vigorous northward flow velocities bringing colder water masses into the Peruvian area from the south (note that *Thalassiothrix longissima* sediment assemblages are found today in the North Pacific); "Assemblage 3" is a documentation of increased oceanic/temperate surface-water conditions, which are a result of

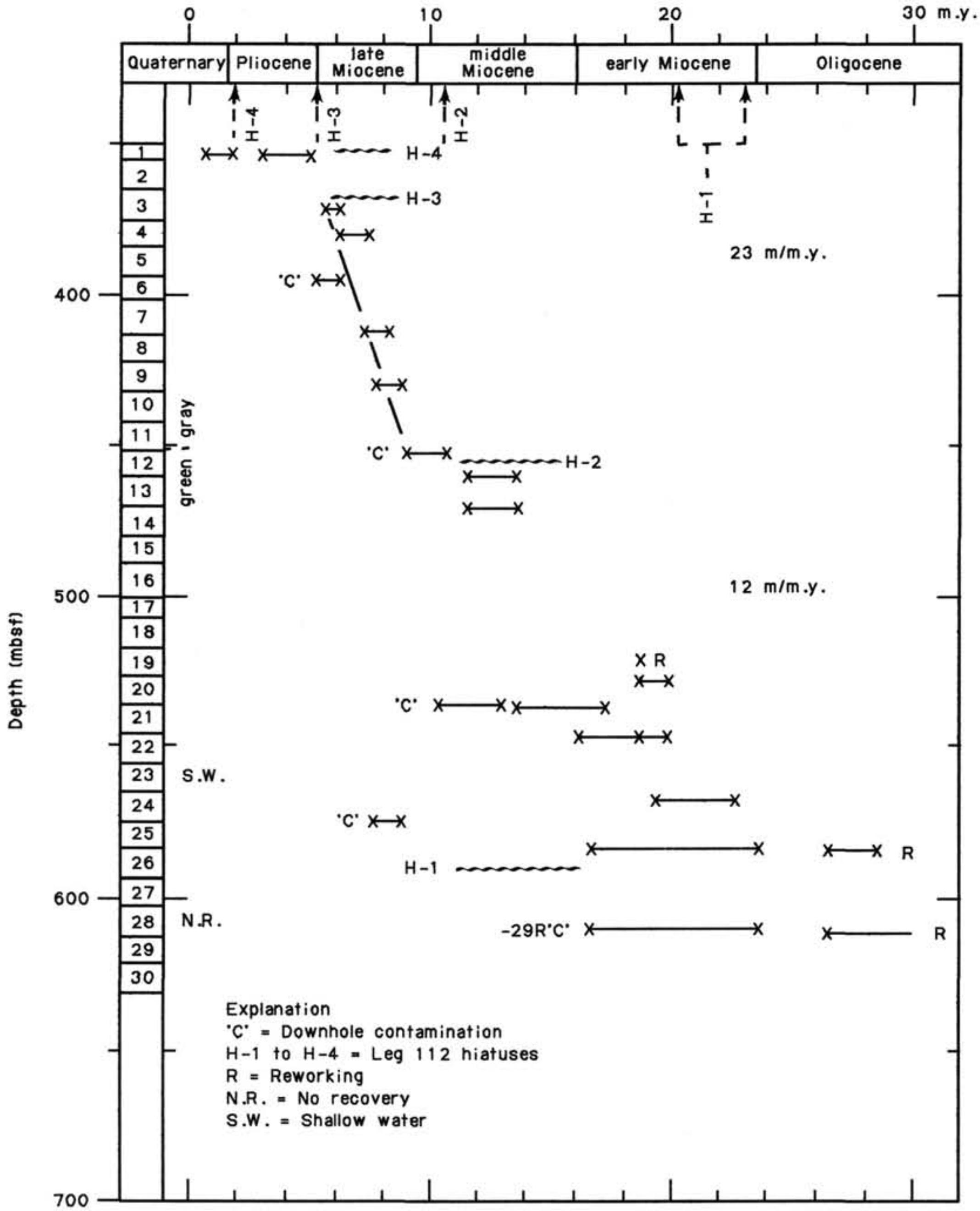

Figure 31. Plot of age vs. corrected depth of Hole 688E samples, based on diatom biostratigraphy. Major hiatuses H-1 through H-4 with simplified lithology next to the core sample log down to Core 112-688E-30R.

either a decreased flow velocity or a migration farther inshore; and "Assemblage 4" is similar to "Assemblage 1."

Rhizosolenia curvirostris was detected in Section 112-688A-8X, CC (68.55 mbsf) and in samples taken from sponges (see paragraph below) occurring in Cores 112-688A-21X (188.8 to 192.9 mbsf), 112-688A-32X (293.3 to 304.6 mbsf), and 112-688A-35X (321.8 to 331.2 mbsf); this is the first reported occurrence in the southern Pacific Ocean. Even though the range of this species is slightly time transgressive in the North Pacific, its biostratigraphic use in the Peruvian area is important. *Rhizosolenia barboi* commonly occurs throughout the section.

Thalassiosira leptopus var. *elliptica* was found in Section 112-688A-7H, CC (65.7 mbsf). This species was reported by Schrader (1974) from TIODZ 1 (Tropical Indian Ocean Diatom Zone), which is equivalent to the *Pseudoeunotia doliolus* Zone of Burckle (1972). The acme of this specialized form may prove useful for Peruvian oceanic sections.

A detailed study to determine the environmental nature of some frequently occurring sponges was undertaken in the following sponge samples: (1) 112-688A-21-2, 91 cm; (2) 112-688A-28-2, 12.5 cm; (3) 112-688A-28X-2, 12.5 cm; (4) 112-688A-28X-2, 12.5 cm; (5) 112-688A-32X-4, 142 cm; (6) 112-688A-32X-5, 63 cm; (7) 112-688A-32X-5, 143.5 cm; (8) 112-688A-32X-6, 82 cm; (9) 112-688A-32X-6, 110 cm; (10) 112-688A-32X-8, 36 cm; (11) 112-688A-32X-9, 43.5 cm; (12) 112-688A-32X-9, 44 cm; (13) 112-688A-33X-3, 92 cm; (14) 112-688A-33X-5, 124 cm; (15) 112-688A-35X-1, 136.5 cm; (16) 112-688A-35X-1, 134 cm; (17) 112-688A-35X-1, 6 cm; (18) 112-688A-35X-2, 102 cm; (19) 112-

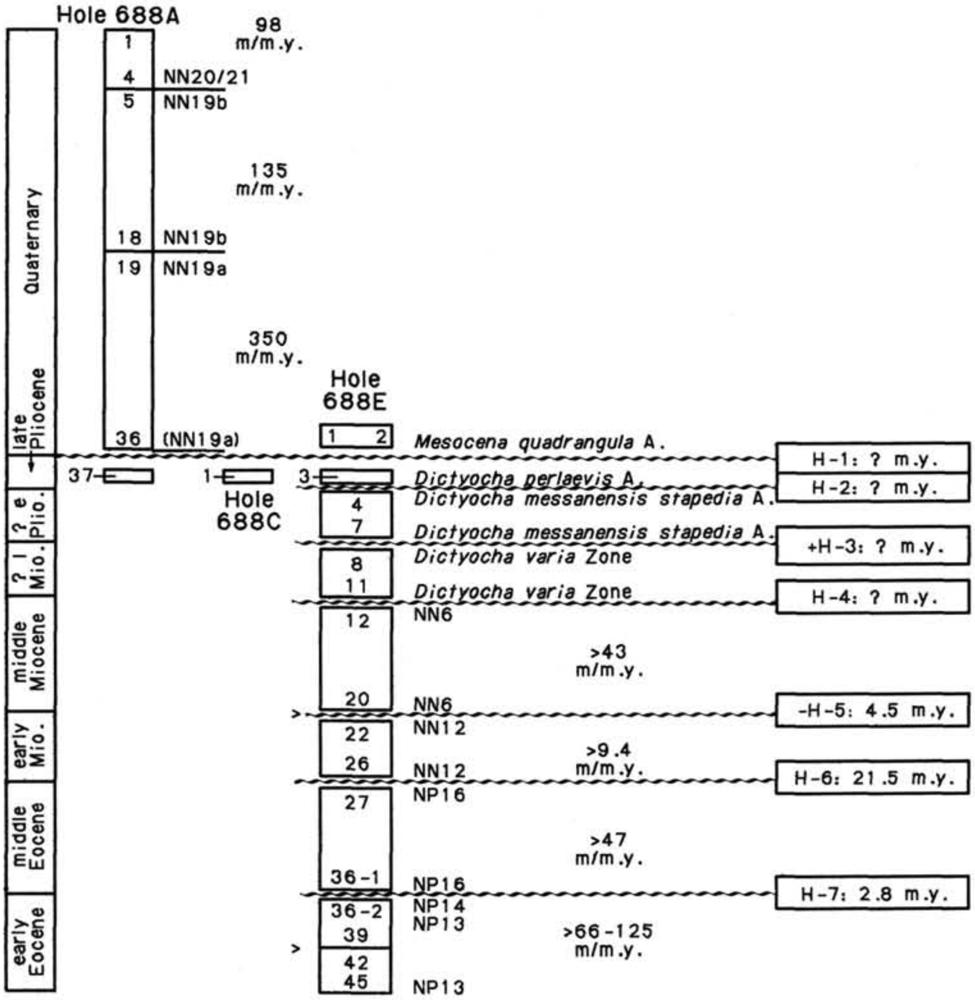

Figure 32. Hiatus stratigraphy and sedimentation rates at Site 688, based on calcareous nannoplankton and silicoflagellates (numbers in left column refer to cores in Hole 688E).

688A-35X-4, 110 cm; (20) 112-688A-35X-5, 35 cm; (21) 112-688A-35X-6, 131 cm; (22) 112-688A-35X-6, 131.5 cm; (23) 112-688A-35X-7, 7 cm; (24) 112-688A-35X-7, 41 cm; (25) 112-688A-6H-7, 64 cm; (26) 112-688A-6H-4, 67 cm; (27) 112-688A-5H-6, 66 cm; (28) 112-688A-5H-3, 44 cm; (29) 112-688A-5H-2, 101 cm; (30) 112-688A-3H-6, 3 cm; (31) 112-688A-2H-1, 85 cm; (32) 112-688A-2H-1, 85 cm; and (33) 112-688A-1H-4, 47 cm. Although sponge material was taken from inside the oval compressed sponges to avoid contamination with surrounding matrix material, we could not do this successfully in every case (contamination did occur in samples 12 and 13).

Sponge contents can be grouped into the following five classes:

Sponge class 1: barren of diatoms and of sponge spicules (samples 8, 9, 11, and 18).

Sponge class 2: with diatoms and sponge spicules; diatoms contain *Rhizosolenia curvirostris* among other members; all these samples should be in the range of 0.3–1.4 Ma (maximum bracket ranges from Koizumi, 1986; (samples 2, 4, 10, 14, and 16).

Sponge class 3: with diatoms and sponge spicules; diatoms include species that are known from Pliocene/Miocene strata, including *Goniothecium odontella*, *Rhizosolenia praebarboi*, and *Rhizosolenia barboi* (samples 1, 2, 17, 24, 25, 26, 27, 31, and 32).

Sponge class 4: with diatoms and sponge spicules; diatom flora are contemporaneous to the matrix and include *Thalassiosira oestrupii*, *Pseudoeunotia doliolus*, *Nitzschia reinholdii*, *Mesocena quadrangula* (samples 3, 4, 5, 6, 7, 12, 13, 15, 19, 20, 21, 22, 30, and 29).

Sponge class 5: with diatoms and sponge spicules; diatoms include shallow-water benthic species (*Diploneis bomboides*; sample 28).

Sponge spicules belong to the amphiox, acanthostyl, oxycalthrop, nephroid rhax, and hooked amphiox classes (see Locker and Martini, 1986). The incorporation of long-bowed *Rhizosolenia barboi*, *R. curvirostris*, and *Chaetoceros setae* into spongy skeletal material is of biological interest; these diatom species are quite rare in the surrounding matrix. The two sponges grouped into class 5 originate from the shelf (water depth of less than 100 m); class 3 sponges originate from continental-margin outcrops of Pliocene/Miocene age, whereas sponges of class 4 may be *in situ*. On the other hand, sponges do not occur in high population densities at water depths below 2000 m, and these may all be displaced.

Hole 688E

Marine planktonic diatoms are abundant and well preserved in Cores 112-688E-1R through 112-688E-25R (350.0–576.7

mbsf); these are abundant to common and moderately well preserved in Cores 112-688E-26R through 112-688E-29R (583.5–612.0 mbsf). Samples below Core 112-688E-29R are barren in diatoms. Assemblages are highly variable and include typical coastal-upwelling assemblages, Humboldt Current assemblages, and shallow-water neritic assemblages. Diatom assemblages having excellent preservation were frequently retrieved from dissolved (by diluted HCl) dolomites and dolomicrites. Well-preserved assemblages were retrieved from fillings of worm structures in Core 112-688E-26R (583.5–584.7 mbsf). Samples below Section 112-688E-29R, CC occasionally contained large recrystallized diatom valves of *Coscinodiscus* sp. and *Stephanopyxis* sp.

We recognized four hiatuses (H-1 through H-4), with H-1 located in the early Miocene, H-2 in the middle Miocene, H-3 in the late Miocene and early Pliocene, and H-4 at the Pleistocene/Pliocene boundary. Sedimentation rates were 23 m/m.y. for the interval at 370 to 450 mbsf, and 12 m/m.y. for the interval at 460 to 580 mbsf (see Fig. 31).

The *Thalassiothrix longissima* zone was observed in Section 112-688E-14R, CC in the *Coscinodicus lewisianus* Zone. *Macrora stella* (a *Synuraceae* skeleton; see Tappan, 1980) was frequent in this sample, as well as in Section 112-688E-17R, CC. Shallow-water and neritic assemblages were found in Core 112-688E-23R, as well as frequent sponge spicules, large *Aulacodiscus* sp., *Triceratium* sp., and *Auliscus* sp.; Section 112-688E-22R, CC contained abundant fish remains in the coarse fraction (Fig. 33).

Abundant recrystallized diatoms and radiolarians were retrieved from a phosphorite nodule taken from the top of Section 112-688E-30R-1 (Fig. 34); these abundant remains indicate that diatom production did occur in the Eocene (see calcareous nannofossils for biostratigraphic age) in the Peruvian continental margin area and that their absence in sediments may be primarily related to diagenetic processes and dissolution of opal.

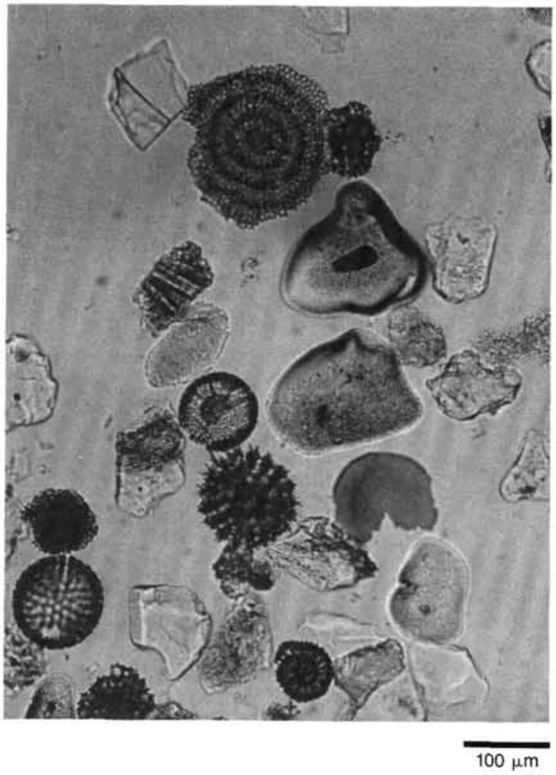

Figure 33. Transmitted light micrograph of the coarse fraction of Hole 688E, Section 112-688E-22R, CC. Also indicated are fish remains with very smoothed edges, specimen in right corner with glauconite filling, radiolarians, diatoms, and quartz/feldspar grains. Scale indicated at bottom of figure.

Dolomite and dolomicrite Samples 112-688E-34R-1, 80 cm, 112-688E-33R-1, 0–10 cm, and 112-688E-38R-3, 126 cm, were dissolved and checked for diatoms. The observed flora included *Rhaphidodiscus marylandicus*, *Synedra jouseana*, *Annellus californicus*, *Rossiella paleacea*, *Coscinodiscus lewisianus*, *Eucampia balaustium*, *Asterolampra acutiloba*, *Rocella gelida*, and *Coscinodiscus rhombicus*. All these samples were cored from farther uphole and partially represent zones that were not recovered during "normal" drilling.

The common and consistent occurrence of *Eucampia antarctica* (*Eucampia balaustium*) in middle Miocene assemblages, coupled with sporadic occurrences of *Coscinodiscus deformans* and *Denticulopsis antarctica*, implies a much stronger and enhanced Humboldt Current system than occurs today. Burckle (1984) reported that *Eucampia antarctica* currently occurs throughout the southern oceans as a minor constituent (see also Fenner et al., 1976). This enhanced northward transportation of floral elements apparently occurred in the early Miocene and during the late Miocene through the Holocene. Antarctic components are enriched in Cores 112-688E-8R through 112-688E-18R (412.5–507.5 mbsf) and represent the *Thalassiosira yabei* Zone through the top of the *Craspedodiscus elegans* Zone of early through late Miocene age.

Nitzschia aff. *grunowii* Hasle was found to range from the *Rouxia californica* Zone of Akiba (1985) through the *Pseudoeunotia doliolus* Zone of Barron (1985). Detailed morphologic study will be necessary to confirm the correct placement of this species because illustrated specimens in Koizumi and Tanimura (1985) differ from those of Jouse et al. (1982). *Thalassiosira domifacta* (Hendey) is a common floral constituent in the *Pseudoeunotia doliolus* through *Nitzschia fossilis* Zones of Jouse et al. (1982). *Thalassiosira leptopus* var. *elliptica* (Kolbe) Hasle occurs in the Panama Basin in the *Pseudoeunotia doliolus* Zone through the upper *Rhizosolenia praebergonii* Zone of Jouse et al. (1982). *Delphineis* aff. *sheshukovae* Akiba (1985) was commonly found in a piece of dolomite in Section 112-688E-25R-1 (species differ by being more compressed and egg-shaped and by having a wider structureless central area). Akiba (1985) reported *D. sheshukovae* from the *Neodenticula kamtschatika* Zone of lower Pliocene age; specimens in Hole 688E came from the *Thalassiosira yabei* Zone of late Miocene age. *Nitzschia pliocena* (Brun) Mertz (1966) was found in Section 112-688E-3R, CC and lower; some specimens resemble *Nitzschia jouseae*, except that they are more delicately structured. Akiba (1985) and Akiba and Yanagisawa (1985) reported that this species occurs in the middle-to-high latitudes of the North Pacific and that it is restricted to the *Thalassionema schraderi* Zone (9.0–7.4 Ma) through the middle part of the *Rouxia californica* Zone (7.5–6.7 Ma). *Mediaria splendida* was found in Sections 112-688E-3R, CC, and 112-688E-9R, CC. We observed true *Mediaria splendida* var. *tenera* specimens that range into the Pliocene and thus support the ranges found earlier in Californian marine sections and in the lower Pliocene Trubi marls in Sicily (see Schrader and Gersonde, 1978; Gersonde and Schrader, 1984). A *Mediaria* species having a structured apical field was found in Sample 112-688E-26R-1, 56 cm. A large *Coscinodiscus* aff. *radiatus* having a concentric ring of irregularly placed larger areolae occurred in Section 112-688E-6R, CC; this form was previously found at other Leg 112 sites of similar age. The very delicate *Thalassiosira* sp. assemblage was found in Section 112-688E-7R, CC; this interval is time equivalent with Section 112-684C-10X, CC.

Four hiatuses (Fig. 31) were defined in the interval from 350 to 600 mbsf of Hole 688E. These are discussed as follows:

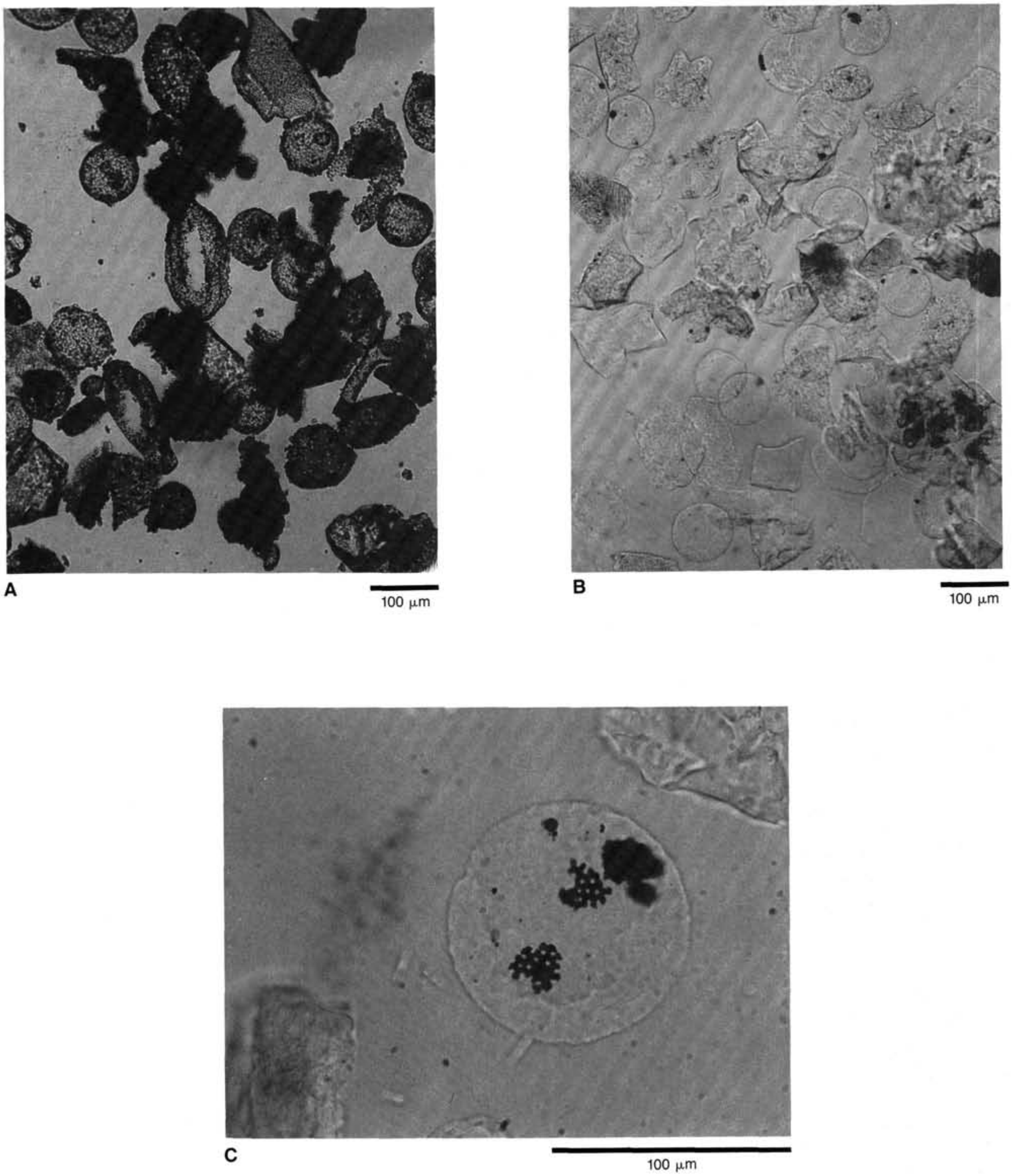

Figure 34. Transmitted light micrographs of the coarse fraction of a phosphorite nodule from Sample 112-688E-30R-1, 10–15 cm. A) Abundant, disk-shaped, recrystallized diatoms, a forked sponge spicule, and spherical recrystallized radiolarians, mounted in Hyrax. B) Disk-shaped recrystallized diatoms with some pyrite structured specks, recrystallized radiolarians at center right, mounted in Canada Balsam. C) Enlarged recrystallized diatom disk with some pyritized internal structure, mounted in Canada balsam. Scale for each section located at bottom of figure.

Hiatus H-1: Based on diatom biostratigraphy, the placement of the Miocene/Oligocene boundary is within the *Rocella gelida* Zone of Barron (1985). *Rocella gelida*, *Rocella vigilans*, and *Bogorovia veniamini* are used to define zonal boundaries within the lowermost Miocene to upper Oligocene. These species did occur in an age-progressing way. The associated occurrence of *Rhaphidodiscus marylandicus* in Sample 112-688E-26R-1, 56 cm, and Section 112-688E-29R, CC makes this assignment weak. J. Barron (pers. comm., 1986) uses the FAD of *Raphidodiscus marylandicus* as the marker for the Oligocene/Miocene boundary. Fenner (1984), Gombos and Ciesielski (1983), Barron (1985), and Schrader and Fenner (1976) reported similar ranges. Assuming that the FAD of *Rhaphidodiscus marylandicus* is correct in the literature and that the range off Peru is not diachronous, all diatom-bearing samples of the lower part of Hole 688E must be early Miocene in age and contain reworked Oligocene *Rocella vigilans* and *Bogorovia veniamini* zonal species. As at Sites 682 and 683, a hiatus that removed most of the Oligocene and part of the Eocene must occur within the lower Miocene. The *Rocella gelida* Zone seemed to be the "oldest" *in-situ* diatom zone, and the hiatus may have occurred in this zone. Floral assemblages of lower Miocene age from Site 688 closely resemble assemblages found in the Caballas Formation, which underlies the Pisco Formation on land. The oldest Caballas Formation samples were also placed into the *Rocella gelida* Zone. However, diatomaceous upper Oligocene must have been deposited, as can be seen by the floral components of the *Rocella gelida*, *Bogorovia veniamini*, and *Rocella vigilans* zones. H-1 may correspond in part NH1 of Barron and Keller (1983).

Hiatus H-2 occurs between Sections 112-688E-11R, CC and 112-688E-12R, CC, removing part of the middle Miocene. We recognized this hiatus in other Leg 112 sites. Barron and Keller (1983) described their NH4 hiatus, which is widely recognized in the North Pacific and the Californian continental margin (DSDP Leg 18, Site 173) at 12 to 11 Ma; this hiatus is related to increased antarctic glaciation and intensified bottom-current circulation.

Hiatus H-3 occurs in Core 112-688E-3R and correlates well with other Miocene/Pliocene hiatuses found during Leg 112. Similar hiatuses were described by Barron and Keller (1983) from DSDP Sites 173 and 470 and from Newport Beach.

Hiatus H-4 was found in Cores 112-688E-1R and 112-688E-2R; this Pliocene–Pleistocene hiatus was detected at other Leg 112 sites as well.

Fish remains (Fig. 33) were common in the NaOH-treated samples from the core catcher of Core 112-688E-22R; these included forms that were illustrated by Doyle and Riedel (1980). Frequently, the cavities of ichthyoliths contained green glauconite and may represent the nuclei of the frequently associated glauconite particles in the untreated coarse fraction.

Sponge spicules were enriched in the interval from Sections 112-688E-22R, CC to 112-688E-24R, CC; spicules were of the amphiox- and nephroid-rhax-type and most likely were displaced from shallow-water environments (water depth of less than 200 m). The following table shows results of our analyses of selected coarse-fraction components. Each component was 63 μm wet sieved with a Canada balsam mount; those requiring special treatment are discussed separately.

Sample	22	23	24	25	26
Component					
Radiolarians	C	R	C	C	C
Fish remains	C	—	—	—	—
Sponge spicules	C	F	R	R	F
Glauconite	F	—	F	R	R
Plant debris	T	R	R	R	R
Craspedodiscus coscinodiscus	—	—	T	T	T
Rocella gelida	—	—	—	—	T

C = common; R = rare; F = few; T = trace.

We noted that reworking occurred frequently in Hole 688E, with Pliocene and Miocene (*Denticulopsis hustedtii*, *Rossiella tatsunokuchiensis*) in Section 112-688E-1R, CC, and undifferentiated Miocene in Cores 112-688E-9R through 112-688E-12R. Downhole cavings were found to occur occasionally and to obscure the age-progressing sequence. Reworked Oligocene into lower Miocene was noted, with elements from the *Bogorovia veniamini* and *Rocella vigilans* zones.

Displaced marine benthic diatoms occurred throughout the Neogene section; Sections 112-688E-11R, CC, 112-688E-10R, CC, 112-688E-9R, CC, and 112-688E-8R, CC seemed to be exceptionally enriched in these floral elements. Displaced freshwater species were found in Sample 112-688E-19R-1, 10–11 cm.

The following diatom zones were recognized: *Nitzschia reinholdii* Zone of Barron (1985) in Section 112-688E-1R, CC; *Neodenticula kamtschatica* Zone of Koizumi (1973; see also Akiba, 1985) of latest late Miocene through early Pliocene age (6.0–3.2 Ma; Barron, 1980) in Section 112-688E-2R, CC; *Thalassiosira convexa* Subzone A of Barron (1985) in Section 112-688E-3R, CC; *Nitzschia miocenica* Zone of Barron (1985) in Section 112-688E-4R, CC; *Thalassiosira convexa* Subzone C of Barron (1985) in Sample 112-688E-6R-1, 145–150 cm; *Thalassiosira yabei* Zone of Barron (1985, listed under *Coscinodiscus yabei* Zone) in Cores 112-688E-8R through 112-688E-9R; *Actinocyclus moronensis* Zone of Barron (1985) in Section 112-688E-12R, CC; *Coscinodiscus gigas* var. *diorama* Zone of Barron (1985) in Section 112-688E-13R, CC; *Coscinodiscus lewisianus* Zone of Barron (1985) in Section 112-688E-14R, CC; *Craspedodiscus elegans* Zone of Barron (1985) in Cores 112-688E-19R through 112-688E-20R; *Bogorovia veniamini* Zone of Barron (1985) in Cores 112-688E-23R through 112-688E-24R (see also Gombos, 1983, and Gombos and Ciesielski, 1983); *Rocella vigilans* Zone of Barron (1985) in Cores 112-688E-26R through 112-688E-29R (note the core catcher of Core 112-688E-29R contained three different lithologies; the diatom-bearing sample was a dark soft mudstone). Note that the oldest non-reworked diatom zone is the *Rocella gelida* Zone of Barron (1985); all Oligocene zones are reworked.

Preparation Method for Diatoms and Radiolarians in Semiconsolidated Hemipelagic Sediments

The consolidation of diatom particles in nondestructive aggregates caused frequent problems during Leg 112. Conventional methods for cleaning these sediments by boiling them in a mixture of HCl and H_2O_2 did not disaggregate these particles. A modification of a rigorous method developed by diatom scientists (summarized by Hustedt, 1924) was applied. Muds were boiled in fumic HNO_3 to destroy organic matter and frequently occurring pyrite. The sample was washed in distilled water and then boiled in a diluted NaOH solution until some flocculation was observed. Immediately washing samples in distilled water prevented the opal from being dissolved. Samples were washed with the aid of a centrifuge (1500 rpm, 3 min). Radiolarians were concentrated by removing all the diatom aggregates and by dissolving diatoms in a stronger NaOH solution. Correct concentration of reagents and time of boiling was empirically determined by taking sample splits and observing the breakdown of aggregates under the microscope. Radiolarian mounts were washed by sieving the material through a 63-μm sieve. Extreme caution was exercised to avoid dissolution of opaline microfossils.

Silicoflagellates and Other Siliceous Groups

All core-catcher samples of Hole 688A were studied for silicoflagellates and some other siliceous microfossil groups. The silicoflagellate assemblages in all core-catcher samples were dominated by members of the *Dictyocha messanensis* group. *Distephanus speculum speculum* f. *speculum* was frequently found throughout the sequence, whereas *D. speculum speculum* f. *pentagonus* occurred in only a few samples. *Mesocena quadrangula* was observed in varying numbers between Section 112-688A-8X, CC (68.5 mbsf) and Section 112-688A-36X, CC (341.2 mbsf); the species has its lowest occurrence at this site in these samples. A Quaternary age was indicated for most of the sequence.

Two samples from Hole 688C at 351.0 (112-688C-1R-1, 75 cm) and 351.5 mbsf (112-688C-1R, CC) contain *Dictyocha perlaevis delicata* and lack both *Mesocena quadrangula* and *Mesocena circulus*, which places these samples in the lowest Pleistocene or uppermost Pliocene.

In Hole 688E, all core-catcher and some additional samples were investigated. *Mesocena quadrangula* occurs in Cores 112-688E-1R and 112-688E-2R (350–356 mbsf), and *Dictyocha perlaevis delicata* has its lowest occurrence in Section 112-688E-3R, CC, duplicating results from the lowest part of Holes 688A and 688C. Cores 112-688E-2R and 112-688E-3R in Hole 688E, as well as Cores 112-688A-36X and 112-688A-37X may be divided by a short hiatus that separates the *Mesocena quadrangula* Assemblage from the *Dictyocha perlaevis* Assemblage. A sudden change to a meager silicoflagellate assemblage between Sections 112-688E-3R, CC and 112-688E-4R, CC may indicate another hiatus. Between Sections 112-688E-4R, CC and 112-688E-7R, CC, the silicoflagellate assemblage consists only of members of the *Distephanus speculum* group and of *Dictyocha messanensis stapedia*. In Section 112-688E-8R, CC (421.7 mbsf) *Dictyocha varia* and members of the *Distephanus crux* group appear. We did not notice any overlap between this assemblage and the occurrence of *Dictyocha messanensis stapedia*, and we suspect another hiatus. The late middle to early upper Miocene *Dictyocha varia* Zone was recognized between Sections 112-688E-8R, CC and 112-688E-12R, CC (421.7–453.0 mbsf). In Section 112-688E-13R, CC, we found the last occurrence of *Corbisema triacantha*. Intervals between Samples 112-688E-14R-3, 13–14 cm, and 112-688E-16R-1, 15–16 cm, can be placed in the *Distephanus stauracanthus* Zone, with *D. stauracanthus* f. *stauracanthus* present throughout this interval. *Distephanus stauracanthus* f. *octogonus* was found in Section 112-688E-16R, CC, which indicates that the interval between Sections 112-688E-13R, CC and 112-688E-16R, CC (460.0–489.8 mbsf) can be placed in the upper part of the middle Miocene *Corbisema triacantha* Zone.

Cores 112-688E-17R, 112-688E-18R, and 112-688E-21R yielded only caved-in middle Miocene material from above this interval. Samples from Cores 112-688E-19R, 112-688E-20R, and 112-688E-22R to 112-688E-24R contain rare specimens of the *Distephanus crux* group, and Section 112-688E-20R, CC also contains *Corbisema triacantha*. These samples cannot be assigned to a certain zone. Sample 112-688E-25R-1, 141 cm, certainly can be placed below the last occurrence of *Naviculopsis* species in the late early Miocene as we found rare *Naviculopsis biapiculata*. We noted *Rocella gelida* in Section 112-688E-25R, CC, indicating the *Rocella gelida* Zone of Barron (1985), which straddles the Oligocene/Miocene boundary. This agrees with the placement of Section 112-688E-25R, CC in nannoplankton Zone NN1/2 (see below). The interval between Core 112-688E-27R and the terminal Core 112-688E-46R (593.0–775.0 mbsf) is barren of silicoflagellates.

Rare reworked *Corbisema triacantha* and *Naviculopsis biapiculata* were found in Sections 112-688A-8X, CC (68.5 mbsf) and 112-688A-23X, CC (208.5 mbsf), most probably derived from lower Miocene strata.

Actiniscidians and ebridians were occasionally noted and include *Actiniscus pentasterias* (Sections 112-688A-1H, CC and 112-688A-19X, CC), *Actiniscus*(?) *elongatus* (Sections 112-688A-4H, CC and 112-688A-36X, CC), and *Parathranium clathratum* (Section 112-688A-3H, CC).

As noted at previous sites, sponge spicules represent a minor component of the regular siliceous microfossil assemblages; however, these were also found in whitish clusters throughout most of the sequence. Preliminary data seem to indicate different composition values for some clusters, especially when compared with those from Site 685. Monaxones of various shapes are the most common forms, but some tetraxons were also observed. From 28 individually selected samples recovered between Cores 112-688A-1H and 112-688A-29X, 16 were processed, and preliminary data are available. Fourteen samples contain resting cysts of diatoms interpreted as *Goniothecium odontella* by Schrader and Fenner (1976) and were found in the middle Miocene to early Pliocene of DSDP Site 348 (Norwegian Sea). However, this species was not plotted in Schrader and Fenner (1976) and an Oligocene–Miocene age was quoted for its distribution. The remaining two samples (112-688A-5H-2, 101 cm, and 112-688A-8X, CC) contained specimens of a *Diploneis* species not found in the other samples. Several of these sponge clusters were aligned along distinct layers, which in the case of Sample 112-688A-2H-1, 85 cm, also contained abundant diatom girdles, which indicates winnowing and transportation. If the ages given for *Goniothecium odontella* are correct, most of these sponges are displaced from older strata. Otherwise, the sponges must have acquired these resting cysts when they were washed out from Miocene/Pliocene strata elsewhere. We will not speculate further as long as the composition value for each recovered sample is unknown.

Calcareous Nannoplankton

All core-catcher and some additional samples from Hole 688A were studied for calcareous nannoplankton. The first four cores, with the exception of the uppermost part of Core 112-688A-1H, contain a moderately well preserved late Quaternary nannoplankton assemblage that includes common *Gephyrocapsa oceanica* and *Gephyrocapsa aperta*, few *Coccolithus pelagicus*, *Cyclococcolithus leptoporus*, and *Helicosphaera carteri*. To date, we have not tried to differentiate the *Emiliania huxleyi* Zone (NN21) from nannoplankton Zone 20 (*Gephyrocapsa oceanica* Zone). Thus, Cores 112-688A-1H to 112-688A-4H were placed in the combined nannoplankton Zones NN20/21 (*Gephyrocapsa oceanica/Emiliania huxleyi* Zone). In Section 112-688A-5H, CC (46.3 mbsf) and below, we found occasional occurrences of *Pseudoemiliania lacunosa*, indicating that most of the sequence belongs to the Quaternary nannoplankton Zone NN19 (*Pseudoemiliania lacunosa* Zone).

From Core 112-688A-14X (122.3 mbsf) downward, barren intervals are common and include part of Cores 112-688A-14X to 112-688A-16X (122.3–157.7 mbsf), 112-688A-23X, 112-688A-25X to 112-688A-27X (226.8–253.4 mbsf), part of Core 112-688A-30X, Cores 112-688A-31X and 112-688A-32X (283.3–304.6 mbsf), as well as Cores 112-688A-35X to 112-688A-37X (321.8–343.4 mbsf).

Cyclococcolithus macintyrei was found in single specimens having poor preservation in Sections 112-688A-6H, CC and 112-688A-9X, CC, which we believe are reworked. The species is found more frequently and is better preserved in Cores 112-688A-19X to 112-688A-22X (169.8–198.7 mbsf), which indicates the lower part of nannoplankton Zone 19 (*Pseudoemiliania lacunosa* Zone) at this level. The remaining parts (Cores 112-688A-17X, 112-688A-18X, 112-688A-24X, 112-688A-28X, 112-688A-29X, and part of 112-688A-32X to 112-688A-34X) contain only rare and, in most cases, poorly preserved *Gephyrocapsa* species as well as *Coccolithus pelagicus* and may represent displaced material from upslope. Because of the impoverished nannoplankton assemblages and barren intervals, no zonal or age assignment was possible for the sequence below Core 112-688A-22X (198.7 mbsf) to the terminal depth of 350.3 mbsf of Hole 688A.

Two samples from Hole 688C at 351.0 (112-688C-1R-1, 75 cm) and 351.5 mbsf (112-688C-1R-1, bottom) are barren in calcareous nannoplankton.

In Hole 688E, Cores 112-688E-1R to 112-688E-11R (350.0–441.0 mbsf), 112-688E-19R (517.0–521.8 mbsf), and 112-688E-

26R (583.5–584.6 mbsf) again are barren in calcareous nannoplankton. Between Cores 112-688E-12R and 112-688E-20R (450.5–528.3 mbsf), we observed middle Miocene calcareous nannoplankton assemblages that contained moderately well preserved *Discoaster exilis*, *Discoaster variabilis*, *Reticulofenestra pseudoumbilica*, *Cyclococcolithus floridanus*, and others in varying numbers. Because we did not observed *Sphenolithus heteromorphus*, the nannoplankton assemblage of Cores 112-688E-12R to 112-688E-20R can be placed in nannoplankton Zone NN6 (*Discoaster exilis* Zone). Cores 112-688E-17R, 112-688E-18R, and 112-688E-21R contained only some caved middle Miocene material. Between Samples 112-688E-22R-1, 2–3 cm (545.5 mbsf) and 112-688E-24R-1, 86–87 cm, and again in Section 112-688E-25R, CC (576.7 mbsf) below a barren interval, we recognized a nannoplankton assemblage dominated by *Discoaster deflandrei*, *Cyclococcolithus floridanus*, and *Reticulofenestra* sp. (small). *Coccolithus miopelagicus*,, *C. pelagicus*, and rare *Sphenolithus dissimilis* and *Coccolithus abisectus* also were observed. Since we did not find *Sphenolithus belemnos* and *Sphenolithus heteromorphus* nor *Dictyococcites dictyodus* and other species that have their last occurrence at or near the Oligocene/Miocene boundary, we believe that the above interval represents the early Miocene nannoplankton Zones NN1 (*Triquetrorhabdulus carinatus* Zone) and NN2 (*Discoaster druggii* Zone).

A major hiatus was found between Cores 112-688E-26R and 112-688E-27R. In Core 112-688E-27R, a middle Eocene nannoplankton assemblage is present in Sample 112-688E-27R-1, 120 cm (594.2 mbsf), which includes *Chiasmolithus solitus*, *Reticulofenestra umbilica*, *Cyclococcolithus formosus*, *Cribrocentrum reticulatum*, *Discoaster saipanensis*, *Discoaster barbadiensis*, and *Neococcolithus dubius*. This assemblage can be placed in nannoplankton Zone NP16 (*Discoaster tani nodifer* Zone) and can be followed down to Sample 112-688E-36R-1, 60–61 cm (670.5 mbsf), although several intervals between these cores are barren or contain only rare and poorly preserved nannoplankton species. A change in the nannoplankton assemblage obviously related to a hiatus was noted between Samples 112-688E-36R-1, 60–61 cm, and 112-688E-36R-2, 18–19 cm. In the latter sample, *Discoaster saipanensis*, *Cribrocentrum reticulatum*, and *Reticulofenestra umbilica* are missing, but rare *Discoaster sublodoensis* is present, which indicates nannoplankton Zone NP14 (*Discoaster sublodensis* Zone). Below, *Discolithina* and *Transversopontis* species show a significant increase, and we also found *Braarudosphaera bigelowi*, which indicates a shallower water depth than in the overlying middle Eocene. Sample 112-688E-36R-2, 140–141 cm, contains moderately well-preserved *Discoaster lodoensis*, *Discoaster distinctus*, *Discoasteroides kuepperi*, *Cyclococcolithus formosus*, *Chiasmolithus solitus* and others, indicating the presence of the early Eocene nannoplankton Zone NP13 (*Discoaster lodoensis* Zone). The remaining cores down to the terminal Core 112-688E-46R (terminal depth of 779.0 mbsf) also contain the nannoplankton assemblage of Zone NP13. The exception are Cores 112-688E-40R and 112-688E-41R (616.5–735.5 mbsf), which are barren in calcareous nannoplankton.

Based on calcareous nannoplankton and silicoflagellates, sedimentation rates at Site 688 (Fig. 32) are increasing downhole from approximately 98 m/m.y. in the late Quaternary (0–46 mbsf) to approximately 135 m/m.y. in the late early Quaternary (46–179 mbsf), and to approximately 350 m/m.y. in the earliest Quaternary (179–340 mbsf). This assumption is true if the first occurrence of *Mesocena quadrangula* at this site really is near the Pliocene/Pleistocene boundary. Sedimentation rates for the upper part of Hole 688E down to Core 112-688E-11R cannot be evaluated at present because of suspected hiatuses of an as yet unknown duration (Fig. 31). In the middle Miocene (450–528 mbsf), the sedimentation rate may exceed 43 m/m.y., based on the occurrence of nannoplankton Zone NN6 in this interval. In the lower Miocene (545–593 mbsf) a rate of at least 9.4 m/m.y. is indicated by calcareous nannoplankton, but this rate may be considerably higher as the interval between Cores 112-688E-22R and 112-688E-26R may represent only part of nannoplankton Zone NN1/2. The middle Eocene is represented by nannoplankton Zone NP16 in Cores 112-688E-27R to 112-688E-35R, and a sedimentation rate of more than 47.5 m/m.y. may be expected between 593 and 678 mbsf. In the lower Eocene, a sedimentation rate between at least 66 and up to 125 m/m.y. was calculated. This depends on whether nannoplankton Zone NP14 (*Discoaster sublodoensis* Zone) is present in Core 112-688E-36R, which we tentatively assigned to nannoplankton Zone NP13 (678 to 775 mbsf). Note that sedimentation rates were not adjusted to dipping values.

Based on calcareous nannoplankton and silicoflagellates, the stratigraphy of the hiatuses at Site 688 is summarized in Figure 31. We found or suspected seven hiatuses, numbered LH-1 to LH-7 (LH for local hiatus) from top to bottom. Hiatuses LH-1 to LH-3 within the earliest Pleistocene to late Miocene interval were indicated by sudden changes in silicoflagellate assemblages, with some overlapping ranges of species missing. LH-3 seems to represent a major regional hiatus also known from Sites 683, 684, and 685 in the late Miocene. However, as calcareous microfossils were not available for comparison, these preliminary data must be confirmed by other siliceous microfossil groups. LH-4 occurred in the late middle Miocene and is indicated by another sudden change in the silicoflagellate assemblage and a change to calcareous sedimentation that incorporates nannoplankton Zone NN6. Again, the duration of the hiatus is somewhat uncertain without further data. Hiatus LH-5 divides the middle Miocene nannoplankton Zone NN6 from the early Miocene Zone NN1/2 at approximately 545 mbsf. We calculated its duration as 4.5 m.y. The next observed hiatus, LH-6, is one of the major regional hiatuses and separates the middle Eocene nannoplankton Zone NP-16 from the early Miocene Zone NN1/2 at Site 688. This hiatus also occurs at Site 682 between the middle Eocene (Zone NP16) and lower Oligocene (Zone NP21) and at Site 683 between the middle Eocene (Zone NP17) and middle Miocene (Zone NN5). A large-scale erosional change is already indicated by the occasional presence of reworked Cretaceous nannoplankton at Site 682 and 688 in the highest levels of the preserved middle Eocene. Reworked material is particularly abundant in the basal Oligocene of Site 682. This major regional hiatus covers an interval of approximately 21.5 m.y. at Site 688. The lowest hiatus discovered (LH-7) has a duration of about 2.8 m.y. and separates the middle Eocene nannoplankton Zone NP16 from the early Eocene nannoplankton Zones NP13 and NP14.

Radiolarians

To extract radiolarians from Section 112-688E-16R, CC (489.8 mbsf) downhole, the techniques used for shales and Mesozoic rocks were employed (De Wever et al., 1979; De Wever, 1982). One hiatus was documented between Sections 112-688E-26R, CC (584.6 mbsf) and 112-688E-27R, CC (595.7 mbsf) by radiolarians between early Miocene and Eocene age.

Hole 688A

All core-catcher samples from Hole 688A were studied for radiolarians. These are generally well preserved in all samples and common to abundant.

A radiolarian assemblage containing *Didymocyrtis tetrathalamus* and *Lamprocyrtis nigriniae* was found in Sections 112-688A-1H, CC (8.3 mbsf) to 112-688A-23X, CC (208.5 mbsf), and 112-688A-25X, CC (229.1 mbsf) to 112-688A-30X, CC (275.6 mbsf). This assemblage indicates a Quaternary age.

Lamprocyrtis neoheteroporos was found in Section 112-688A-30X, CC (275.5 mbsf) coexisting with *L. nigriniae*. Thus, this sample is younger than earliest Quaternary in age.

L. neoheteroporos, *Didymocyrtis tetrathalamus*, and *Theocorythium vetulum* were found in Sections 112-688A-32X, CC to 112-688A-37X, CC (304.6–331.2 mbsf). These indicate an earliest Quaternary to late Pliocene age.

Section 112-688A-24X, CC (21.85 mbsf) was not available for radiolarian investigations.

Hole 688E

All core-catcher samples as well as other additional samples from this hole were studied for radiolarians. Preservation of radiolarians was well to poor and deteriorated downhole. These are rare, except in Section 112-688E-1R, CC, which contains few radiolarians. These are diluted by diatoms in the upper part of the section.

Sections 112-688E-2R, CC (356.1 mbsf) to 112-688E-7R, CC (412.5 mbsf), 112-688E-9R, CC (430.5 mbsf), 112-688E-13R, CC to 112-688E-16R, CC (460 to 489.8 mbsf), 112-688E-24R, CC (567.5 mbsf), and 112-688E-29R, CC (621 mbsf) yielded too few specimens to allow any dating.

Sections 112-688E-21R, CC (536.5 mbsf) and 112-688E-28R, CC (602.5 mbsf) were unavailable for radiolarian investigation.

A radiolarian assemblage containing *Lamprocyclas neoheteroporos* was found in Section 112-688E-1R, CC (353 mbsf). Although we searched for *L. nigriniae*, we found no specimens. Thus, this assemblage indicates an early Quaternary to Pliocene age.

Didymocyrtis hughesi or *D. pettersoni* and *Stichocorys delmontensis* were found in Section 112-688E-8R, CC (421.7 mbsf). These species indicate an early middle Miocene age. Although *S. delmontensis* was found in Section 112-688E-10R, CC (438.5 mbsf), it still belongs to Miocene age.

Didymocyrtis mammifera was found in Section 112-688E-11R, CC (441 mbsf). The species ranges from the base of the *D. pettersoni* Zone to the base of the *Calocycletta costata* Zone, which represents the early middle Miocene to the late early Miocene. Taking into account the results from Sections 112-688E-8R, CC (421.7 mbsf) and 112-688E-12R, CC (453.4 mbsf), an early middle Miocene age is most probable.

Didymocyrtis laticonus and *Stichocorys delmontensis* were found in Section 112-688B-12R, CC (453.4 mbsf). These indicate the middle Miocene to the lowermost upper Miocene. Taking into account the results from previous samples, a middle Miocene age is probable for this sample.

Phormocyrtis fistula, *Lithopera thornburgi*, and *Stichocorys delmontensis* were found in Section 112-688E-17R, CC (498 mbsf). This association indicates the top of the *Dorcadospyris alata* Zone to the bottom of the *Didymocyrtis pettersoni* Zone, which represents the middle Miocene.

Stichocorys delmontensis and a fragment of *Dorcadospyrys dentata* were found in Section 112-688E-18R, CC (507 mbsf). These indicate the *Calocycletta costata* Zone to the lowermost part of the *Stichocorys wolffii* Zone, which corresponds to the late early Miocene.

S. delmontensis, *Didymocyrtis tubarius*, and *Calocycletta costata* were found in Sections 112-688E-19R, CC and 112-688E-20R, CC (521.8–528.3 mbsf). These indicate the earliest middle Miocene to the late early Miocene.

Cyrtocapsella tetrapera was found in Section 112-688E-22R, CC (545.7 mbsf). This species indicates the base of the *C. tetrapera* Zone or a younger age. Thus, only a Miocene age is assumed.

S. delmontensis was found in Section 112-688E-23R, CC (559.4 mbsf) and indicates a Miocene age. *Siphostichartus praecorona* and *S. corona* were found in Section 112-688E-25R, CC (576.7). According to Nigrini (1977), these indicate the early Miocene.

Lychnocanomma elongata was found in Section 112-688E-26R, CC (584.6 mbsf). It indicates early early Miocene to the latest Oligocene age. *Lithocyclia ocellus* or *L. aristotelis* along with fish scales was found in Section 112-688E-27R, CC (595.7 mbsf). This specimen indicates an Eocene age.

Theocampe mongolfieri was tentatively identified in Section 112-688E-30R, CC (623.2 mbsf), which would indicate an Eocene age. *Dictyoprora amphora* group was tentatively identified in Section 112-688E-30R, CC (623.2 mbsf), which according to Nigrini (1977) indicates an Eocene age.

Eusyringium fistuligerum and *Theocampe mongolfieri* were found and *Thyrsocyrtis rhizodon* and *Lychnocanomma bellum* were tentatively identified in Sample 112-688E-33R-2, 62–64 cm (652.1 mbsf). These indicate the late early to middle Eocene.

Lychnocanomma bellum was identified in Section 112-688E-34R, CC (661.8 mbsf). According to Kling (1978) this species indicates the late early to middle Eocene.

Dictyoprora amphora group was tentatively identified in Section 112-688E-34R-1, 102–103 cm (660 mbsf), which according to Nigrini (1977) indicates an Eocene age.

Thyrsocyrtis rhizodon was tentatively identified in Section 112-688E-35R, CC (670.5 mbsf), which according to Kling (1978) indicates an Eocene age. Radiolarians were present mainly as inner molds and thus were unidentifiable for the most part.

Sections 112-688E-32R, CC (642.4 mbsf), 112-688E-33R, CC, and 112-688E-36R, CC to 112-688E-38R, CC (683.6 to 702.9 mbsf), 112-688E-40R, CC, 112-688E-41R, CC, 112-688E-43R, CC, and 112-688E-45R, CC yielded specimens that were too rare and too poorly preserved to allow us to assign ages. The samples often yielded inner molds of radiolarians, crystallized with silicified foraminifers (e.g., Section 112-688E-37, CC). Sections 112-688E-42R, CC and 112-688E-44R, CC were barren.

Section 112-688E-39R, CC (710.9 mbsf) presented an inner mold that may correspond to *Eusyringium lagena* from late early Eocene to early late Eocene.

Planktonic Foraminifers

Core-catcher samples from Holes 688A and 688E were examined for planktonic foraminifers. Age-diagnostic species were recognized in Sections 112-688A-12, CC (105.5 mbsf), 112-688A-37X, CC (343.4 mbsf), 112-688E-12R, CC (453.4 mbsf), 112-688E-37R, CC (691.2 mbsf), and 112-688E-44R, CC (757 mbsf). Hole 688A can be placed in the Quaternary age, and Section 112-688A-37X, CC (343.4 mbsf) is 1.8 m.y. or older. Section 112-688E-12R, CC (453.4 mbsf) can be placed in the early Miocene, and Sections 112-688E-37R, CC (691.2 mbsf), and 112-688E-44R, CC (757 mbsf) can be dated as early Eocene.

Hole 688A

In Sections 112-688A-1H, CC through 112-688A-15X, CC (8.3–141.1 mbsf), planktonic foraminifers were abundant to rare and well or moderately well preserved. Below Section 112-688A-16X, CC (152.7 mbsf), core-catcher samples were barren of planktonic foraminifers, except for Sections 112-688A-19X, CC (176.7 mbsf), 112-688A-21X, CC (192.9 mbsf), 112-688A-22X, CC (198.7 mbsf), 112-688A-27X, CC (253.4 mbsf), 112-688A-34X, CC (321.7 mbsf), and 112-688A-37X, CC (343.4 mbsf), in which planktonic foraminifers were few or rare and moderately to poorly preserved.

Sections 112-688A-1H, CC (8.3 mbsf) through 112-688A-7H, CC (65.7 mbsf) contain *Globigerinoides ruber*, *Globorotalia menardii*, *G. tumida tumida*, *Pulleniatina obliquiloculata*, and *Sphaeroidinella dehiscens dehiscens*; these species indicate a subtropical environment. Below Section 112-688A-8X, CC (68.5 mbsf), planktonic foraminifer assemblages indicate temperate conditions, except in Section 112-688A-21X, CC (192.9 mbsf), where *Globigerinoides sacculifer*, *Globorotalia menardii*, and *Pulleniatina obliquiloculata* indicate warm water.

Hastigerinopsis riedeli was found in Sections 112-688A-7H-2 (57.3 mbsf), 112-688A-8X, CC (68.5 mbsf), and 112-688A-13X, CC (122.1 mbsf). *Globorotalia bermudezi* was found in Sections 112-688A-8X, CC (68.5 mbsf) and 112-688A-12X, CC. Both species occur only in the Quaternary (Poore, 1979; Rögl and Bolli, 1973). *Globigerinoides tenellus* was found in Section 112-688A-28X, CC (257.0 mbsf); it ranges from N21 to the Holocene. The last occurrence of *Neogloboquadrina humerosa* is in Section 112-688A-3H, CC (27.5 mbsf). This species ranges from Zone N18 to Zone N22, late Miocene to Pleistocene. *Globigerinoides obliquus obliquus* was found in Section 112-688A-37X, CC (343.4 mbsf). The last occurrence of this species is at 1.8 Ma (Berggren et al., 1983). Based on planktonic foraminifers, the age of the lowermost sample, 112-688A-37X, CC is 1.8 m.y. or older.

Hole 688C

In the core-catcher sample from Hole 688C at 351.5 mbsf, planktonic foraminifers were rare and well preserved; however, no age-diagnostic species were recognized.

Hole 688E

Planktonic foraminifers were found in Sections 112-688E-12R, CC through 112-688E-18R, CC (453.4–507.5 mbsf), 112-688E-37R, CC (691.2 mbsf), 112-688E-38R, CC (702.9 mbsf), and 112-688E-44R, CC(757 mbsf). These are rare and well to moderately well preserved, except in Sections 112-688E-37R, CC (691.2 mbsf), 112-688E-38R, CC (702.9 mbsf), and 112-688E-44R, CC (757 mbsf), where they are poorly preserved.

Globigerinoides sacculifer and *Catapsydrax unicavus* were found in Section 112-688E-12R, CC (453.4 mbsf), and *Catapsydrax unicavus* and *Globigerinita uvula* were found in Section 112-688E-18R, CC (5.7.5 mbsf). The range of *Globigerinoides sacculifer* is N6 to Holocene; the range of *Catapsydrax unicavus* is P14 to N6, and the range of *Globigerinita uvula* is P22 to the Holocene (Blow, 1969; Poore, 1979). We placed both sections in N6, the early Miocene. *Acarinina intermedia* was found in Section 112-688E-37R, CC (691.2 mbsf); the range of this species is from P4 to P6, late Paleocene to early Eocene (Berggren, 1977), and the sample was placed in late Paleocene to early Eocene. We could not ascertain the age of Section 112-688E-38R, CC (702.9 mbsf) because planktonic foraminifers were rare and poorly preserved. *Acarinina esnaensis* and *A. pentacamerata* were found in Section 112-688E-44R, CC (757 mbsf). The range of *Acarinina esnaensis* is from P4 to P6, while *Acarinina pentacamerata* ranges from P6 to P9 (Berggren, 1977). This sample was placed in P6, the early Eocene.

Benthic Foraminifers

Hole 688A

Benthic foraminifers are common to abundant and well to moderately well preserved in Sections 112-688A-1H, CC through 112-688A-13X, CC (8.3–122.2 mbsf). In lower levels of this hole, these are generally few or rare and moderately well to poorly preserved, except for Sections 112-688A-19X, CC (176.7 mbsf) and 112-688A-27X, CC through 112-688A-30X, CC (253.5–275.6 mbsf), where these are common and moderately well preserved. Sections 112-688A-26X, CC (236.9 mbsf), 112-688A-31X, CC (284.6 mbsf), and 112-688A-35X, CC through 112-688A-37X, CC (331.3–343.5 mbsf) are barren of benthic foraminifers.

One assemblage, dominated by *Uvigerina senticosa* and indicative of the lower-bathyal environment in which the hole was drilled (water depth of 3828 m), occurs throughout the cored section, except in the barren intervals and in Section 112-688A-13X, CC (122.2 mbsf), which is size-sorted. This sorted section contains only small species and those with small juvenile stages (*Bolivina costata*, *Bulimina exilis tenuata* juv., *Epistominella levicula*, *Cassidulina depressa*, and *Stainforthia complanata* juv.). About one-half of the species were transported from the shelf and slope. This sample marks approximately the base of the upper part of the cored section in which benthic foraminifers are most abundant. Iron monosulfides and abundant pyrite, which are noticeable in the cores from Section 112-688A-9X, CC (84.2 mbsf) downward, do not immediately affect the abundance or preservation of the foraminifer tests but may have some effect below the size-sorted sample, where etched and pyrite-infilled tests are common.

The *Uvigerina senticosa* Assemblage, previously sampled at Sites 682 and 683, generally has common to abundant *Melonis pompilioides*, *M. affinis*, *Oridorsalis umbonatus*, and *Pullenia bulloides*. In Sections 112-688A-3X, CC (27.6 mbsf) and 112-688A-5X, CC (46.4 mbsf), *Astrononion schwageri* and *Hoeglundina elegans* also are abundant. The significance of the variability in the lower-bathyal assemblage is not known at this time, but eventually may be linked to variation in environment; planktonic foraminifers indicate warm surface waters coincident with these assemblages.

Transported tests (mostly *Bolivina costata* from the outer-shelf/upper-bathyal environment) occur throughout the cored section. Their greatest frequency occurs in Sections 112-688A-2X, CC (17.9 mbsf), 112-688A-6X, CC (56.2 mbsf), and 112-688A-29X, CC (274.2 mbsf), where about 50% of the tests are transported.

Hole 688E

The benthic foraminifers recovered in this hole reflect a general subsidence of the seafloor through time, from shelf and mid- to upper-bathyal environments of the Eocene to the lower-bathyal environment revealed in the Pliocene through Quaternary sequence of Hole 688A. Barren intervals and hiatuses prevented us from determining a subsidence curve.

The late Miocene part of this hole, including Sections 112-688E-1R, CC through 112-688E-11R, CC (353–441 mbsf) is barren of benthic foraminifers, presumably due to diagenetic destruction of the tests. In the middle Miocene part of the cored section, benthic foraminifers occur in Sections 112-688E-12R, CC through 112-688E-16R, CC (453.4–488.5 mbsf), where they are few to rare and poorly preserved, except for Section 112-688E-15R, CC (482 mbsf), where they are common, moderately well preserved, and indicative of an upper-middle bathyal environment (~500–1500 m). In an assemblage in Section 112-688E-15R, CC, *Bulimina alligata* and *Stilostomella* spp. are abundant and *Melonis affinis*, *Nodosaria longiscata*, and *Eilohedra levicula* are common. *Uvigerina mantaensis* and *Gyroidina altiformis* occur in Section 112-688E-16R, CC (488.5 mbsf). *Bolivina* cf. *vaughani* occurs rarely in Section 112-688E-14R, CC (474 mbsf) and was probably transported from the shelf. This species also occurs rarely in middle Miocene bathyal assemblages at Site 683 and in late Miocene bathyal assemblages at Site 685. In each case, the downslope transportation of tests was much less in the Miocene part of the sections than in Pliocene–Quaternary strata. Sections 112-688E-17R, CC through 112-688E-20R, CC (498–528.4 mbsf) in the lower part of the middle Miocene sequence are barren of foraminifers.

The early Miocene part of the cored sequence is barren of benthic foraminifers. The sequence contains rare, poorly preserved specimens in Sections 112-688E-21R, CC (536 mbsf) and 112-688E-24R, CC through 112-688E-26R, CC (567.5–584.7 mbsf) in an assemblage marked by the occurrence of *Uvigerina gallowayi*, similar to Sites 682 and 683. *Gyroidina altiformis* and *Uvigerina mantaensis* as well as *Oridorsalis umbonatus* are the most abundant species in this assemblage, which indicates an upper-middle bathyal environment.

In the middle Eocene interval from Sections 112-688E-27R, CC through 112-688E-35R, CC (595.7–670.5 mbsf), foraminifers are rare and poorly preserved or the samples are barren of foraminifers, except for Section 112-688E-34R, CC (661.9 mbsf), where they are few to common and moderately well to poorly preserved. The foraminifer assemblage of this sample, which is a dolomitized mudstone, contains *Uvigerina mantaensis*, *Plectofrondicularia vaughani*, *P.* cf. *packardi multilineata*, *Anomalina chirana*, *Guttulina irregularis*, *Nodosaria longiscata*, and *Oridorsalis umbonatus*, which indicates an upper-middle bathyal to upper-bathyal environment. The coarse sandstones characterizing the low-yield benthic foraminifers of the middle Eocene interval appear to have been deposited on the shelf, but the few foraminifers contained in these sandstones are not indicative of shelf conditions. All these middle Eocene species were reported in the Chira Shale (Cushman and Stone, 1947).

The lower Eocene interval from Sections 112-688E-36R, CC through 112-688E-42R, CC (683.6–737.5 mbsf) and Section 112-688E-45R, CC (767.8 mbsf) is sandy and contains rare, poorly preserved, shelf-dwelling species. Among them are *Hanzawaia* sp., *Buliminella peruviana* (the Eocene counterpart of *Buliminella elegantissima*), *Spiroplectammina gryzbowskii*, and *Cyclammina* spp. A middle-bathyal assemblage occurs in Section 112-688E-43R, CC (750.5 mbsf). Foraminifers are few to common and moderately well preserved, including *Cibicidoides grimsdalei*, *C. perlucidus*, *C. martinezensis*, *Anomalina venezuelana*, *Oridorsalis umbonatus*, and *Cassidulina globosa*. Section 112-688E-44R, CC (757 mbsf) contains abundant, moderately well preserved benthic foraminifers in which the association of *Bulimina jacksonensis*, *Cassidulina globosa*, *Valvulineria* spp., and *Buliminella chirana* suggests an upper-bathyal (150–500 m) environment.

Biogenic Groups in Coarse-Fraction Analysis

The semiquantitative distribution of percentages of the biogenic groups recorded in the coarse fraction is shown in Figure 35. Note that radiolarians are the dominant group throughout Hole 688A, reaching up to 100% of the population in Sections 112-688A-15X, CC (141.1 mbsf) and 112-688A-16X, CC (152.7 mbsf). In these samples, sediments exhibit the character of a siliceous ooze.

Benthic foraminifers vary from 10% to 20% between Sections 112-688A-1H, CC and 112-688A-13, CC (8.3 to 122.1 mbsf). Below Section 112-688A-18X, CC (161.8 mbsf), the relative percentage of the benthic foraminifers is no higher than 10%.

Planktonic foraminifers range from 5% to 30% between Sections 112-688A-1H, CC and 112-688A-13X, CC (8.3–122.1 mbsf). Below this interval, the only significant occurrences were observed in Sections 112-688A-19X, CC (176.7 mbf) and 112-688A-28X, CC (257.2 mbsf).

The diatoms in Hole 688A appear to be scarce but are continuously present from Sections 112-688A-3H, CC to 112-688A-13X, CC (27.5–122.1 mbsf). Below this interval, diatoms occur sporadically in the coarse fraction.

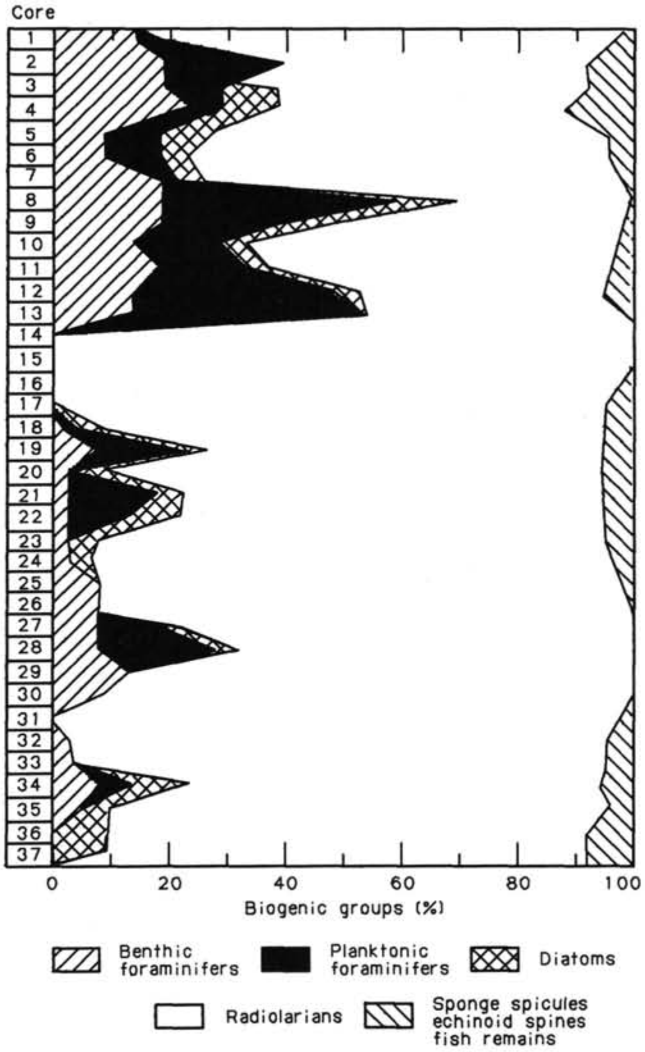

Figure 35. Biogenic groups in the coarse fraction of Hole 688A.

Correlation with the Onshore Basins

The stratigraphic interval cored between Sections 112-688E-38R, CC and 112-688E-44R, CC was referred to the upper Eocene Chira-Verdun sequence of the Talara and Sechura basins on the basis of the occurrence of the benthic foraminifers *Cyclammina simiensis*, *Bathysiphon eocenicus*, *Valvulineria duboisi*, *Bulimina debilis*, *Anomalina chirana*, *Uvigerina chirana*, and *Cyclammina deformis*. The planktonic foraminifers assigned to *Globorotalia* cf. *increbescens* range from Eocene to early Oligocene in age.

Section 112-688E-44R, CC (760 mbsf) contains the planktonic forms *Globorotalia bolivariana* and *Clavigerinella akersi*, which are considered indicative species of the middle Eocene in the coastal basins of Peru. The benthic foraminifer assemblage in this section consists of *Tritaxilina pupa*, *Vulvulina nummulina*, *Marginulina mexicana*, *Discorbis berryii*, *Bulimina brachycostata*, and *Rotalia constans*. These faunas indicate the Talara Shale Formation in the Talara Basin.

Section 112-688E-45R, CC (767.8 mbsf) contains mostly arenaceous foraminifers of relatively nondiagnostic significance; however, a few chambers of *Clavigerinella colombiana* were observed, and on this basis the sample was assigned a middle Eocene age, in accordance with today's stratigraphic standards of the Peruvian coastal basins.

A chert pebble encountered in Sample 112-688E-45R-1, 1–4 cm (765 mbsf) was examined micropaleontologically; it contained biserial planktonic foraminifer indicative of the Cenomanian similar to forms of the genus *Heterohelix* and *Globigerinelloides*. These faunas were reported from the Albian–Cenomanian cherts and limestones of the El Muerto and Pariatambo formations of the Central Andes and the Talara Basin.

ORGANIC GEOCHEMISTRY

Holes 688A and 688E were drilled in lower-slope deposits of the Peru Outer Continental Margin at a water depth of about 3820 m. This water depth is similar to that at Site 682 (3800 m). Site 688 is the fourth site located in waters deeper than 3000 m, well within the pressure-temperature field in which gas hydrates are stable. The same organic geochemical approaches were taken here as at previous deep-water sites. Details of methods and procedures are found in "Organic Geochemistry" sections, Site 679 and 682 chapters. Instruments are described in the "Explanatory Notes" (this volume).

Hydrocarbon Gases

Vacutainer Gases

Starting with Core 112-688A-4H (31.8 mbsf), gas pockets were sampled to the bottom of Holes 688A-688E. Almost every core contained enough gas to be sampled using the vacutainer technique. This provided a complete record of the composition of hydrocarbon gases to a depth of 769 mbsf (Table 5). Carbon concentrations were variable and ranged from 0.77% (obviously contaminated with air) to 99.2%. Carbon dioxide was a component of the balance gas; CO_2 was measured in about one-half of the samples. Concentrations of this gas ranged from 0.05% to 42.4%. As at previous deep-water sites, the shallow occurrence of large amounts of C_1 results from the rapid depletion of sulfate (see "Inorganic Geochemistry" section, this chapter) that allows microbial methanogenesis to proceed without being inhibited by microbial sulfate reducers (Claypool and Kaplan, 1974).

Besides C_1 and CO_2, the gases collected by vacutainers also contained C_2 and C_3, both of which generally increase in concentration with increasing depth. The amount of C_2 ranged from from 5.6 to 3500 ppm, and the amount of C_3 from 1.7 to 2100 ppm. The highest concentrations were found in the deeper sediments of Hole 688E.

C_1/C_2 ratios decrease exponentially with depth overall (Table 5 and Fig. 36), although some distinct breaks in the record represent changes in the gas composition of different geologic units. For example, the high ratios in the upper part of the section represent gas composition in the Quaternary. These high values give way to lower values below about 340 mbsf that correspond to the boundary between lithologic Units I and II. The abrupt change in ratios between 584 and 641 mbsf corresponds to a tectonic melange (see "Lithostratigraphy" section, this chapter), and the high ratios between 600 and 700 mbsf represent the anomalous compositions of gas in a major sandstone unit. Because of its anomalous composition, we believe that this gas may have migrated into the sandstone.

Table 5. Vacutainer gases at Site 688.

Core-section interval (cm)	Depth (mbsf)	C_1 (%)	CO_2 (%)	C_2 (ppm)	C_3 (ppm)	C_1/C_2
112-688A-4H-4, 2	31.8	87.0		9.5		92,000
5H-6, 148	45.8	87.8	7.5	12	5.6	72,000
6H-3, 90	50.2	67.8		8.7		78,000
7H-5, 90	62.7	85.3	9.9	12	5.7	71,000
9X-2, 1	76.3	62.7	8.8	10	3.4	61,000
10X-1, 114	85.4	58.5	24.0	9.0	8.5	65,000
11X-8, 97	103.0	84.2		9.4	4.6	90,000
12X-1, 32	103.6	53.1	16.2	7.9	8.5	67,000
13X-4, 90	118.2	83.3		16		51,000
14X-4, 104	127.8	64.2		12	5.4	54,000
15X-6, 44	139.7	81.8	3.7	17		48,000
16X-7, 15	150.4	63.8		17		38,000
17X-5, 12	156.9	56.0	15.8	8.2	3.6	68,000
18X-1, 106	161.4	64.6		12		53,000
19X-3, 79	173.6	46.1	28.8	6.5	4.2	71,000
21X-2, 105	191.4	80.4	17.6	15	1.7	53,000
23X-1, 36	208.2	50.9	32.3	6.1	3.8	83,000
25X-2, 35	228.7	56.7	42.4	13	12	42,000
27X-5, 105	252.9	42.1	41.7	15	10	29,000
28X-1, 76	256.1	55.0		13	8.0	41,000
29X-5, 65	271.5	66.7	12.9	15	7.1	45,000
30X-2, 45	274.8	17.2		16	14	11,000
32X-6, 112	301.9	82.9	11.6	28	9.0	30,000
33X-4, 86	308.2	25.7		38	19	6,800
35X-3, 46	325.3	69.8	15.5	200	17	3,600
36X-7, 42	340.7	25.1	16.1	69	22	3,600
112-688E-4R-3, 30	377.8	59.9	17.3	380	250	1,600
5R-6, 90	392.4	56.4	27.3	620	450	910
6R-2, 135	396.4	0.77		5.6		1,400
7R-2, 104	405.5	0.97		17	4.3	567
8R-4, 140	418.4	26.9	16.3	240	53	1,100
9R-6, 1	429.5	18.8		140	23	1,300
10R-4, 109	437.1	68.3	19.9	750	100	910
14R-3, 15	472.7	11.5	1.6	160		730
15R-2, 10	480.6	71.0		1100	42	670
16R-1, 90	489.4	22.3	6.8	480	20	460
19R-1, 144	518.4	69.7		1100	23	650
20R-1, 34	526.8	49.7	7.9	980	22	510
23R-3, 126	559.3	79.2		2000	43	400
24R-2, 121	567.2	77.3	3.6	1200	18	620
25R-2, 110	576.6		19.2	410		470
26R-1, 25	583.8	34.4	2.6	650		530
32R-1, 78	641.3	13.0		9.7		13,000
35R-1, 40	669.4	67.7	0.2	210		3,300
36R-2, 140	681.4	95.5		1700	55	550
37R-2, 100	690.5	56.4	0.07	1200	44	460
38R-1, 132	698.8	89.5	0.13	3100	210	290
41R-1, 82	726.8	22.7	0.05	490	41	470
43R-4, 34	749.8	99.2		1800	412	550
44R-2, 15	756.2	84.9		1900	520	440
45R-2, 128	766.8	85.9		3500	2100	250

Units of (%) and (ppm) are in volume of gas component per volume of gas mixture. Hydrocarbon gases were analyzed using the Hach-Carle Gas Chromatograph; CO_2 was analyzed with the Hewlett-Packard Gas Chromatograph.

Extracted Gases

Hydrocarbon gases were extracted using the headspace and can procedures on sediment samples collected from both Holes 688A and 688E. Results are shown in Table 6. High concentrations of C_1 are already present at 14.3 mbsf (53,000 μL/L), and high values continue to the bottom of Hole 688E. The zone of sulfate reduction at this site is very thin, which allows microbial generation of abundant C_1 to occur near the surface (see "Inorganic Geochemistry" section, this chapter). Figure 37 shows the profile with depth of C_1 concentrations for both Holes 688A and 688E. Results of both the can and headspace procedures indicate the same general trends, but the amount of C_1 recovered using the can procedure is lower. C_1 concentrations reach a maximum value of 120,000 μL/L at 33.3 mbsf and then decrease slightly through the remainder of the Quaternary section. In the older sediments to the bottom of Hole 688E, the concentrations of C_1 appear to increase. The low C_1 concentration measured at 436 mbsf may reflect a real decrease in the amount of C_1 present at this stratigraphic level because the results from the can procedure also show a minimum at a nearby depth of 452 mbsf.

C_2 and C_3 were not detected in Quaternary samples analyzed by the headspace procedure and were found in very low amounts (1.4 to 4.2 μL/L for C_2 and 7.0 to 8.9 μL/L for C_3) using the can procedure (Table 6). Between 307.3 and 340.3 mbsf, concentrations of these compounds increase abruptly and tend to continue to increase with depth. C_2 concentrations, as measured by the headspace procedure, range from 20 to 2900 μL/L and those of C_3 from 23 to 1600 μL/L in the pre-Quaternary sediments. For some unknown reason, $C_{2:1}$ was detected in only a few samples. This result is contrary to what was observed at previous sites (see "Organic Geochemistry" section, Site 683 and 685 chapters).

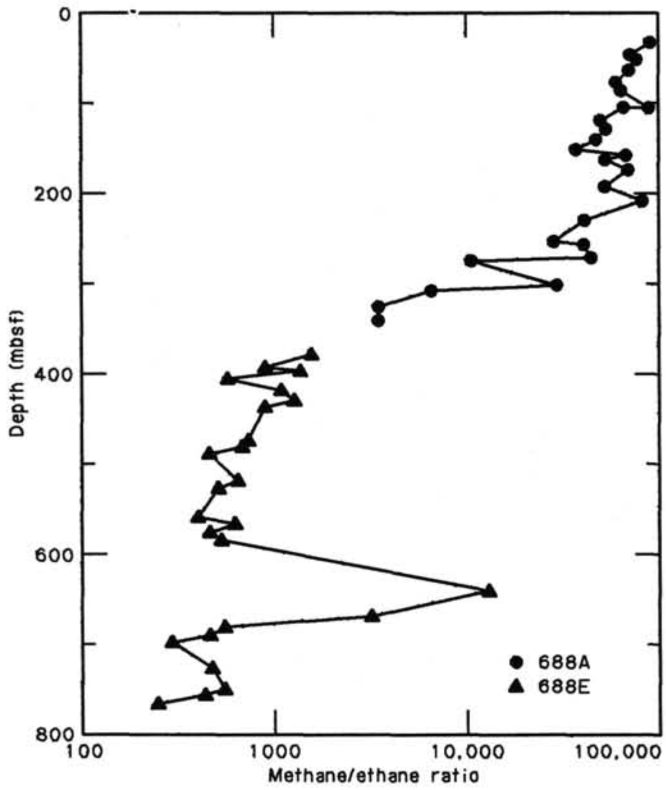

Figure 36. Methane/ethane ratios in gas collected by means of vacutainers from Holes 688A and 688E.

Gas Hydrates

Gas hydrates were recovered from Core 112-688A-15X-7 (141 mbsf). Figure 38 shows that the gas hydrate is closely mixed with dark grayish-black fine silt and clay. Two samples, called A and B, were confined in pressure vessels described by Kvenvolden et al. (1984). After photography, a third sample, called C, was placed in a beaker where the gas hydrate dissociated. A fourth sample was placed in a special container for long-term storage (Sloan, 1985); however, the seals may have failed because there was no pressure increase during the initial storage at −20°C. The information obtained is as follows:

Sample A
Equilibrium pressure at 25.4 °C = 85 psig
Total volume of gas = 160 cm^3 (STP)
Total volume of C_1 = 147 cm^3 (STP)
Total volume of H_2O = 11.3 mL
Ratio C_1/H_2O by volume = 13
Weight of sediment = 2.5 g
Sediment associated with gas hydrate = 18%
Geochemistry: salinity = 7.8 g/kg;
chlorinity = 90.60 mmol/L;
sulfate = 0 mmol/L;
phosphate = 173.82 μmol/L;
ammonia = 12.34 μmol/L;
silica = 444 μmol/L;
C_1 = 91.5%;
C_2 = 22 ppm;
C_1/C_2 = 42,000.

Sample B (all gas transferred to a stainless steel cylinder)
Equilibrium pressure at 25.1°C = 95 psig
Total volume of gas = 176 cm^3 (STP)
Composition of gas = assumed to be the same as Sample A
Total volume of C_1 = 162 cm^3 (STP)
Total volume of H_2O = 6.2 mL
Ratio C_1/H_2O by volume = 26
Weight of sediment = 3.1 g
Sediment associated with gas hydrate = 67%
Inorganic geochemistry: salinity = 20.0 g/kg;
chlorinity = 232.27 mmol/L;
sulfate = 0 mmol/L;
phosphate = 111.88 μmol/L;
ammonia = 34.48 μmol/L;
silica = 635 μmol/L.

Table 6. Extracted gases at Site 688.

Core/section interval (cm)	Depth (mbsf)	C_1 (μL/L)	C_2 (μL/L)	C_3 (μL/L)	C_1/C_2
Headspace gases					
112-688A-2H-5, 0-1	14.3	53,000			
4H-5, 0-1	33.3	120,000			
9X-6, 0-1	82.3	8,100			
10X-3, 0-1	87.3	20,000			
12X-1, 139-140	104.7	24,000			
14X-4, 0-1	126.8	22,000			
15X-3, 149-150	136.3	28,000			
16X-5, 0-1	147.3	15,000			
18X-1, 149-150	161.8	9,900			
20X-1, 53-54	179.8	8,200			
21X-3, 107-108	192.9	22,000			
25X-2, 0-1	228.3	6,500			
27X-5, 0-1	251.8	13,000			
30X-1, 114-115	275.5	19,000			
33X-4, 0-1	307.3	20,000			
36X-7, 0-1	340.3	21,000	25	38	835
Canned gases					
112-688A-1H-4, 140-145	6.0	230	1.4		170
3H-4, 140-145	23.8	94,000	1.7		55,000
6H-3, 140-145	50.8	24,000	1.4		17,000
9X-5, 135-140	82.2	28,000	4.1	8.9	6,800
16X-4, 135-140	147.2	11,000	1.9		5,800
25X-1, 135-140	228.2	6,200	4.2	7.0	1,500
33X-3, 135-140	307.2	5,300	3.5	7.5	1,500
Headspace gases					
112-688E-1R-2, 0-1	351.5	49,000	160	700	300
3R-4, 134-135	370.9	29,000	140	360	210
6R-5, 0-1	399.5	60,000	140	300	440
9R-6, 0-1	429.5	98,000	250	250	390
10R-4, 0-1	436.0	2,200	21		110
12R-2, 0-1	452.0	43,000	410	150	110
13R, CC, 0-1	469.0	220,000	1600	400	130
14R-3, 0-1	472.5	270,000	800	160	340
19R-4, 0-1	520.1	85,000	600	80	140
23R-2, 0-1	556.5	150,000	550	34	280
24R-2, 0-1	556.5	150,000	1100	42	140
26R-1, 116-117	584.7	400,000	2700	93	150
27R-2, 0-1	594.5	270,000	1100	23	250
30R-1, 134-135	622.9	250,000	110		2,200
32R-1, 0-1	640.5	34,000	20		1,700
34R-2, 0-1	661.0	290,000	110		2,700
36R-3, 0-1	681.5	39,000	1100	220	37
37R-2, 0-1	689.5	62,000	900	160	68
38R-2, 0-1	699.0	67,000	940	200	71
39R-3, 0-1	710.0	60,000	2900	1300	21
41R-2, 0-1	727.5	65,000	650	240	100
43R-4, 0-1	749.5	300,000	2300	1600	130
Canned gases					
112-688E-3R-4, 135-140	370.9	10,000	50	180	210
12R-1, 135-140	451.9	4,700	47	15	100
19R-3, 135-140	521.4	23,000	170	16	140
30R-1, 135-140	622.9	37,000	11		3,700
38R-1, 145-150	699.0	31,000	690	180	45

Units are in microliters (μL) of gas component per liter (L) of wet sediment. All measurements were performed on the Hach-Carle Gas Chromatograph.

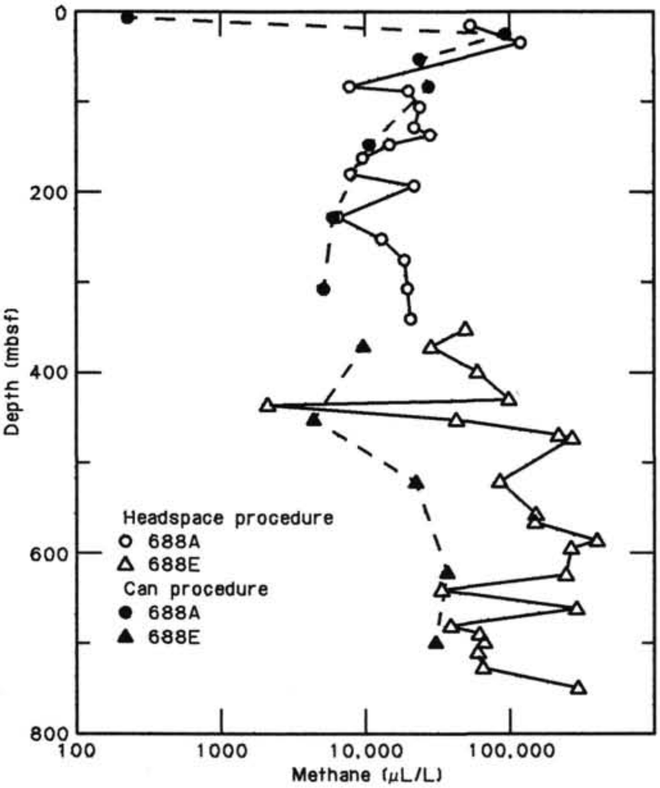

Figure 37. Comparison of extracted methane concentrations with depth as obtained by the headspace and can procedures for Holes 688A and 688E.

Figure 38. Photograph of a sample of gas hydrate from Core 112-688A-15X-7 (141 mbsf).

Sample C (gas hydrate decomposed in open beaker; a major part of the water was retained for isotopic determinations)

Inorganic geochemistry: salinity = 11.8 g/kg;
chlorinity = 136.62 mmol/L.

The waters of the gas-hydrate samples from Site 688 apparently were contaminated with seawater, as indicated by salinity and chlorinity as well as other pore-water parameters (see "Organic Geochemistry" section, this chapter). The volume of C_1 released was only 13 and 26 times the volume of water that composed the gas hydrate; at Site 685 about 100 volumes of gas were released per volume of water. The results indicate that the gas hydrates at Site 688 underwent significant decomposition before our measurements were conducted.

A bottom-simulating reflector (BSR) was observed in seismic records about 2.5 km seaward of Site 688. This reflector, which occurs at 0.55 s (two-way traveltime) or about 500 mbsf, is inferred to correspond to the base of the zone of gas hydrates. Using Shipley et al.'s method (1979) and an assumed bottom-water temperature of 1.7°C, we estimated that the temperature at the base of the gas-hydrated zone was 25.4°C and that the geothermal gradient at this site was about 47°C/km. This geothermal gradient is within the range of those estimated for the other deep-water sites (43° to 57°C/km). Thus, the average geothermal gradient for deep-water, continental-slope sediments of the Peru Continental Margin is 49° ± 6°C/km, as estimated from the occurrences of gas hydrates.

Carbon

Total-carbon, carbonate-carbon, and organic-carbon values were determined for 13 sediment samples from Hole 688A and 12 sediment samples from Hole 688E, which are the "squeeze cakes" from pore-water geochemistry studies (Table 7 and Fig. 39). Organic-carbon contents of sediments generally decrease at this site below about 200 mbsf. Within the major sandstone unit (between 600 and 700 mbsf), the organic-carbon values are as low as 0% at 651 mbsf. Toward the bottom of Hole 688E, organic-carbon values increase, as do the amounts of C_1, C_2, and C_3.

Rock-Eval pyrolysis results are given in Table 8 and Figure 40. The results show that sediments from Hole 688A are organic-rich (TOC ranges from 1.99% to 7.97%). Below about 556 mbsf in Hole 688E, the sediments are organic-poor, except for the deepest sample, with TOC values ranging from 0.01% to 0.71%. In all cases, the organic matter is immature; that is, T_{max} values are all less than 430°C. In general, all of the Rock-Eval parameters decrease with depth. Most values associated with Sample 112-688E-33R-1, 140–150 cm, should be discarded because S_2 = 0 and TOC = 0.01. The diagram of the hydrogen and oxygen indices (HI and OI, respectively; Fig. 41) shows wide scatter between organic matter of type II and III. Much of this organic matter is probably of marine origin and immature, which is reflected by the relatively high oxygen content.

Table 7. Organic carbon and carbonate carbon at Site 688.

Core-section interval (cm)	Depth (mbsf)	Total carbon (%)	Inorganic carbon (%)	Organic carbon (%)	TOC (%)
112-688A-1H-4, 145–150	6.0	3.33	0.12	3.21	2.71
3H-4, 145–150	23.8	4.72	2.11	2.61	2.54
6H-3, 145–150	50.8	3.19	1.05	2.14	1.99
9X-5, 140–150	82.2	5.92	1.03	4.89	4.73
12X-1, 140–150	104.7	4.96	0.94	4.02	3.74
16X-4, 140–150	147.2	5.04	0.27	4.77	3.13
19X-3, 140–150	174.2	4.31	0.64	3.67	3.24
21X-3, 108–118	192.9	4.13	0.33	3.80	3.41
25X-1, 140–150	228.2	8.98	0.29	8.69	7.97
27X-4, 140–150	251.7	4.91	0.17	4.74	2.71
30X-1, 115–125	275.5	5.82	0.21	5.61	5.16
33X-3, 140–150	307.2	5.61	0.64	4.97	4.46
36X-6, 140–150	339.9	4.12	0.11	4.01	3.72
112-688E-3R-4, 140–153	370.9	4.34	0.15	4.19	3.02
6R-4, 140–150	399.4	2.62	0.32	2.30	2.03
9R-5, 140–150	429.4	2.55	0.20	2.35	1.72
12R-1, 140–150	451.9	4.39	0.47	3.92	3.41
19R-3, 140–150	521.2	2.45	0.57	1.88	1.63
23R-1, 140–150	556.4	3.09	2.23	0.86	1.04
27R-1, 140–150	594.4	0.60	0.21	0.39	0.28
30R-1, 140–150	622.9	0.63	0.38	0.25	0.20
33R-1, 140–150	651.4	1.21	1.23	0.00	0.01
35R-1, 140–150	670.4	1.10	0.45	0.65	0.53
37R-1, 140–150	689.4	1.39	0.56	0.83	0.71
43R-4, 87–97	750.4	1.88	0.53	1.35	1.27

TOC = total organic carbon from Rock-Eval pyrolysis.

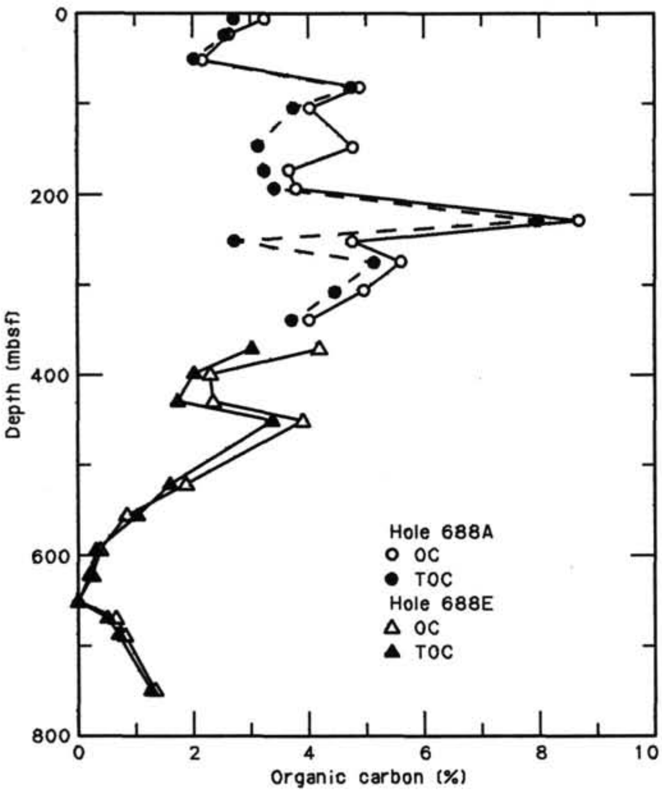

Figure 39. Comparison of organic carbon (OC) and total organic carbon (TOC) from Rock-Eval pyrolysis with depth at Holes 688A and 688E.

Examination of Core 112-688E-39R

When Core 112-688E-39R was sawed, we noticed that the dark gray siltstone contained a few zones having numerous black carbonaceous particles that resembled carbonized-wood fragments. These fragments were concentrated at bedding surfaces, especially in small pockets that might correspond to shallow depositional hollows. Under ultraviolet light, a few bright spots of fluorescence were seen. These corresponded to millimeter-sized white objects, possibly foraminifers. A small part of this sediment-filled depression in Sample 112-688E-39R-1, 130–131 cm, was transferred to an evaporating dish, and methylene chloride was added. The white objects and their fluorescence dispersed in the solvent. Under the microscope, the numerous black particles appeared as brownish-red amorphous fragments that were not clearly of woody or terrestrial origin.

Three samples were taken and extracted with methylene chloride, evaporated, and transferred to a small volume of hexane. Part of each sample was analyzed by gas chromatography. The first two samples (about 200 mg each, TOC = 3.53% and 2.15%) came from the sawed surface of the depression and from immediately beneath this depression. Both gave similar gas chromatographic traces (Fig. 42) and exhibited a range of n-alkanes from about C_{11} to C_{40} as a smooth distribution maximizing at about C_{19}, with prominent peaks at the retention times of pristane and phytane. The quantity of n-C_{20}, for example, is estimated to be about 500 μg/g of sediment. The n-alkanes are accompanied by an unresolved complex mixture. The overall gas chromatographic pattern resembles a partially weathered marine bitumen, for which the most likely origin was syndepositional with the fossils and presumed woody fragments. This interpretation was supported by the gas-chromatographic data for the third sample (30 cm higher in the core) at another bedding surface. This sample was a light gray siltstone that was representative of the general lithology of the section and that displayed few black fragments (TOC = 0.87%). The gas-chromatographic trace showed a very small amount of hydrocarbons (individual n-alkanes less than 5 μg/g).

INORGANIC GEOCHEMISTRY

Introduction and Operation

At Site 688, on the lower slope of the Peru Trench, cores were recovered from three holes: Holes 688A, 688C (only one core), and 688E. We analyzed 11 whole-round, squeezed sediment samples (three of 5 cm and nine of 10 cm) and two *in-situ*, interstitial-water samples from Hole 688A; seven whole-round (10 cm), squeezed sediment samples were analyzed in Hole 688E. Five additional whole-round sediment samples were analyzed from Cores 112-688E-30R, 112-688E-33R, 112-688E-35R, 112-688E-37R, and 112-688E-43R. These samples were also squeezed at 40,000 psi for >2 hours each, but unfortunately yielded no interstitial waters. Therefore, the chemical data only span the first 600 m of the section drilled at Site 688. The chemical data are summarized in Tables 9 and 10. For procedures to prepare samples of indurated sediment fragments, see "Inorganic Geochemistry" section, Site 685 chapter (this volume).

In Table 10, the data obtained from neighboring interstitial waters in squeezed sediments are compared with the *in-situ* sample data. The *in-situ* samples have 0% sulfate concentrations, which indicates no contamination by drill-hole water.

The *in-situ* samples have higher salinity, chloride, Ca^{2+}, Mg^{2+}, and lower phosphate concentrations than the neighboring samples. This is the fourth Leg 112 site where most of the cored sediment section lies within the stability field of marine gas-hydrates (Kvenvolden and McMenamin, 1980). Disseminated gas hydrates "dilute" the interstitial waters already at about 30 m below the sediment/water interface at this site, as can be seen from methane data and chloride profiles (Fig. 43).

Similar to the other three gas-hydrate sites (Sites 682, 683, and 685), systematic chemical variations with pronounced minima and maxima were observed downhole and are shown in Figures 43 through 50. The most significant trends in the chemical

Table 8. Summary of Rock-Eval pyrolysis data for Holes 688A and 688E.

Core/section interval (cm)	Depth (mbsf)	Weight (mg)	T_{max}	S_1	S_2	S_3	PI	S_2/S_3	PC	TOC (%)	HI	OI
112-688A-1H-4, 145–150	5.95	99.9	424	1.09	8.15	3.00	0.12	2.71	0.77	2.71	300	110
4H-4, 145–150	23.75	99.6	422	1.00	6.96	3.41	0.13	2.04	0.66	2.54	274	134
6H-3, 145–150	50.75	103.0	424	0.68	5.07	2.58	0.12	1.96	0.47	1.99	254	129
9X-5, 140–150	82.20	100.4	418	2.16	16.37	3.94	0.12	4.15	1.54	4.73	346	83
12X-1, 140–150	104.70	101.1	422	1.53	12.50	3.89	0.11	3.21	1.16	3.74	334	104
16X-4, 140–150	147.20	101.6	425	1.54	15.32	5.01	0.09	3.05	1.40	3.13	489	160
19X-3, 140–150	174.20	101.2	424	0.88	10.35	3.51	0.08	2.94	0.93	3.24	319	108
21X-3, 108–118	192.88	100.3	417	1.05	9.86	3.33	0.10	2.96	0.90	3.41	289	97
25X-1, 140–150	228.20	100.1	417	3.69	35.16	5.79	0.10	6.07	3.23	7.97	441	72
27X-4, 140–150	251.70	100.7	413	1.36	16.66	3.27	0.08	5.09	1.50	2.71	614	120
30X-1, 115–125	275.45	98.9	419	1.67	19.52	3.86	0.08	5.05	1.76	5.16	378	74
33X-3, 140–150	307.20	100.2	418	1.28	16.44	4.85	0.07	3.38	1.47	4.46	368	108
36X-6, 140–150	339.90	102.8	427	1.15	15.81	2.78	0.07	5.68	1.41	3.72	425	74
112-688E-3R-4, 140–153	370.90	83.4	391	2.42	18.88	3.21	0.11	5.88	1.77	3.02	625	106
6R-4, 140–150	399.40	74.4	397	0.96	9.07	1.90	0.10	4.77	0.83	2.03	446	93
9R-5, 140–150	429.40	97.6	400	1.18	9.12	1.65	0.11	5.52	0.85	1.72	530	95
12R-1, 140–150	451.90	90.0	401	1.84	16.96	3.55	0.10	4.77	1.56	3.41	497	104
19R-3, 140–150	521.20	98.0	417	0.36	6.90	1.37	0.05	5.03	0.60	1.63	423	84
23R-1, 140–150	556.40	101.0	413	0.21	2.11	1.69	0.09	1.24	0.19	1.04	202	162
27R-1, 140–150	594.40	99.0	412	0.05	0.48	0.53	0.10	0.90	0.04	0.28	171	189
30R-1, 140–150	622.90	101.5	409	0.05	0.23	0.66	0.18	0.34	0.02	0.20	115	330
33R-1, 140–150	651.40	100.6	246	0.02	0.00	0.18	1.00	0.00	0.00	0.01	0	1800
35R-1, 140–150	670.40	97.9	417	0.08	0.75	0.43	0.10	1.74	0.06	0.53	141	81
37R-1, 140–150	689.40	103.8	423	0.04	1.49	0.73	0.03	2.04	0.12	0.71	209	102
43R-4, 87–97	750.37	99.8	418	0.12	3.87	0.87	0.03	4.44	0.33	1.27	304	68

Note: Rock-Eval parameters are defined in "Inorganic Geochemistry" section, Site 679 chapter.

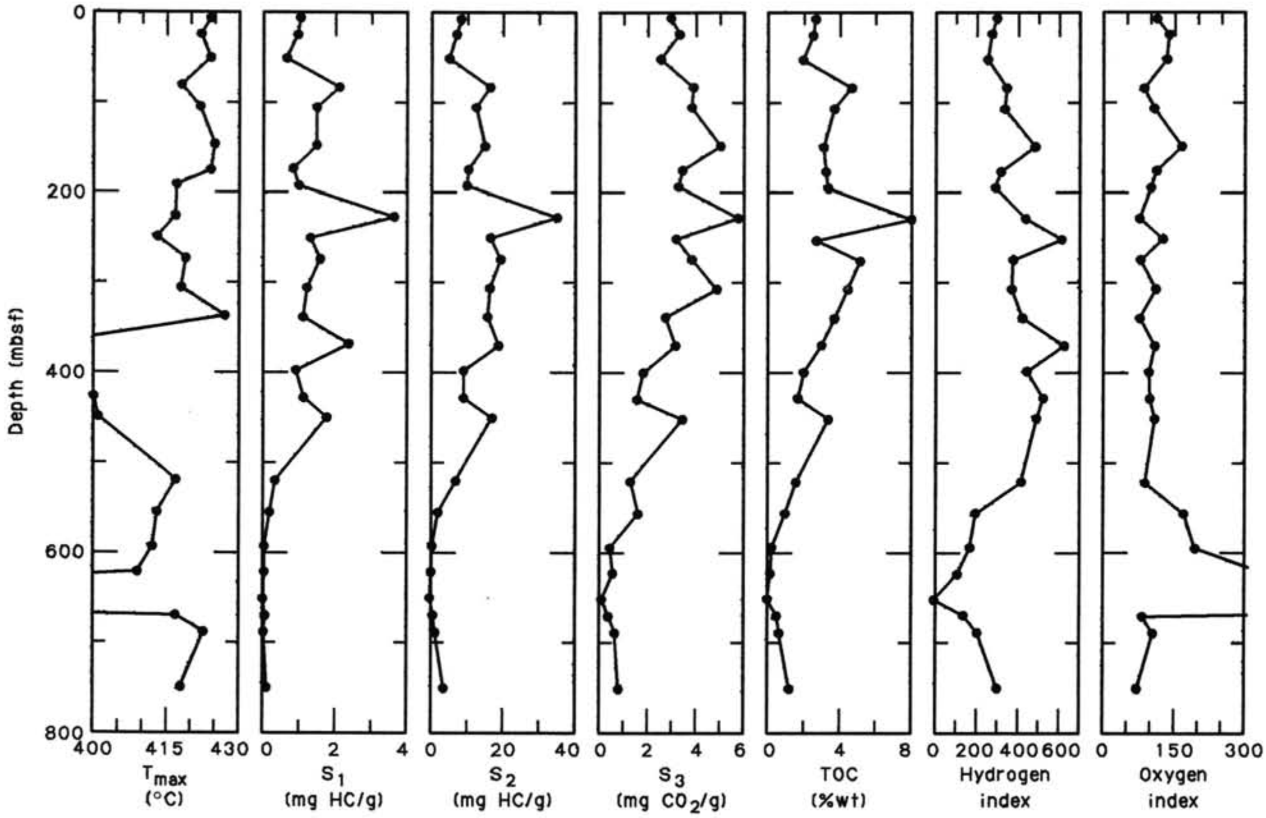

Figure 40. Comparison of Rock-Eval parameters T_{max}, S_1, S_2, S_3, TOC, HI, and OI in sediments at Site 688.

concentration profiles are downhole decreases in Cl^-, rapid depletion of SO_4^{2-}, as well as increases with subsequent decreases in salinity, alkalinity, Mg^{2+}, NH_4^+, phosphate, and silica. Calcium first decreases and then increases strongly downhole. The profiles in the allochthonous sediment sequence, to approximately 370 mbsf, the depth of the Miocene/Pliocene hiatus (see "Biostratigraphy" section, this chapter), are similar to those observed at the other deep-water tectonic sites cored during Leg 112. Except for dilution by dissociation of gas hydrates, which is more pronounced at Site 683, all the other chemical gradients are significantly more extreme at Site 688, compared with Sites 682, 683, and 685.

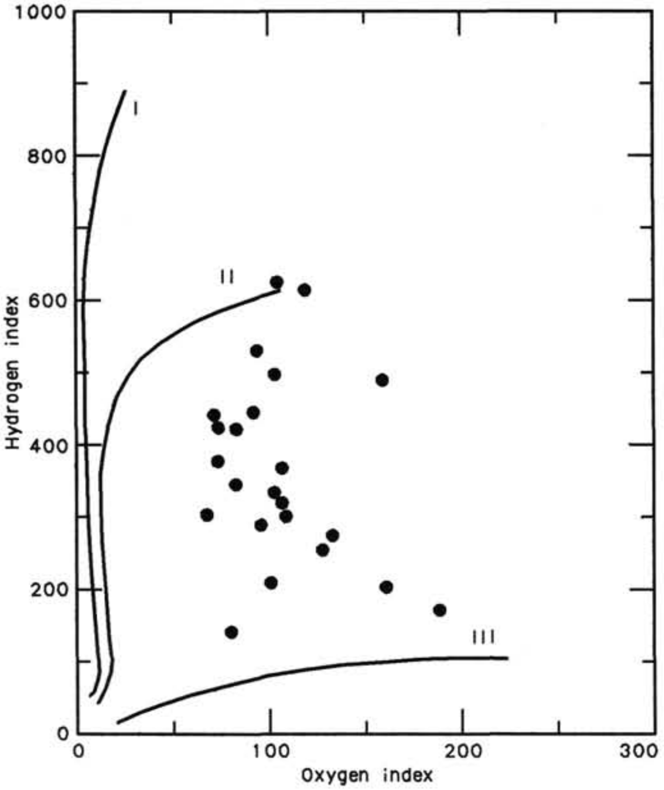

Figure 41. Hydrogen and oxygen indices (HI and OI) obtained from Rock-Eval pyrolysis of sediments from Site 688 and plotted on a van Krevelen-type diagram.

Below ~370 m, the concentrations and gradients are distinct from those above. This is obvious, especially with the Cl^-, Ca^{2+}, Mg^{2+}/Ca^{2+}, and silica concentration profiles shown in Figures 43, and 47 through 49, respectively.

The following sharp changes or reversals in chemical gradients occur at ~370 mbsf. This depth still remains in the stability field of marine gas hydrates, but is close to the lower boundary of the stability field (at about 500 mbsf at this site; Kvenvolden and McMenamin, 1980; and "Organic Geochemistry" section, this chapter). Cl^- shows a distinct freshening spike and concentrations remain generally low (below 500 mmol/L). Ca^{2+} concentrations increase sharply, and Mg^{2+} concentrations decrease sharply with depth. The slope of Ca^{2+} vs. Mg^{2+} concentrations is −1. Initially, silica increases, but then abruptly decreases at about 550 mbsf. Methane concentrations also indicate a distinct spike at this depth interval (see "Organic Geochemistry" section, this chapter). The freshening spike most probably indicates dilution with fresher water that originates from either dewatering of an accretionary complex at greater depth (Hanshaw and Coplen, 1973; Marine and Fritz, 1981) or dehydration of clay minerals and/or opal-A. Another possibility is that decomposing gas hydrates below the stability field produce freshwater. Inversely, strong Ca^{2+} and Mg^{2+} concentration gradients reflect chemical reactions with volcanogenic matter and/or with basement. The waters from below seem to be flowing out from within this zone, where the sediments are considerably more silty and sandy than those above (see "Lithostratigraphy" section, this chapter). The sediment section below ~370 m thus acts as a dewatering conduit at this lower slope of the Peru Trench section.

The previous record of 156.4 mmol/L in alkalinity, observed at Site 685, was short-lived. A new record alkalinity value of 265.7 mmol/L was determined at this site. A record ammonia concentration of 63.02 mmol/L has never been observed before in the history of scientific ocean drilling. Phosphate concentrations are also extremely high and reach 746.8 μmol/L. Similar high phosphate values were observed at Site 685.

Chloride and Salinity

The main cause of the progressive freshening with depth that we observed in Figure 43 (and also at all other gas-hydrate sites) is discussed in the "Inorganic Geochemistry" sections of the Site 682 and 683 chapters (Figs. 43 and 44; Tables 9 and 10). The Cl^- concentrations in the first 30 m of the section are about 3 to 4 mmol/L higher than the average seawater concentration. This probably reflects the expected chloride maximum immediately above the stability field of marine gas hydrates.

Two pristine *in-situ* interstitial-water samples were obtained at Site 688. These samples have higher Cl^- and salinity values than waters from adjacent squeezed sediment samples, which indicates less dilution by decomposing gas-hydrates, as expected (Table 11).

The salinity profile in the allochthonous sediment pile at this site is primarily controlled by the extreme alkalinity values that were observed. The correspondence between the salinity and alkalinity profiles between a depth of 6 and ~370 m is remarkable (Fig. 44). At greater depths, where alkalinity values decrease, salinity also decreases considerably; those alkalinity values that are significantly below seawater salinity are controlled by both decomposition of the gas hydrates and freshening that results from the dewatering and dehydrating of an accretionary complex or of subducted sediments below.

Alkalinity and Sulfate

Alkalinity values are unexpectedly high. Water samples of 2 mL, instead of 5 mL, were used for analyzing alkalinity (Fig. 45 and Table 10) Between measurements, the combination electrode was rested in seawater (IAPSO) for 30 to 60 min. The GRAN plot and titration record of Sample 112-688A-19X-3, 140–150 cm (at 174.20 mbsf) indicate that 264.65 mmol/L is the highest alkalinity value ever recorded in the history of the drilling program (see Fig. 46).

Such high alkalinity values trigger diagenetic carbonate reactions, which also affect the depth of the observed alkalinity maximum. Carbonate reactions and CO_2 reduction to CH_4 are the main reactions responsible for decreasing alkalinity with depth.

The sulfate-reduction zone is very thin at this site because of high sedimentation rates (>100 m/m.y.). At ~6 mbsf, sulfate concentration is below 5 mmol/L. From about 30 mbsf to the bottom of the site, sulfate concentrations are almost 0 mmol/L, and methane concentrations are high (see "Organic Geochemistry" section, this chapter). The slight (<1 mmol/L) sporadic increases in sulfate concentrations in five of the deepest samples may be caused by contamination with drill-hole water because all cracks in the rotary-drilled, indurated sediment samples were soaked with drill-hole water. We took special precautions for preparing samples before squeezing. However, very small contamination levels were unavoidable in a few of these deeper samples; the total volume of interstitial water recovered from these samples ranged between 1 and 5 mL.

Ammonia and Phosphate

Ammonia concentrations reach a record high value of 63.02 mmol/L at 192.88 mbsf (Sample 112-688A-21X-3, 108–118 cm), about 20 m below the alkalinity maximum. At Site 685, which held the previous alkalinity record value, the maximum NH_4^+ value determined was only 32.32 mmol/L, which is ~50% of the maximum value at Site 688.

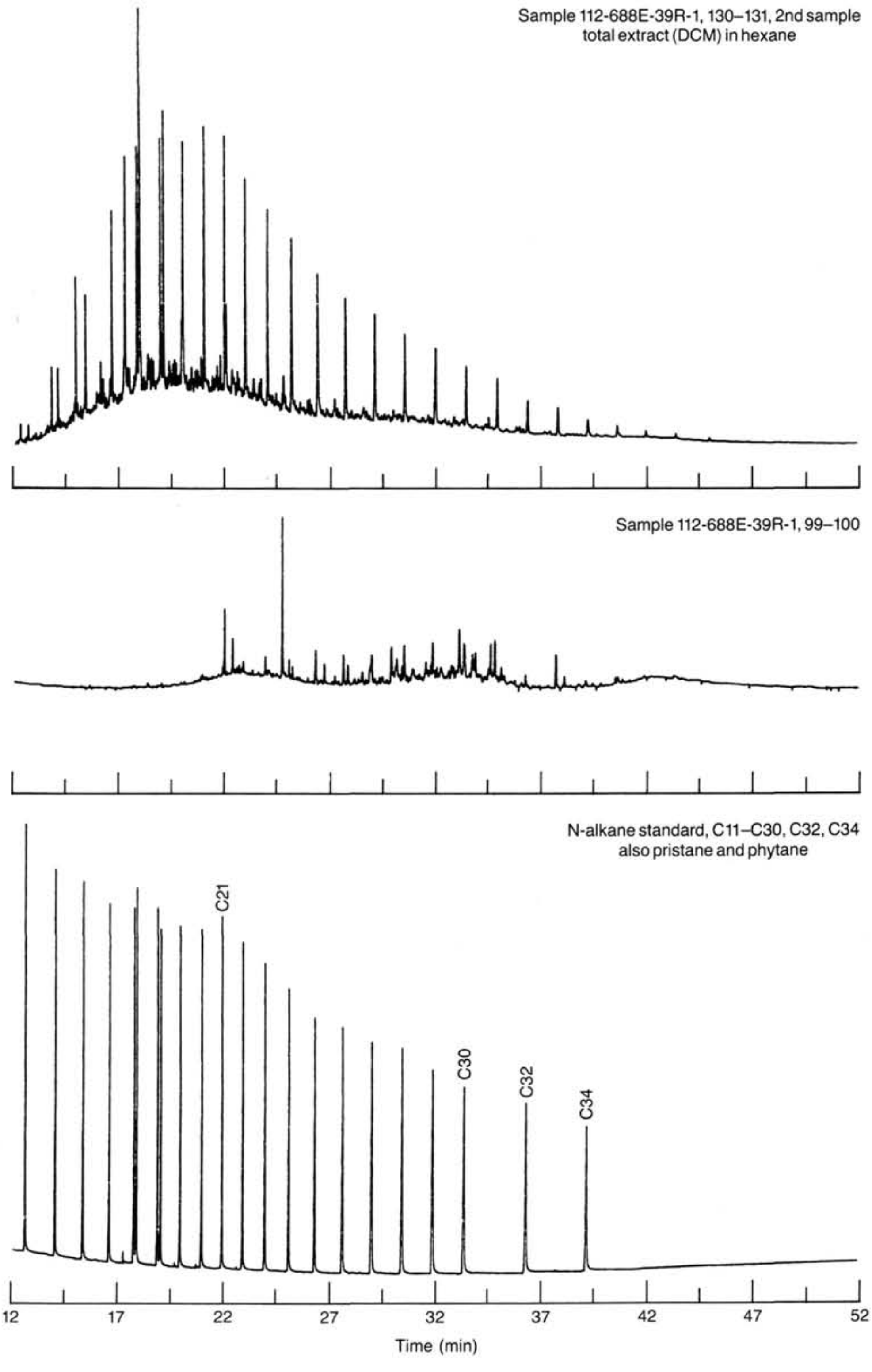

Figure 42. Gas chromatograms of extracts of Samples 112-688E-39R-1, 130–131 cm, and 112-688E-39R-1, 99–100 cm, in hexane and of a standard mixture of alkanes in hexane.

We observed a phosphate maximum at 104.7 mbsf, about 70 m above the alkalinity maximum. The depth sequence of concentration maxima of first phosphate, then alkalinity, and finally ammonia was maintained, even at this site of extremely high sedimentation rates in the Quaternary sequence.

Silica

The solubility of diatoms controls the silica concentration values between ~20 and 350 mbsf. We believe that opal-A dissolution rates control the silica values in the uppermost 20 m of

Table 9. Interstitial-water geochemical data for Site 688.

Core/section interval (cm)	Depth (mbsf)	Salinity (g/kg)	Cl^- (mmol/L)	Alkalinity (mmol/L)	SO_4^{2-} (mmol/L)	PO_4^{3-} (μmol/L)	NH_4^+ (mmol/L)	SiO_2 (μmol/L)	Ca^{2+} (mmol/L)	Mg^{2+} (mmol/L)	Mg^{2+}/Ca^{2+}
112-688A-1H-4, 145-150	5.95	33.8	563.82	28.44	4.48	45.68	3.20	920	7.35	50.51	6.87
3H-4, 145-150	23.75	36.3	562.86	70.35	1.59	187.97	10.07	1078	4.62	53.80	11.65
6H-3, 145-150	50.75	37.4	546.47	99.49	0.0	191.63	20.90	1248	4.61	55.41	12.02
9X-5, 140-150	82.20	40.8	544.54	153.31	0.0	554.51	34.24	1133	4.72	71.18	15.08
12X-1, 140-150	104.70	44.2	531.05	189.27	0.0	746.76	41.18	1080	6.12	85.41	13.96
16X-4, 140-150	147.20	47.2	528.16	244.46	0.0	462.56	52.07	1089	7.29	96.49	13.24
19X-3, 140-150	174.20	49.0	527.19	264.65	0.0	303.74	60.69	1104	7.51	98.84	13.16
21X-3, 108-118	192.88	48.3	522.38	265.68	0.0	175.52	63.02	1047	7.40	96.78	13.08
27X-4, 140-150	251.70	46.0	520.45	231.48	0.23	462.56	57.89	1082	6.52	86.78	13.31
30X-1, 115-125	275.45	44.5	517.56	220.95	0.0	178.36	56.65	1135	5.86	78.58	13.41
33X-3, 140-150	307.20	43.8	507.92	195.19	0.0	295.38	52.53	1186	6.32	70.07	11.09
112-688E-3R-4, 140-150	365.00	36.5	470.84	123.50	0.0	274.04	37.36	1254	2.92	45.20	15.48
6R-4, 140-150	393.50	34.2	493.12	101.30	0.46	141.55	31.31	1332	3.79	39.43	10.40
9R-5, 140-150	422.00	32.8	494.09	78.48	0.0	59.19	27.57	1359	5.93	29.48	4.97
12R-1, 140-150	450.50	32.2	483.43	66.91	0.32	20.10	25.08	1409	8.87	26.78	3.02
19R-3, 140-150	521.40	31.2	492.15	—	(1.24)	9.17	15.52	1322	15.27	25.45	1.67
23R-1, 140-150	556.40	30.0	487.51	—	0.54	7.60	10.60	993	18.58	22.78	1.23
27R-1, 140-150	594.40	30.2	502.81	—	0.32	—	—	632	25.59	20.71	0.70

Table 10. Interstitial-water chemical data squeezed from sediment samples compared with *in-situ* samples in Hole 688A.

Core/section interval (cm)	Depth (mbsf)	Salinity (g/kg)	Cl^- (mmol/L)	Alkalinity (mmol/L)	SO_4^{2-} (mmol/L)	PO_4^{3-} (μmol/L)	NH_4^+ (mmol/L)	SiO_2 (μmol/L)	Ca^{2+} (mmol/L)	Mg^{2+} (mmol/L)	Mg^{2+}/Ca^{2+}
112-688A-3H-4, 145-150	23.75	36.3	562.86	70.35	0	187.97	10.07	1078	4.62	53.80	11.65
In-situ 1	46.30	37.5	550.33	97.96	0	122.16	18.46	1100	5.04	57.64	11.44
6H-3, 145-150	50.75	37.4	546.47	99.49	0	191.63	20.90	1248	4.61	55.41	12.02
16X-4, 140-150	147.20	47.2	528.16	244.46	0	462.56	52.07	1089	7.29	96.49	13.24
In-situ 2	160.30	49.3	533.94	261.65	0	128.20	54.98	1106	7.84	103.36	13.18
19X-3, 140-150	174.20	49.0	527.19	264.65	0	303.74	60.69	1104	7.51	98.84	13.16

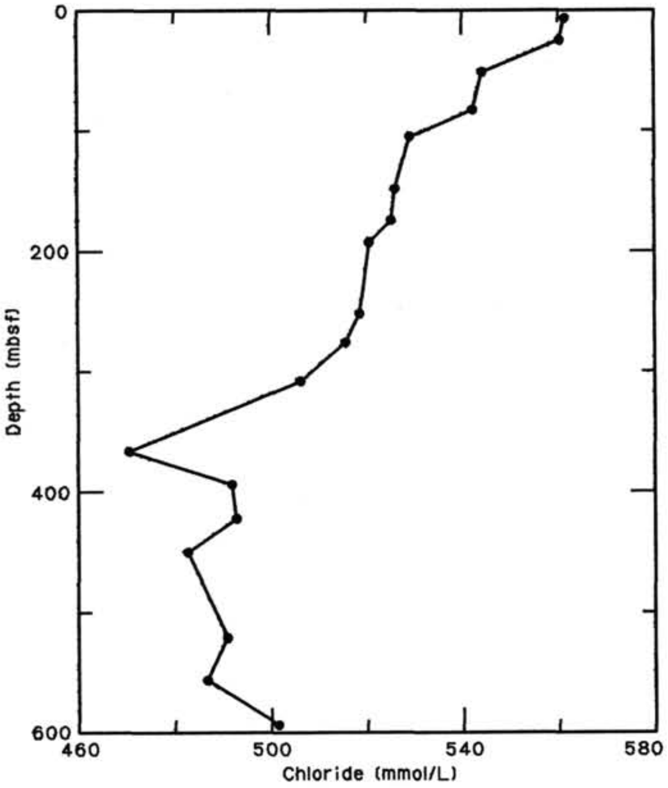

Figure 43. Interstitial chloride for Site 688.

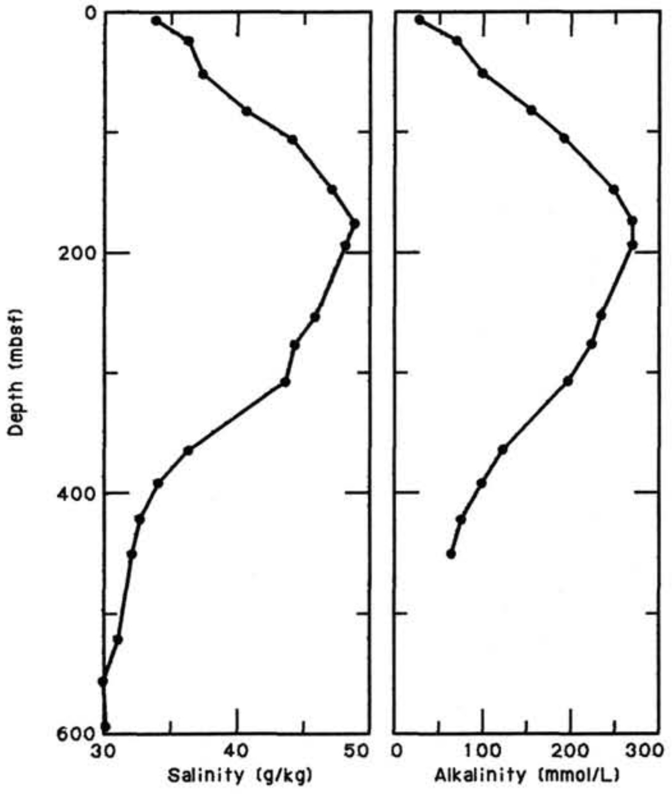

Figure 44. Interstitial salinity and alkalinity for Site 688.

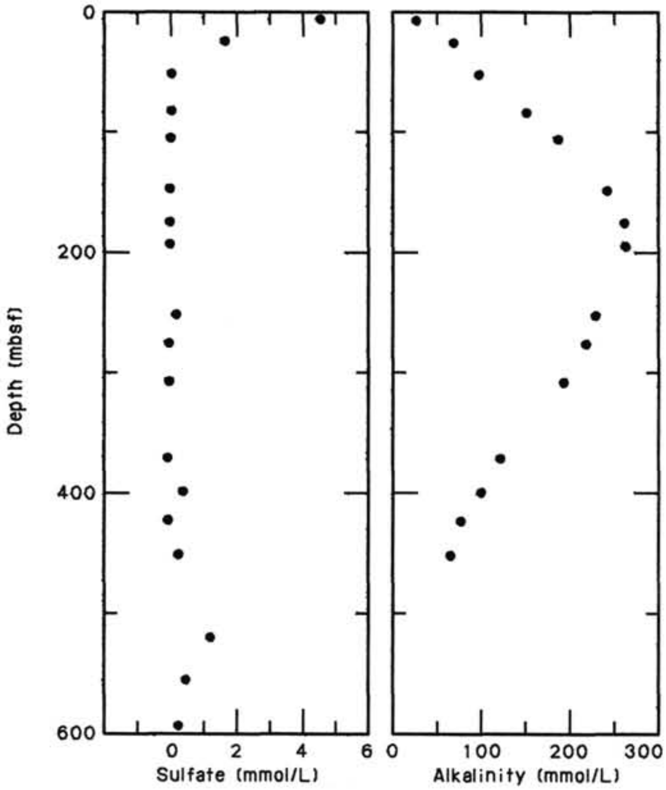

Figure 45. Interstitial sulfate and alkalinity for Site 688.

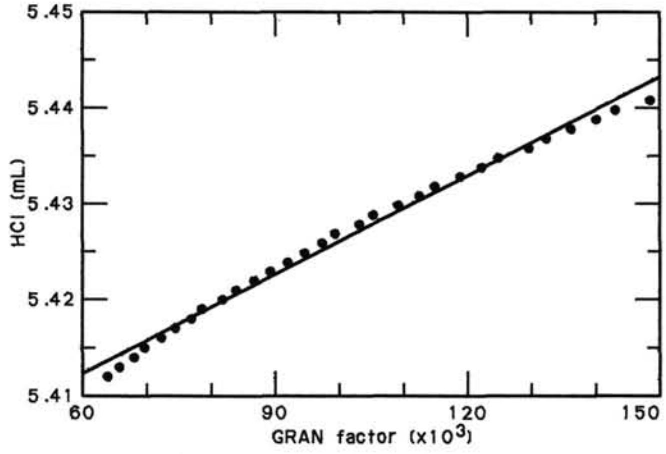

Figure 46. GRAN plot and titration alkalinity record for Sample 112-688A-19X-3, 140–150 cm.

the hole (Fig. 48 and Table 9). In the uppermost 20 m, opal-A dissolution rates control silica values. Silica values are significantly higher between about 350 to ~500 m; these values range between 1250 and 1410 μmol/L. Within this depth interval, diatoms are abundant and well preserved (see "Biostratigraphy" section, this chapter). The section with abundant, well-preserved diatoms continues to 577 mbsf, while silica values decrease sharply from 1409 to 993 μmol/L at 556 mbsf. This value is below the solubility of opal-A at the *in-situ* pressure and temperature. Between 584 and 612 mbsf, diatoms are still common and moderately preserved, while below 612 mbsf, the sediments are barren of diatoms (see "Biostratigraphy" section, this chapter). Silica concentrations decrease sharply within this zone.

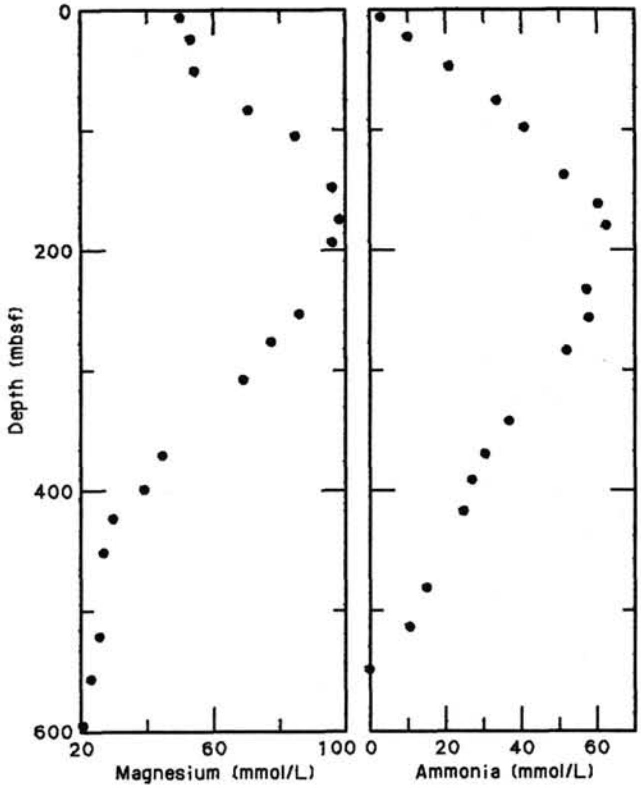

Figure 47. Interstitial magnesium and ammonia for Site 688.

The behavior of the silica profile below ~350 mbsf suggests that the advecting waters also are rich in silica. The depth zone between 350 and ~500 mbsf is probably a mixing zone between the two solutions. This continuous water flow affects the diatoms below the zone, where they dissolve more rapidly than in the upper section, which is controlled only by diffusion; eventually, all the siliceous remains will dissolve and disappear from the silty-sandy section.

Calcium and Magnesium

The reaction scheme of carbonates characteristic to this sedimentological and tectonical environment was discussed in detail in the Site 682 and 683 chapters.

Here, an unusual increase in Mg^{2+} concentrations to a maximum level of 98.8 mmol/L at 174 m is caused by an ion-exchange reaction driven by the extreme ammonia concentrations that were observed (Figs. 47, 49, and 50; Table 9). The correspondence between the Mg^{2+} and NH_4^+ profiles (between 100 and 300 mbsf) is indicated in Figure 47. The distinct water masses discussed in the introduction are clearly seen in the Ca^{2+}, Mg^{2+}, and Mg^{2+}/Ca^{2+} profiles shown in Figures 49 and 50.

In a Quaternary sequence between ~193 and 307 mbsf, significant decreases in Mg^{2+} concentrations were observed (from 96.8 to 70.1 mmol/L). The gradient of decrease is 2.3 mmol/L (Fig. 49). Within the same depth interval, Ca^{2+} concentrations are almost constant and show an insignificant decrease of only 1.1 mmol/L (from 7.4 to 6.3 mmol/L). This appears to be a zone of calcite dolomitization. The decreases in the Mg^{2+}/Ca^{2+} ratio are small and suggest that the amount of dolomite formed per unit of sediment volume is not large.

Between 365 and 594 mbsf, in the section influenced by these advecting fluids, Ca^{2+} concentrations increase from 2.9 to 25.6 mmol/L, at an average gradient of 1 mmol/L/10 m; Mg^{2+} concentrations decrease from 45.2 to 20.7 mmol/L, again at an average gradient of 1 mmol/L/10 m. The Ca^{2+} vs. Mg^{2+} slope

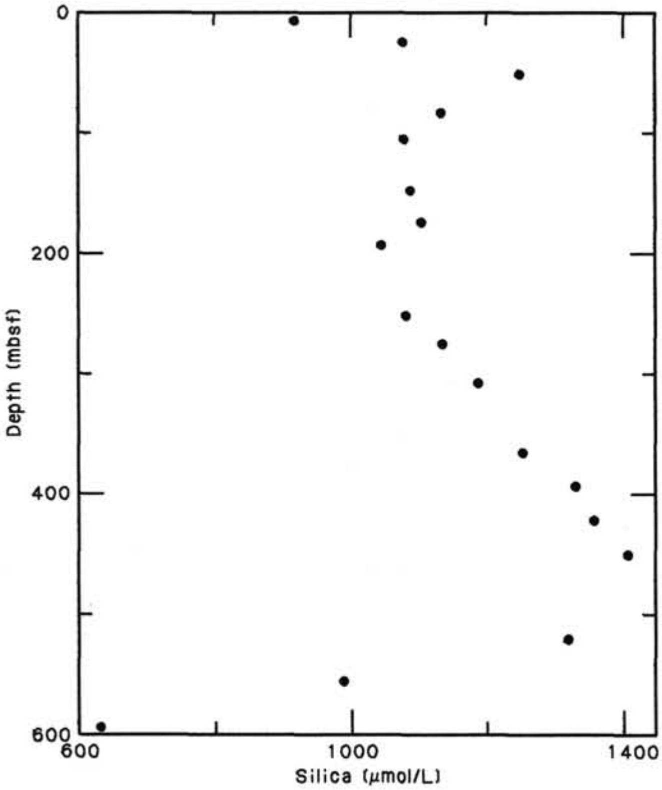

Figure 48. Interstitial silica for Site 688.

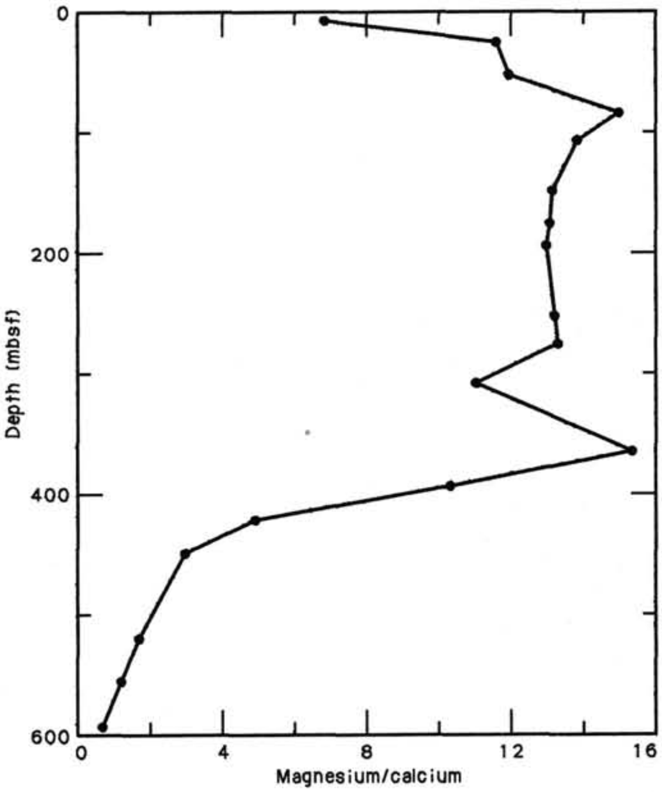

Figure 50. Mg^{2+}/Ca^{2+} ratio for Site 688.

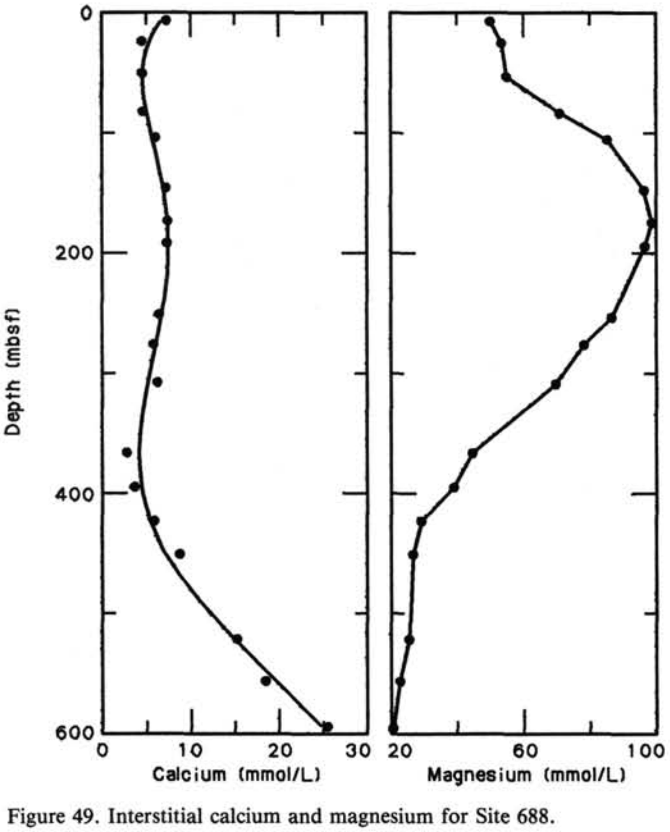

Figure 49. Interstitial calcium and magnesium for Site 688.

equals −1, which is a typical volcanogenic and/or basement signal (see review by Gieskes, 1983).

The large increases in Ca^{2+} do not seem to be controlled by calcite dissolution; the observed concentrations are above the calcite solubility at the *in-situ* temperature and pressure; however, alkalinity does not increase, but even decreases.

The sharp inverse Ca^{2+} and Mg^{2+} gradients are reflected in the steep slope of the profile for Mg^{2+}/Ca^{2+} ratios (Fig. 50). At 450 mbsf, the ratio is 3. With ratios between 1 and 3, one can expect co-formation of dolomite and calcite for kinetic reasons. Below a ratio of 1 (at this site below ~560 mbsf), only calcite is stable. Calcite cementation and calcite veins are common within this depth interval; calcite cementation of sandstone is pervasive (see "Lithostratigraphy" section, this chapter).

Chemistry of Gas Hydrates

On the basis of chemical gradients within the depth interval 82.2 to 174.2 mbsf, Samples 112-688A-9X-5, 140–150 cm through 112-688A-16X-4, 140–150 cm, and the chemistry of the interstitial waters at 141 mbsf, the chemistry of the three hydrate samples recovered at this site from Core 112-688A-15X, is as follows:

Salinity	46.8 (g/kg)
Cl^-	528.6 (mmol/L)
NH_4^+	51.5 (mmol/L)
SiO_2	1088 (μmol/L)
PO_4^{3-}	500.5 (μmol/L)
Ca^{2+}	7.2 (mmol/L)
Mg^{2+}	94.9 (mmol/L)
Mg^{2+}/Ca^{2+}	13.2

Table 11. Chemical data of gas hydrates and of nearby interstitial waters from squeezed sediments, Site 688.

Core/section interval (cm)	Type	Depth (mbsf)	Salinity (g/kg)	Cl^- (mmol/L)	SO_4^{2-} (mmol/L)	PO_4^{3-} (μmol/L)	NH_4^+ (mmol/L)	SiO_2 (μmol/L)	Ca^{2+} (mmol/L)	Mg^{2+} (mmol/L)	Mg^{2+}/Ca^{2+}
112-688A-12X-1, 140-150	Squeezed sediment	104.7	44.2	531.05	0	746.76	41.18	1080	6.12	85.41	13.96
15X-7A	Gas hydrate	~141	7.8	90.60	0	139.95	12.34	449	1.48	12.54	8.47
15X-7C	Gas hydrate	~141	11.8	136.86	0	61.69	15.08	491	1.35	18.07	13.39
15X-7B	Gas hydrate	~141	20.0	232.27	0	75.92	34.43	635	2.42	28.36	11.72
16X-4, 140-150	Squeezed sediment	147.2	47.2	528.16	0	462.56	52.07	1089	7.29	96.49	13.24

The percent of dilution for the three gas-hydrate samples (112-688A-15X-7A, -7B, and -7C) by interstitial water is calculated for each component analyzed in the following table:

Percent Dilution by Interstitial Water

Gas-hydrate samples	Salinity (g/kg)	Cl^- (mmol/L)	NH_4^+ (mmol/L)	SiO_2 (μmol/L)	PO_4^{3-} (μmol/L)	Ca^{2+} (mmol/L)	Mg^{2+} (mmol/L)
15X-A	16.7	17.1	24.5	41.3	28.0	20.6	13.3
15X-B	25.2	25.9	29.9	45.1	12.3	18.8	19.1
15X-C	42.7	43.9	68.3	58.4	15.2	33.6	29.9

Results for salinity and chloride are practically the same. Calculated percentage of dilution for ammonia and silica are systematically higher than for salinity and chloride. This strongly suggests that, in addition to methane, ethane, and ice, these gas-hydrate samples also contain ammonia and silica.

Except for phosphate and calcium in Sample 15X-7A, the calculated percentage of dilution for phosphate, Ca^{2+}, and Mg^{2+}, is significantly lower than that of salinity and chloride. Because of their high reactivity, these substances may have been involved in almost instantaneous inorganic reactions triggered by the pressure-temperature changes induced by coring and sample handling.

PALEOMAGNETICS

Introduction

The shipboard paleomagnetic study for Site 688 yielded results distinctly different from those of previous Leg 112 holes. The pattern in previous holes was a decrease in the intensity of magnetization to a level below which the Molspin spinner magnetometer could not measure, usually at a depth, just below the Brunhes-Matuyama boundary. In Hole 688A, the magnetic intensity decreased at this depth, but then strengthened; thus, with appreciable recovery, we were able to obtain good results from all cores. We believe that the presence of iron monosulfides in cores is partially responsible, which implies that magnetization is linked to diagenesis. In Hole 688E, we were able to measure samples from the first few cores, below which the signal deteriorated and accurate measurements with the Molspin were not possible.

Holes 688A and 688E constitute by far the longest interval of core from which we obtained paleomagnetic measurements during Leg 112, although many voids exist even in one of the most completely recovered intervals. This paleomagnetic signal may tell us more about diagenetic processes involving the production of iron sulfides than the chronology of the cores. The magnetic data from Site 688 thus may be the most difficult to interpret.

Results

The declination, inclination, and intensity of magnetization are plotted vs. depth in Figure 51. A wide range of intensities can be seen in the samples. In Figure 51, the data were filtered so that only measurements taken after an alternating-field (AF) treatment of 150 Oe (15 mT) remain. Note that intensity declines in the first few cores of Hole 688E, which is below the sensitivity of the Molspin. This was also observed in other sites during Leg 112. Another interesting feature is that samples down to Section 112-688A-29X-5, far downhole and having an intensity greater than 2.0 mA/m, are normally magnetized (Fig. 51). Below that point, both normally and reversely magnetized samples have magnetizations greater than 2.0 mA/m. If the magnetization of these samples is owing to the presence of iron sul-

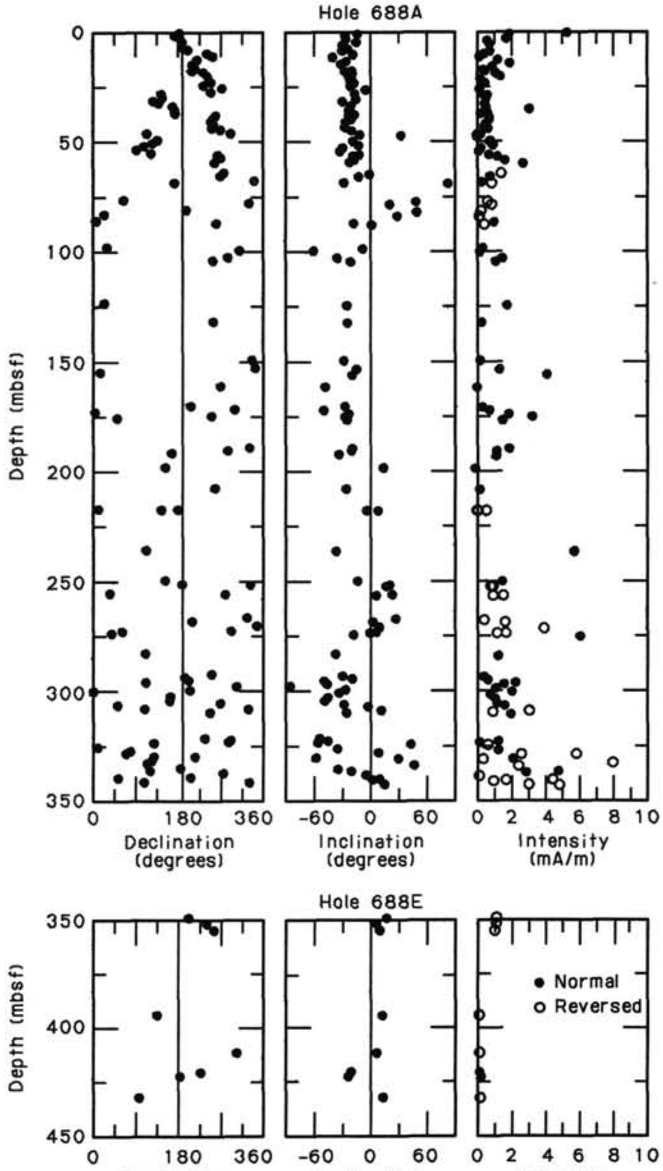

Figure 51. Declinations, inclinations, and intensities for samples from Holes 688A and 688E after an AF treatment of 150 Oe. Only statistically significant measurements are included.

fides, then the polarity changes observed downhole may represent the timing of the monosulfide formation.

An attempt at defining a reversal chronology for Site 688 is presented in Figure 52. However, because of the diagenesis care must be used when applying these results to a time scale. Holes 688A and 688E are abutted at a depth of 350 m in Figure 52. This depth is where coring began in Hole 688E. Selected lithologic features were added to the diagrams. Several reversals can be seen in these data. First, is the Brunhes/Matuyama boundary in Section 112-688A-9X-2. However, below Section 112-688A-11X-14, magnetization again has normal polarity; this polarity is predominant down to Core 112-688A-23X. One possibility for this predominance of normal polarity is that much of this section of the core was remagnetized during the Brunhes Normal Chron. Several hypotheses can be stated as follows:

1. Zones where the core is black (between Cores 112-688A-11X and 112-688A-23X) indicate that iron sulfides are probably present and are predominantly of normal magnetization. In deeper cores, several reversed intervals can be seen. This may indicate that the normal overprinting associated with iron sulfides is weaker or fades at depth. It may also indicate that the iron sulfides in the deeper intervals were formed and acquired their magnetization during a reversed period.
2. The first occurrence of pervasive iron sulfide impregnation coincides with a reversal in polarity from reversed to normal.
3. The occurrence of dark gray and dark olive gray mud in Sections 112-688A-27X-5 to 112-688A-29X coincides with a reversed interval.
4. Two lithologic boundaries coincide with magnetic reversals. These are the Unit I/Unit II boundary at 338 mbsf in Hole 688A and the Subunit IIB/Subunit IIC boundary in Hole 688E. This may be coincidence but is often an indication that the boundary reflects a hiatus. Between lithologic Units I and II, however, this contact coincides with the basal occurrence of the black mud. The reversal thus may be related to the presence of iron sulfides and does not reflect a stratigraphic boundary.

What these points seem to indicate is that the iron sulfides were either generated diagenetically and recorded the field at the time of their formation, or that the lower cores contain complex magnetization made up of two or more magnetic phases. One may be the original magnetization of the samples. In some cases, the observed magnetizations may be related to the presence or absence of a diagenetic process. For this reason, the first reversal was labeled a maximum depth for the Brunhes-Matuyama boundary. Evidently, this is the boundary because none of the samples from higher in the hole exhibit any indication of a reversed magnetization. The sedimentation rate predicted by paleontological investigation during the Quaternary is certainly high enough to allow for this possibility (>100 m/m.y.).

Other interpretations of the reversal pattern shown in Figure 52 require that a hiatus at the base of Core 112-688E-9R represent a considerable length of time. The required break would abut the Matuyama Chron with either the Olduvai Chron or the Gauss Chron, a gap of either 0.9 Ma or 1.5 Ma, with little supportive paleontological evidence. Other evidence indicates that post-depositional remagnetization occurred in these cores (discussed next). Results from samples in the major intervals shown in Figure 52 are presented and described in the next section.

Discussion of Zijderveld Plots

Zijderveld plots, intensity of magnetization vs. AF treatment, and stereonets of directions of magnetization are shown in Figure 53 and discussed below.

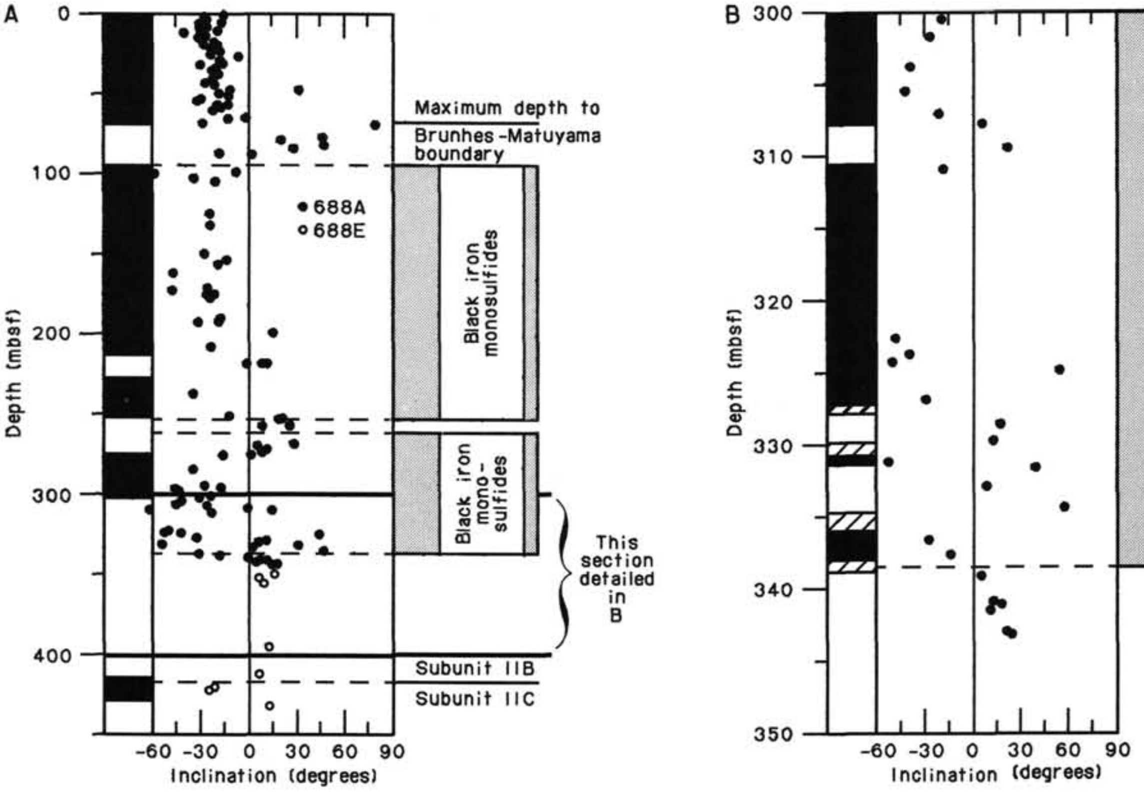

Figure 52. A) The inclinations of samples from Holes 688A and 688E. Some lithologic information is included, and the polarity of the magnetization has been added; black indicates normal and white indicates reversed intervals. B) Details of the lower portion of Hole 688A also are shown.

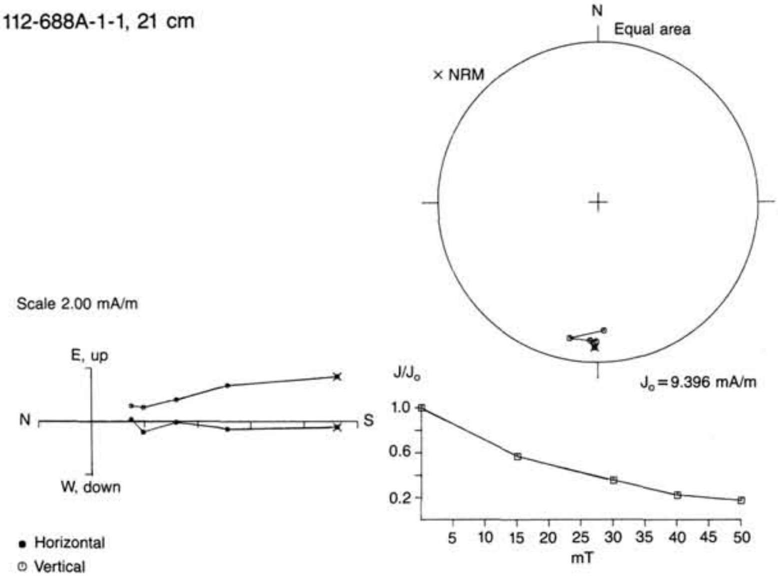
112-688A-1-1, 21 cm

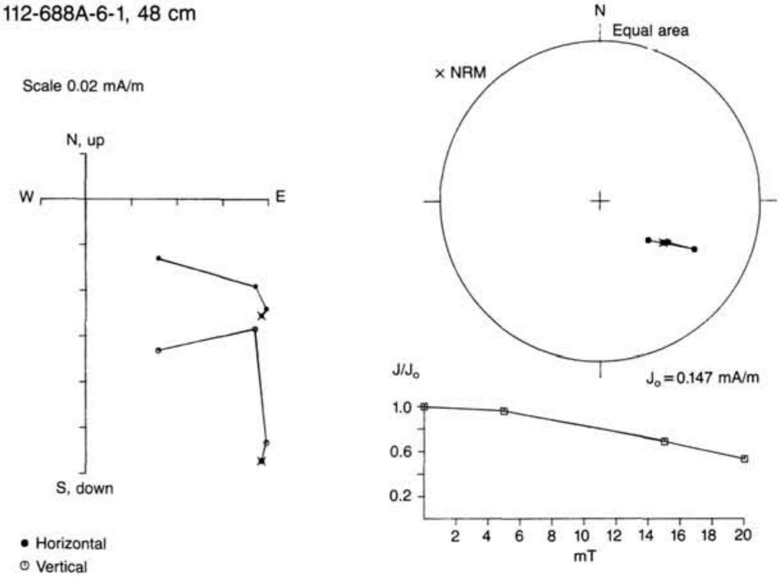
112-688A-6-1, 48 cm

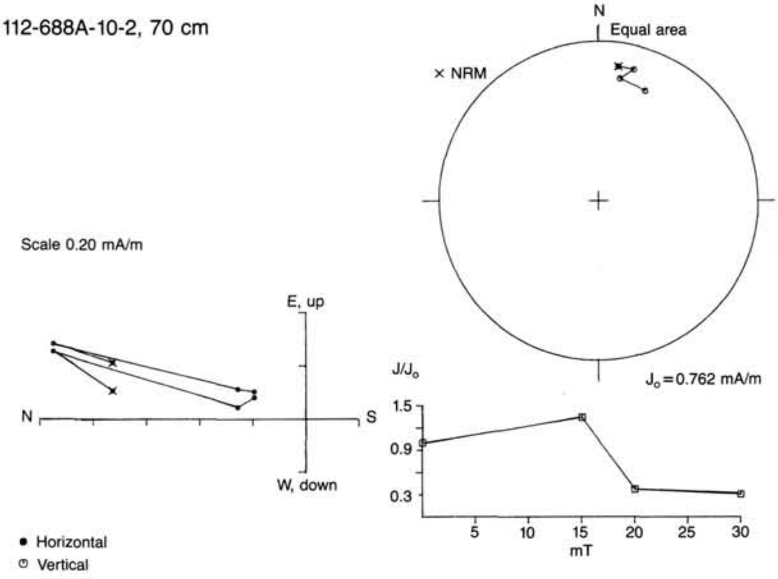
112-688A-10-2, 70 cm

Figure 53. A series of Zijderveld, stereonet, and intensity plots. Each summarizes the results from a single sample typical of an interval of core. See text for discussion.

112-688A-17-2, 71 cm

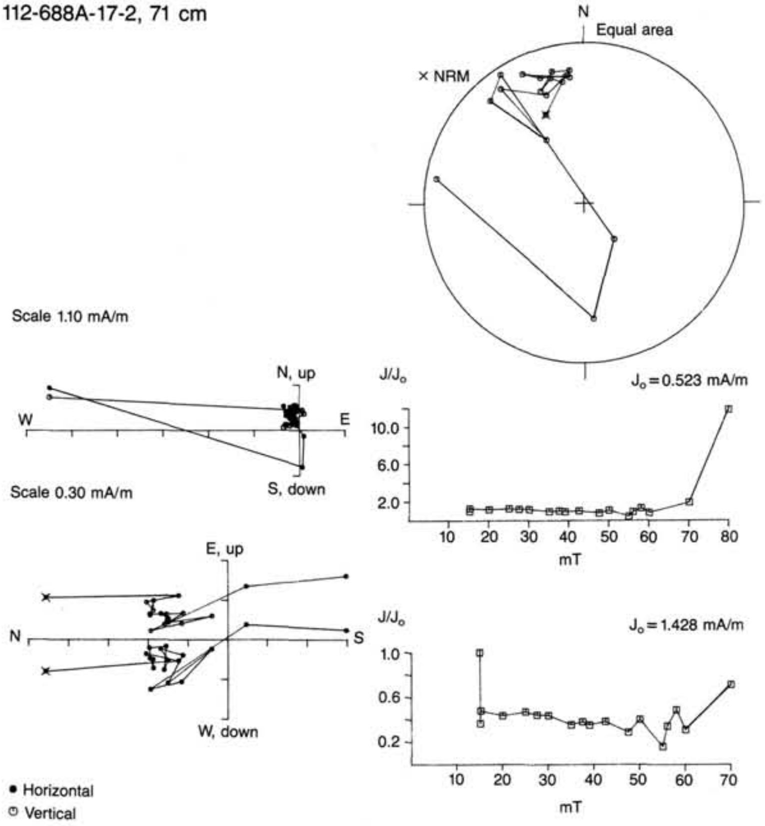

112-688A-24-1, 75 cm

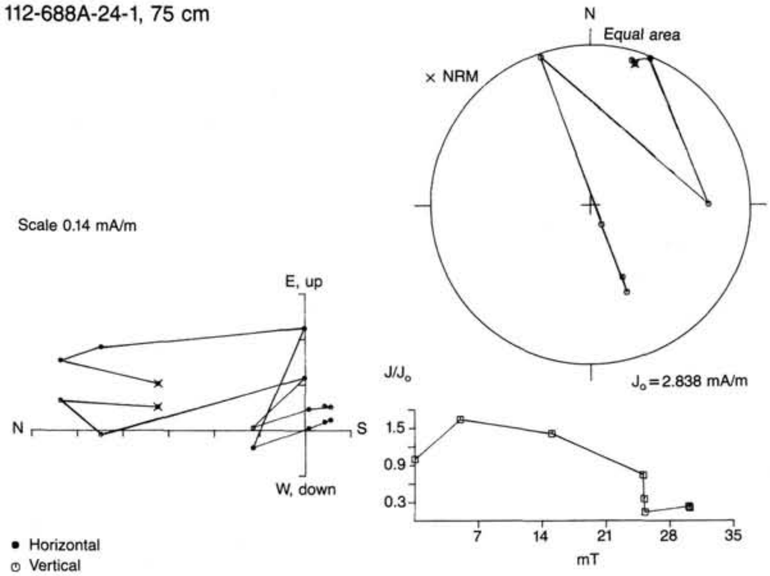

Figure 53 (continued).

1. Sample 112-688A-1H-1, 21 cm (0.21 mbsf); this sample shows a decay consistent with a single magnetization of normal polarity from very near the mud line.

2. Sample 112-688A-6H-1, 48 cm (46.78 mbsf); this sample is within the normally magnetized interval above the first reversal. The decay is certainly not classic, but the direction indicated is consistent. However, a large, circular standard deviation of 20.2 warrants caution when interpreting these results.

3. Sample 112-688A-10X-2, 70 cm (86.50 mbsf); this sample is from just below the first reversed interval of Hole 688A and exhibits a decay consistent with the presence of two magnetizations of opposite polarity but similar direction. The increased intensity between the natural remanent magnetization (NRM) and 150-Oe measurements and the Zijderveld plot supports this finding. The normal component of the magnetization is stronger. We are tempted to assign the status of overprint to the reversed magnetization.

4. Sample 112-688A-17X-2, 71 cm (153.01 mbsf); this sample is from the black mud and exhibits a magnetization that remains fixed in orientation to high AF treatments (roughly 550 Oe). The direction changes slightly in different treatments and indicates that the sample was not successfully demagnetized.

112-688A-24-1, 74 cm

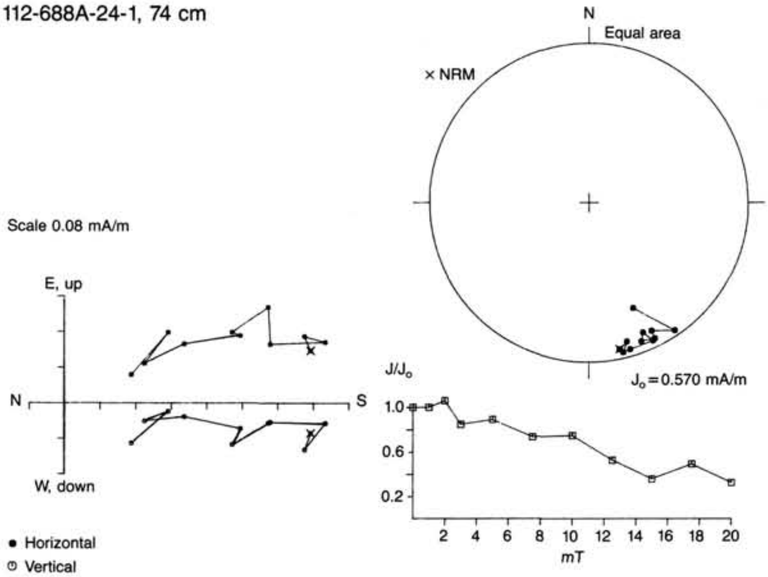

112-688A-24-1, 61 cm

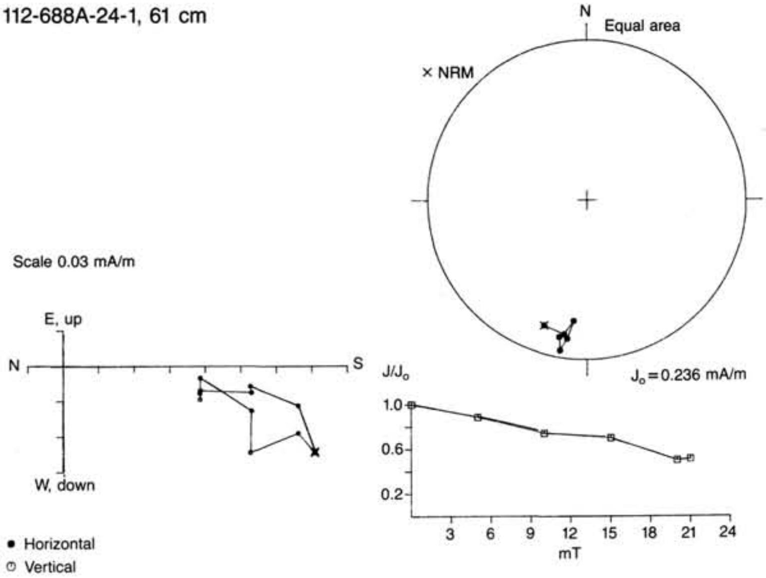

112-688A-21-1, 75 cm

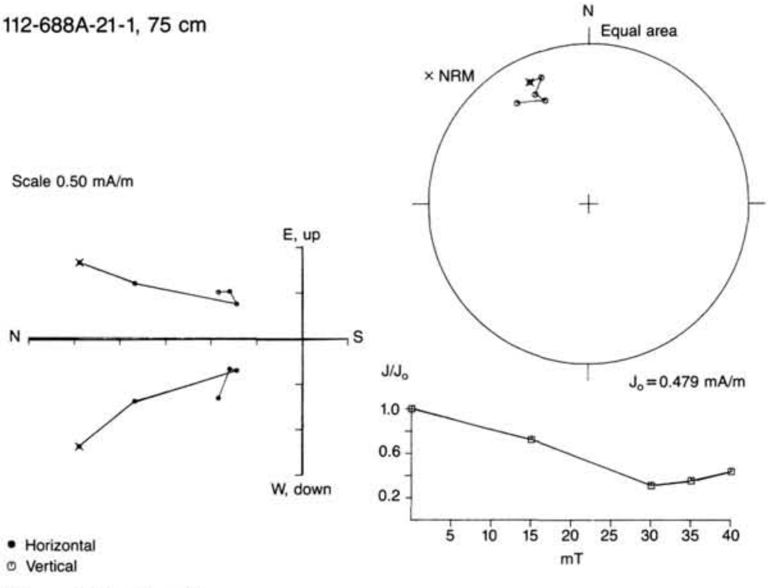

Figure 53 (continued).

112-688A-27-5, 70 cm

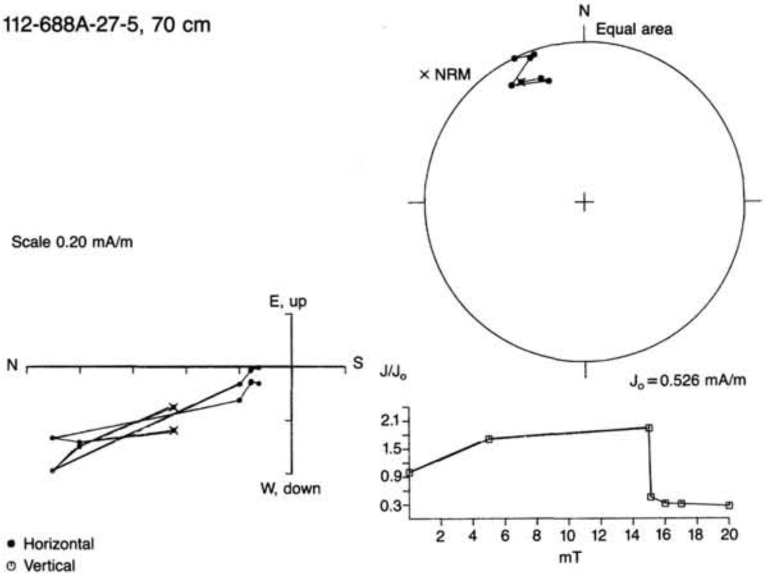

112-688A-29-7, 18 cm

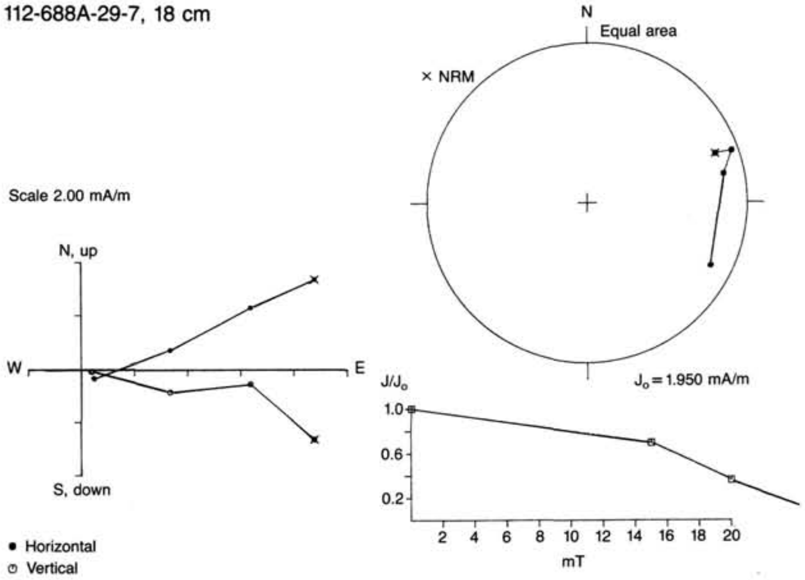

112-688A-30-1, 68 cm

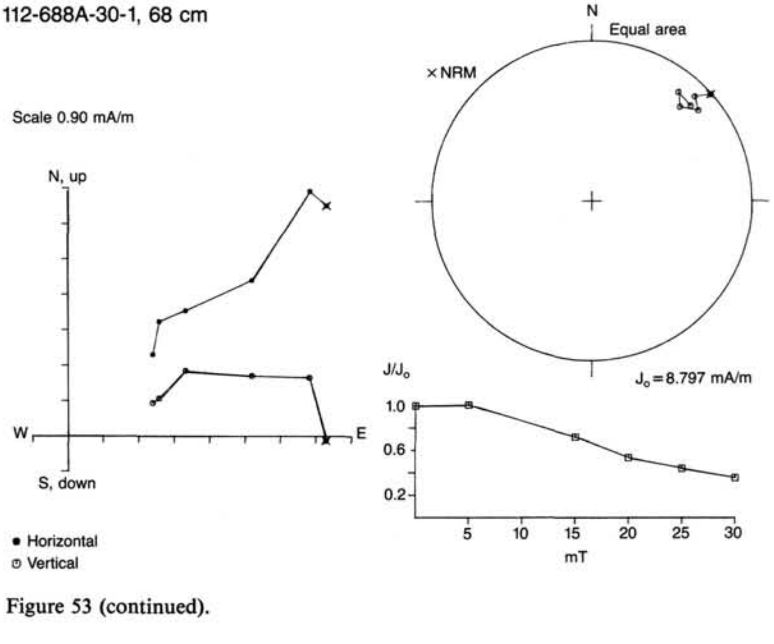

Figure 53 (continued).

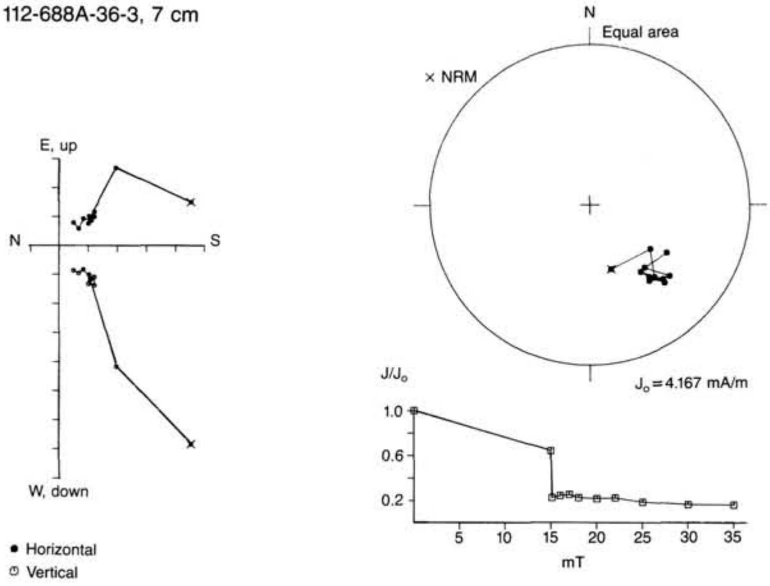

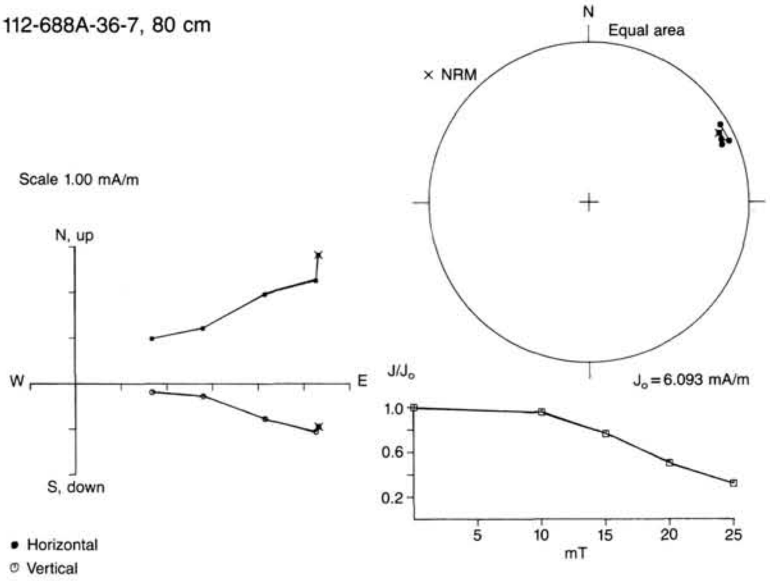

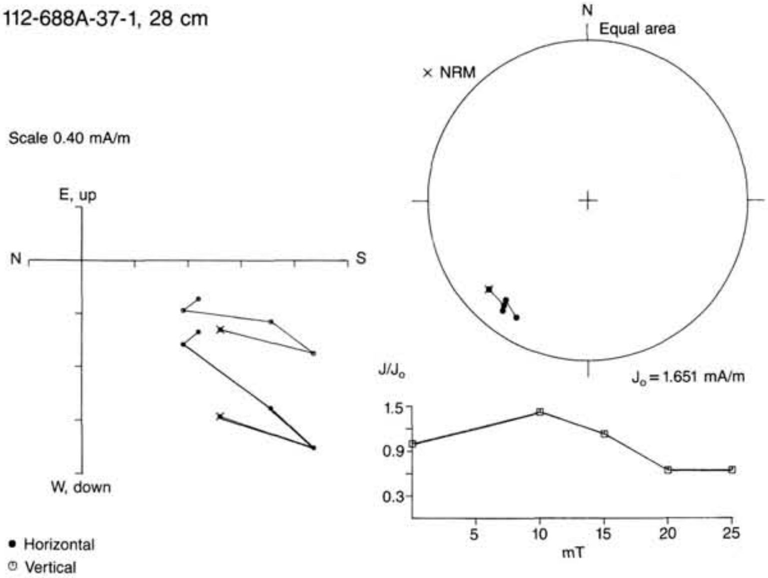

Figure 53 (continued).

Thermal demagnetization of some of these specimens will be tried during shore-based studies. This pattern suggests that hematite or pyrrhotite is the magnetic carrier.

5. Samples 112-688A-24X-1, 75 cm (218.05 mbsf); 112-688A-24X-1, 61 cm (217.91 mbsf); and 112-688A-24X-1, 74 cm (218.04 mbsf); these three samples were retrieved from Core 112-688A-24X, which recovered only 1.2 m of sediments. The first sample selected was at 75 cm and although it depicted erratic behavior during demagnetization, the last three steps fall on a great circle. This pattern indicates the presence of two magnetizations, both of which are being destroyed in a similar way by the successive AF steps. Thus, one sample contained both a normal and a reversed component, and two samples were retrieved from a nearby core to see if they were reversely magnetized. Though neither sample shows excellent decay, both exhibit positive inclinations and indicate that they carry a reversed magnetization. This also indicates that other reversely magnetized intervals in the black mud may have been missed and that more detailed sampling is required to locate them.

6. Sample 112-688A-21X-1, 75 cm (189.55 mbsf); a sample from within the black mud interval that exhibits a straightforward decay and is normally magnetized.

7. Samples 112-688A-27X-5, 70 cm (252.50 mbsf) and 112-688A-29X-7, 18 cm (273.98 mbsf); these samples are from a lighter interval within the black muds of Subunit IB. Both indicate a reversed polarity. The former also shows a normal overprint and reduced intensity over a period of two days.

8. Sample 112-688A-30X-1, 68 cm (274.98 mbsf); this sample shows a normal magnetization and a simple intensity plot.

9. Samples 112-688A-36X-3, 7 cm (334.37 mbsf) and 112-688A-36X-7, 80 cm (340.80 mbsf); both these samples are reversely magnetized. The intensity plot of the former shows that the intensity decreased over the time between the initial 150-Oe treatment and the second treatment, which suggests a viscous component in this sample. Both samples have reasonably good decays and a single direction of magnetization.

10. Sample 112-688A-37X-1, 28 cm (341.08 mbsf); this sample is reversely magnetized but displays a Zijderveld plot and intensity curve consistent with the presence of two magnetizations: a stronger reversed component and a weaker, more easily destroyed normal component.

Discussion

The correlation between the iron sulfide-bearing black mud and the reversal pattern of Figure 52 is compelling evidence that at least some, if not all, reversals in Holes 688A and 688E were generated by diagenetic processes that produced iron sulfides. The Brunhes-Matuyama boundary is the only date we obtained from the paleomagnetic data at this site. This is a maximum depth, although indications are that it is close to the true depth. Further dating may be possible after more detailed sampling and more precise measurements are conducted during shore-based studies. By combining studies about diagenetic processes and paleomagnetic data, we may be able to supply a chronology of diagenesis from Site 688.

Core Orientation

We were able to orient a structure using paleomagnetic measurements with a fault surface having slickensides that was found in Sample 112-688A-37X-2, 68–73 cm. A sample was retrieved from the working half of the same drilling biscuit. The direction of magnetization obtained from this sample was used to determine the true orientation of the fault. Procedures are discussed in the "Lithostratigraphy" section (this chapter).

Orienting a core using the paleomagnetic information obtained from a single sample depends greatly on the quality of the results for the sample and on the care taken during sampling. The accuracy of a single measurement as an orienting tool can be shown by looking at measurements of samples taken from APC cores. In Hole 688A, the first seven cores were recovered using the APC tool. Figure 54 shows the declination values obtained from these cores. The measurements indicate that the cores do indeed act as reasonably coherent pieces. Some scattering can be correlated with drilling disturbance and gaps in the cores. The data show that a single measurement could orient a core to ± 15°. Assuming no obvious breaks in continuity, several measurements over the length of a core should provide an excellent orientation for a core. When obvious breaks do occur, local sampling should be undertaken to orient specific features. When orienting a feature in a small biscuit, the retrieved sample certainly is local, and the orientation most probably is as accurate as that of a single measurement performed on an APC core.

Paleomagnetic Orientation

The fault at Sample 112-688A-37X-2, 66–73 cm, was found in a drilling biscuit of mudstone roughly 7 cm in length and thus unlikely to be inverted during drilling. One can see it best in the archive half of the core. An oriented sample (a 6-cm^3 minicube) was retrieved from the working half of the same biscuit and treated as a standard paleomagnetic sample with the goal of determining the original orientation of the biscuit and of the fault. Measurements of up to 30 mT were conducted during AF demagnetization.

Results of these magnetic measurements are shown in Figure 55. The sample proved to be excellent for our purposes. Aside from a small normal component that disappears at a low level of demagnetization, the magnetization is reversed (positive inclination, Southern Hemisphere). This combination indicates that the biscuit almost certainly is not inverted. The direction of magnetization, determined by a least-squares fit to the treat-

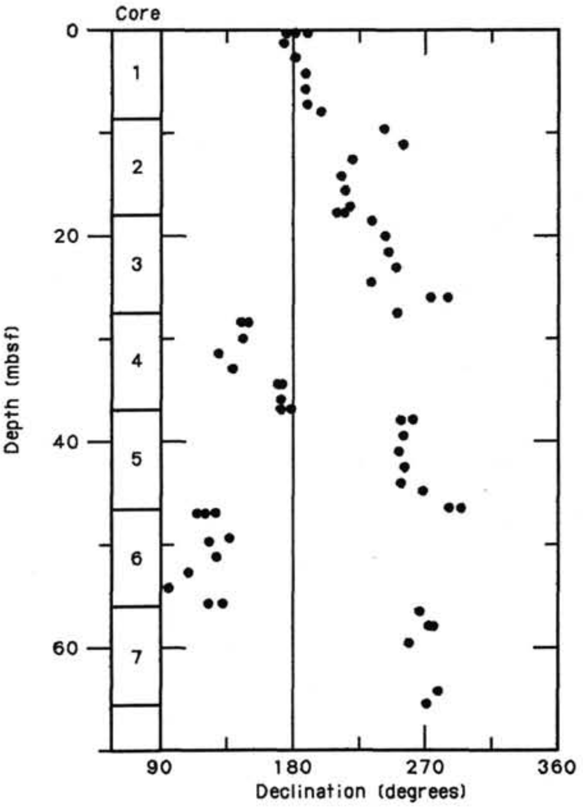

Figure 54. Declination data from the APC-cored interval in Hole 688A.

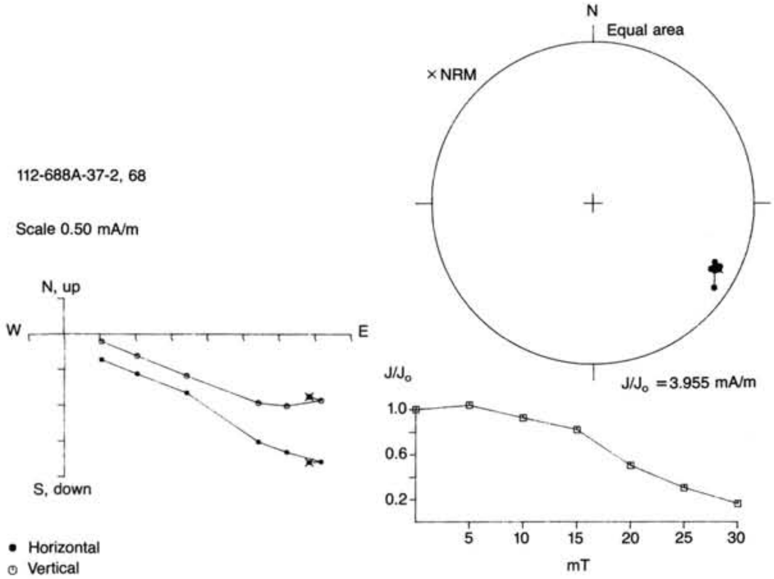

Figure 55. Paleomagnetic results from Sample 112-688A-37X-2, 68 cm, from Hole 688A. Plots are (1) Zjiderveld plot, (2) intensity vs. AF treatment value, and (3) a stereonet of the directions of magnetization. Treatments over 100 mT define a magnetization with a direction having a declination of 118° (wrt core) and inclination of 14°.

ments above 15 mT, is a declination of 118° (with respect to the core) and an inclination of 14°. The reversed polarity is consistent with nearby samples. Although the inclination is lower than anticipated for this site (22°), it is not inconsistent with the range in values observed during Leg 112. This magnetization must be aligned with the geographic south to obtain the orientation of the fault.

Orientation of the core by measuring a single sample is unusual enough to warrant discussion. This particular sample has a well-defined magnetization that is at least as old as the Brunhes/Matuyama boundary and that is stable in orientation up to treatments of 30 mT. The magnetization was probably acquired diagenetically, which represents a reasonable time average. This is further supported by evidence from APC cores of similar but less indurated sediments from this hole and previous holes that show declinations often consistent to within 10° over the length of the core. Part of the error was incurred when splitting and sampling the cores. We took care to be consistent, but a misalignment of 5° is certainly possible. A lesser problem is the rare occurrence of assignment of the working half to the archive half and vice versa. However, this should be checked. If reasonable care was taken in sampling, with a sample exhibiting a well-defined magnetization, the error in alignment of the core from a single sample is probably 10° to 15°.

Figure 28, which is a projection (lower hemisphere) of the structural elements and paleomagnetic measurements in a plane perpendicular to the core axis, summarizes these results. The fault strikes 297°. This result and its structural implications are discussed in the "Lithostratigraphy" section (this chapter).

PHYSICAL PROPERTIES

Physical-properties measurements at Site 688 were performed on split cores, generally at an interval of one every two sections (3 m) in good quality APC and XCB cores. The quality of recovery provided a good suite of index-property samples and vane shear tests in Hole 688A. We had more difficulty obtaining samples from the cores of Hole 688E because the material was either too lithified to perform vane shear tests or too fractured to provide reliable samples. Several samples obtained in Hole 688E were used to measure velocity with the Hamilton Frame.

Index Properties

The index properties measured at Site 688 include water content (presented as a percentage of dry sample weight), porosity, bulk density, and grain density (Table 12). The methods specified in the "Explanatory Notes" (this volume) were used to measure the index properties at Site 688. The measured salinity of the pore water (see "Inorganic Geochemistry" section, this chapter) was used in the calculations.

Figure 56 illustrates downhole trends in water content and porosity with depth and lithology for this site. Figure 57 shows the bulk-density data obtained from samples of the split cores and from GRAPE profiles. All apparently undisturbed APC and XCB core sections were run through the GRAPE, with the index-properties sample data showing good correlation to the GRAPE profile. The rotary core barrel (RCB), used in Hole 688E, provided cores that were too disturbed for meaningful GRAPE data.

Discernible trends are evident in the index-property data at Site 688. The water contents in lithologic Subunit IA decrease rapidly from a high of 142% near the mud line to 76% at the base of the unit (Fig. 56). The porosities in Unit I also decrease within the unit, from 80% near the mud line to 70% at 66 mbsf. Bulk densities increase rapidly within the upper 35 m of Subunit IA, from 1.4 g/cm^3 near the mud line to 1.51–1.53 g/cm^3. A marked increase in bulk density occurs at this depth, to 1.58 g/cm^3 at 39 mbsf (Fig. 57). This depth appears to correspond to an increase in content of nannofossils and foraminifers and the accompanying decrease in silt content. The average bulk density in the remainder of Subunit IA remains fairly constant with depth, but individual values vary between 1.5 and 1.67 g/cm^3.

Subunit IB appears to have constant or perhaps slightly increasing water content with depth and an approximate mean value of 95%. The porosities continue to decrease slightly with depth through Subunit IB. The bulk densities in this unit appear to decrease slightly with depth and vary between 1.51 and

Table 12. Summary of index properties data for Holes 688A and 688E.

Core/section interval (cm)	Depth (mbsf)	Water contents (% dry wt)	Porosity (%)	Bulk density (g/cm³)	Grain density (g/cm³)
112-688A-1H-2, 87	2.37	133.39	80.09	1.44	2.51
1H-4, 73	5.23	126.92	79.59	1.46	2.51
1H-6, 17	7.67	142.25	81.16	1.42	2.38
2H-2, 41	10.21	129.78	77.88	1.41	2.46
2H-4, 83	13.63	132.73	78.85	1.42	2.42
2H-6, 87	16.67	102.60	73.59	1.49	2.45
3H-1, 92	18.72	122.90	78.42	1.46	2.35
3H-3, 86	21.66	101.45	74.63	1.52	2.63
3H-5, 88	24.68	102.35	75.69	1.53	2.52
4H-1, 95	28.25	120.64	80.29	1.50	2.71
4H-3, 83	31.13	107.90	76.98	1.52	2.45
4H-5, 117	34.47	115.11	79.07	1.51	2.53
5H-2, 82	39.12	87.73	72.28	1.58	2.43
5H-4, 96	42.26	79.63	72.12	1.67	2.54
6H-2, 69	48.49	95.18	74.11	1.56	2.48
6H-4, 94	51.74	89.82	72.17	1.56	2.52
6H-6, 85	54.65	81.20	72.06	1.65	2.63
7H-2, 98	58.28	87.46	72.33	1.59	2.49
7H-4, 106	61.36	103.34	74.35	1.50	2.35
7H-6, 106	64.36	75.90	69.61	1.65	2.48
8X-1, 118	66.48	80.69	70.04	1.61	2.61
9X-2, 137	77.67	111.60	78.56	1.53	2.46
9X-4, 88	80.18	79.68	70.12	1.62	2.43
9X-6, 137	83.67	78.74	69.55	1.62	2.36
10X-1, 76	85.06	74.08	66.98	1.61	2.38
10X-3, 47	87.77	96.68	75.45	1.57	2.52
11X-3, 132	97.34	100.52	74.09	1.51	2.39
11X-7, 77	101.17	106.58	76.61	1.52	2.34
11X-9, 25	101.85	109.58	77.81	1.52	2.39
12X-1, 77	104.07	98.29	73.25	1.51	2.36
13X-2, 94	115.24	95.10	73.06	1.54	2.40
13X-6, 78	121.08	97.34	74.20	1.54	2.32
14X-1, 90	123.20	77.21	69.22	1.63	2.45
14X-4, 38	127.18	109.37	77.47	1.52	2.37
14X-6, 52	130.32	106.70	74.60	1.48	2.41
15X-1, 18	131.98	110.18	76.04	1.49	2.36
15X-7, 10	140.90	85.46	71.61	1.59	2.42
16X-2, 34	143.14	115.79	78.98	1.51	2.31
16X-5, 20	146.12	109.64	78.28	1.53	2.27
16X-6, 18	147.40	90.42	73.20	1.58	2.34
17X-2, 92	153.22	99.07	74.19	1.53	2.33
17X-4, 13	155.43	97.02	74.83	1.56	2.49
17X-6, 35	158.65	97.24	73.46	1.53	2.38
18X-1, 124	161.54	111.56	76.50	1.49	2.36
19X-1, 53	170.33	84.05	71.29	1.60	2.44
19X-3, 36	173.16	79.09	69.56	1.61	2.48
19X-5, 57	176.37	68.44	66.80	1.68	2.51
20X-1, 18	179.48	95.17	74.36	1.56	2.30
21X-2, 42	190.72	103.15	75.16	1.52	2.29
21X-3, 93	192.73	86.56	72.43	1.60	2.32
22X-1, 26	198.56	89.25	73.91	1.61	2.44
24X-1, 58	217.88	88.81	73.12	1.59	2.25
25X-2, 76	229.06	102.50	76.16	1.54	2.16
26X-1, 31	236.61	87.09	72.96	1.61	2.41
27X-5, 9	251.89	86.92	72.95	1.61	2.43
28X-1, 54	255.84	83.93	75.55	1.70	2.65
29X-2, 133	267.63	95.81	73.19	1.53	2.42
29X-3, 73	268.53	78.21	70.36	1.64	2.53
30X-1, 69	274.99	83.47	71.40	1.61	2.37
31X-1, 26	284.06	85.58	70.64	1.57	2.31
32X-2, 8	294.88	70.20	66.79	1.66	2.55
32X-5, 65	297.67	76.64	69.05	1.63	2.48
32X-8, 107	301.87	81.81	69.95	1.59	2.44
33X-4, 53	307.83	92.41	71.42	1.52	2.24
33X-5, 117	309.97	104.60	72.91	1.46	2.24
35X-1, 84	322.64	83.21	69.58	1.57	2.38
35X-2, 74	324.04	43.73	68.74	2.31	4.34
35X-6, 84	330.14	93.38	70.84	1.50	2.30
36X-1, 32	331.62	82.57	70.02	1.59	2.32
36X-6, 53	339.03	106.66	73.01	1.45	2.17
112-688E-5R-2, 96	386.46	115.97	76.27	1.46	2.18
5R-5, 55	390.55	54.65	59.12	1.71	2.31
6R-2, 12	395.12	54.44	60.99	1.77	2.31
8R-6, 71	420.71	43.35	52.36	1.77	2.44
9R-5, 101	429.01	64.86	64.69	1.68	2.44
10R-1, 54	432.04	42.39	53.23	1.83	2.39
12R-1, 29	450.79	26.29	41.85	2.06	2.55
12R-2, 129	453.29	87.83	68.66	1.50	2.19
14R-3, 10	472.60	68.35	61.83	1.56	2.33
23R-1, 90	555.90	20.77	35.10	2.09	2.53
25R-1, 68	574.68	41.43	50.22	1.76	2.39

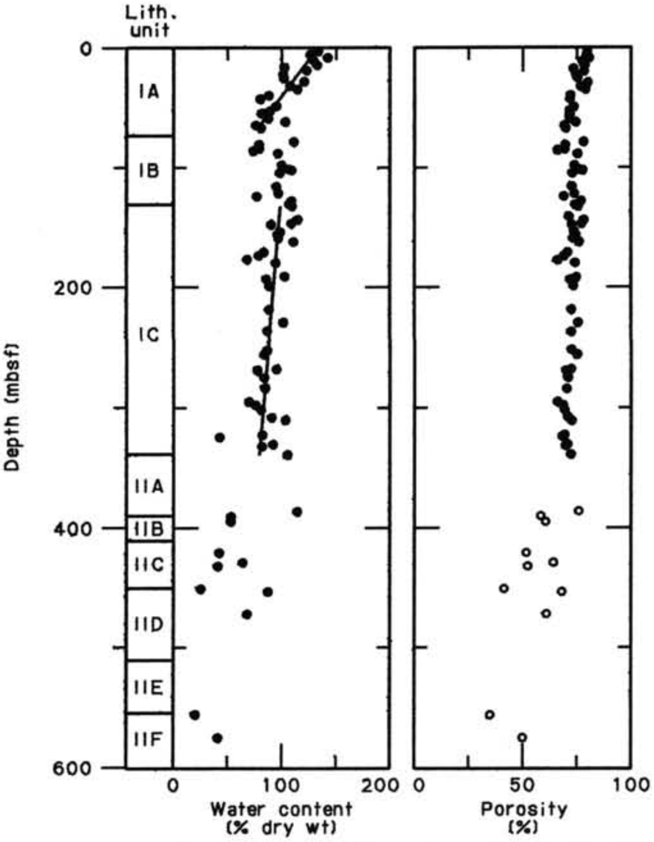

Figure 56. Downhole water-content and porosity profiles for Site 688. Schematic of units is also shown.

1.63 g/cm³. The behavior of the index properties in Subunit IB is contrary to that normally found in a consolidating sediment sequence. This reversal of behavior changes at the Subunit IB/Subunit IC boundary, with the water contents gradually decreasing with depth through Subunit IC. Although values as low as 44% and as high as 105% occur throughout Subunit IC, the mean provides an approximate water content of 80% at the base of Subunit IC. Porosity continues to decrease through Subunit IC to values of 69% to 73% at the base of the unit (330–340 mbsf). With the exception of local fluctuations, bulk densities in Subunit IC appear to remain constant with depth, with a mean of approximately 1.58 g/cm³.

The data obtained in lithologic Unit II is scattered. This unit consists of slumped and deformed sediments, and these variable lithologies most likely cause the variability in the index-property data. Water contents and porosities continue to decrease through Unit II, as would be expected. Bulk densities continue to increase. No samples were obtained in lithologic Unit III.

Compressional-Wave Velocity

The *P*-wave logger, which is run in conjunction with the GRAPE, was used to measure velocities through the sediments of unsplit APC cores. However, the plots of velocity vs. depth produced immediately by the logger system indicated that, as at previous sites, the quality of data was poor. The usefulness of the *P*-wave logger for providing downhole profiles of velocity is particularly limited in gasous sediments.

Hamilton Frame samples were obtained for several samples in Hole 688E to help us interpret seismic data. These velocities are presented in Table 13. In some cases, the signal obtained during measurement was not clear, which was probably caused by fracturing within the sample; the resulting low velocities are not reported. The mudstone samples in lithologic Unit II (e.g.,

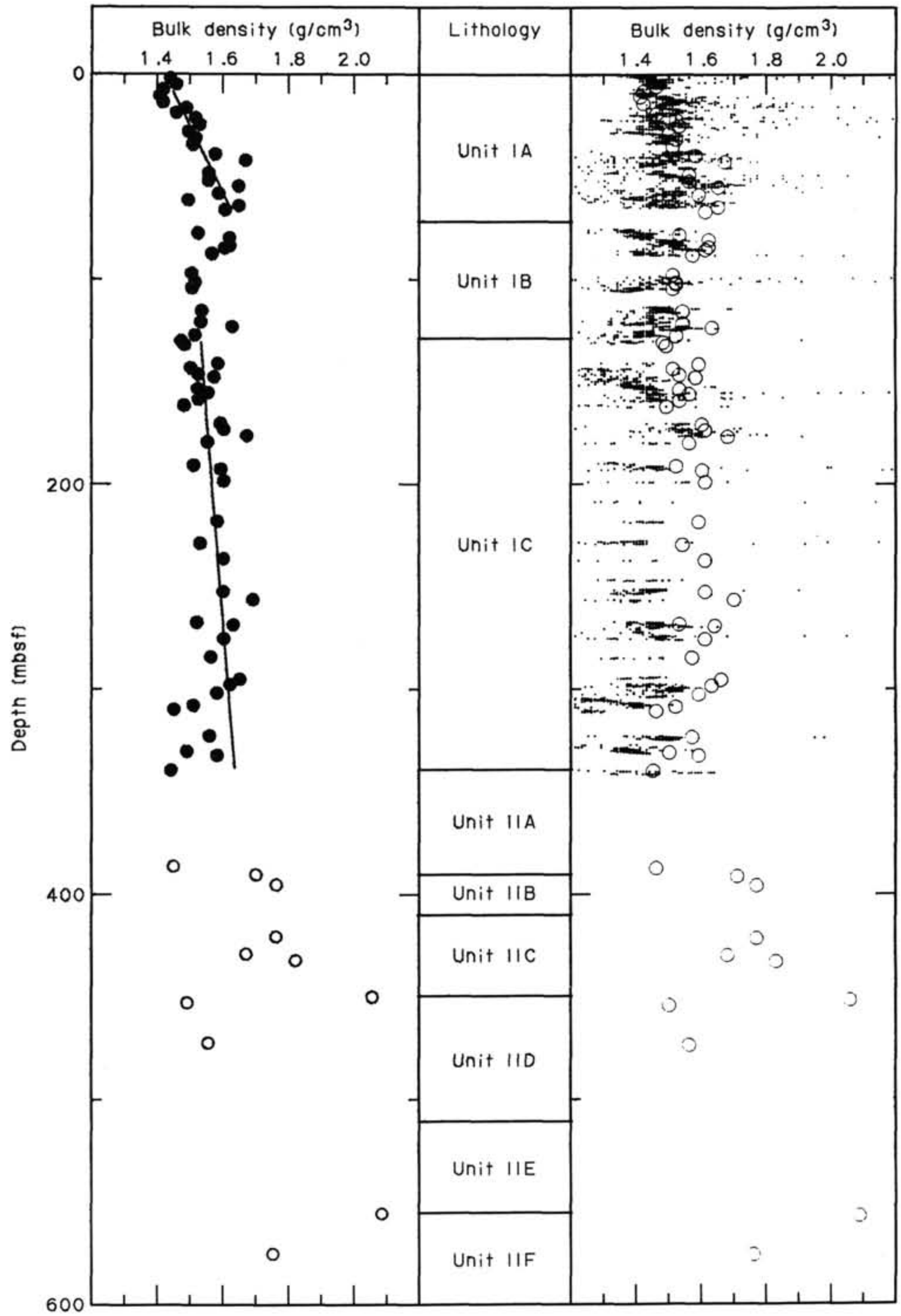

Figure 57. Bulk-density measurements of discreet samples and GRAPE bulk-density profile of Site 688. Schematic of lithologic units is also shown.

Sample 112-688E-8R-6, 71 cm) provided velocities of almost 1.8 km/s. A dolomite sample (112-688E-9R-6, 95 cm) gave a velocity of 3.8 km/s. Velocities increase downhole, with a value of 2.1 km/s for a mudstone from Sample 112-688E-23R-1, 90 cm. The cemented sandstones (e.g., Sample 112-688E-33R-2, 118 cm) gave a velocity of 2.34 km/s. The mudstones become more lithified with depth, and a value of 2.34 km/s was obtained from Sample 112-688E-43R-4, 53 cm. A limestone sample (112-688E-41R-1, 16 cm) gave a velocity of 2.65 km/s.

Vane Shear Strength

The undrained vane shear strength measurements for Site 688 were performed with the Wykham Farrance vane apparatus. Values obtained for peak undrained vane shear strengths are presented in Table 14 and are shown vs. depth below seafloor in Figure 58. Van shear strength increases rapidly within lithologic Subunit IA from a low of 22 kPa at the mud line to 68 kPa at 31 mbsf, which corresponds to the rapid decrease in water con-

Table 13. Profile of compressional-wave velocity data for Hole 688E.

Core/section interval (cm)	Depth (mbsf)	Velocity A (km/s)	Velocity B (km/s)	Comments
112-688E-6R-1, 97	394.47	1.66		mudstone
8R-6, 71	420.71	1.79		mudstone
9R-6, 95	430.45	3.81	3.80	dolomite
10R-1, 54	432.04	1.71		mudstone
23R-1, 90	555.90	2.12	2.10	mudstone
24R-1, 14	564.64	1.92	1.93	mudstone
25R-1, 67	574.67	1.76		mudstone
32R-1, 100	641.50	1.94		sandstone
33R-2, 118	652.68	2.34	2.34	mudstone
39R-1, 106	708.06	2.23		mudstone
41R-1, 16	726.16	2.65		limestone
43R-4, 53	750.03	2.34	2.36	mudstone
44R-2, 6	756.06	2.14	2.14	mudstone

Note: Velocity A is velocity in vertical direction; Velocity B is velocity in horizontal direction.

Table 14. Summary of vane-shear-strength data for Hole 688A.

Core/section interval (cm)	Depth (mbsf)	Peak (kPa)
112-688A-1H-2, 87	2.37	21.64
1H-4, 73	5.23	30.79
1H-6, 17	7.67	22.47
2H-2, 41	10.21	33.29
2H-4, 83	13.63	61.82
2H-6, 87	16.67	58.59
3H-1, 92	18.72	59.05
3H-3, 86	21.66	47.52
3H-5, 88	24.68	67.36
4H-3, 83	31.13	67.82
4H-5, 117	34.47	104.27
6H-2, 69	48.49	73.82
6H-4, 94	51.74	85.81
6H-6, 85	54.65	71.51
7H-2, 99	58.29	43.83
7H-4, 107	61.37	81.20
7H-6, 107	64.37	94.58
9X-4, 88	80.18	82.58
9X-6, 138	83.68	89.04
10X-1, 77	85.07	109.34
10X-3, 48	87.78	87.20
11X-3, 133	97.34	56.29
11X-7, 78	101.17	78.89
13X-2, 95	115.25	65.97
14X-1, 91	123.21	107.50
14X-4, 38	127.18	67.82
15X-7, 10	140.90	88.12
16X-5, 20	147.50	64.59
16X-6, 18	148.98	106.11
17X-4, 13	155.43	59.98
17X-6, 35	158.65	63.67
19X-1, 54	170.34	110.26
19X-3, 34	173.14	138.87
21X-3, 93	192.73	111.95
26X-1, 31	236.61	122.44
28X-1, 54	255.84	99.12
29X-2, 134	267.64	103.79
29X-3, 74	268.54	130.61
30X-1, 70	275.00	97.96
32X-2, 9	294.89	165.59
32X-5, 66	297.67	153.93
32X-8, 108	301.87	159.76
35X-1, 85	322.65	111.95
35X-2, 75	324.05	120.11
35X-6, 84	330.14	129.44
36X-6, 54	339.04	104.95

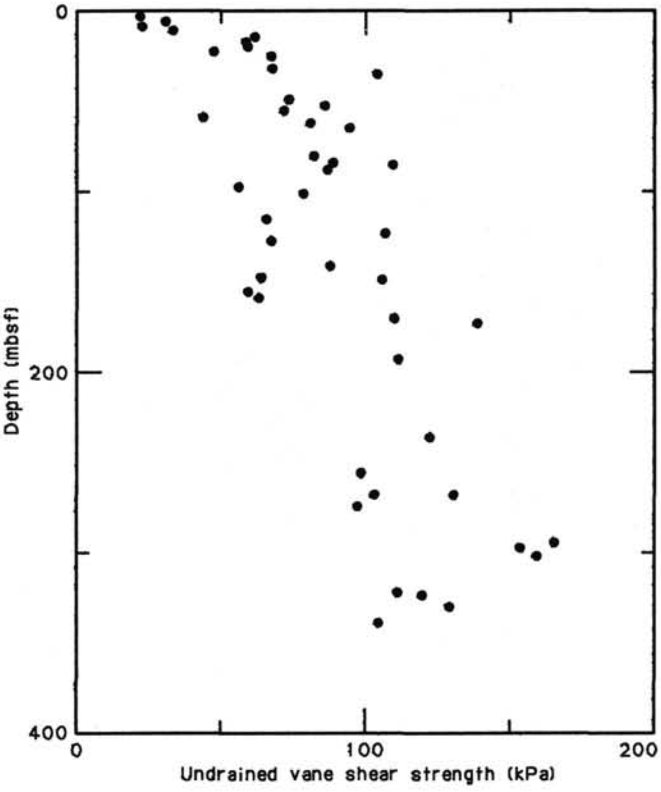

Figure 58. Peak undrained vane-shear-strength profile for Site 688.

tent over the same interval. A range of highs (104 kPa) and lows (44 kPa) occurs throughout the remainder of Subunit IA from 31 mbsf to 72 mbsf, with an apparent trend of increasing shear strength with depth. Throughout Subunits IB and IC (72 to 340 mbsf), vane shear strengths continue to increase with depth, although the considerable scatter reflects variations in the index-property data.

Total overburden stress for Hole 688A was calculated using bulk-density determinations and assuming hydrostatic pore-pressure conditions. The total stress and assumed hydrostatic profiles are shown vs. depth below seafloor in Figure 59. The slope of the data profile appears constant, although some scatter occurs at the lower part of the curve, which reflects the variable bulk-density values at this depth. The ratio of peak undrained shear strength to effective overburden pressure (C_u/P') is plotted vs. depth below seafloor in Figure 60. The data follow the theoretical curve, with the exception of the value at 14 mbsf. The sudden increase in vane shear strength at this depth is emphasized. This depth corresponds to the occurrence of nannofossils and foraminifers in the sediments, but may also be an artifact. We changed the vane spring before this test and this sharp change may be an artifact of the testing. Other variations in this profile result from the variable shear-strength and bulk-density profiles.

Thermal Conductivity

Thermal conductivity was measured by the needle-probe method in Hole 688A cores. The probes were inserted into the ends of the split sections parallel to the core axis. We had difficulty finding undisturbed samples at the ends of the sections below 120 mbsf, so only a few measurements were possible. The results are presented in Table 15 and Figure 61.

In lithologic Subunit IA, the thermal conductivity seems to increase with depth. This tendency is consistent with the variation in index properties (Figs. 56 and 57). In Subunit IB, thermal conductivity decreases with depth. Although the water content and bulk density seem to vary correspondingly in the same depth range, these variations are not large compared with that in thermal conductivity. On the other hand, the grain density in

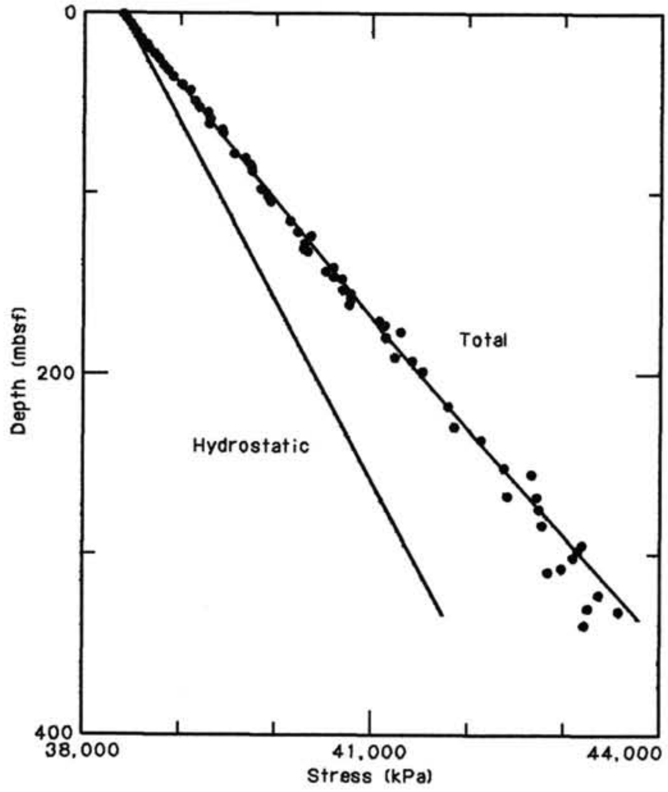

Figure 59. Assumed hydrostatic stress and calculated total stress profiles for Site 688.

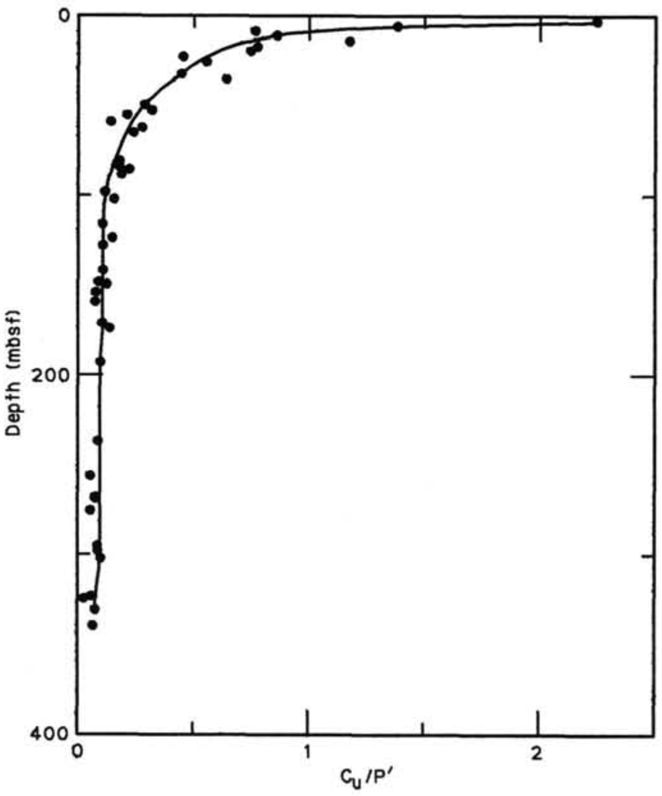

Figure 60. Profile of the ratio of peak undrained vane shear strength to effective overburden pressure for Site 688.

Table 15. Thermal-conductivity data for Hole 688A.

Core/section interval (cm)	Depth (mbsf)	Thermal conductivity (W/m·K)
112-688A-1H-2, 3	1.53	0.955
1H-3, 3	3.03	0.906
1H-5, 3	6.03	0.968
1H-6, 3	7.53	0.841
2H-2, 3	9.83	0.991
2H-3, 3	11.33	0.944
2H-4, 3	12.83	0.865
2H-5, 3	14.33	0.955
3H-1, 147	19.27	0.936
3H-4, 3	22.33	1.040
3H-7, 3	26.83	0.861
4H-2, 3	28.83	0.939
4H-3, 3	30.33	0.956
4H-5, 3	33.33	0.952
4H-6, 3	34.83	0.841
4H-7, 53	36.83	1.058
5H-6, 147	45.77	1.050
5H-7, 3	45.83	1.025
6H-3, 125	50.14	1.013
6H-4, 122	51.61	0.976
6H-5, 3	51.92	0.951
6H-5, 147	53.36	1.130
7H-5, 147	62.93	1.055
7H-6, 147	64.43	0.955
8X-2, 147	68.27	0.993
9X-3, 147	79.27	0.911
9X-7, 3	83.83	0.955
10X-2, 147	87.27	0.889
11X-4, 31	97.44	0.923
11X-4, 147	98.12	0.915
11X-9, 3	102.51	0.786
13X-1, 147	114.27	0.854
13X-3, 3	115.83	0.873
16X-9, 3	149.63	1.018
17X-5, 3	156.83	0.836
29X-2, 147	266.41	0.925
29X-3, 147	267.91	0.789
29X-6, 147	269.90	0.928
30X-1, 113	275.43	0.950
32X-2, 3	294.83	1.045
35X-1, 147	323.21	0.878
35X-6, 147	329.12	0.867

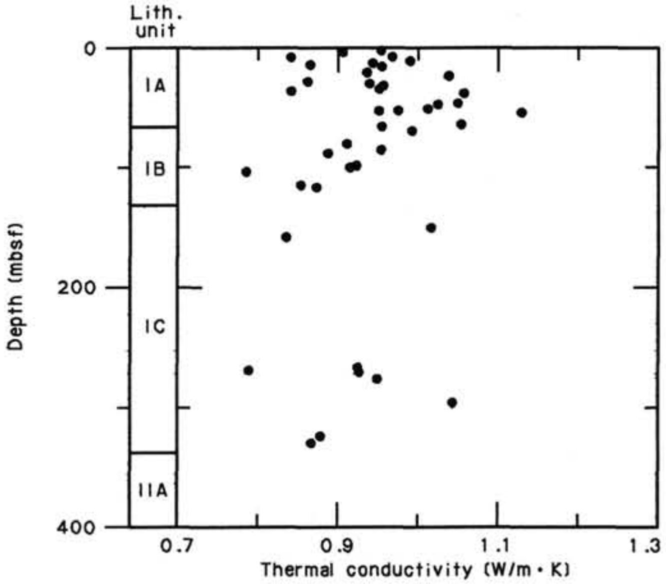

Figure 61. Thermal conductivity vs. depth below seafloor at Site 688.

Subunit IB is somewhat lower than that in Subunit IA (Table 12). Possibly a change in the mineral composition resulted in decreased thermal conductivities and grain densities.

Figure 62 shows the relation between thermal conductivity and water content for Leg 112 samples. Thermal conductivity correlates well with the water content. However, we observed that the thermal conductivity of XCB cores was generally lower than that of APC cores for the same water content. Most likely the XCB cores were more disturbed by drilling and have small cracks that lower the thermal conductivity.

Summary and Discussion

The physical-properties data obtained at Site 688 provide profiles having discernible trends that emphasize changes in lithology. A rapid decrease in water contents and increase in bulk densities occurs within Subunit IA (0–72 mbsf). Such profiles may be caused by the rapid sedimentation rates in this unit. Subunit IB appears to have slightly increasing water contents and slightly decreasing bulk densities, a reverse behavior from that expected of a normally consolidating sediment sequence. The decreased water contents and the increased bulk densities occur gradually throughout Subunit IC.

Unit II contains predominantly slumped and deformed sediments and variable lithologies, which is apparent in the scattering of obtained data. Insufficient data exist for establishing the behavior of the index properties within each subunit of lithologic Unit II. However, a trend of continuing decrease in water contents and porosities and increase in bulk densities occurs through Unit II. Results of thermal-conductivity measurements are consistent with the variations observed in the index properties.

Hamilton Frame samples provided velocities that were useful for interpreting the seismic data. The cemented sandstones tested (from Section 112-688E-33R) gave a velocity of 2.34 km/s. The oldest mudstone sampled (from Section 112-688E-43R) resulted in a velocity of 2.34 km/s, and a sample of limestone from Section 112-688E-41R gave a velocity of 2.65 km/s.

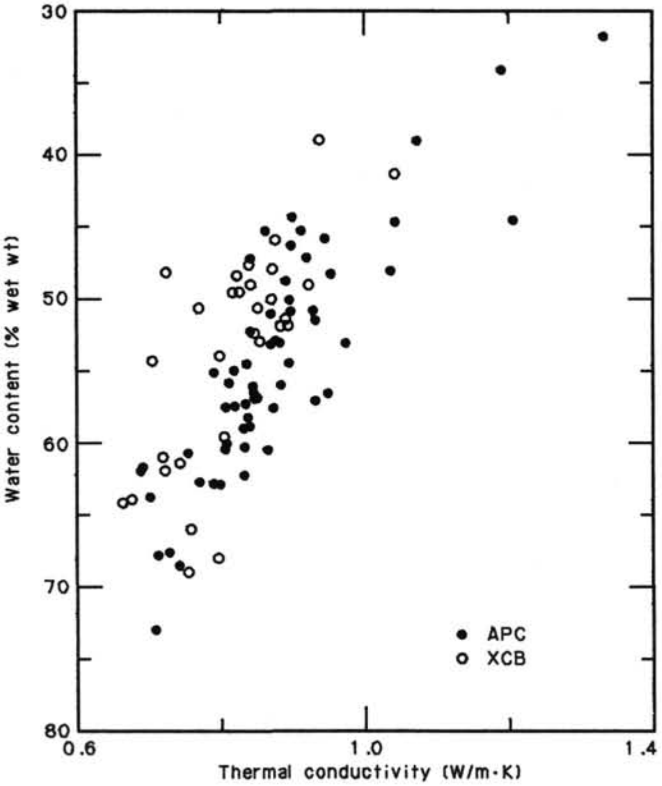

Figure 62. Thermal conductivity vs. water content for Leg 112 samples.

GEOPHYSICS

Seismic-Reflection Records

Site 688 was selected after drilling at Site 682 failed to reach the basement objective. This basement objective was to verify that the frontal part of the Peruvian margin consists of continental crust. If true, the Peruvian margin has been extensively eroded during plate convergence and subduction. We had problems reaching basement during Leg 112 because of the fractured condition of the rock, which made it impossible to penetrate more than about 450 m before a hole collapsed. Identifying the degree of fracturing required excellent seismic data.

Seismic record CDP-1 was shot for the Nazca Plate Project and was processed to a "first-pass level" common to seismic processing during the early 1970s (Hussong and Wipperman, 1981). About two weeks before beginning Leg 112, this record was reprocessed by stacking all of the 24 channels recorded and applying migration (R. von Huene and Miller, unpubl. data). This processing improved the seismic image greatly by collapsing many of the diffractions. Thus, we were able to see more clearly the areas of coherent reflections and to differentiate from those having many faults and fractures.

Site 688 is located on the lower-slope terrace of the Peru Trench (Fig. 63). The outgoing signal contains reflections from a small basin that were also seen in the 3.5-kHz transducer record of the site approach. Sediment filling the top of the basin corresponded to the high-frequency reflections from 0 to 0.4 s below the seafloor. From 0.4 to 0.67 s, one can see six reflections of lower frequency and greater amplitude. Before drilling, we inferred that these reflections were from Eocene rock because of a character similar to the reflections from Eocene rock at Site 682. However, during drilling we discovered that the reflections were from rocks of Pliocene through lower Miocene.

The high-amplitude reflection at 0.67 s indicates a change in lithology. Such a change in lithology was cored at 600 m, where a cataclasite separates the Neogene mudstones above from Eocene sandstones, siltstones, and conglomerate below. Although this 600-m depth does not fall on the time intercept of the high-amplitude reflection when applying the average velocity/depth curve for the area, the 0.03-s discrepancy was easily accounted for by a lower-than-normal velocity in the uppermost 300-m-thick section of Quaternary diatomaceous mud. In the absence of a velocity log, our preferred interpretation was to correlate the 0.67-s reflection with the top of the Eocene section. When the velocities measured for the Eocene rocks (see "Physical Properties" section, this chapter) were weighted in accordance with the lithology cored (see "Lithostratigraphy" section, this chapter), the estimated velocity was 2.36 km/s. Applying this velocity to the intercepts of the seismic record indicated basement at about 836 m, or 57 m more than the depth drilled.

The base of gas-hydrate reflection was observed across the lower slope to a point 2.5 km downslope; that is, 0.52 s below the seafloor. The depth corresponding to this time intercept was passed without incident during drilling, despite the visible gas hydrate in the upper part of the hole (see "Organic Geochemistry" section, this chapter).

Heat Flow

Temperature Measurements

At Site 688, temperatures were measured once with the APC tool during APC coring (Core 112-688A-4H). Further measurements were impossible because of the stiff sediments. The temperature record is presented in Figures 64 and 65. The equilibrium temperature at 36.8 mbsf was calculated as 3.8 ±0.2°C.

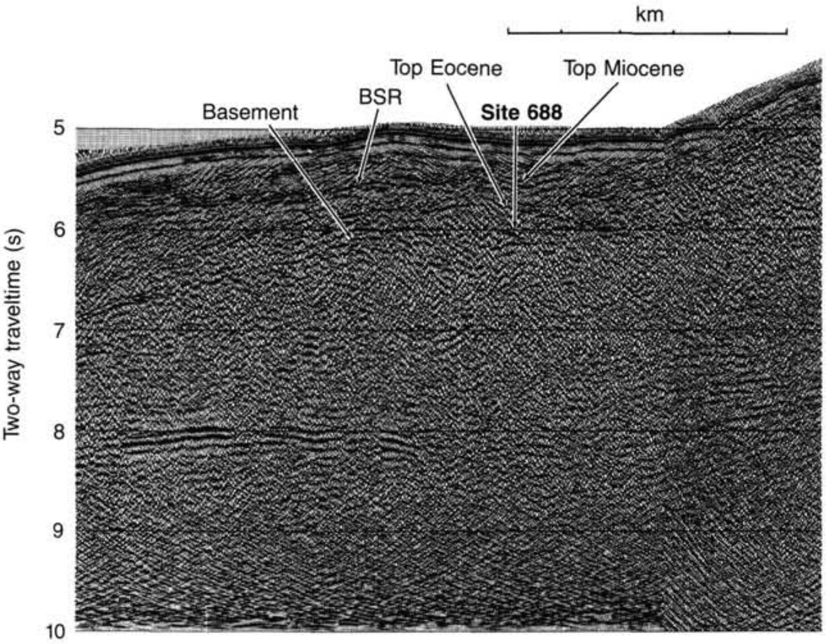

Figure 63. Location of Site 688 on MCS line CDP-1 with age assignments of reflectors.

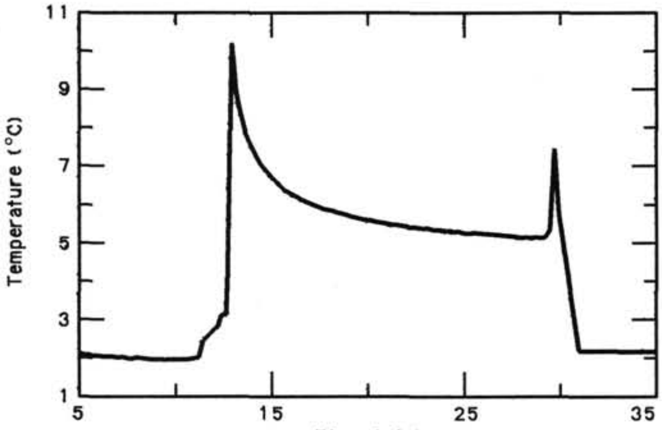

Figure 64. Record of temperature vs. time using the APC tool, obtained while retrieving Core 112-688A-4H.

Temperatures were also measured using the APC tool during pore-water sampling following Core 112-688A-5H (46.3 mbsf). The maximum temperature recorded before we pulled out of the hole was 4.2°C. This value should be used only for reference (see "Explanatory Notes," this volume).

Heat-Flow Estimation

From oceanographic data, the bottom-water temperature at Site 688 was estimated as about 1.7°C. To combine this data with the equilibrium temperature at 36.8 mbsf, one should take into account the characteristic of the APC tool. The temperature was corrected from 3.8° to 3.6°C (see "Explanatory Notes," this volume). Thus, the mean temperature gradient was 52 m K/m. The thermal resistance for the same depth range was calculated as 41.6 m^2 K/W from the thermal-conductivity data in Hole 688A corrected to *in-situ* conditions. Hence, the heat flow at Site 688 is 46 m/W/m^2. This value is not much different from 39 m/W/m^2 at Site 683 or 49 m/W/m^2, measured by the ordinary surface heat-flow probe.

SUMMARY AND CONCLUSIONS

Our major objectives at Site 688 were to recover a more complete Paleogene section and to penetrate basement. A well-stratified Quaternary basin was selected for drilling to provide stable hole conditions. The thick Quaternary section we recovered gave us insight into Quaternary subsidence and basin formation. Although we did not reach the basement, substantial information was obtained from a 180-m-thick early and middle Eocene sequence of shelf affinities.

The three distinct tectono-sedimentary environments encountered in the 770 m that were penetrated record progressively deeper water sedimentation from early Eocene to Quaternary time. The first sequence represents a substantial 339-m-thick accumulation of bioturbated Quaternary diatomaceous muds. The uppermost 132 m is composed of dark olive gray to greenish-gray nannofossil- and foraminifer-bearing diatomaceous muds. Common foraminifer, terrigenous turbidites in the top 66 m indicate reworked sediment influx. Within the diatomaceous muds, benthic foraminifer assemblages are representative of today's water depths. The remainder of the Quaternary sequence is a diatomaceous mud having low carbonate content. From 75 to 312 mbsf, the sediment has a uniform black coloration that is associated with a significant amount of pyrite and iron monosulfide. This represents a substantially thicker black section than that encountered at Site 685 (90 m). The black color and enrichment in monosulfide and pyrite are characteristic of high sedimentation rates. Biostratigraphic data indicate sedimentation rates of around 300 m/m.y. for the Quaternary section. An incipient fissility developed in the Quaternary section below 100 mbsf.

The second major sedimentary unit is made up of diatomaceous and diatom-bearing muds of lower Miocene to Pliocene-Pleistocene age, between 339 and 593 mbsf. The boundary between the second and first lithological units is marked by the occurrence of the black, pyrite- and monosulfide-bearing muds and by a decrease in diatom content. Fissility is better developed from 339 mbsf. A biostratigraphic hiatus separating the Quaternary and Pliocene can be seen between 341 and 350 mbsf in

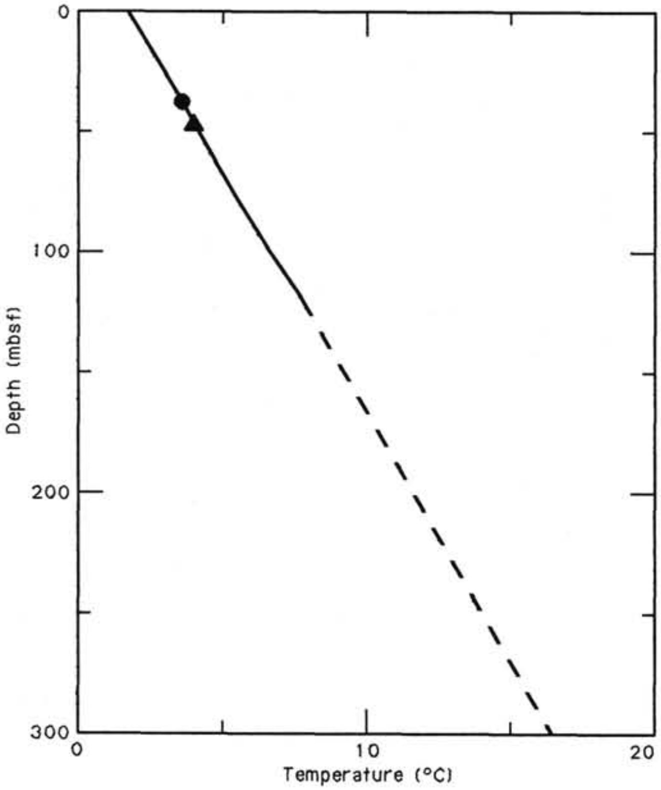

Figure 65. Plot of temperature vs. depth for Hole 688A. Circle and triangle indicate the extrapolated equilibrium temperature and the lower limit temperature, respectively. Solid line represents the temperature profile, based on the heat-flow and thermal-conductivity data from 0-38.6 mbsf in Hole 688A. Broken line represents continuation of the profile, assuming that the thermal conductivity is 0.9 and 1.1 W/m · K.

Hole 688A and between 350 and 356 mbsf in Hole 688E. Dolomite occurs as a disseminated authigenic phase throughout this sequence, and discrete dolomite zones are developed at several intervals. A particularly dolomite-rich section occurs in the lower Miocene at 446 to 565 mbsf. Finely laminated sediment of alternating diatomite and mudstone with associated minor phosphorite is present in the late Miocene and Pliocene-Miocene. This facies association is similar to that of the contemporaneous sediments of the onshore Pisco Basin and modern coastal upwelling deposits. Intervals of terrigenous sedimentation with reduced diatom content occur in the lower Miocene and in the Pliocene-Miocene. Upper mid-bathyal benthic foraminifer faunas indicate deposition of the Pliocene-Miocene sequence in substantially shallower water (500-1500 m) than at today's depths. Throughout the Pliocene-Miocene sequence, pervasive soft-sediment deformation is evident. The deformation style is facies-dependent and includes folding in laminated sequences, complex conjugate subvertical microfaults, dissection of more competent beds by faults exhibiting ramp and flat geometries, and anastomosing bedding subparallel faults. Many of the faults are mud-filled. The structures observed indicate deformation within a predominantly extensional stress field consistent with slide emplacement. Four breaks in the biostratigraphic record, which represent missing zones within the Pliocene-Miocene sequence, may also have formed by extensional faulting. The most substantial of these hiatuses involves a 4.5-Ma break between the lower and mid-Miocene between 535 and 555 mbsf. Thus, an explanation for the emplacement of the Pliocene-Miocene section as an essentially intact sedimentary slide into today's water depths seems most likely. Sedimentation rates for the Pliocene-Miocene section are approximately 23 m/m.y.

A marked lithological break to diatom-free calcareous sediment rich in terrigenous clastic detritus occurs at 593 mbsf. This coincides with a hiatus that spans the mid-Eocene to the earliest Miocene, a period of approximately 21.5 m.y. The sediments at the top of the Eocene section showed an intense cataclastic deformation, and recovery was poor between 593 and 621 mbsf. The sediments recovered from 621 to 659 mbsf are predominantly greenish-gray to dark greenish-gray, poorly sorted, quartzo-litho-feldspathic sandstones interbedded with sandy siltstones and black mudstones. The sandstones have a dominantly calcitic cement. The sediments show evidence of syngenetic deformation. Beneath the sandstones (from 659 to 678 mbsf), a siltier sequence contains nannofossil chalks and marls, which represent a more quiescent marine-influenced sedimentation. Reworked Cretaceous calcareous nannoplankton are recorded from the highest levels of the middle Eocene. Benthic foraminifer assemblages for this section indicate a mid- and upper-bathyal (150-500 m) range of water depths.

A hiatus from early to mid-Eocene occurs at 678 mbsf. The early Eocene sequence from 745 to 678 mbsf includes abundant transported plant matter, coarse pebbly layers, and bioclastic material. Toward the base of this unit, calcareous mudstones and sandstones and silty, bioclastic limestones contain well-preserved mollusks, some of which are still articulated and evidence little transport before deposition. Bioclastic material decreases in abundance and coincides with more sandstone intervals and pebbly sandstone, and with the development of conglomeratic zones that contain clasts of milky quartz, metamorphic rocks, volcanics, micritic limestone, and chert. Benthic foraminifer and nannofossil assemblages indicate shelf depths for the deposition of this sequence. The interval from 745 to 764 mbsf contains predominantly dark olive gray mudstones, with minor siltstones and interbedded nannofossil chalks and marls. Foraminifer faunas indicate depths of 150 to 500 m. The last sediments recovered from 764 to 769.5 mbsf are composed of interbedded sandstones, siltstones, and mudstones, with abundant plant material and foraminifer assemblages indicative of shelf depths. A chert pebble at this level contains a planktonic foraminifer fauna of Cenomanian age identical to faunas of Albian to Cenomanian limestones and cherts of the Central Andes and the onshore Talara Basin. Planktonic and benthic foraminifer faunas throughout the Eocene sequence show close affinities with those of the coastal basins of Peru. Sedimentation rates for the Eocene section are approximately 12 m/m.y. and are indicative of breaks between pulses of sedimentation.

Site 688 provided the most extreme geochemical gradients of Leg 112. Maximum values of alkalinity, ammonia, and phosphate exceeded previous records for DSDP or ODP sites. The upper part of this hole showed downhole interstitial-water profiles similar to the other deep-water sites of Leg 112, except for the very high gradients. The near-surface, sulfate-reduction zone was very thin and contained sulfate only to 30 mbsf. Methanogenesis and carbonate diagenesis dominate both inorganic- and organic-geochemical profiles in the Quaternary sequence.

Predictions were that the methane generated in these sediments would be present in the gas-hydrate phase; Site 688 provided one of the best-documented occurrences of gas hydrates to date. A large sample of gas hydrate, filling several centimeters of the core, was recovered from a depth of 141 mbsf. The samples consisted of gas hydrate and mud in a heterogeneous mixture. Although equilibrium pressures were lower than for samples at Site 683, the large samples provided excellent material for gas and water analyses.

The hiatus at 350 m marks the boundary between the signals from two very different bodies of interstitial water. This can best be seen in the chloride profile, where a distinct freshening of the water is observed below 350 m. This freshening may indicate dilution by water that originates at depth from dewatering of subducted sediments. Mg^{2+} is replaced in an exact molar ratio by Ca^{2+} through the lower part of the sequence, which suggests reaction with volcanogenic or basement rocks. The CDP-1 seismic record and the subsidence history at Site 688 strongly suggest that continental crust underlies the site. Deeper reflections in CDP-1 indicate the presence of a subducted oceanic crust below 8 s two-way traveltime. Thus, it is possible that the interstitial water records both dewatering of subducted sediments and reaction with basement rocks.

These pore-water characteristics are reflected in the sequence of carbonate diagenesis. Calcite and dolomite occur as authigenic phases at Site 688. The upper 75 m of the section is dominated by precipitation of calcite with a corresponding decrease in the calcium content and increase in the Mg^{2+}/Ca^{2+} ratio of pore waters. Lithified carbonates first become common at 422 mbsf; between this depth and 660 m, dolomite is the main authigenic carbonate phase, and the magnesium content and the Mg^{2+}/Ca^{2+} ratio in pore water decrease rapidly. From 660 to 779 mbsf, calcite again becomes the major authigenic carbonate phase within a zone of increasing calcium in pore waters, possibly derived from the underlying subducted sediments. The lower part of this zone shows extensive calcitization of sandstone and numerous calcite-filled veins.

The methane/ethane ratio also shows the differentiation between the thick Quaternary sediments and the older sequence. The ratio continues to decrease to values well below 1000, except for a sharp increase at approximately 650 m, which corresponds to the middle Eocene sandy sequence at the top of lithologic Unit III. This sharp increase probably records a zone of gas migration. The high methane/ethane ratio indicated a biogenic origin for the gas, so that there was no danger in continued drilling.

The paleomagnetic results for Site 688 proved to be some of the most interesting encountered during Leg 112. The Brunhes-Matuyama boundary was found near the base of Core 112-688A-8X. Below this level, no correlation with the biostratigraphy could be established. However, the excellent correlation between a strong normal magnetization and the presence of possible iron monosulfides suggests overprinting of the magnetization through a diagenetic process related to the production of monosulfides. The production of such a thick sequence of monosulfide-bearing sediment is difficult to explain, but is probably related to high sedimentation rates, methanogenesis, and the limited availability of metal cations for sulfide formation.

High sedimentation rates also strongly influence physical properties at Site 688. Although water content is low in near-surface sediments, compared to sites where more diatomaceous sediments dominate, the water content shows a relatively slow decrease with depth through lithologic Unit I. Bulk densities and seismic velocities thus remain low to depths of 350 m. The slide-deformed sequence of lithologic Unit II is characterized by erratic but lower water content and correspondingly higher bulk density.

The early and mid-Eocene sequences record an influx of basement-derived clastic sediments to developing basins of shallow and shallow-to-intermediate depths founded on continental crust. The facies involved suggest a fault-controlled fan-delta environment. Alternations between clastic and biogenic sedimentation were probably associated with pulses of fault activity. The mid-Eocene to Pliocene environment at Site 688 is unknown. The area must have subsided to mid-slope depths by Pliocene–Quaternary time, however, when the allochthonous Pliocene–Miocene sequence was emplaced as a sediment slide. The slide block was derived from the area seaward of Lima Basin because the upper Miocene and perhaps most of the middle Miocene eroded from the Lima Basin area. The Quaternary sequence records rapid subsidence and deposition as infill of a fault-bounded slope basin.

REFERENCES

Akiba, F., 1985. Middle Miocene to Quaternary diatom biostratigraphy in the Nankai Trough and Japan Trench, and modified lower Miocene through Quaternary diatom zones for the middle-to-high latitudes of the North Pacific. *In* Kagami, H., Karig, D. E., Coulbourn, W. C., et al., *Init. Repts. DSDP*, 87: Washington (U.S. Govt. Printing Office), 393–481.

Akiba, F., and Yanagisawa, Y., 1985. Taxonomy, morphology and phylogeny of the Neogene diatom zonal marker species in the middle-to-high latitudes of the North Pacific. *In* Kagami, H., Karig, D. E., Coulbourn, W. C., et al., *Init. Repts. DSDP*, 87: Washington (U.S. Govt. Printing Office), 483–554.

Barron, J. A., 1980. Lower Miocene to Quaternary diatom biostratigraphy of Leg 57, off northeastern Japan, Deep Sea Drilling Project. *In* Scientific Party, *Init. Repts. DSDP*, 56, 57, Pt. 2: Washington, (U.S. Govt. Printing Office), 641–685.

Barron, J. A., 1985. Late Eocene to Holocene diatom biostratigraphy of the equatorial Pacific Ocean, Deep Sea Drilling Project Leg 85. *In* Mayer, L., Thayer, F., Thomas, E., et al., *Init. Repts. DSDP*, 85: Washington (U.S. Govt. Printing Office), 413–456.

Barron, J. A., and Keller, G., 1983. Paleotemperature oscillations in the middle and late Miocene of the northeastern Pacific. *Micropaleontology*, 29:150–181.

Berggren, W. A., 1977. Atlas of Paleogene planktonic foraminifera. Some species of the genera, *Subbotina*, *Planorotalites*, *Morozovella*, *Acarinina* and *Truncorotaloides*. *In* Ramsay, A.T.S. (Ed.), *Oceanic Micropaleontol.*, 1:205–300.

Berggren, W. A., Aubry, M. P., and Hamilton, N., 1983. Neogene magnetobiostratigraphy of DSDP Site 516 (Rio Grande Rise, South Atlantic). *In* Barker, P. F., Carlson, R. L., Johnson, D. A., et al., *Init. Repts. DSDP*, 72: Washington (U.S. Govt. Printing Office), 675–706.

Berner, R. A., 1974. Iron sulfides in Pleistocene deep Black Sea sediments and their paleo-oceanographic significance. *In* Degens, E. T., and Ross, D. A. (Eds.), *The Black Sea—Geology, Chemistry, and Biology*. AAPG Mem., 20:526–531.

Blow, W. H., 1969. Late middle Eocene to Recent planktonic foraminiferal biostratigraphy. *In* Bronnimann, P., and Renz, H. H. (Eds.), *Proc. First Int. Conf. Plankt. Microfossils*, 1:199–421.

Bourgois, J., Pautot, G., Bandy, W., Boinet, T., Chotin, P., Huchon, P., Lepinay, B., Monge, F., Montau, J., Pelletier, B., Sosson, M., and von Huene, R., 1987. Tectonic regime of the Andean convergent margin off Peru (SeaPERC cruise of the R/V *Jean Charcot*, July, 1986). *C. R. Acad. Sci. Paris*, 33:1599–1604.

Burckle, L. H., 1972. Late Cenozoic planktonic diatom zones from the eastern equatorial Pacific. *Nova Hedwigia, Beihefte*, 39:217–246.

Burckle, L. H., 1977. Pliocene and Pleistocene diatom datum levels from the equatorial Pacific. *Quat. Res.*, 7:330–340.

Burckle, L. H., 1984. Ecology and paleoecology of the marine diatom *Eucampia antarctica* (Castracane) Manguin. *Mar. Micropaleontol.*, 9:77–86.

Burckle, L. H., Hammond, S. R., and Seyb, S. M., 1982. A stratigraphically important new diatom from the Pleistocene of the North Pacific. *Pacific Sci.*, 32:209–214.

Ciesielski, P. F., 1983. The Neogene and Quaternary diatom biostratigraphy of subantarctic sediments, Deep Sea Drilling Project Leg 71. *In* Ludwig, W. J., Krasheninnikov, V. A., et al., *Init. Repts. DSDP*, 71: Washington (U.S. Govt. Printing Office), 635–665.

Claypool, G. E., and Kaplan, I. R., 1974. The origin and distribution of methane in marine sediments. *In* Kaplan, I.R. (Ed.), *Natural Gases in Marine Sediments*: New York (Plenum), 94–129.

Cushman, J., and Stone, B., 1947. An Eocene foraminiferal fauna from the Chira Shale of Peru. *Cushman Lab. Foram. Res. Spec. Publ.*, 20:1–27.

De Wever, P., 1982. Radiolaires du Trias et du Lias de la Téthys (taxonomie, stratigraphie). *Soc. Géol. Nord, Publ.*, 7:599.

De Wever, P., Riedel, W. R., et al., 1979. Recherches actuelles sur les Radiolaires en Europe. *Annu. Soc. Géol. Nord*, 98:205–222.

Doyle, P. S., and Riedel, W. R., 1980. Ichthyoliths from Site 436, northwest Pacific, Leg 56, Deep Sea Drilling Project. *In* Scientific Party, *Init. Repts. DSDP*, 56, 57, Pt. 2: Washington (U.S. Govt. Printing Office), 887–893.

Fenner, J., 1984. Eocene–Oligocene planktic diatom stratigraphy in the low latitudes and the high southern latitudes. *Micropaleontology*, 30:319–342.

Fenner, J., Schrader, H., and Wienigk, H., 1976. Diatom phytoplankton studies in the southern Pacific Ocean, composition and correlation to the Antarctic Convergence and its paleoecological significance. *In* Hollister, C. D., Craddock, C., et al., *Init. Repts. DSDP*, 36: Washington (U.S. Govt. Printing Office), 757–813.

Gersonde, R., and Schrader, H., 1984. Marine planktonic diatom correlation of the lower Messinian deposits in the western Mediterranean. *Mar. Micropaleontol.*, 9:93–110.

Gieskes, J. M., 1983. The chemistry of interstitial waters of deep sea sediments: interpretation of deep sea drilling data. *Chem. Oceanogr.*, 8:221.

Gombos, A. M., 1983. Middle Eocene diatoms from the South Atlantic. *In* Ludwig, W. J., Krasheninnikov, V. A., et al., *Init. Repts. DSDP*, 71: Washington (U.S. Govt. Printing Office), 565–581.

Gombos, A. M., and Ciesielski, P. F., 1983. Late Eocene to early Miocene diatoms from the southwest Atlantic. *In* Ludwig, W. J., Krasheninnikov, V. A., et al., *Init. Repts. DSDP*, 71: Washington (U.S. Govt. Printing Office), 583–634.

Hanshaw, B. B., and Coplen, T. B., 1973. Ultrafiltration by a compacted clay membrane; II. Sodium ion exclusion at various ionic strengths. *Geochim. Cosmochim. Acta*, 37:2311.

Hussong, D. M., and Wipperman, C. K., 1981. Vertical movement and tectonic erosion of the continental wall of the Peru-Chile Trench near 11°30′S latitude. *In* Kulm, L. D., Dymond, J., Dasch, E. J., and Hussong, D. M. (Eds.), *Nazca Plate: Crustal Formation and Andean Convergence*. Geol. Soc. Am. Mem., 154:509–524.

Hustedt, Fr., 1924. Vom Sammeln und Präparieren der Kieselalgen sowie Angaben über Untersuchungs- und Kulturmethoden. *In Handbuch der biologischen Arbeitsmethoden*: Abt. 11, Teil 4, Sonderdruck J. Cramer (Weinheim).

Jouse, A. P., Kazarina, G. Kh., and Mukhina, V. V., 1982. Distribution of diatoms in Pliocene and Pleistocene deposits from the middle America trench off Guatemala. *In* Aubouin, J., von Huene, R., et al., *Init. Repts. DSDP*, 67: Washington (U.S. Govt. Printing Office), 455–471.

Kling, S. A., 1978. Radiolaria. *In* Haq, B. U., and Boersma, A., *Introduction to Marine Micropaleontology*: Amsterdam (Elsevier), 9: 203–244.

Koizumi, I., 1973. The late Cenozoic diatoms of Sites 183-193, Leg 19. *In* Creager, J. S., Scholl, D. W., et al., *Init. Repts. DSDP*, 19: Washington (U.S. Govt. Printing Office), 805–855.

________, 1986. Pliocene and Pleistocene diatom datum levels related with paleoceanography in the northwest Pacific. *Mar. Micropaleontol.*, 10:309–325.

Koizumi, I., and Tanimura, Y., 1985. Neogene diatom biostratigraphy of the middle latitude western North Pacific, Deep Sea Drilling Project Leg 86. *In* Heath, G. R., Burckle, L. H., et al., *Init. Repts. DSDP*, 86: Washington (U.S. Govt. Printing Office), 269–300.

Kvenvolden, K. A., and McMenamin, M. K., 1980. Hydrates of natural gas: a review of their geologic occurrence. *U.S. Geol. Surv. Circ.*, 815.

Kvenvolden, K. A., Claypool, G. E., Threlkeld, C. N., and Sloan, E. D., 1984. Geochemistry of a naturally occurring massive marine gas hydrate. *Org. Geochem.*, 6:703–713.

Locker, S., and Martini, E., 1986. Silicoflagellates and some sponge spicules from the southwest Pacific, Deep Sea Drilling Project, Leg 90. *In* Kennett, J. P., von der Borsch, C. C., et al., *Init. Repts. DSDP*, 90: Washington (U.S. Govt. Printing Office), 887–924.

Marine, I. W., and Fritz, S. J., 1981. Osmotic model to explain anomalous hydraulic heads. *Water Pressure Res.*, 17:73.

Mertz, D., 1966. Mikropalaeontologische und sedimentologische Untersuchungen der Pisco Formation Suedperus. *Palaeontographica*, 118(Abt. B.):1–51.

Nigrini, C., 1977. Tropical Cenozoic artostrobiidae (Radiolaria). *Micropaleontology*, 23:241–265.

Poore, R. Z., 1979. Oligocene through Quaternary planktonic foraminiferal biostratigraphy of the north Atlantic: DSDP Leg 49. *In* Luyendyk, B. P., Cann, J. R., et al., *Init. Repts. DSDP*, 49: Washington (U.S. Govt. Printing Office), 675–706.

Rögl, F., and Bolli, H. M., 1973. Holocene to Pleistocene planktonic foraminifera of Leg 15, Site 147 (Cariaco Basin (Trench), Caribbean Sea) and their climatic interpretation. *In* Edgar, N. T., Saunders, J. B., et al., *Init. Repts. DSDP*, 15: Washington (U.S. Govt. Printing Office), 553–616.

Sancetta, C., 1982. Diatom biostratigraphy and paleoceanography, Deep Sea Drilling Project 68. *In* Prell, W. L., Gardner, J. V., et al., *Init. Repts. DSDP*, 68: Washington (U.S. Govt. Printing Office), 301–309.

Schrader, H., 1974. Cenozoic marine planktonic diatom stratigraphy of the tropical Indian Ocean. *In* Fisher, R. L., Bunce, E. T., et al., *Init. Repts. DSDP*, 24: Washington (U.S. Govt. Printing Office), 887–967.

________, 1976. Cenozoic planktonic diatom biostratigraphy of the southern Ocean. *In* Hollister, C. D., Craddock, C., et al., *Init. Repts. DSDP*, 35: Washington (U.S. Govt. Printing Office), 605–671.

Schrader, H., and Fenner, J., 1976. Norwegian Sea Cenozoic diatom biostratigraphy and taxonomy. *In* Talwani, M., Udintsev, G., et al., *Init. Repts. DSDP*, 38: Washington (U.S. Govt. Printing Office), 921–1099.

Schrader, H., and Gersonde, R., 1978. Diatoms and silicoflagellates. *In* Zachariasse, W. J., et al. (Eds.), Micropaleontological counting methods and techniques—an exercise on an 8-m section of the lower Pliocene of Capo Rossello, Sicily. *Utrecht Micropaleontol. Bull.*, 17: 129–176.

Schrader, H., and Cruzado, J., 1987. Diatom biostratigraphy of the Ballena and Delfin wells off the coast of central Peru. *Trans. Geol. Con. Peru* (Lima, July 1987).

Shipley, T. H., Houston, M. H., Buffler, R. T., Shaub, F. J., McMillan, K. J., Ladd, J. W., and Worzel, J. L., 1979. Seismic evidence for widespread possible gas hydrate horizons on continental slopes and rises. *AAPG Bull.*, 63:2204–2213.

Sloan, E. D., 1985. Shore-based laboratory experimental measurements on a gas hydrate sample recovered at Site 570. *In* von Huene, R., Aubouin, J., et al., *Init. Repts. DSDP*, 84: Washington (U.S. Govt. Printing Office), 695–698.

Tappan, H., 1980. *The Paleobiology of Plant Protists*: San Francisco (W. H. Freeman).

Thornburg, T. M., 1985. Seismic stratigraphy of Peru forearc basins. *In* Hussong, D. M., et al. (Eds.), *Atlas of the Ocean Margin Drilling Program, Peru Continental Margin, Region VI*: Woods Hole (Marine Science Int.).

Ms 112A-119

SITE 688 HOLE A CORE 1H CORED INTERVAL 3819.8-3828.1 mbsl; 0.0-8.3 mbsf

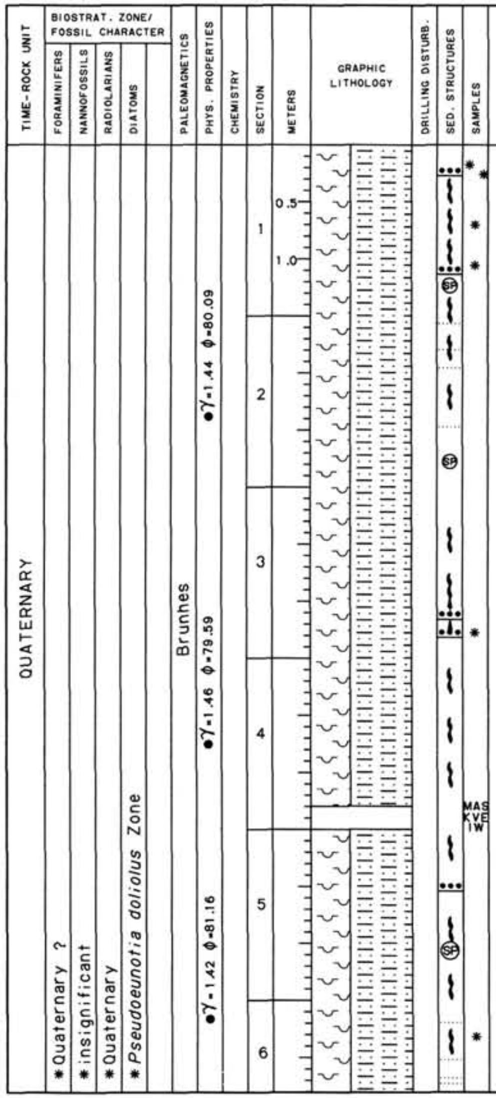

LITHOLOGIC DESCRIPTION

DIATOMACEOUS MUD

Major lithology: diatomaceous mud, dark olive gray (5Y 3/2), homogeneous to moderately bioturbated with small irregular patches of monosulfides and pockets of sponge spicules throughout.

Minor lithologies:
1. grayish (N 4), quartz-feldspathic, ungraded, well-sorted sand, e.g., Section 1, 111 cm, and Section 6, 45 cm.
2. brownish gray (5Y 4/1) benthic-foraminifer-bearing turbidite. Detrital input is about 15% to 20%, e.g., Section 1, 25 cm, and Section 3, 120-130 cm.

SMEAR SLIDE SUMMARY (%):

	1, 23 M	1, 26 M	1, 76 D	1, 108 M	3, 130 M	6, 35 D
TEXTURE:						
Sand	30	70	—	80	80	—
Silt	40	20	20	10	15	55
Clay	30	10	80	10	5	45
COMPOSITION:						
Quartz	15	9	5	40	25	7
Feldspar	15	8	Tr	30	25	8
Rock fragments	5	3	—	5	15	—
Mica	Tr	Tr	—	—	—	—
Clay	20	10	35	5	5	45
Volcanic glass	—	—	—	5	Tr	—
Calcite/dolomite	Tr	—	20	5	—	Tr
Accessory minerals						
Phosphorite	—	2	—	—	Tr	—
Glauconite	—	5	Tr	—	Tr	Tr
Opaques	—	—	—	5	—	—
Foraminifers	30	60	—	5	30	—
Nannofossils	2	Tr	10	—	—	—
Diatoms	5	3	30	—	Tr	40
Radiolarians	—	—	—	—	Tr	—
Sponge spicules	—	—	Tr	—	Tr	—
Silicoflagellates	—	—	Tr	—	Tr	—

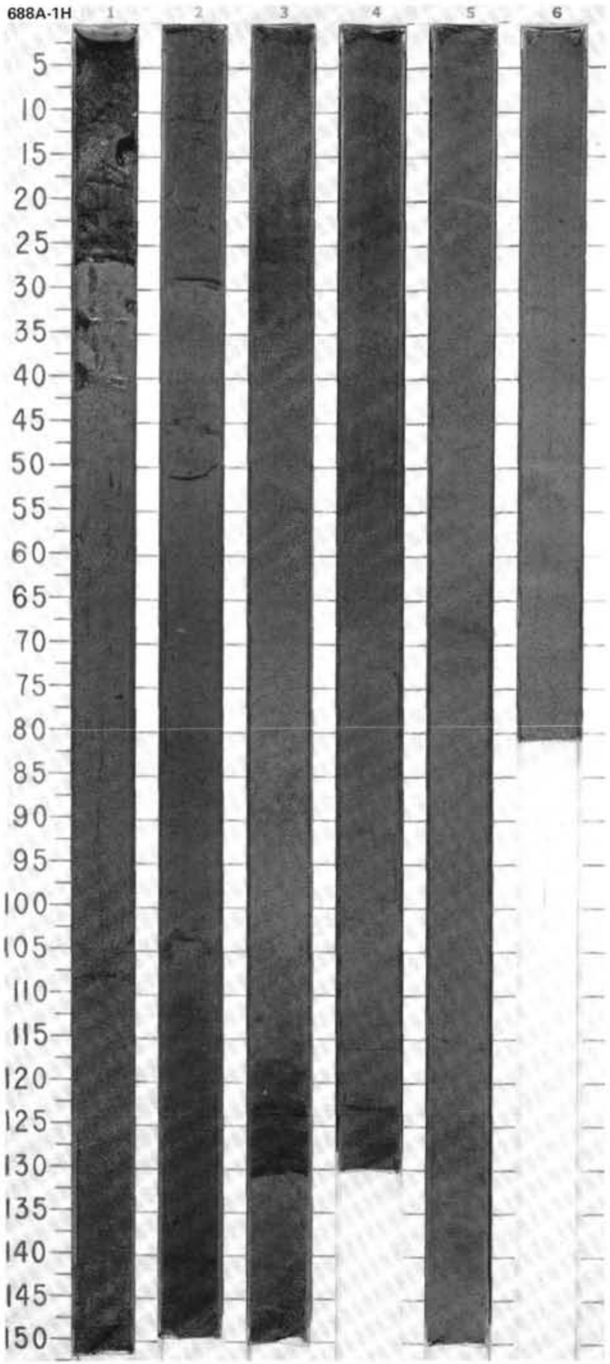

SITE 688 HOLE A CORE 2H CORED INTERVAL 3828.1-3837.6 mbsl; 8.3-17.8 mbsf

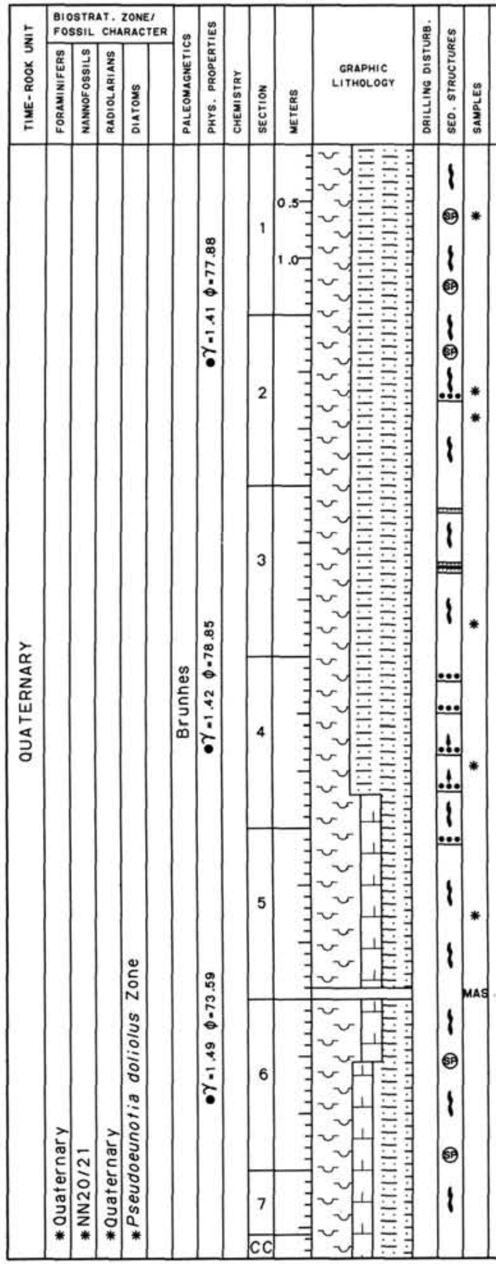

LITHOLOGIC DESCRIPTION

DIATOMACEOUS MUD

Major lithology: diatomaceous mud, dark olive gray (5Y 3/2) to olive gray (5Y 4/2), extensively bioturbated with small irregular patches of monosulfides and pockets of sponge spicules throughout. Foraminifer-bearing in the lowest part of the core.

Minor lithologies:
1. grayish (N 4/),quartz-feldspathic, ungraded, well-sorted sand.
2. brownish gray (5Y 4/1) benthic-foraminifer-bearing turbidite.

SMEAR SLIDE SUMMARY (%):

	1, 68 D	2, 73 M	2, 85 D	3, 127 M	4, 94 D	5, 78 D	7, 38 D
TEXTURE:							
Sand	5	50	—	80	—	10	15
Silt	60	25	63	10	55	60	75
Clay	35	25	37	10	45	30	10
COMPOSITION:							
Quartz	8	10	7	35	5	2	10
Feldspar	8	10	8	25	5	3	10
Rock fragments	4	—	5	5	—	1	4
Mica	—	—	—	2	—	Tr	1
Clay	35	25	37	10	20	27	17
Volcanic glass	5	—	—	3	—	Tr	—
Calcite/dolomite	—	7	3	3	10	5	5
Accessory minerals	—	—	—	2	—	—	1
Glauconite	Tr	5	Tr	2	—	1	2
Hornblende	—	—	—	5	—	—	3
Pyrite	—	—	—	3	—	3	2
Micrite	—	—	—	—	—	—	2
Foraminifers	Tr	40	Tr	Tr	20	2	15
Nannofossils	—	3	—	—	10	5	2
Diatoms	40	—	40	5	15	50	25
Radiolarians	Tr	—	Tr	—	—	—	1
Sponge spicules	—	—	—	Tr	—	1	Tr
Silicoflagellates	Tr	—	Tr	—	—	—	—
Pellets?	—	—	—	—	15	—	—

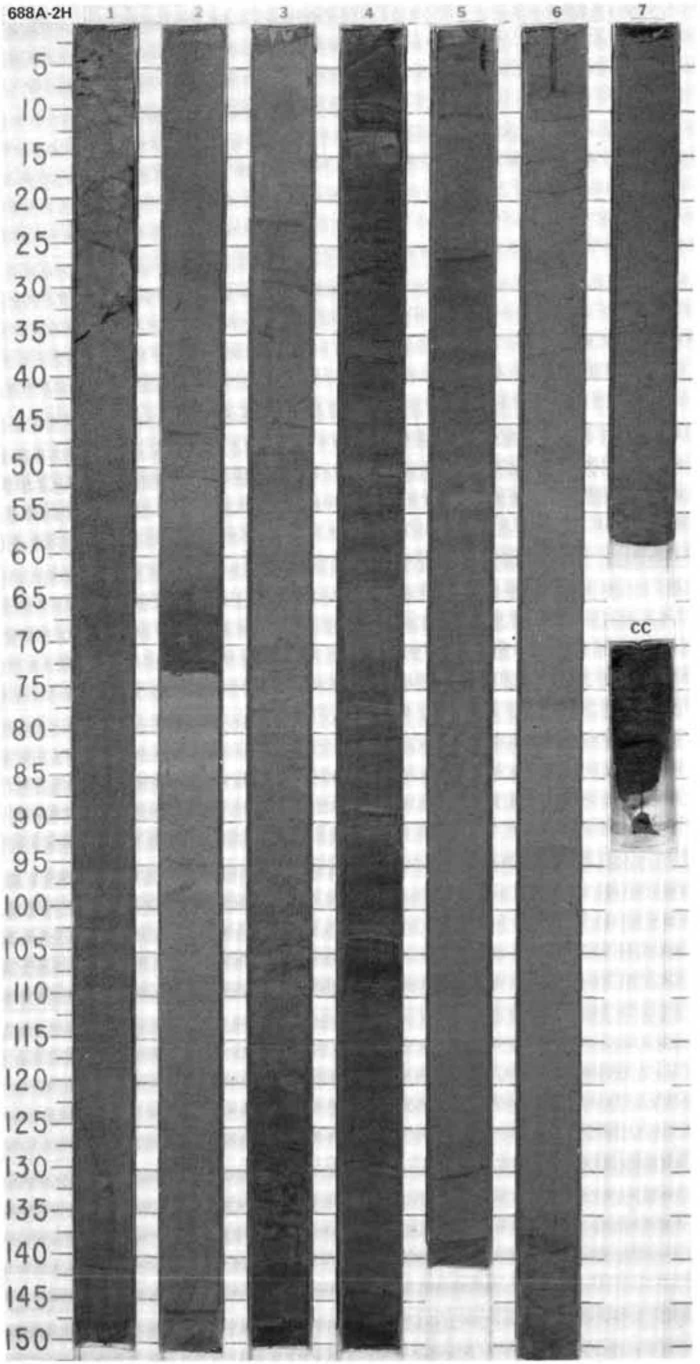

SITE 688 HOLE A CORE 3H CORED INTERVAL 3837.6-3847.1 mbsl; 17.8-27.3 mbsf

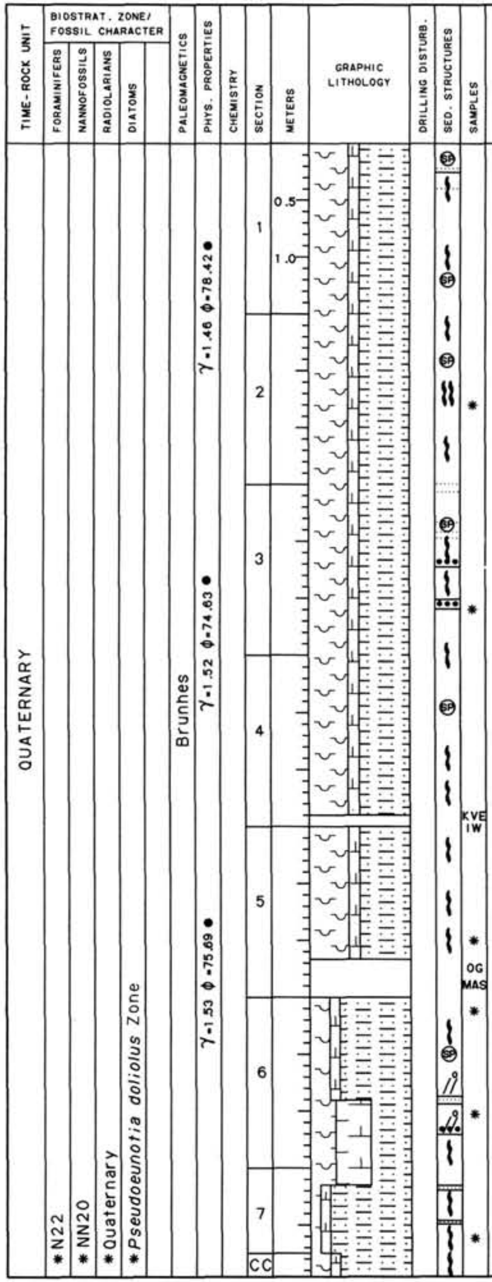

LITHOLOGIC DESCRIPTION

FORAMINIFER-BEARING DIATOMACEOUS MUD

Major lithology: foraminifer-bearing diatomaceous mud, dark olive gray (5Y 3.5/2) to dark greenish gray (5GY 4/1), extensively bioturbated with small irregular patches of monosulfides and pockets of sponge spicules throughout. Slight color changes from lighter to darker.

Minor lithologies:
1. black (5Y 2.5/2), monosulfide-rich diatomaceous mud.
2. grayish (N 4/), quartz-feldspathic ungraded sand.
3. brownish gray (5Y 4/1) benthic-foraminifer-bearing turbidite.

SMEAR SLIDE SUMMARY (%):

	2, 78 D	3, 117 M	5, 100 D	6, 14 D	6, 111 D	7, 63 D
TEXTURE:						
Sand	—	85	—	—	10	—
Silt	65	15	65	50	40	35
Clay	35	—	35	50	50	65
COMPOSITION:						
Quartz	5	20	15	5	7	2
Feldspar	5	20	15	5	7	3
Rock fragments	—	15	—	2	2	1
Mica	—	—	—	1	1	1
Clay	35	—	35	52	34	64
Volcanic glass	—	—	—	1	—	3
Calcite/dolomite	5	—	8	3	3	—
Accessory minerals	—	10	—	—	—	—
Glauconite	—	5	—	1	1	—
Phosphate	—	5	—	—	—	—
Pyrite	—	—	—	3	1	2
Hornblende	—	—	—	1	1	—
Collophane	—	—	—	2	—	2
Micrite	—	—	—	—	1	—
Foraminifers	10	25	7	1	20	2
Nannofossils	Tr	—	Tr	—	15	3
Diatoms	40	—	20	20	5	15
Radiolarians	—	—	—	2	1	1
Sponge spicules	—	—	Tr	1	1	—
Silicoflagellates	—	—	—	—	—	1

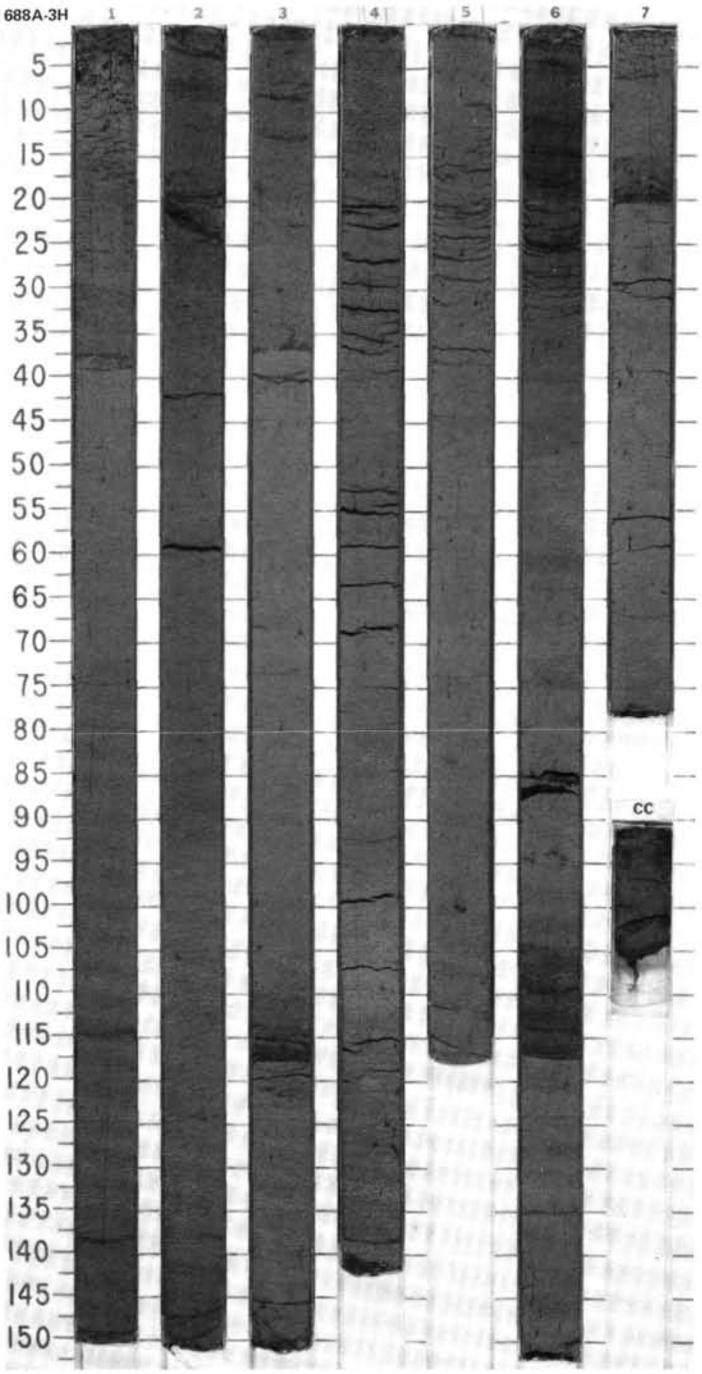

SITE 688 HOLE A CORE 4H CORED INTERVAL 3847.1-3856.6 mbsl; 27.3-36.8 mbsf

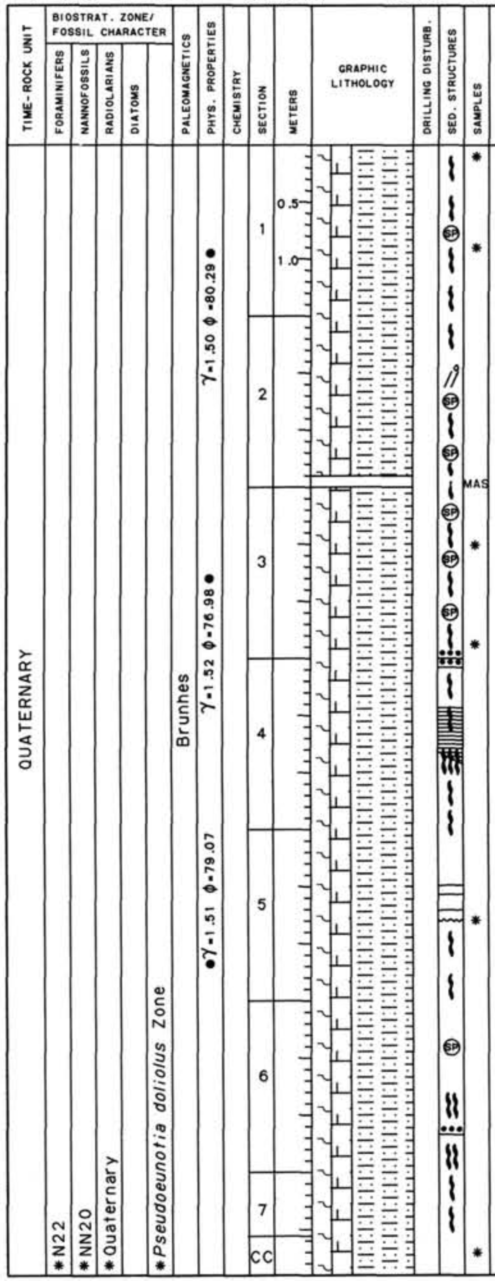

LITHOLOGIC DESCRIPTION

FORAMINIFER-NANNOFOSSIL-BEARING DIATOMACEOUS MUD

Major lithology: foraminifer-nannofossil-bearing diatomaceous mud, dark greenish gray (5GY 4/1) to greenish gray (5Y 5/1) and dark olive gray (5Y 3/2). Moderately bioturbated with small irregular patches of monosulfides and pockets of sponge spicules throughout.

Minor lithologies:

1. quartz-feldspathic, ungraded, well-sorted sand. Mica is abundant. Associated with erosional features.
2. brownish gray (5Y 4/1), benthic-foraminifer-bearing turbidite.

SMEAR SLIDE SUMMARY (%):

	1, 10 M	1, 82 M	3, 55 D	3, 137 M	5, 81 M	CC, 12 D
TEXTURE:						
Sand	—	5	—	50	80	—
Silt	45	50	30	40	15	50
Clay	55	45	70	10	5	50
COMPOSITION:						
Quartz	—	5	5	20	25	10
Feldspar	—	—	—	5	25	—
Rock fragments	—	—	—	—	20	—
Mica	—	10	5	5	Tr	5
Clay	20	10	20	10	5	—
Volcanic glass	—	—	—	—	—	Tr
Calcite/dolomite	10	20	20	30	Tr	40
Accessory minerals	—	—	—	—	10	—
Iron sulfides	10	—	Tr	10	Tr	—
Biotite	—	Tr	—	—	—	—
Hornblende	—	—	—	—	Tr	Tr
Foraminifers	15	—	10	20	15	5
Nannofossils	25	Tr	10	Tr	—	15
Diatoms	20	50	30	—	—	20
Radiolarians	—	—	Tr	—	—	—
Sponge spicules	—	Tr	Tr	—	—	5
Silicoflagellates	Tr	5	Tr	—	—	Tr
Fish remains	—	—	—	—	—	Tr

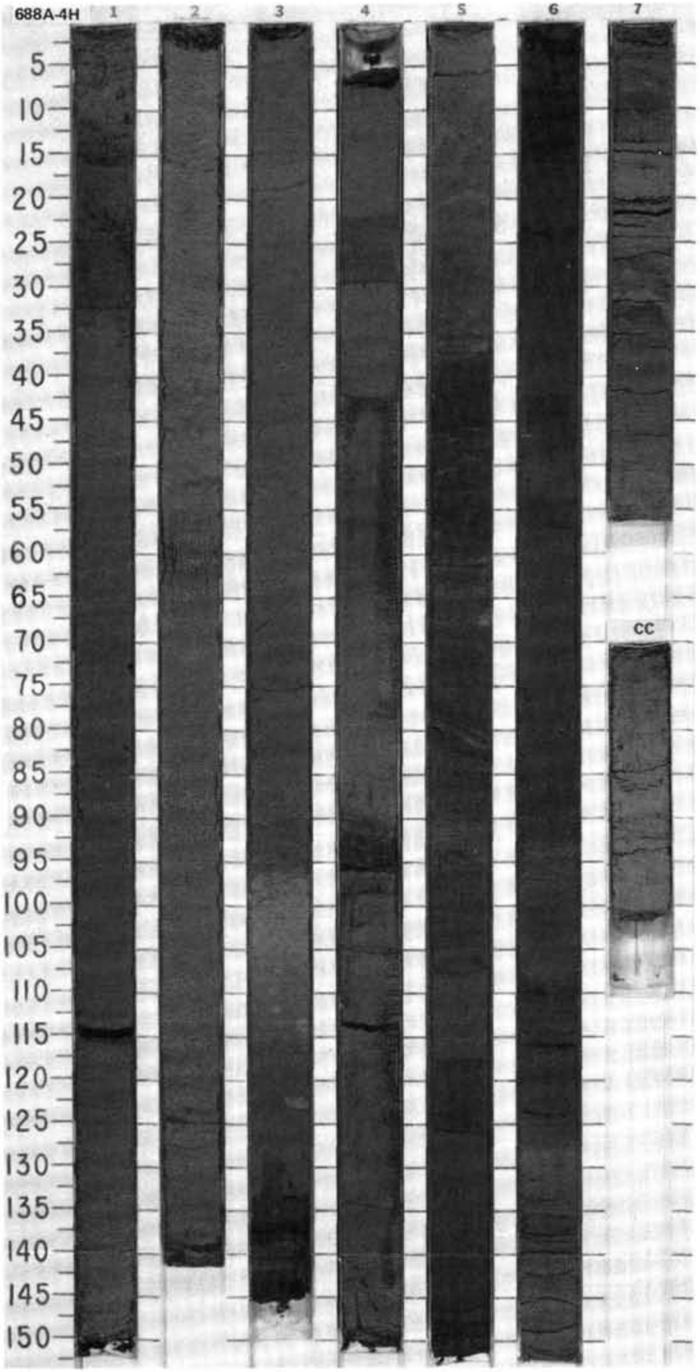

SITE 688 HOLE A CORE 5H CORED INTERVAL 3856.6-3866.1 mbsl; 36.8-46.3 mbsf

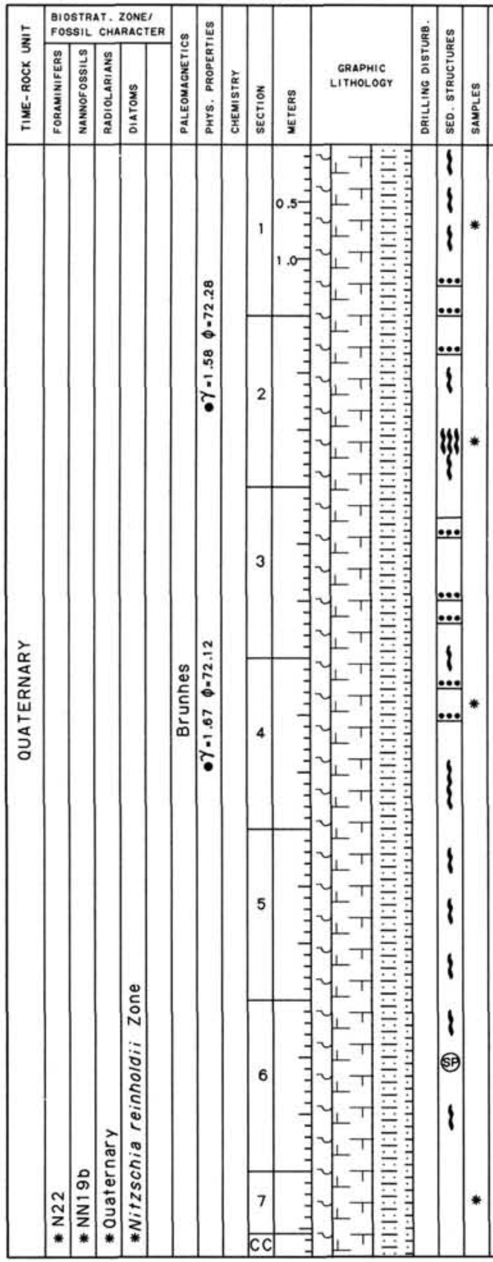

LITHOLOGIC DESCRIPTION

DIATOM-BEARING FORAMINIFER-NANNOFOSSIL MUD

Major lithology: diatom-bearing foraminifer-nannofossil mud, dark olive gray (5GY 3/2) to olive (5Y 5/3) and dark greenish gray (5GY 4/1) to greenish gray (5GY 5/1). Extensively bioturbated with small dots of monosulfides and sponge spicule nests throughout.

Minor lithologies:
1. quartz-feldspathic foraminifer-bearing sandy turbidite, brownish gray (5Y 4/1). Sequences are 5–10-cm thick.
2. very finely laminated sandy to silty detrital material. Interbedded with mud, <1-mm thick.

SMEAR SLIDE SUMMARY (%):

	1, 75 D	2, 118 M	4, 48 M	7, 27 D
TEXTURE:				
Sand	5	30	85	—
Silt	40	40	10	30
Clay	55	30	5	70
COMPOSITION:				
Quartz	5	30	20	5
Feldspar	5	10	20	—
Rock fragments	—	—	25	—
Mica	—	—	Tr	5
Clay	30	—	5	30
Calcite/dolomite	10	35	—	20
Pyrite	Tr	—	—	—
Hornblende	—	5	—	—
Phosphorite	—	—	5	—
Foraminifers	5	5	15	Tr
Nannofossils	30	15	—	20
Diatoms	10	—	—	20
Sponge spicules	Tr	—	—	Tr
Pellets	5	—	—	—

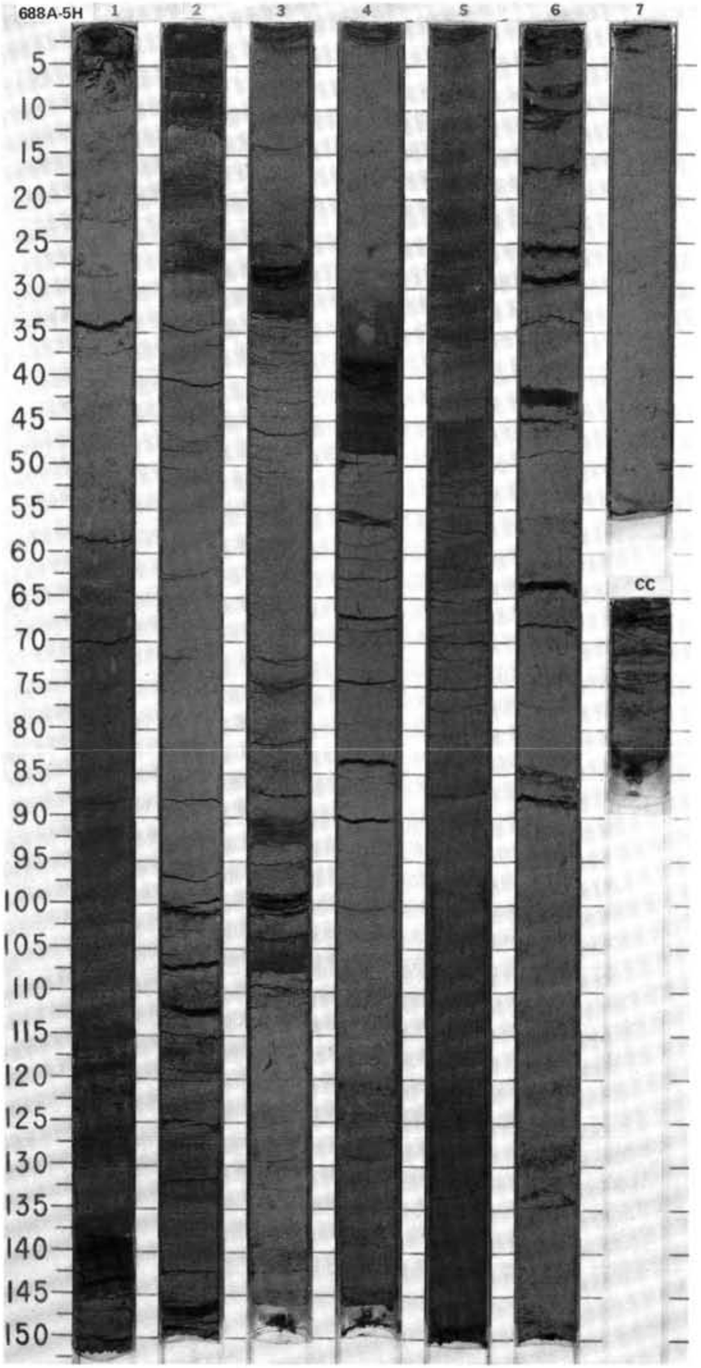

SITE 688 HOLE A CORE 6H CORED INTERVAL 3866.1-3875.6 mbsl; 46.3-55.8 mbsf

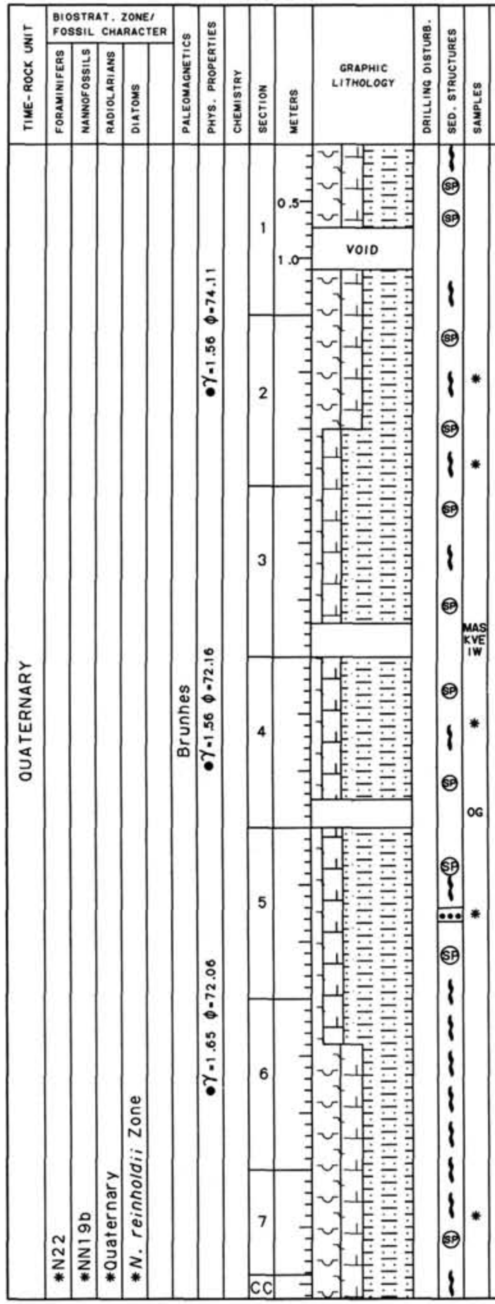

LITHOLOGIC DESCRIPTION

FORAMINIFER-NANNOFOSSIL-BEARING DIATOMACEOUS MUD

Major lithology: foraminifer-nannofossil-bearing diatomaceous mud, dark greenish gray (5GY 4/1) to greenish gray (5GY 5/1). Moderately to extensively bioturbated, rare isolated to very abundant sponge spicule nests with irregular patches of monosulfides associated with pyrite.

Minor lithology: quartz-rich, calcareous, brownish (5Y 3/2), foraminifer-bearing turbidite.

SMEAR SLIDE SUMMARY (%):

	2, 53 D	2, 136 D	4, 54 D	5, 78 M	7, 39 D
TEXTURE:					
Sand	—	—	—	30	5
Silt	60	40	60	20	35
Clay	40	60	40	50	60
COMPOSITION:					
Quartz	5	15	7	20	10
Feldspar	5	5	8	5	—
Rock fragments	—	15	—	—	—
Mica	—	Tr	—	5	10
Clay	30	30	40	10	30
Calcite/dolomite	10	10	10	30	—
Accessory minerals					
Pyrite	—	7	—	—	5
Opaques	—	—	5	5	—
Hornblende	—	—	—	5	—
Foraminifers	15	2	15	10	—
Nannofossils	10	1	Tr	10	15
Diatoms	25	15	15	—	30
Silicoflagellates	Tr	Tr	Tr	—	—

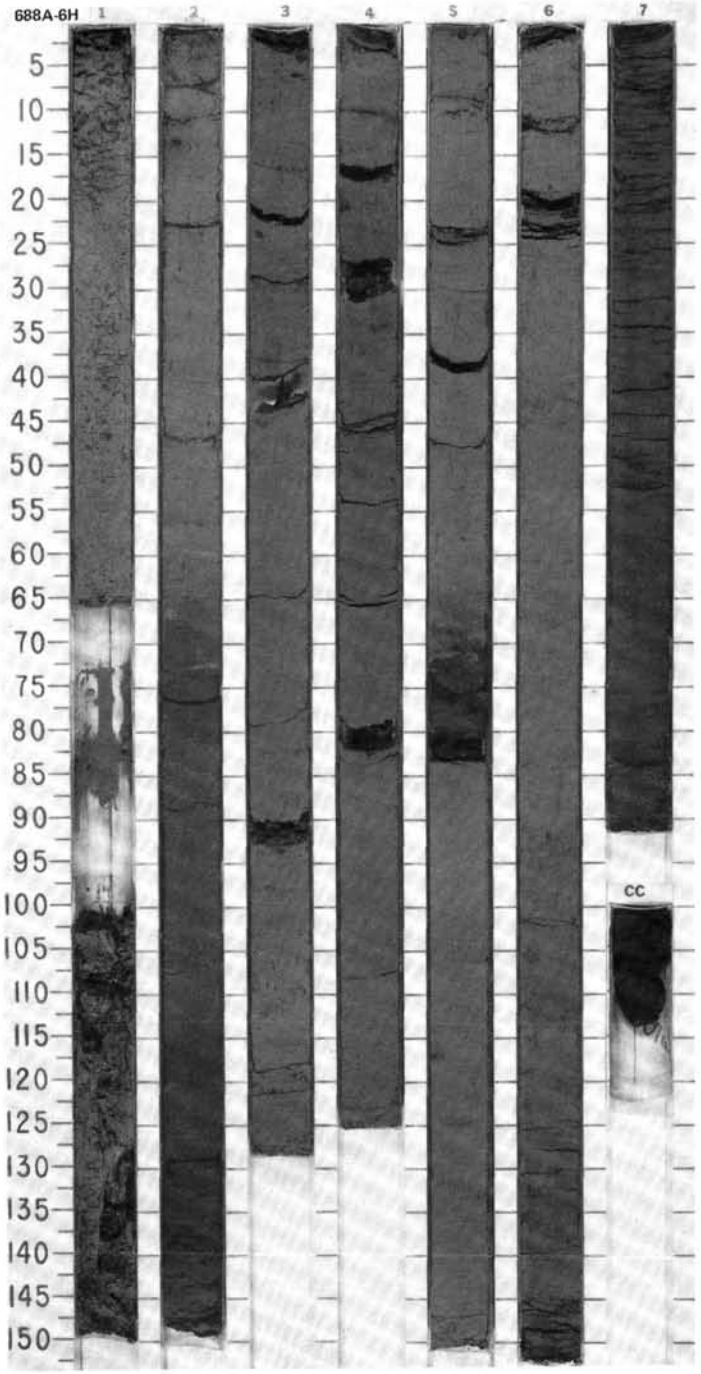

SITE 688 HOLE A CORE 7H CORED INTERVAL 3875.6-3885.1 mbsl; 55.8-65.3 mbsf

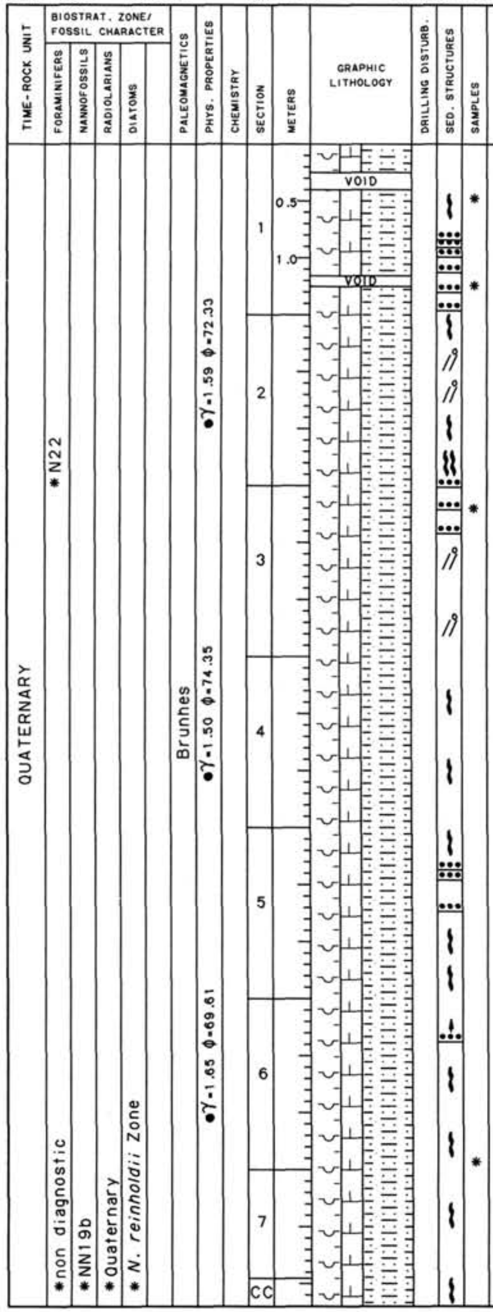

LITHOLOGIC DESCRIPTION

FORAMINIFER-NANNOFOSSIL-BEARING DIATOMACEOUS MUD

Major lithology: foraminifer-nannofossil-bearing diatomaceous mud, dark olive gray (5Y 4/1) to olive (5Y 4.5/2) and dark gray (3Y 3/2) to greenish gray (5GY 5/1). Extensively bioturbated, patches of monosulfides associated with pyrite (3 to 15%).

Minor lithology: quartzo-feldspathic, brownish (2.5Y 3/2) turbidite, with 14 well-graded sequences throughout core. Dewatering vein structures.

SMEAR SLIDE SUMMARY (%):

	1, 57 D	1, 128 M	3, 23 D	6, 143 D
TEXTURE:				
Sand	5	95	35	5
Silt	50	5	25	55
Clay	45	—	40	40
COMPOSITION:				
Quartz	4	20	10	4
Feldspar	8	15	10	10
Rock fragments	8	30	5	5
Mica	—	Tr	—	—
Clay	30	Tr	20	28
Volcanic glass	2	Tr	—	3
Calcite/dolomite	5	—	8	5
Accessory minerals	3	3	—	3
Pyrite	3	15	7	4
Phosphate	—	5	—	—
Amphibole	—	10	—	—
Foraminifers	5	2	15	8
Nannofossils	4	Tr	5	2
Diatoms	28	—	20	26
Radiolarians	Tr	—	—	—
Sponge spicules	—	Tr	—	2
Silicoflagellates	Tr	—	—	Tr

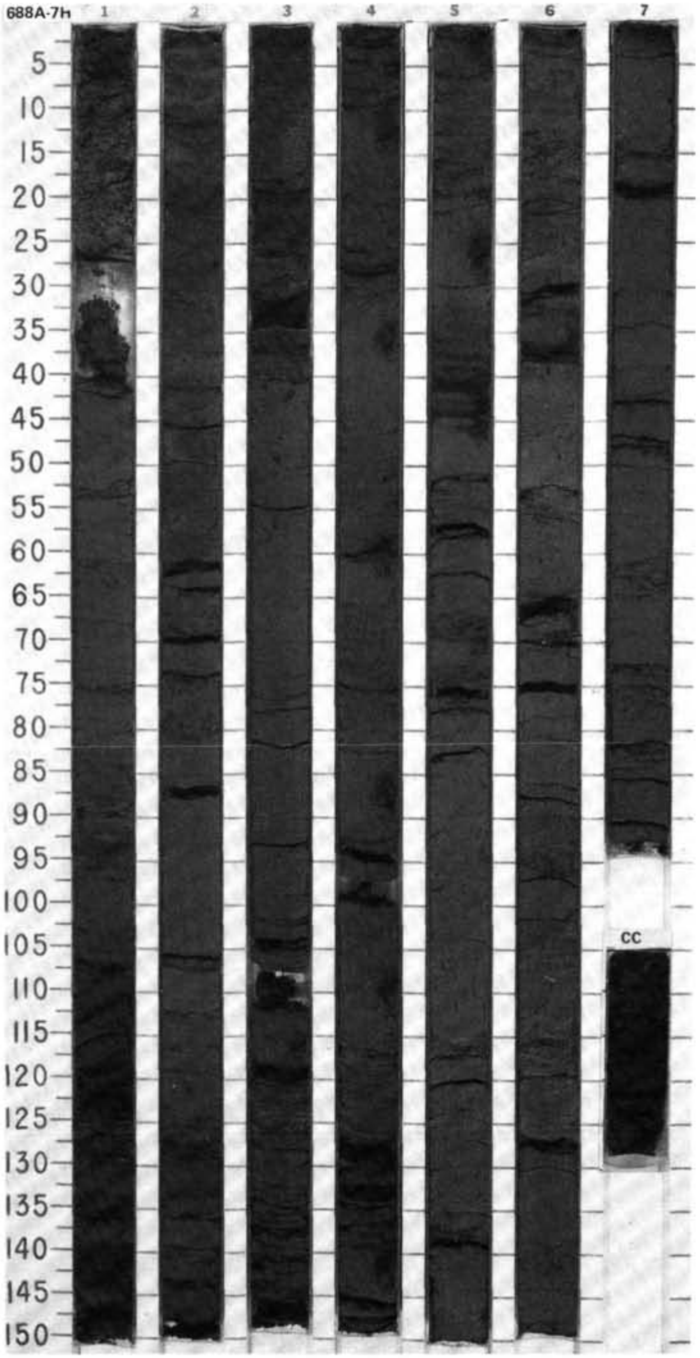

SITE 688 HOLE A CORE 8X CORED INTERVAL 3885.1-3894.6 mbsl; 65.3-74.8 mbsf

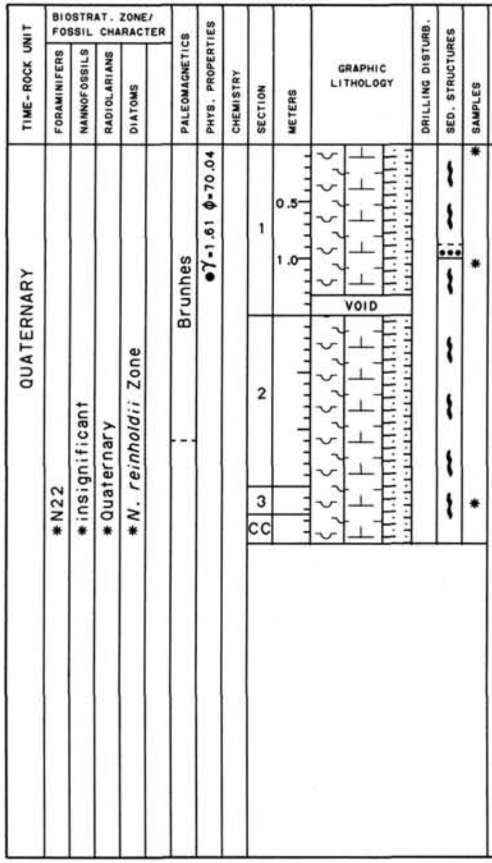

LITHOLOGIC DESCRIPTION

DIATOM-BEARING FORAMINIFER-NANNOFOSSIL MUD

Major lithology: diatom-bearing foraminifer-nannofossil mud, olive green (5GY 4/2) to dark olive gray (5Y 3/2) and very dark brown (5Y 2/2). Moderately bioturbated, pyrite associated with monosulfides.

Minor lithology: black (5Y 2.5/1) graded sand, foraminifer-bearing quartzo-feldspathic turbidite.

SMEAR SLIDE SUMMARY (%):

	1, 10 D	1, 105 D	3, 14 D
TEXTURE:			
Sand	15	5	5
Silt	45	40	50
Clay	40	55	45
COMPOSITION:			
Quartz	2	5	5
Feldspar	5	4	2
Rock fragments	5	Tr	—
Clay	29	40	15
Volcanic glass	2	—	—
Calcite/dolomite	3	2	20
Accessory minerals	—	Tr	—
Pyrite	3	10	2
Foraminifers	30	—	5
Nannofossils	5	—	20
Diatoms	15	35	30
Radiolarians	Tr	2	1
Sponge spicules	—	Tr	—
Silicoflagellates	1	2	Tr

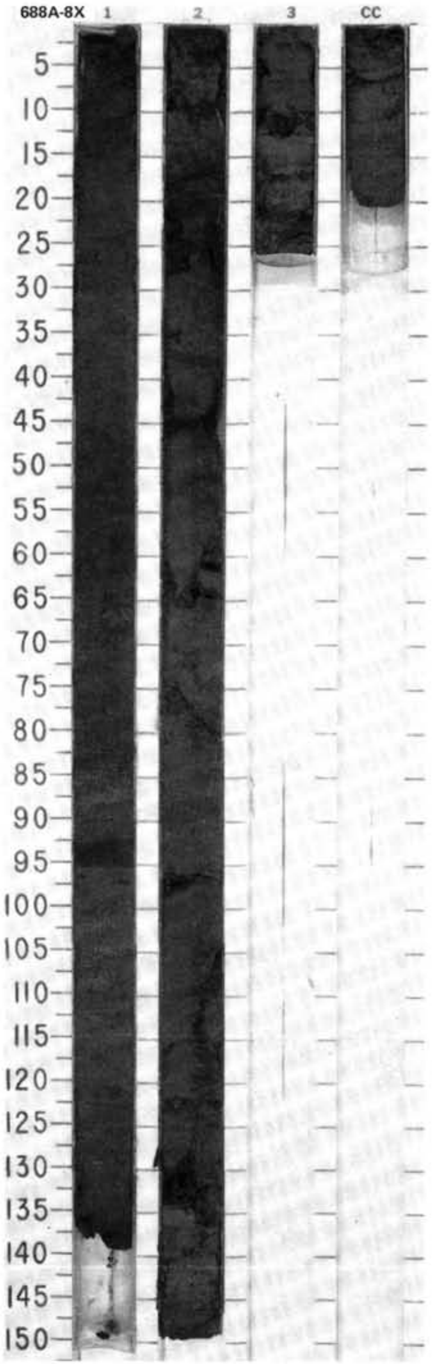

SITE 688 HOLE A CORE 9X CORED INTERVAL 3894.6-3904.1 mbsl; 74.8-84.3 mbsf

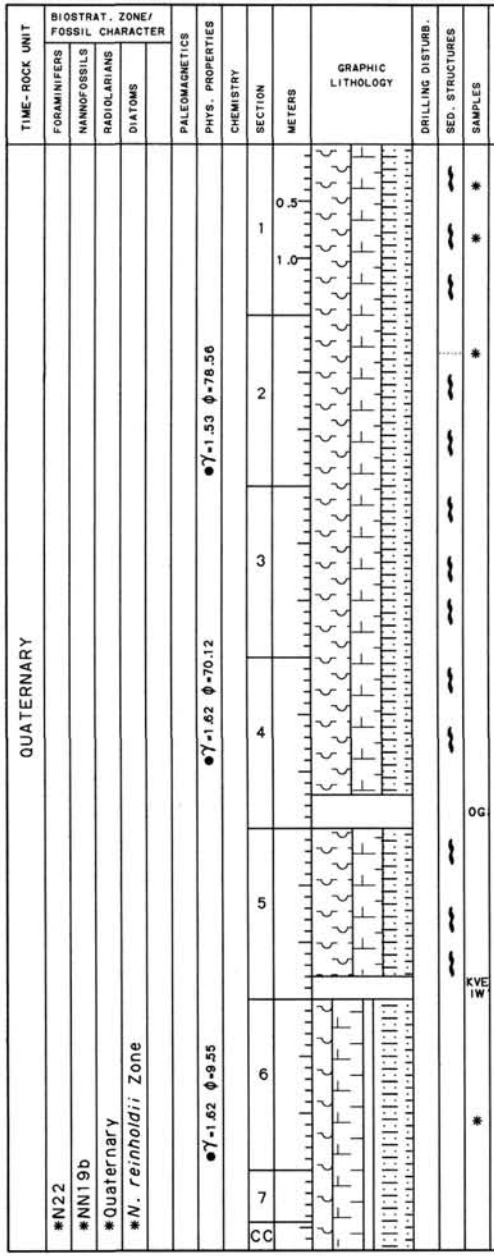

LITHOLOGIC DESCRIPTION

FORAMINIFER-NANNOFOSSIL-BEARING DIATOMACEOUS MUD and IRON MONOSULFIDE-RICH FORAMINIFER-BEARING DIATOMACEOUS MUD

Major lithology: Sections 1 through 5: foraminifer-nannofossil-bearing diatomaceous mud, olive gray (5Y 4/2), dark olive gray (5Y 3/2), and dark gray (5Y 3/1). Moderately bioturbated, pyrite associated with monosulfides.

Sections 6, 7, and CC: iron monosulfide-rich foraminifer-bearing diatomaceous mud, black (2.5Y 2/0). Moderately bioturbated. Note: component with no symbol is pyrite/monosulfides.

Color change from black (2.5Y 2/0) to olive black (5Y 2.5/2) which occurs in 1 to several hours is related to oxidation of iron monosulfides.

Minor lithology: diatom nannofossil ooze, Sections 1–5.

SMEAR SLIDE SUMMARY (%):

	1, 27 D	1, 87 D	2, 39 M	6, 105 D
TEXTURE:				
Sand	20	5	15	15
Silt	45	55	50	40
Clay	35	40	35	45
COMPOSITION:				
Quartz	2	2	10	3
Feldspar	5	5	5	8
Rock fragments	3	2	—	2
Mica	—	—	5	—
Clay	15	15	25	29
Volcanic glass	2	—	—	3
Calcite/dolomite	4	—	—	2
Accessory minerals				
Pyrite/monosulfide	5	2	5	3
Amphibole	—	—	Tr	—
Foraminifers	30	10	—	25
Nannofossils	2	20	—	5
Diatoms	30	40	40	20
Radiolarians	1	2	7	—
Sponge spicules	—	2	2	Tr
Silicoflagellates	1	Tr	1	Tr

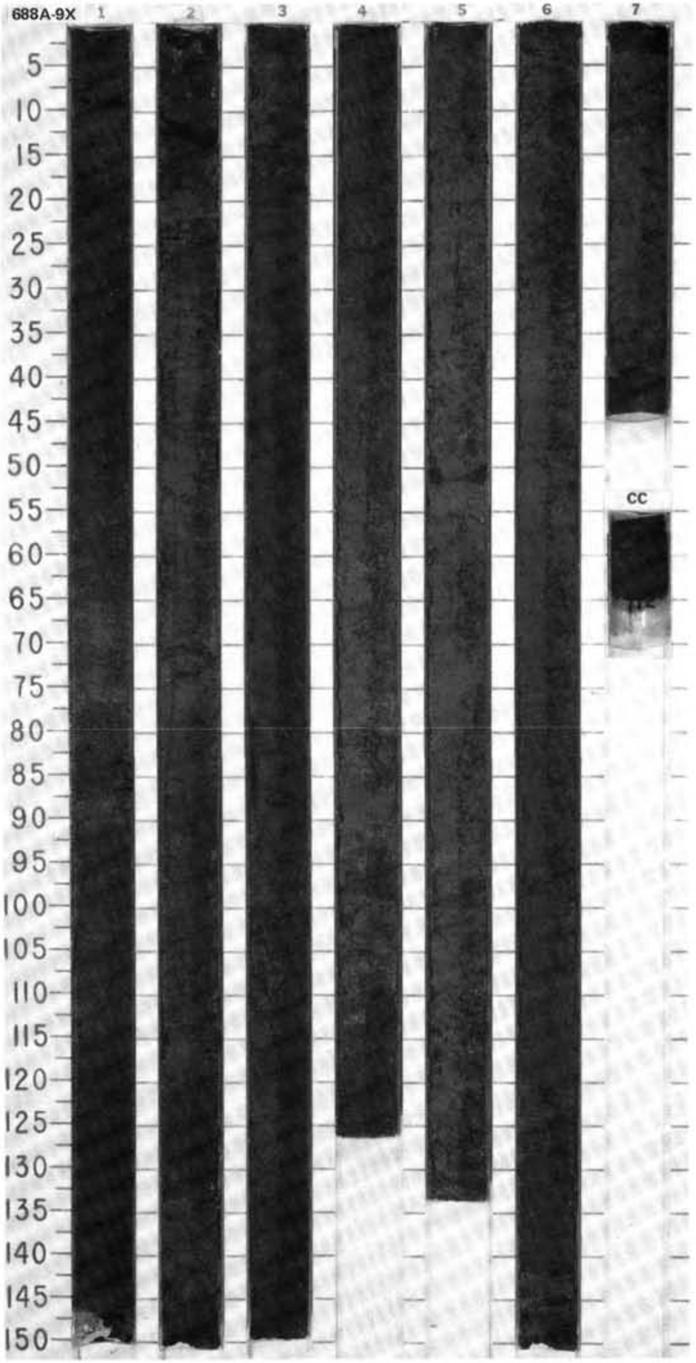

SITE 688 HOLE A CORE 10X CORED INTERVAL 3904.1-3913.6 mbsl; 84.3-93.8 mbsf

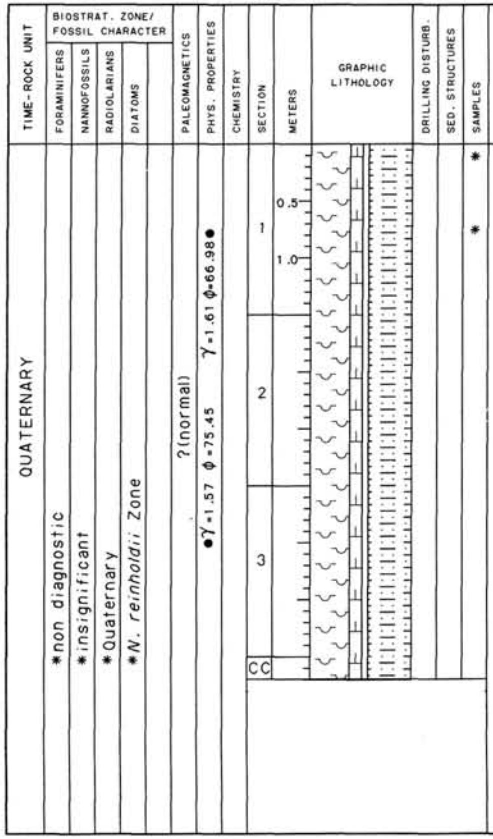

LITHOLOGIC DESCRIPTION

FORAMINIFER-NANNOFOSSIL-BEARING DIATOMACEOUS MUD

Major lithology: foraminifer-nannofossil-bearing diatomaceous mud, black (2.5Y 2/0). Pyrite and iron monosulfide-rich. Rapid color change after core splitting related to oxidation of iron monosulfide. Moderately bioturbated. Note: component with no symbol is *pyrite/monosulfides.*

Minor lithology: rare sponge spicule nests, 1 to 5–6 mm.

SMEAR SLIDE SUMMARY (%):

	1, 17 M	1, 80 D
TEXTURE:		
Sand	—	5
Silt	2	65
Clay	98	30
COMPOSITION:		
Quartz	—	4
Feldspar	—	6
Rock fragments	—	2
Clay	—	25
Calcite/dolomite	Tr	3
Accessory minerals	—	3
Pyrite	85	6
Iron sulfides	15	—
Foraminifers	—	10
Nannofossils	—	2
Diatoms	—	37
Radiolarians	Tr	—
Sponge spicules	Tr	Tr
Silicoflagellates	—	—

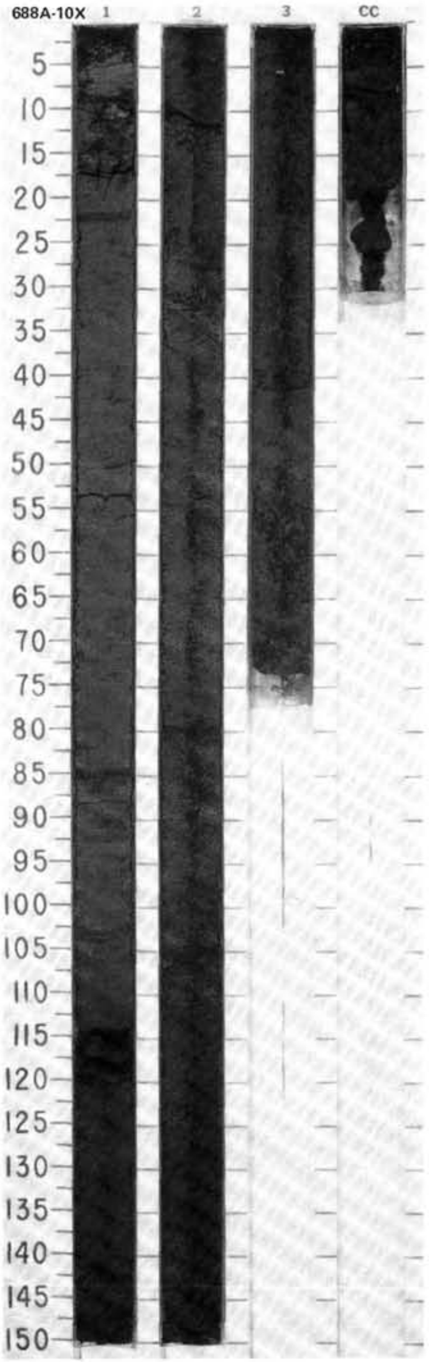

SITE 688 HOLE A CORE 11X CORED INTERVAL 3913.6-3923.1 mbsl; 93.8-103.3 mbsf

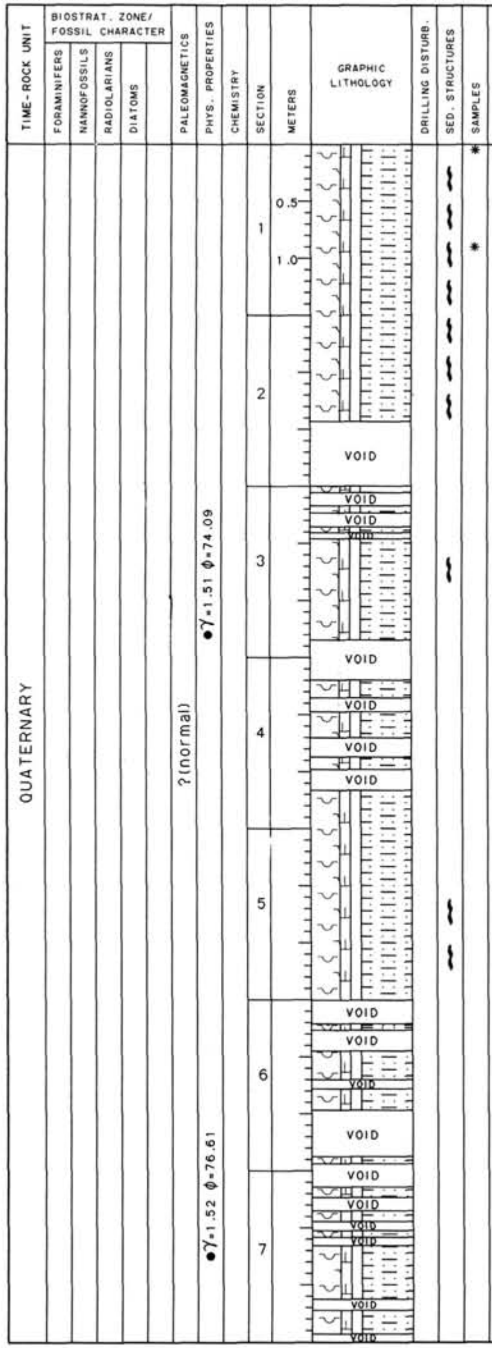

LITHOLOGIC DESCRIPTION

FORAMINIFER-NANNOFOSSIL-BEARING DIATOMACEOUS MUD

Major lithology: foraminifer-nannofossil-bearing diatomaceous mud, black (2.5Y 2/0). Pyrite and iron monosulfide-rich. Rapid color change after core splitting related to oxidation of iron monosulfide. Moderately bioturbated. Note: component with no symbol is pyrite/monosulfides.

Minor lithology: rare sponge spicule nests, 1 to 5–6 mm.

SMEAR SLIDE SUMMARY (%):

	1, 4 M	1, 93 D
TEXTURE:		
Sand	5	1
Silt	40	34
Clay	55	65
COMPOSITION:		
Quartz	10	10
Feldspar	10	10
Clay	30	45
Calcite/dolomite	10	2
Accessory minerals		
Pyrite	5	5
Glauconite	Tr	Tr
Hornblende	—	Tr
Foraminifers	5	2
Nannofossils	5	—
Diatoms	25	25
Radiolarians	Tr	—
Sponge spicules	Tr	1

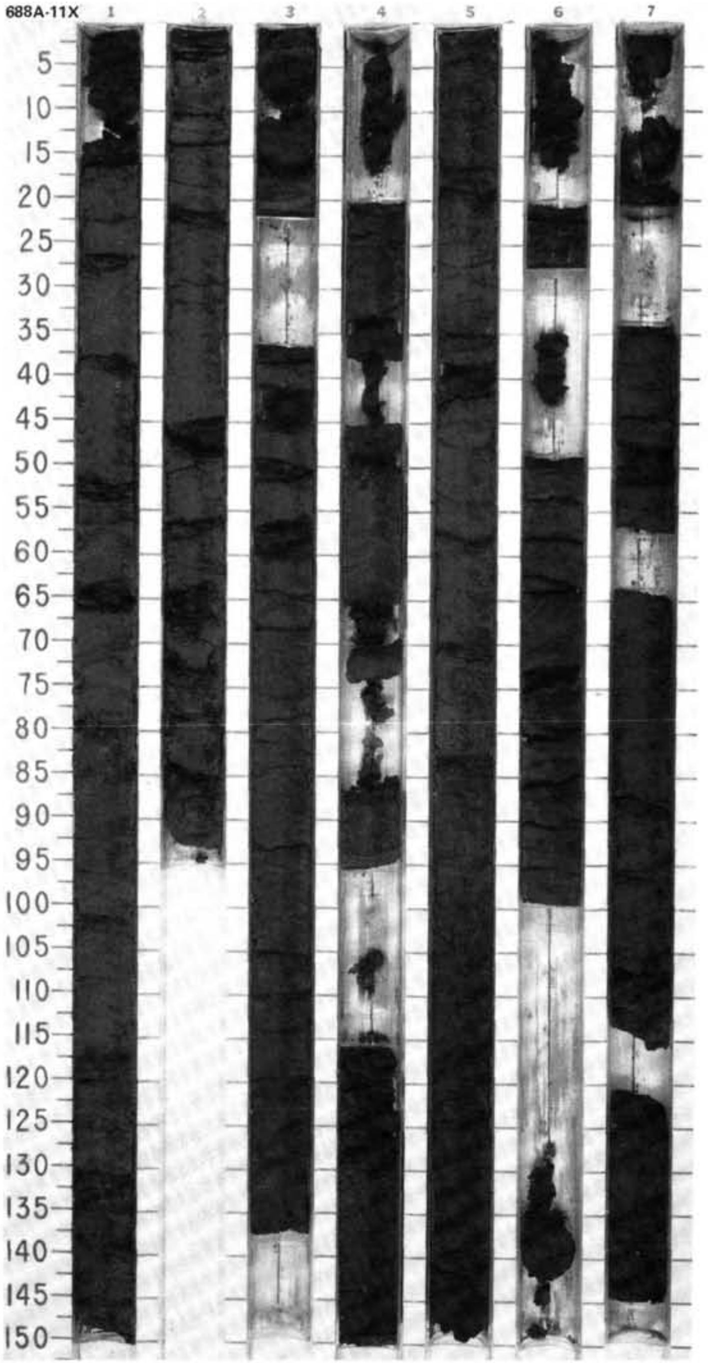

SITE 688 HOLE A CORE 11X CORED INTERVAL 3913.6-3923.1 mbsl; 93.8-103.3 mbsf

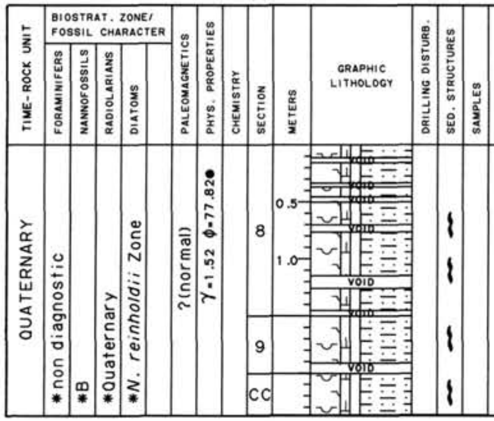

LITHOLOGIC DESCRIPTION

cont.

SITE 688 HOLE A CORE 12X CORED INTERVAL 3923.1-3932.6 mbsl; 103.3-112.8 mbsf

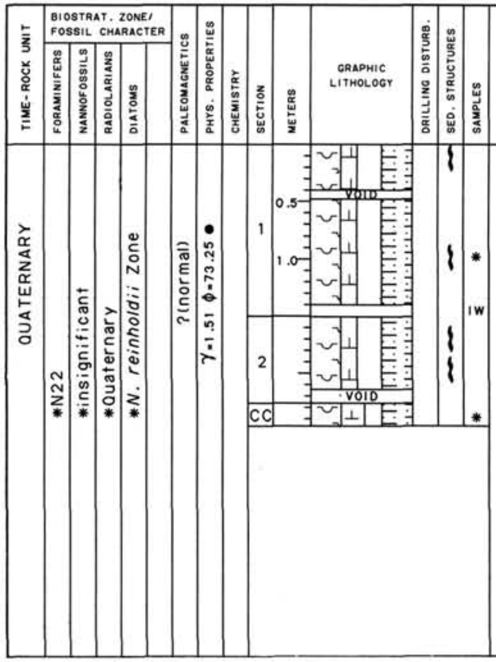

LITHOLOGIC DESCRIPTION

FORAMINIFER-NANNOFOSSIL-BEARING DIATOMACEOUS MUD

Major lithology: foraminifer-nannofossil-bearing diatomaceous mud, black (2.5Y 2/0). Pyrite and iron monosulfide-rich. Rapid color change after core splitting related to oxidation of iron monosulfide. Moderately bioturbated. Note: component with no symbol is pyrite/monosulfides.

Minor lithology: rare sponge spicule nests, 1 to 5–6 mm.

SMEAR SLIDE SUMMARY (%):

	1, 99 D	CC, 15 M
TEXTURE:		
Sand	5	10
Silt	80	35
Clay	15	55
COMPOSITION:		
Quartz	5	4
Feldspar	5	4
Clay	15	40
Calcite/dolomite	5	5
Accessory minerals		
Pyrite	15	2
Iron sulfide	15	—
Foraminifers	15	10
Nannofossils	Tr	5
Diatoms	25	30
Radiolarians	Tr	Tr
Sponge spicules	—	Tr
Silicoflagellates	Tr	—

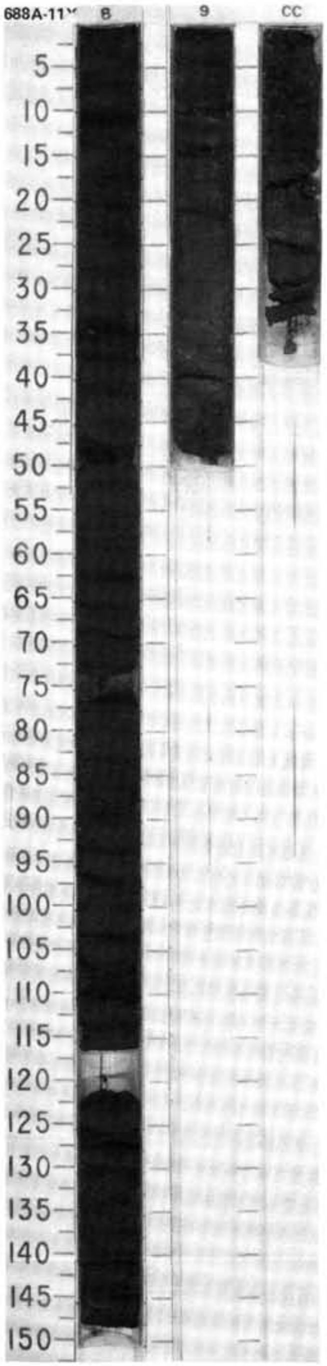

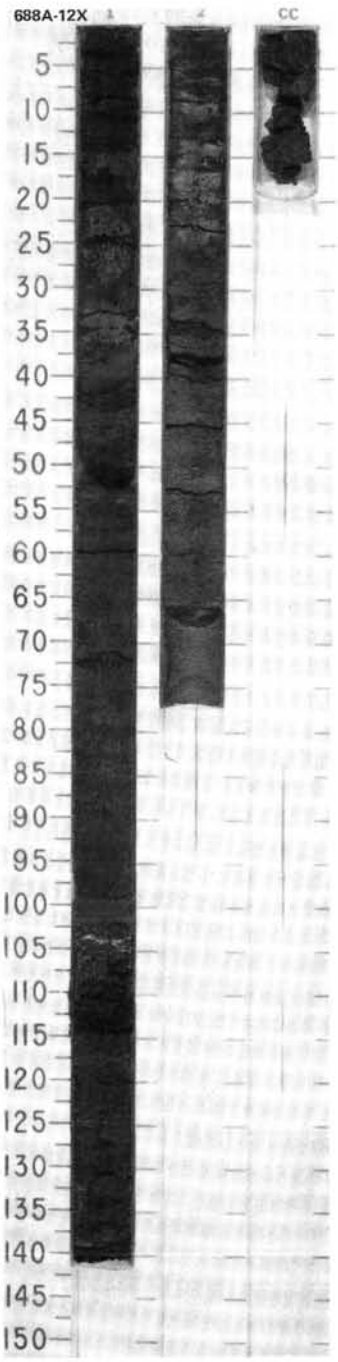

SITE 688 HOLE A CORE 13X CORED INTERVAL 3932.6-3942.1 mbsl; 112.8-122.3 mbsf

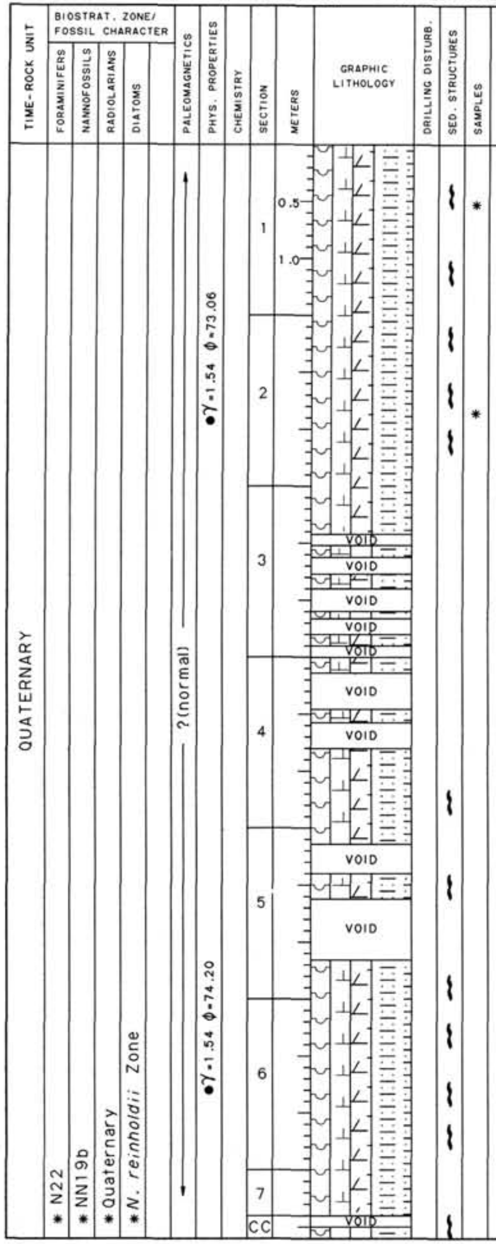

LITHOLOGIC DESCRIPTION

FORAMINIFER-NANNOFOSSIL-BEARING DIATOMACEOUS MUD

Major lithology: foraminifer-nannofossil-bearing diatomaceous mud, black (2.5Y 2/0). Pyrite and iron monosulfide-rich. Rapid color change after core splitting related to oxidation of iron monosulfides. Moderately bioturbated.

Minor lithology: rare sponge spicule nests, 1 to 5–6 mm.

SMEAR SLIDE SUMMARY (%):

	1, 50 D	2, 86 M
TEXTURE:		
Sand	10	10
Silt	35	40
Clay	55	50
COMPOSITION:		
Quartz	5	5
Feldspar	2	5
Rock fragments	—	4
Clay	30	30
Calcite/dolomite	10	10
Accessory minerals		
Pyrite	8	6
Iron sulfides	10	5
Foraminifers	15	10
Diatoms	20	25
Silicoflagellates	Tr	Tr

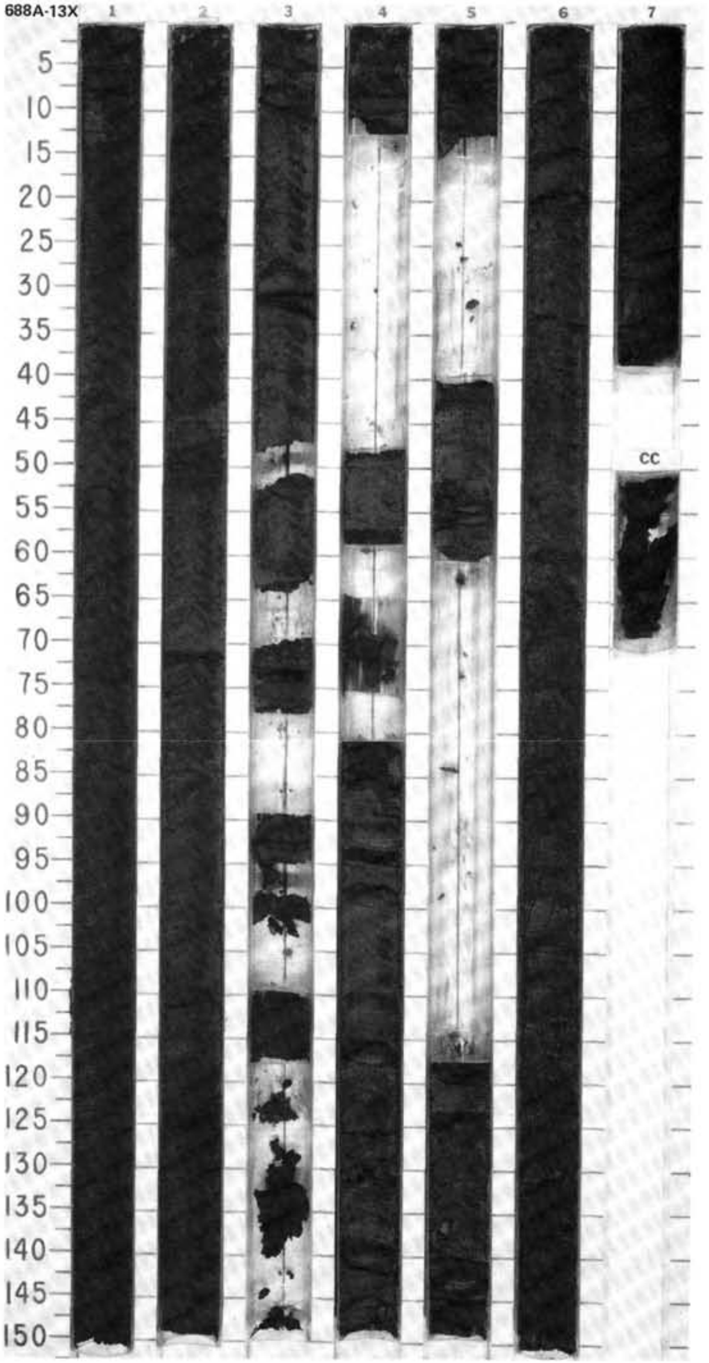

SITE 688 HOLE A CORE 14X CORED INTERVAL 3942.1-3951.6 mbsl; 122.3-131.8 mbsf

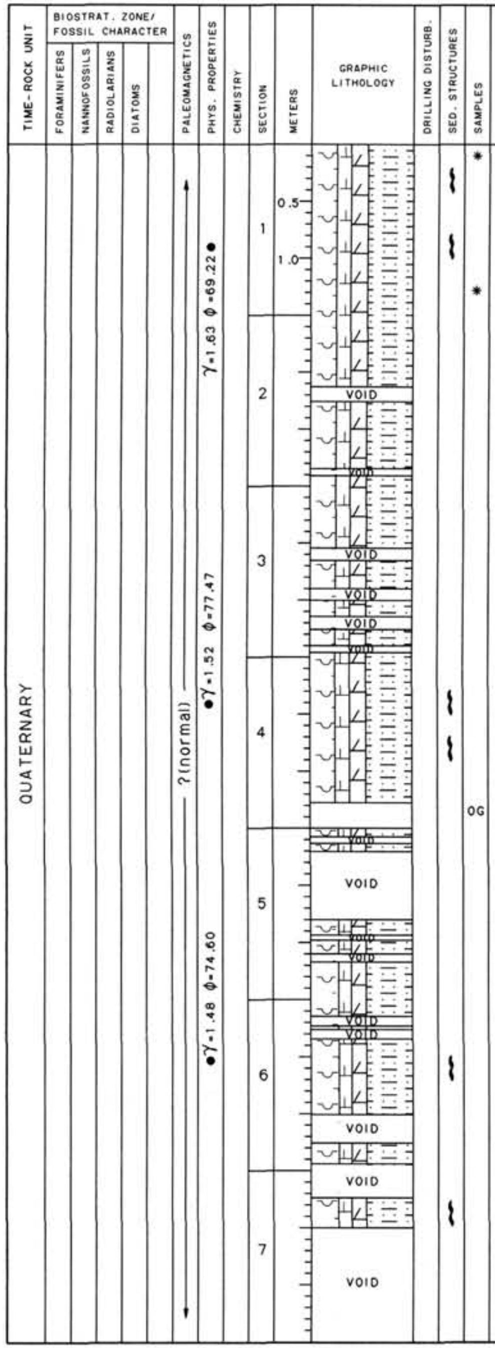

LITHOLOGIC DESCRIPTION

FORAMINIFER-NANNOFOSSIL-BEARING DIATOMACEOUS MUD

Major lithology: foraminifer-nannofossil-bearing diatomaceous mud, black (2.5Y 2/0). Pyrite and iron monosulfide-rich. Rapid color change after core splitting related to oxidation of iron monosulfides. Moderately bioturbated.

Minor lithology: rare sponge spicule nests, 1 to 5–6 mm.

SMEAR SLIDE SUMMARY (%):

	1, 14 D	1, 130 D
TEXTURE:		
Sand	20	5
Silt	30	45
Clay	50	50
COMPOSITION:		
Quartz	6	5
Feldspar	4	5
Rock fragments	Tr	—
Clay	30	35
Calcite/dolomite	10	5
Accessory minerals		
Pyrite	3	4
Iron sulfides	12	11
Glauconite	—	Tr
Foraminifers	15	10
Nannofossils	Tr	Tr
Diatoms	20	25
Radiolarians	Tr	Tr
Sponge soicules	Tr	Tr

cont.

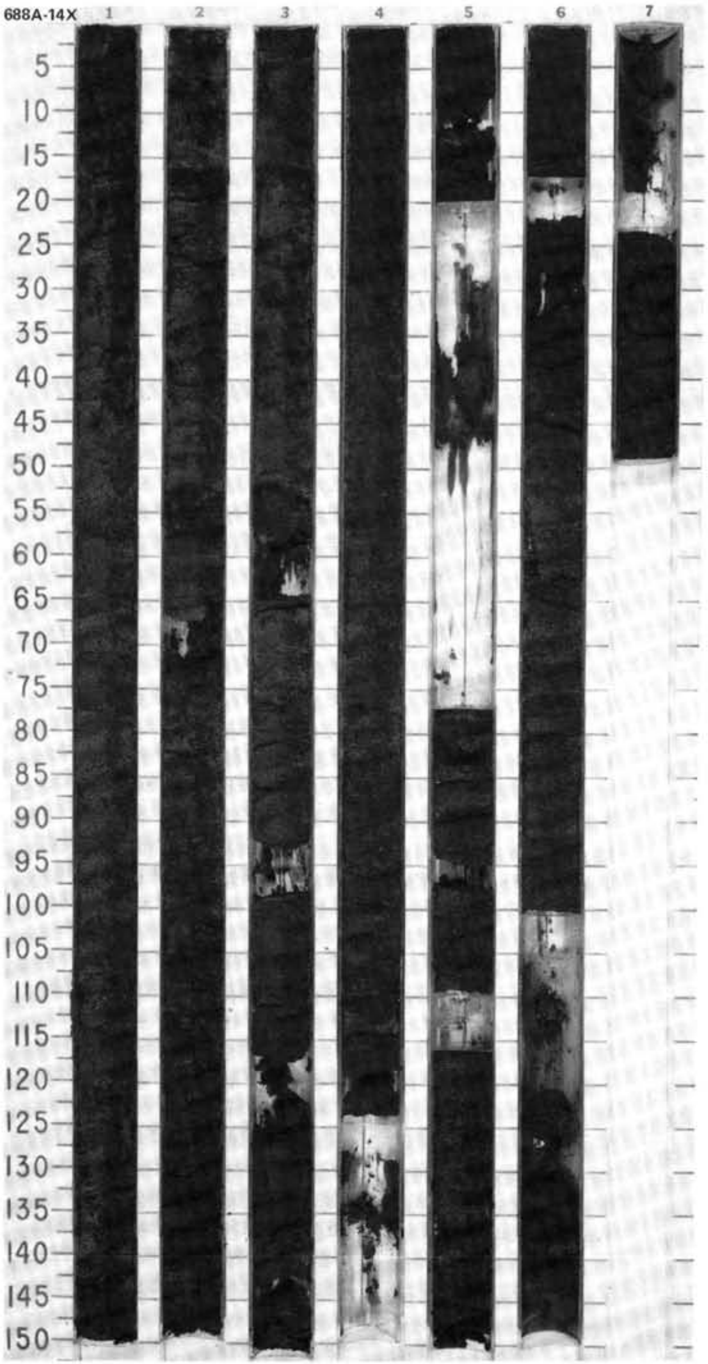

SITE 688 HOLE A CORE 14X CORED INTERVAL 3942.1-3951.6 mbsl; 122.3-131.8 mbsf

TIME-ROCK UNIT	BIOSTRAT. ZONE/ FOSSIL CHARACTER					PALEOMAGNETICS	PHYS. PROPERTIES	CHEMISTRY	SECTION	METERS	GRAPHIC LITHOLOGY	DRILLING DISTURB.	SED. STRUCTURES	SAMPLES	LITHOLOGIC DESCRIPTION
	FORAMINIFERS	NANNOFOSSILS	RADIOLARIANS	DIATOMS											
QUATERNARY	*non diagnostic	*B	*Quaternary	*N. reinholdii Zone		?(normal)	γ-1.49 ϕ-73.25 ●		8 9 CC	0.5 1.0	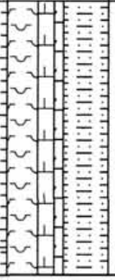	|	~		cont.

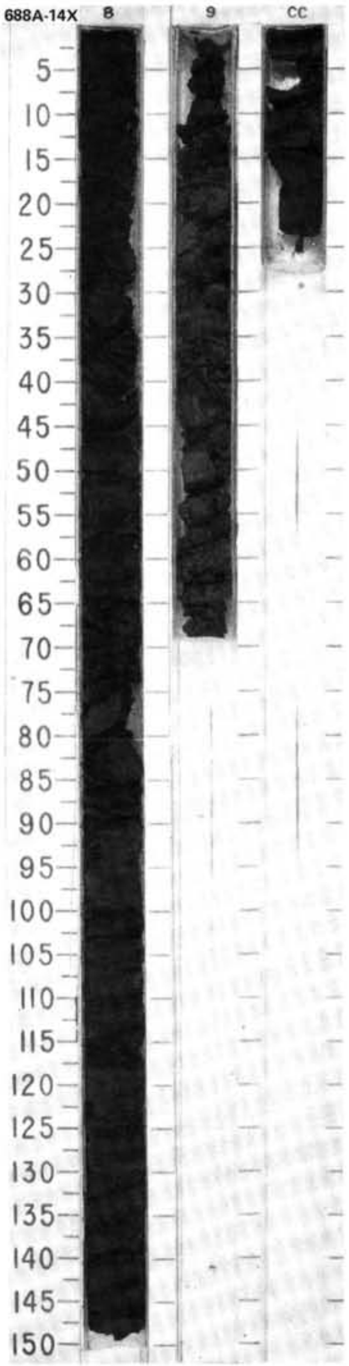

SITE 688 HOLE A CORE 15X CORED INTERVAL 3951.6-3961.1 mbsl; 131.8-141.3 mbsf

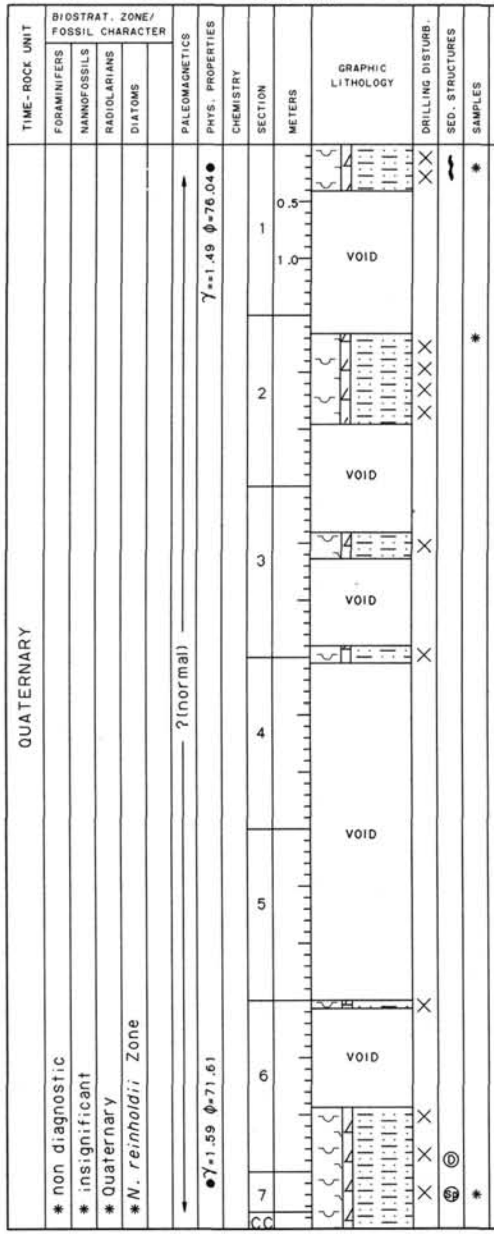

LITHOLOGIC DESCRIPTION

DIATOMACEOUS MUD and GAS HYDRATE

Major lithology: diatomaceous mud, black (2.5Y 2/0). Pyrite and iron monosulfide-rich (5 to 10%). Rapid color change related to oxidation of iron monosulfides. Rare sponge spicule nests, 1 to 3–5 mm. Extreme gas expansion due to gas hydrate throughout the core.

SMEAR SLIDE SUMMARY (%):

	1, 20 D	2, 27 D	7, 14 M
TEXTURE:			
Sand	5	5	100
Silt	35	30	—
Clay	60	65	—
COMPOSITION:			
Quartz	5	5	—
Feldspar	5	5	—
Rock fragments	3	—	—
Mica	—	Tr	—
Clay	45	53	—
Calcite/dolomite	3	2	100
Accessory minerals			
Pyrite	4	5	—
Iron sulfides	5	—	—
Nannofossils	—	Tr	—
Diatoms	30	30	—
Radiolarians	Tr	—	—
Sponge spicules	Tr	Tr	—
Silicoflagellates	—	Tr	—

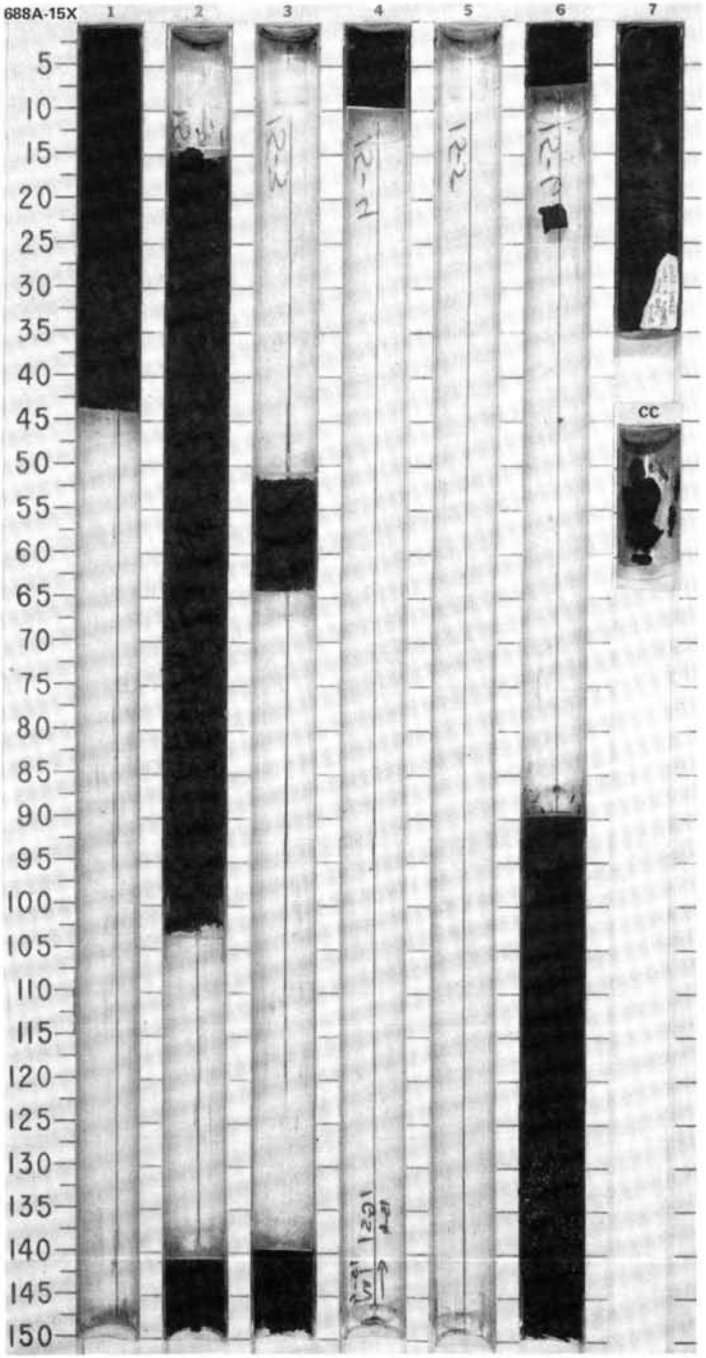

SITE 688 HOLE A CORE 16X CORED INTERVAL 3961.1-3970.6 mbsl; 141.3-150.8 mbsf

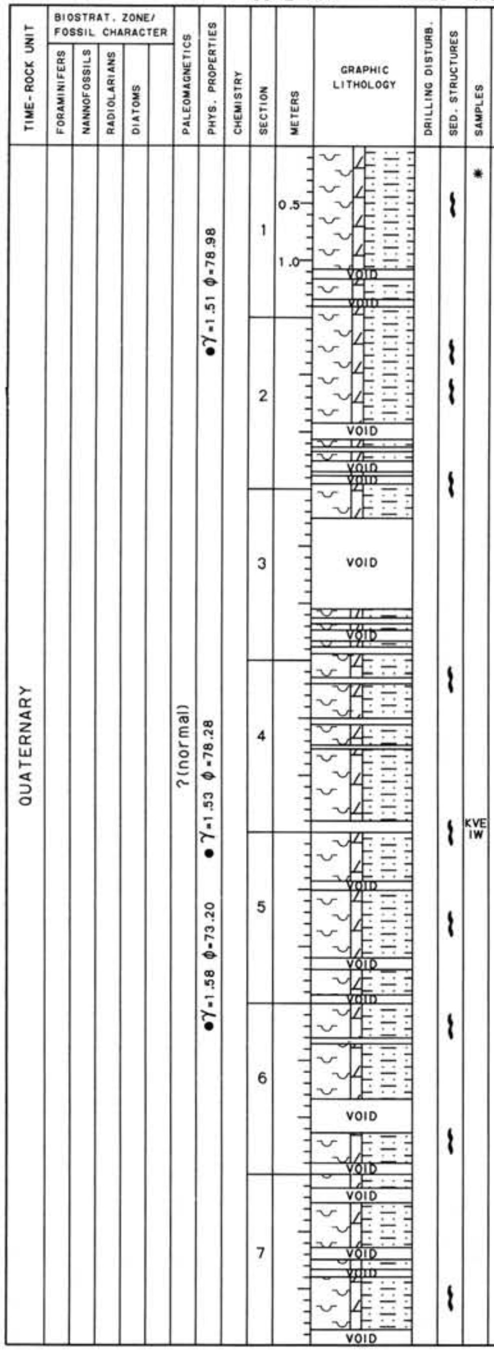

LITHOLOGIC DESCRIPTION

DIATOMACEOUS MUD

Major lithology: diatomaceous mud, black (2.5Y 2/0). Pyrite and iron monosulfide-rich (5 to 10%), oxidizing to olive black (5Y 2.5/2), moderately burrowed.

Minor lithology: rare sponge spicule clots, 1 to 5–6 mm.

SMEAR SLIDE SUMMARY (%):

	1, 26 D
TEXTURE:	
Silt	50
Clay	50
COMPOSITION:	
Quartz	5
Feldspar	3
Rock fragments	2
Clay	50
Calcite/dolomite	Tr
Accessory minerals	
Pyrite	3
Iron sulfides	2
Diatoms	35
Radiolarians	Tr
Silicoflagellates	Tr

cont.

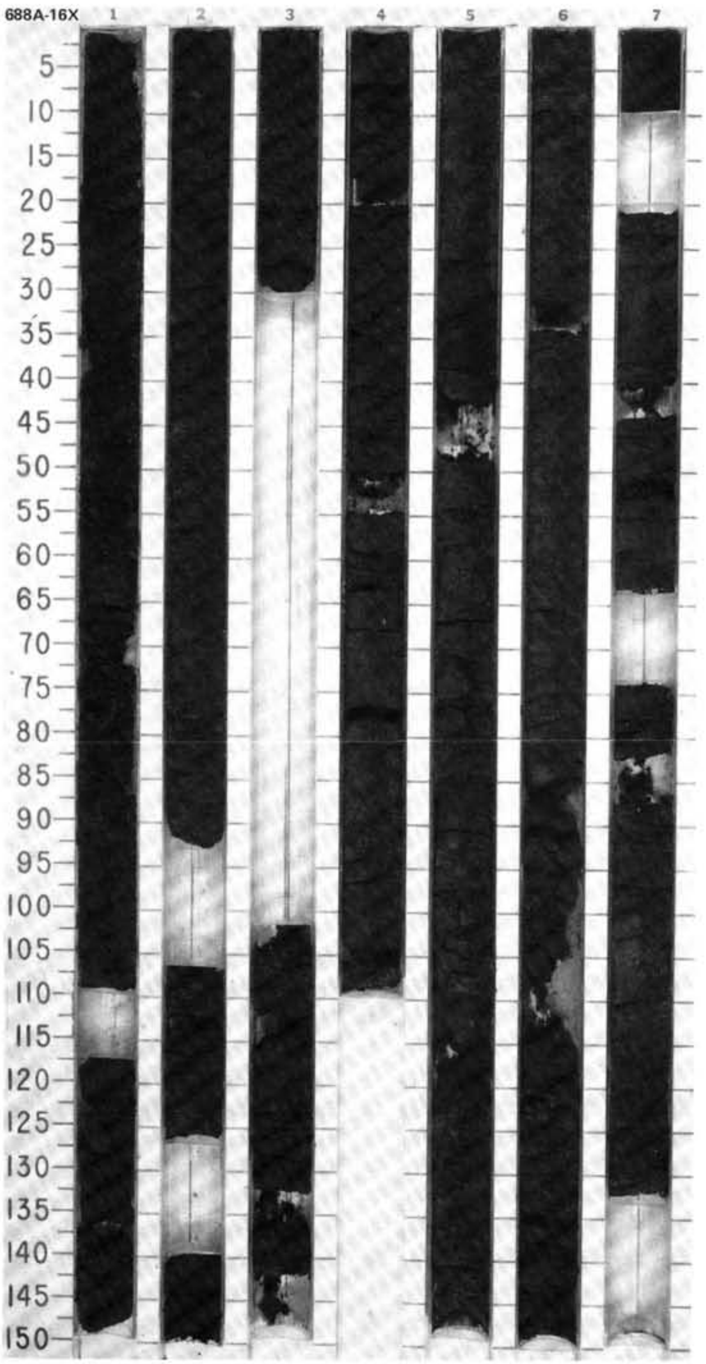

SITE 688 HOLE A CORE 16X CORED INTERVAL 3961.1-3970.6 mbsl; 141.3-150.8 mbsf

TIME-ROCK UNIT	BIOSTRAT. ZONE/ FOSSIL CHARACTER				PALEOMAGNETICS	PHYS. PROPERTIES	CHEMISTRY	SECTION	METERS	GRAPHIC LITHOLOGY	DRILLING DISTURB.	SED. STRUCTURES	SAMPLES	LITHOLOGIC DESCRIPTION
	FORAMINIFERS	NANNOFOSSILS	RADIOLARIANS	DIATOMS										
QUATERNARY	*B	*B	*Quaternary	*N. reinholdii Zone	?(normal)			8 9 CC	0.5 1.0	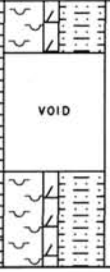 VOID	┆	~ ~ ~		

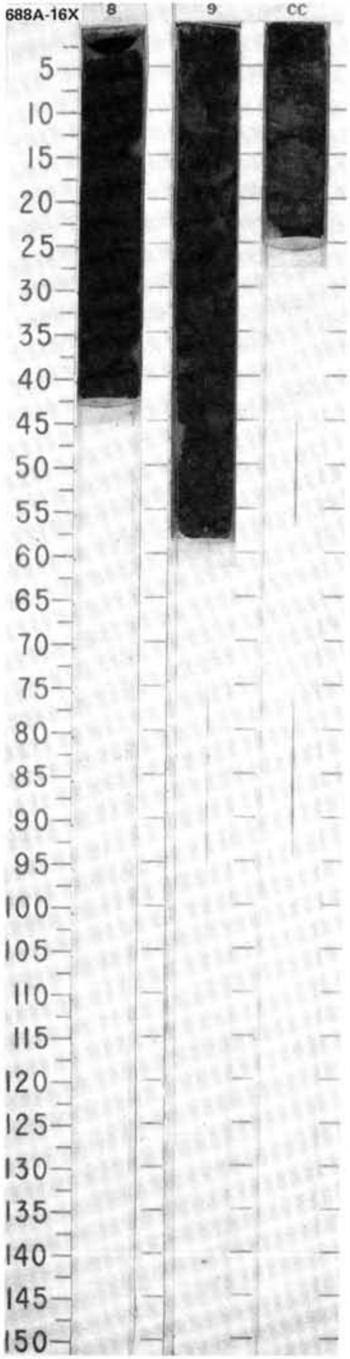

SITE 688 HOLE A CORE 17X CORED INTERVAL 3970.6-3980.1 mbsl; 150.8-160.3 mbsf

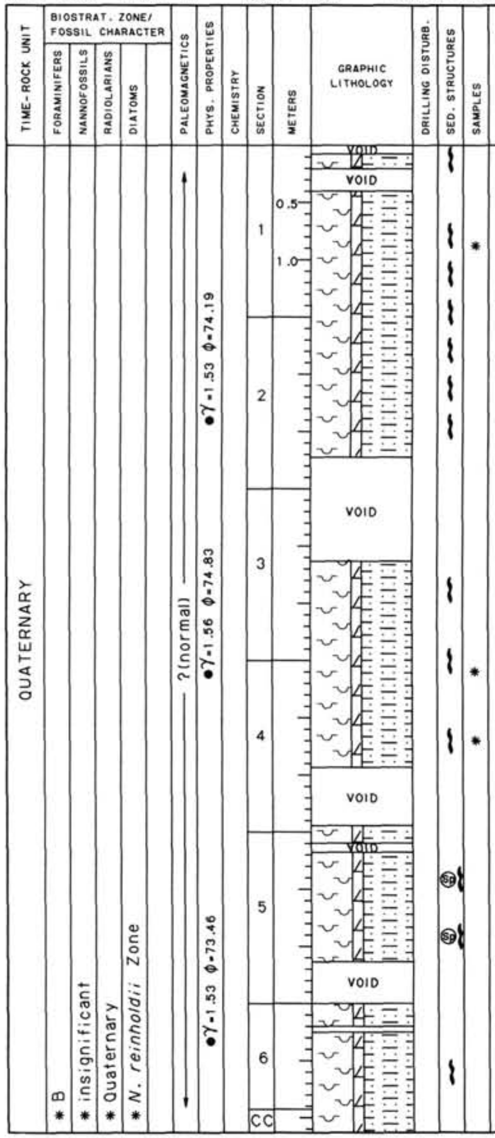

LITHOLOGIC DESCRIPTION

DIATOMACEOUS MUD

Major lithology: diatomaceous mud, black (2.5Y 2/0). Pyrite and iron monosulfide-rich (5 to 10%), oxidizing to olive black (5Y 2.5/2), moderately burrowed.

Minor lithology: rare sponge spicule clots, 1 to 5–6 mm.

SMEAR SLIDE SUMMARY (%):

	1, 89 D	4, 15 D	4, 73 M
TEXTURE:			
Sand	10	10	2
Silt	40	54	30
Clay	50	36	68
COMPOSITION:			
Quartz	10	5	Tr
Feldspar	5	5	Tr
Rock fragments	10	—	—
Mica	1	—	—
Clay	36	36	10
Volcanic glass	5	2	Tr
Calcite/dolomite	5	5	Tr
Accessory minerals			
Pyrite	3	5	2
Apatite	—	1	—
Foraminifers	Tr	—	—
Nannofossils	—	—	57
Diatoms	25	40	30
Radiolarians	—	1	1
Sponge spicules	1	Tr	Tr
Silicoflagellates	1	—	—

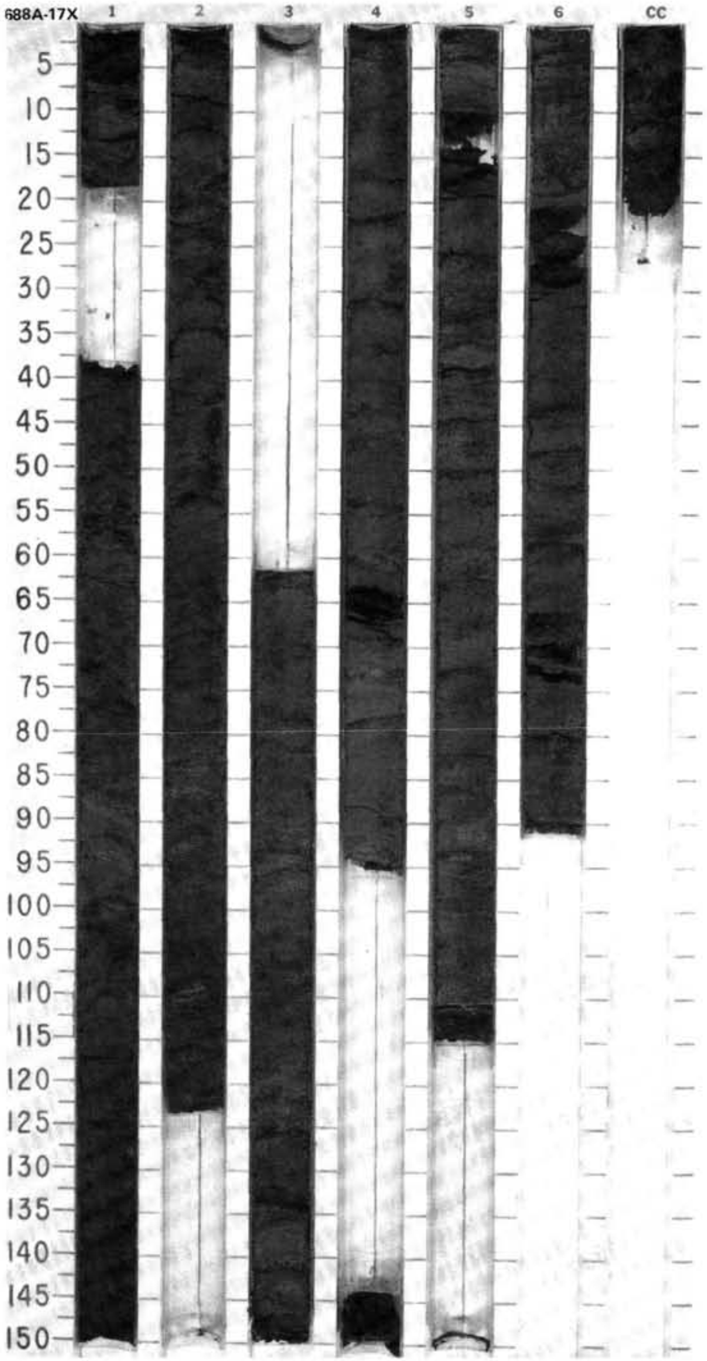

SITE 688 HOLE A CORE 18X CORED INTERVAL 3980.1-3989.6 mbsl; 160.3-169.8 mbsf

TIME-ROCK UNIT	BIOSTRAT. ZONE/ FOSSIL CHARACTER FORAMINIFERS	NANNOFOSSILS	RADIOLARIANS	DIATOMS		PALEOMAGNETICS	PHYS. PROPERTIES	CHEMISTRY	SECTION	METERS	GRAPHIC LITHOLOGY	DRILLING DISTURB.	SED. STRUCTURES	SAMPLES
QUATERNARY	*B	*insignificant	*Quaternary	**N. reinholdii* Zone		?(normal)		●γ-1.49 ϕ-76.50	1 CC	0.5 1.0	VOID			*

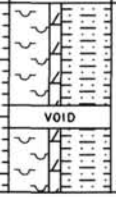

LITHOLOGIC DESCRIPTION

DIATOMACEOUS MUD

Major lithology: diatomaceous mud, black (2.5Y 2/0). Pyrite and iron monosulfide-rich (5 to 10%), oxidizing to olive black (5Y 2.5/2). Moderately burrowed.

Minor lithology: rare sponge spicule clots, 1 to 5–6 mm.

SMEAR SLIDE SUMMARY (%):

	1, 48 D
TEXTURE:	
Sand	15
Silt	45
Clay	40
COMPOSITION:	
Quartz	5
Feldspar	3
Rock fragments	10
Clay	25
Volcanic glass	3
Calcite/dolomite	2
Accessory minerals	
Opaques	8
Pyrite	3
Dolomite rhombs.	1
Nannofossils	3
Diatoms	35
Sponge spicules	2
Silicoflagellates	Tr

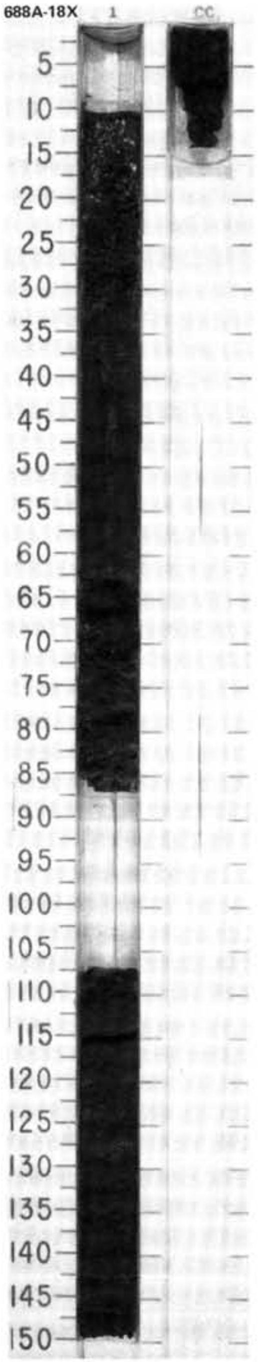

SITE 688 HOLE A CORE 19X CORED INTERVAL 3989.6-3999.1 mbsl; 169.8-179.3 mbsf

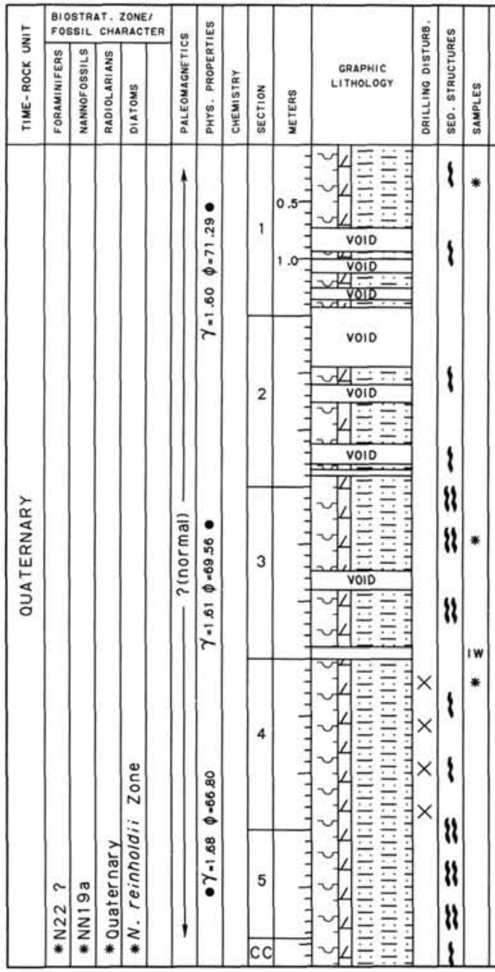

LITHOLOGIC DESCRIPTION

DIATOMACEOUS MUD

Major lithology: diatomaceous mud, black (2.5Y 2/0). Pyrite and iron monosulfide-rich (5 to 10%), oxidizing to dark gray (5Y 3/1) to very dark greenish gray (5GY 3/1). Intensely to moderately burrowed; burrows are filled with black iron monosulfides.

SMEAR SLIDE SUMMARY (%):

	1, 39 D	3, 50 M	4, 25 M
TEXTURE:			
Sand	5	5	5
Silt	30	25	30
Clay	65	70	65
COMPOSITION:			
Quartz	3	2	3
Feldspar	Tr	3	3
Rock fragments	5	2	2
Mica	—	—	Tr
Clay	45	42	65
Volcanic glass	Tr	—	—
Calcite/dolomite	5	3	5
Accessory minerals			
Pyrite	4	–	2
Phosphate	2	2	1
Opaques	10	40	10
Micrite	–	–	2
Glauconite	–	–	2
Foraminifers	–	–	Tr
Nannofossils	–	1	1
Diatoms	25	5	12
Radiolarians	–	Tr	1
Sponge spicules	1	1	1
Silicoflagellates	Tr	–	–

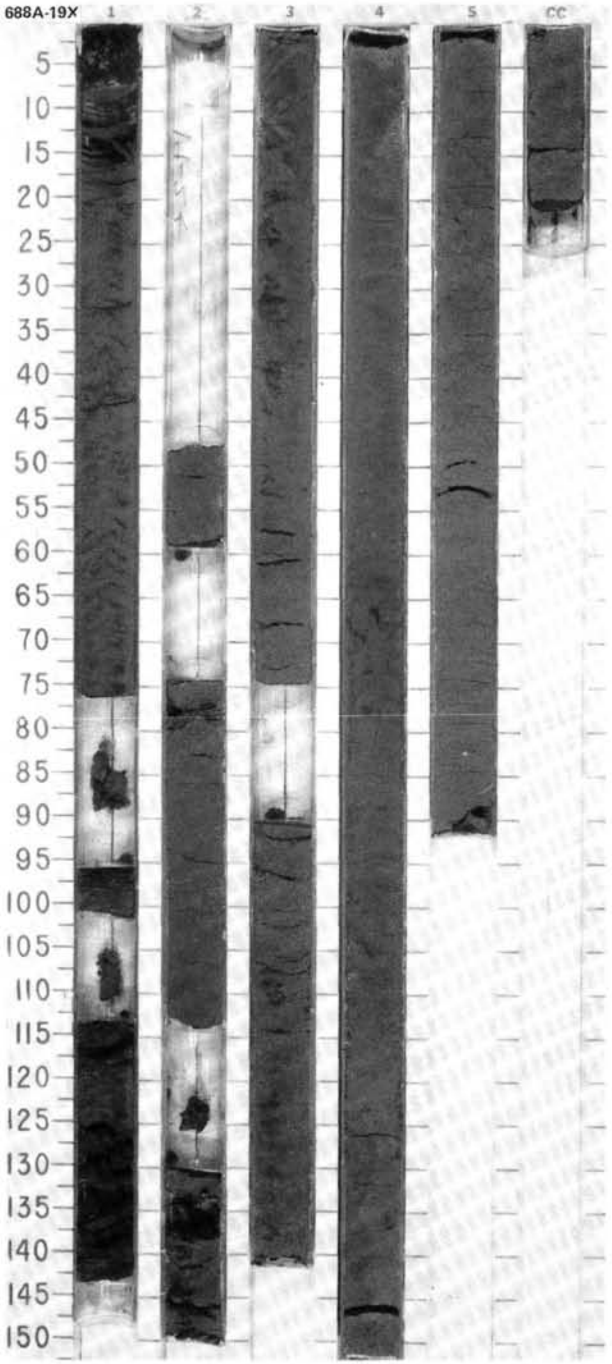

SITE 688 HOLE A CORE 20X CORED INTERVAL 3999.1-4008.6 mbsl; 179.3-188.8 mbsf

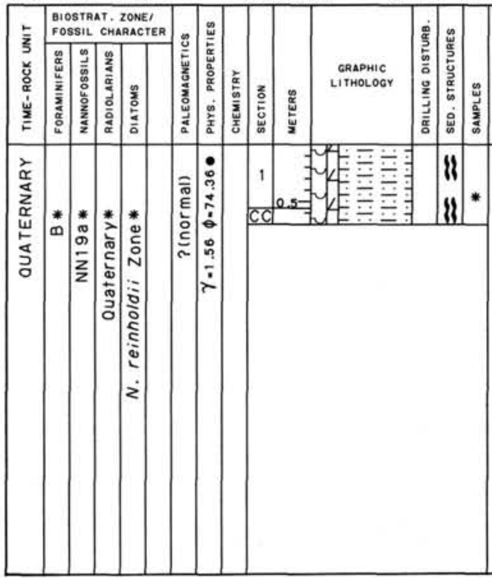

LITHOLOGIC DESCRIPTION

DIATOMACEOUS MUD

Major lithology: diatomaceous mud, black (2.5Y 2/0). Pyrite and iron monosulfide-rich (5 to 10%), oxidizing to dark gray (5Y 3/1) and very dark greenish gray (5GY 3/1). Intensely to moderately burrowed; burrows are filled with black iron monosulfides.

SMEAR SLIDE SUMMARY (%):

	1, 50 D
TEXTURE:	
Silt	40
Clay	60
COMPOSITION:	
Quartz	7
Feldspar	8
Clay	60
Calcite/dolomite	5
Accessory minerals	
Opaques	5
Glauconite	Tr
Nannofossils	Tr
Diatoms	15
Radiolarians	Tr
Sponge spicules	Tr
Silicoflagellates	Tr

SITE 688 HOLE A CORE 21X CORED INTERVAL 4008.6-4018.1 mbsl; 188.8-198.3 mbsf

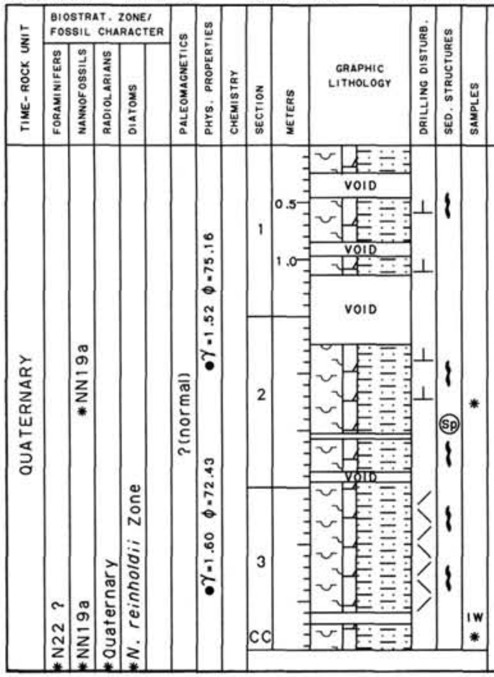

LITHOLOGIC DESCRIPTION

DIATOMACEOUS MUD

Major lithology: diatomaceous mud, black (2.5Y 2/0). Pyrite and iron monosulfide-rich (5 to 10%), *oxidizing to dark gray (5Y 3/1) and very dark greenish gray (5GY 3/1).* Intensely to moderately burrowed; burrows are filled with black iron monosulfides.

Minor lithology: isolated whole sponge in Section 2.

SMEAR SLIDE SUMMARY (%):

	2, 81 D	CC, 17 D
TEXTURE:		
Sand	1	—
Silt	67	70
Clay	32	30
COMPOSITION:		
Quartz	10	12
Feldspar	6	8
Rock fragments	7	5
Mica	1	1
Clay	30	26
Calcite/dolomite	4	6
Accessory minerals	1	—
Pyrite	9	5
Foraminifers	Tr	1
Nannofossils	Tr	1
Diatoms	32	35
Radiolarians	Tr	—
Sponge spicules	Tr	—
Silicoflagellates	Tr	—

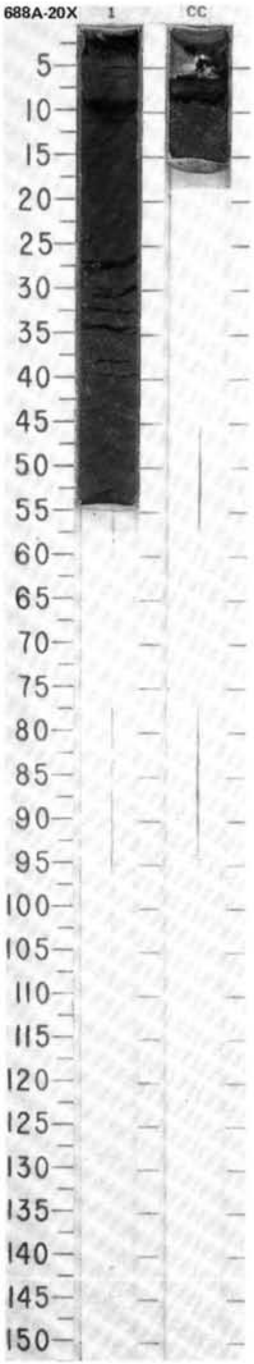

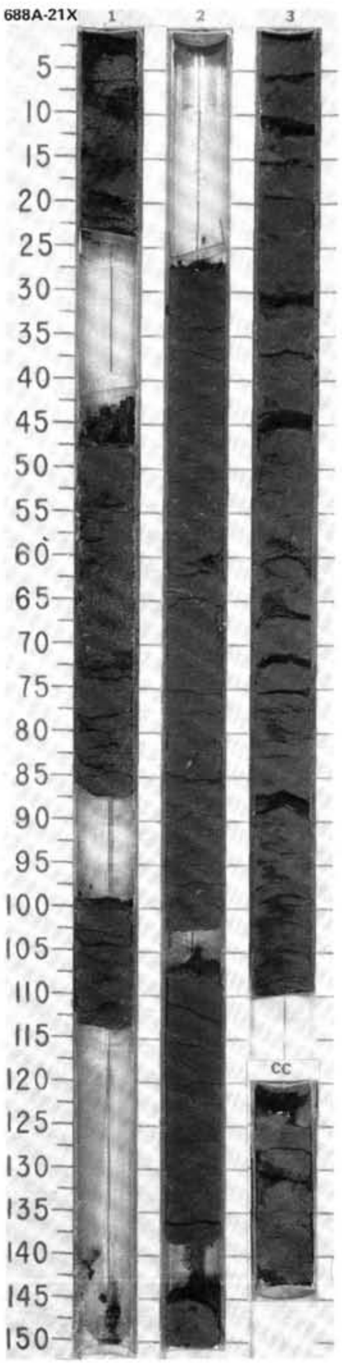

SITE 688 HOLE A CORE 22X CORED INTERVAL 4018.1-4027.6 mbsl; 198.3-207.8 mbsf

TIME-ROCK UNIT	BIOSTRAT. ZONE/ FOSSIL CHARACTER					PALEOMAGNETICS	PHYS. PROPERTIES	CHEMISTRY	SECTION	METERS	GRAPHIC LITHOLOGY	DRILLING DISTURB.	SED. STRUCTURES	SAMPLES
	FORAMINIFERS	NANNOFOSSILS	RADIOLARIANS	DIATOMS										
QUATERNARY	non diagnostic *	NN19a *				?	γ=1.61 ϕ=73.91●		1		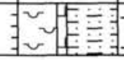	⊥ ⊥	~	*

LITHOLOGIC DESCRIPTION

DIATOMACEOUS MUD

Major lithology: diatomaceous mud, black (2.5Y 2/0). Pyrite and iron monosulfide-rich (5 to 10%), oxidizing to dark gray (5Y 3/1) and very dark greenish gray (5GY 3/1). Intensely to moderately burrowed; burrows are filled with black iron monosulfides.

SMEAR SLIDE SUMMARY (%):

	1, 31 D
TEXTURE:	
Silt	65
Clay	35
COMPOSITION:	
Quartz	10
Feldspar	5
Rock fragments	5
Mica	Tr
Clay	28
Volcanic glass	Tr
Calcite/dolomite	5
Accessory minerals	
Pyrite	4
Foraminifers	5
Nannofossils	1
Diatoms	37

SITE 688 HOLE A CORE 23X CORED INTERVAL 4027.6-4037.1 mbsl; 207.8-217.3 mbsf

TIME-ROCK UNIT	BIOSTRAT. ZONE/ FOSSIL CHARACTER					PALEOMAGNETICS	PHYS. PROPERTIES	CHEMISTRY	SECTION	METERS	GRAPHIC LITHOLOGY	DRILLING DISTURB.	SED. STRUCTURES	SAMPLES
	FORAMINIFERS	NANNOFOSSILS	RADIOLARIANS	DIATOMS										
QUATERNARY	B *	B *	Quaternary *	*N. reinholdii* Zone *		?(normal)			1 CC	0.5	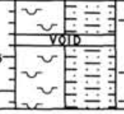	⊥ ⊥ ⊥	~ ≷ ~	* * *

LITHOLOGIC DESCRIPTION

DIATOMACEOUS MUD

Major lithology: diatomaceous mud, black (2.5Y 2/0). Pyrite and iron monosulfide-rich (5 to 10%), oxidizing to dark gray (5Y 3/1) and very dark greenish gray (5GY 3/1). Intensely to moderately burrowed; burrows are filled with black iron monosulfides.

SMEAR SLIDE SUMMARY (%):

	1, 47 D	1, 75 M	CC, 14 D
TEXTURE:			
Silt	65	17	65
Clay	35	83	35
COMPOSITION:			
Quartz	8	4	10
Feldspar	4	—	5
Rock fragments	9	—	12
Mica	Tr	Tr	Tr
Clay	33	—	29
Volcanic glass	—	—	Tr
Calcite/dolomite	3	2	3
Accessory minerals			
Pyrite	3	2	5
Micrite	—	72	—
Foraminifers	—	—	Tr
Nannofossils	Tr	5	Tr
Diatoms	40	15	36
Radiolarians	Tr	—	Tr
Sponge spicules	Tr	—	—
Silicoflagellates	Tr	—	Tr

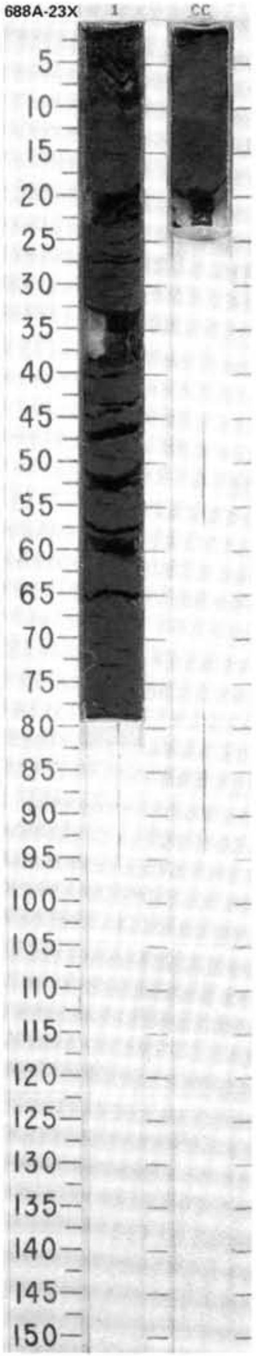

SITE 688 HOLE A CORE 24X CORED INTERVAL 4037.1-4046.6 mbsl; 217.3-226.8 mbsf

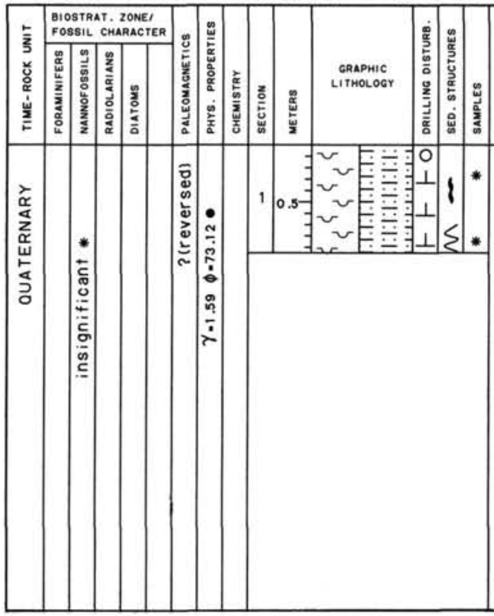

LITHOLOGIC DESCRIPTION

DIATOMACEOUS MUD

Major lithology: diatomaceous mud, black (2.5Y 2/0). Pyrite and iron monosulfide-rich (5 to 10%), oxidizing to dark gray (5Y 3/1) to very dark greenish gray (5GY 3/1). Intensely to moderately burrowed; burrows are filled with black iron monosulfides.

SMEAR SLIDE SUMMARY (%):

	1, 34 D	1, 83 D
TEXTURE:		
Silt	60	55
Clay	40	45
COMPOSITION:		
Quartz	5	6
Feldspar	5	5
Rock fragments	3	3
Mica	Tr	Tr
Clay	37	45
Calcite/dolomite	3	3
Accessory minerals		
Pyrite	4	3
Foraminifers	Tr	Tr
Nannofossils	—	Tr
Diatoms	43	35
Radiolarians	Tr	—
Sponge spicules	—	Tr
Silicoflagellates	Tr	Tr

SITE 688 HOLE A CORE 25X CORED INTERVAL 4046.6-4056.1 mbsl; 226.8-236.3 mbsf

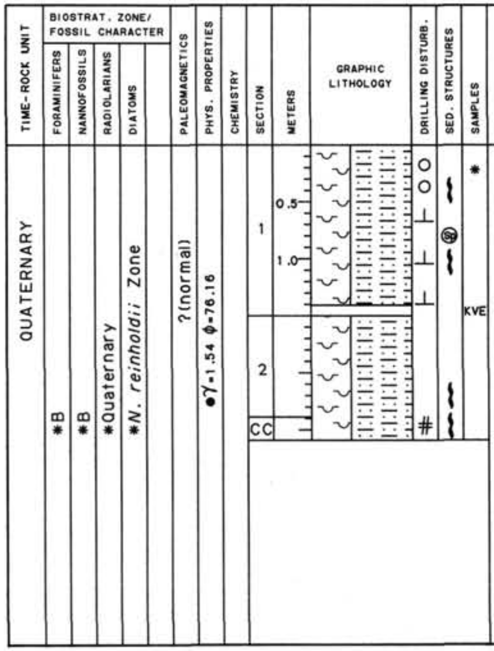

LITHOLOGIC DESCRIPTION

DIATOMACEOUS MUD

Major lithology: diatomaceous mud, black (2.5Y 2/0). Pyrite and iron monosulfide-rich (5 to 10%), oxidizing to dark gray (5Y 3/1) and very dark greenish gray (5GY 3/1). Intensely to moderately burrowed; burrows are filled with black iron monosulfides.

Minor lithology: small sponge spicule nests, 1 to 5–6 mm, throughout.

SMEAR SLIDE SUMMARY (%):

	1, 21 D
TEXTURE:	
Sand	3
Silt	62
Clay	35
COMPOSITION:	
Quartz	8
Feldspar	5
Rock fragments	5
Mica	Tr
Clay	33
Calcite/dolomite	5
Accessory minerals	
Pyrite	6
Glauconite	Tr
Foraminifers	Tr
Diatoms	35
Radiolarians	Tr
Sponge spicules	2
Silicoflagellates	1

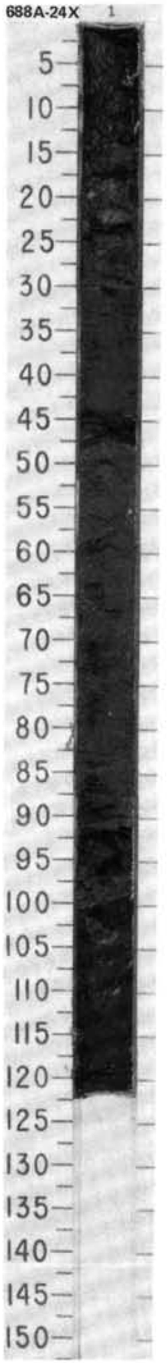

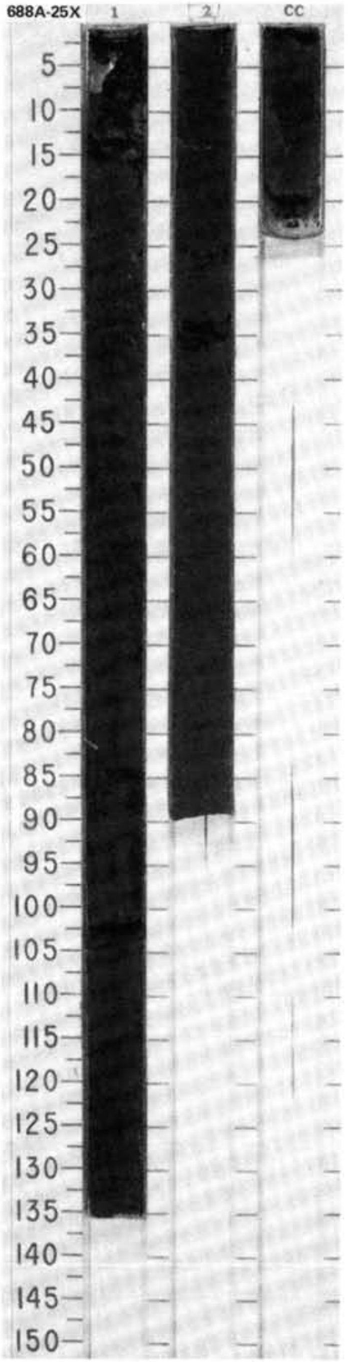

SITE 688 HOLE A CORE 26X CORED INTERVAL 4056.1-4065.6 mbsl; 236.3-245.8 mbsf

TIME-ROCK UNIT	BIOSTRAT. ZONE/ FOSSIL CHARACTER FORAMINIFERS	NANNOFOSSILS	RADIOLARIANS	DIATOMS		PALEOMAGNETICS	PHYS. PROPERTIES	CHEMISTRY	SECTION	METERS
QUATERNARY	B *	B *	Quaternary *	*N. reinholdii* Zone *		?(normal)	γ=1.60 ϕ=72.96 ●		1 CC	0.5

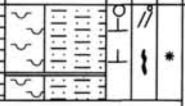

LITHOLOGIC DESCRIPTION

DIATOMACEOUS MUD

Major lithology: diatomaceous mud, black (2.5Y 2/0). Pyrite and iron monosulfide-rich (5 to 10%), oxidizing to dark gray (5Y 3/1) and very dark greenish gray (5GY 3/1). Intensely to moderately burrowed; burrows are filled with black iron monosulfides.

SMEAR SLIDE SUMMARY (%):

	1, 41 D
TEXTURE:	
Sand	3
Silt	67
Clay	30
COMPOSITION:	
Quartz	7
Feldspar	9
Rock fragments	6
Clay	29
Calcite/dolomite	3
Accessory minerals	
Pyrite	6
Diatoms	40
Radiolarians	Tr
Sponge spicules	Tr
Silicoflagellates	Tr

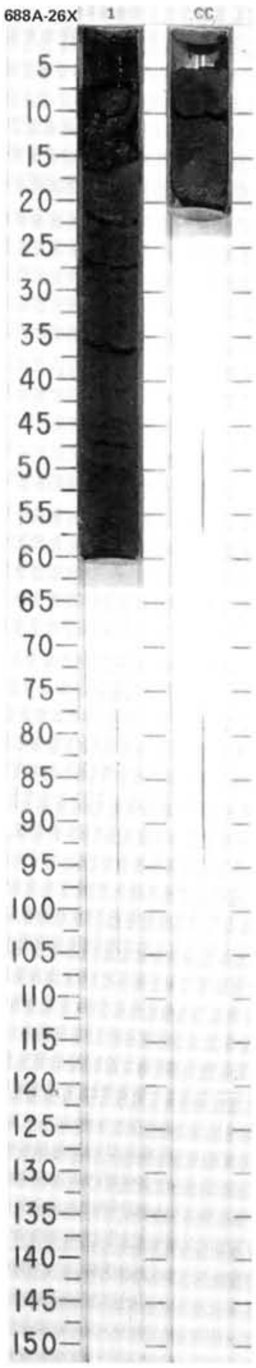

SITE 688 HOLE A CORE 27X CORED INTERVAL 4065.6-4075.1 mbsl; 245.8-255.3 mbsf

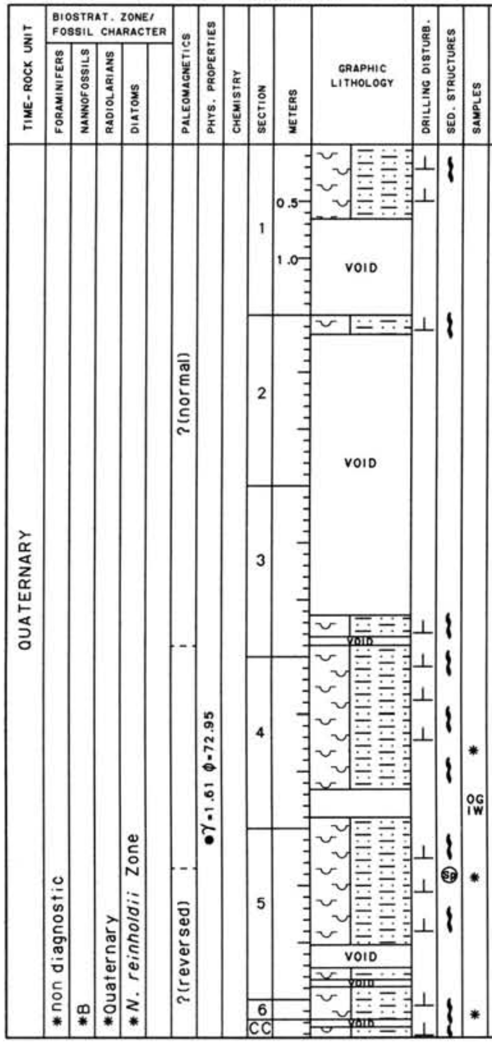

LITHOLOGIC DESCRIPTION

DIATOMACEOUS MUD

Major lithology: diatomaceous mud, black (2.5Y 2/0). Pyrite and iron monosulfide-rich (5 to 10%), oxidizing to dark gray (5Y 3/1) and very dark greenish gray (5GY 3/1). Intensely to moderately burrowed; burrows are filled with black iron monosulfides. Section 6 grades downhole from black to green.

SMEAR SLIDE SUMMARY (%):

	4, 82 D	5, 43 D	6, 7 D
TEXTURE:			
Silt	49	51	50
Clay	51	49	50
COMPOSITION:			
Quartz	2	5	5
Feldspar	2	2	3
Rock fragments	1	2	—
Mica	Tr	Tr	—
Clay	51	49	50
Volcanic glass	—	—	—
Calcite/dolomite	1	—	Tr
Accessory minerals			
Pyrite	2	2	5
Micrite	—	Tr	—
Diatoms	40	40	30
Sponge spicules	1	Tr	3
Silicoflagellates	Tr	—	—
Pellets	—	—	4

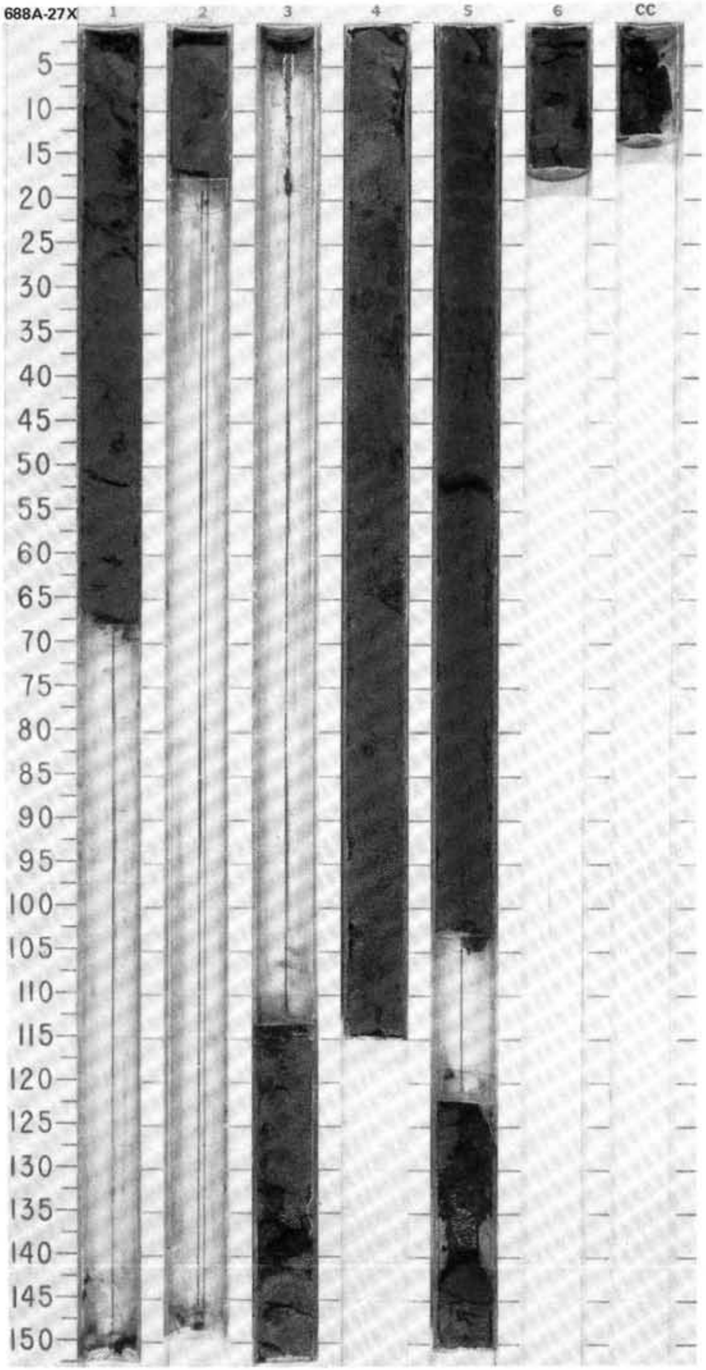

SITE 688 HOLE A CORE 28X CORED INTERVAL 4075.1-4084.6 mbsl; 255.3-264.8 mbsf

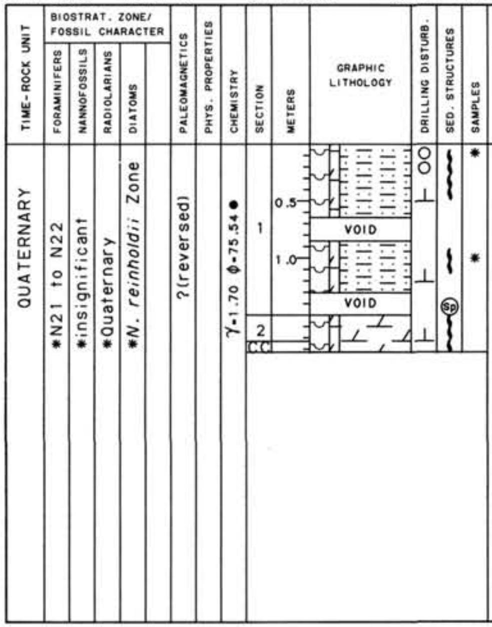

LITHOLOGIC DESCRIPTION

DIATOMACEOUS MUD

Major lithology: very dark greenish gray (5GY 4/1) diatomaceous mud. Intensely to moderately burrowed; burrows are filled with black iron monosulfides.

SMEAR SLIDE SUMMARY (%):

	1, 10 D	1, 93 D
TEXTURE:		
Silt	40	45
Clay	60	55
COMPOSITION:		
Quartz	5	6
Feldspar	5	7
Mica	Tr	—
Clay	60	55
Calcite/dolomite	3	5
Accessory minerals		
Opaques	5	7
Glauconite	—	Tr
Foraminifers	2	Tr
Nannofossils	Tr	—
Diatoms	20	20
Radiolarians	—	Tr
Sponge spicules	Tr	—
Silicoflagellates	Tr	Tr

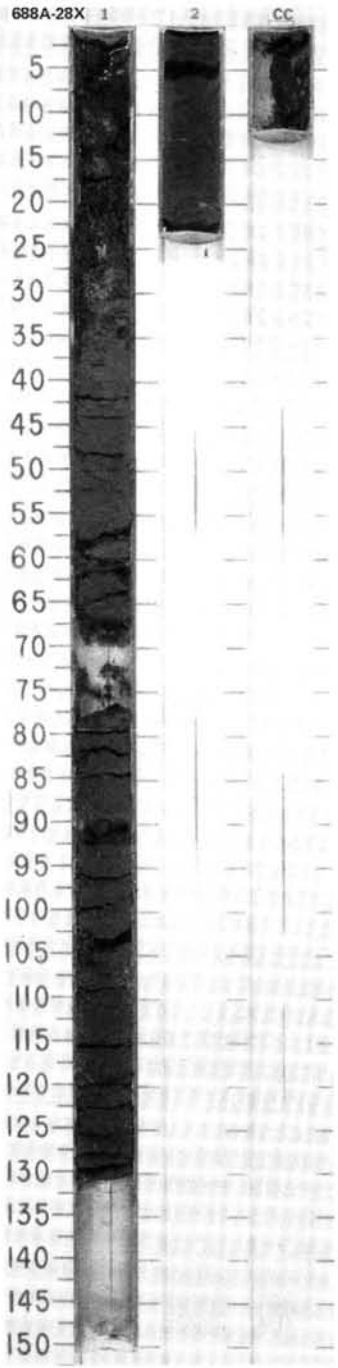

SITE 688 HOLE A CORE 29X CORED INTERVAL 4084.6-4094.1 mbsl; 264.8-274.3 mbsf

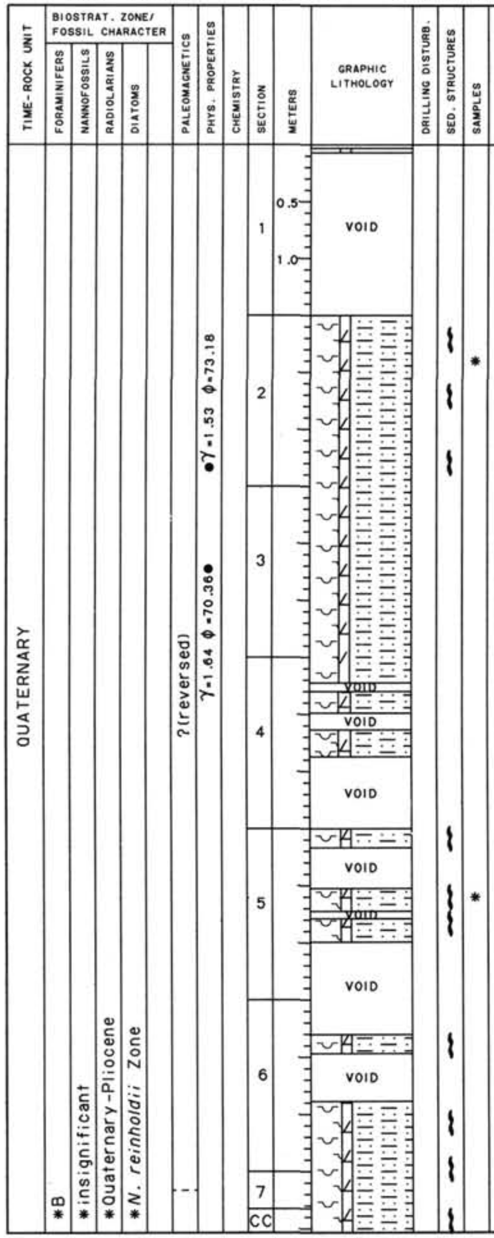

LITHOLOGIC DESCRIPTION

DIATOMACEOUS MUD

Major lithology: diatomaceous mud, black (2.5Y 2/0). Pyrite and iron monosulfide-rich (5 to 10%), oxidizing to dark gray (5Y 3/1) and very dark greenish gray (5GY 3/1). Intensely to moderately burrowed; burrows are filled with black iron monosulfides.

SMEAR SLIDE SUMMARY (%):

	2, 44 D	5, 62 D
TEXTURE:		
Sand	5	10
Silt	35	45
Clay	60	45
COMPOSITION:		
Quartz	4	5
Feldspar	Tr	5
Rock fragments	6	Tr
Clay	50	35
Volcanic glass	3	—
Calcite/dolomite	3	5
Accessory minerals		
Pyrite	8	5
Glauconite	Tr	—
Foraminifers	—	10
Nannofossils	—	5
Diatoms	25	30
Radiolarians	—	Tr
Sponge spicules	1	Tr

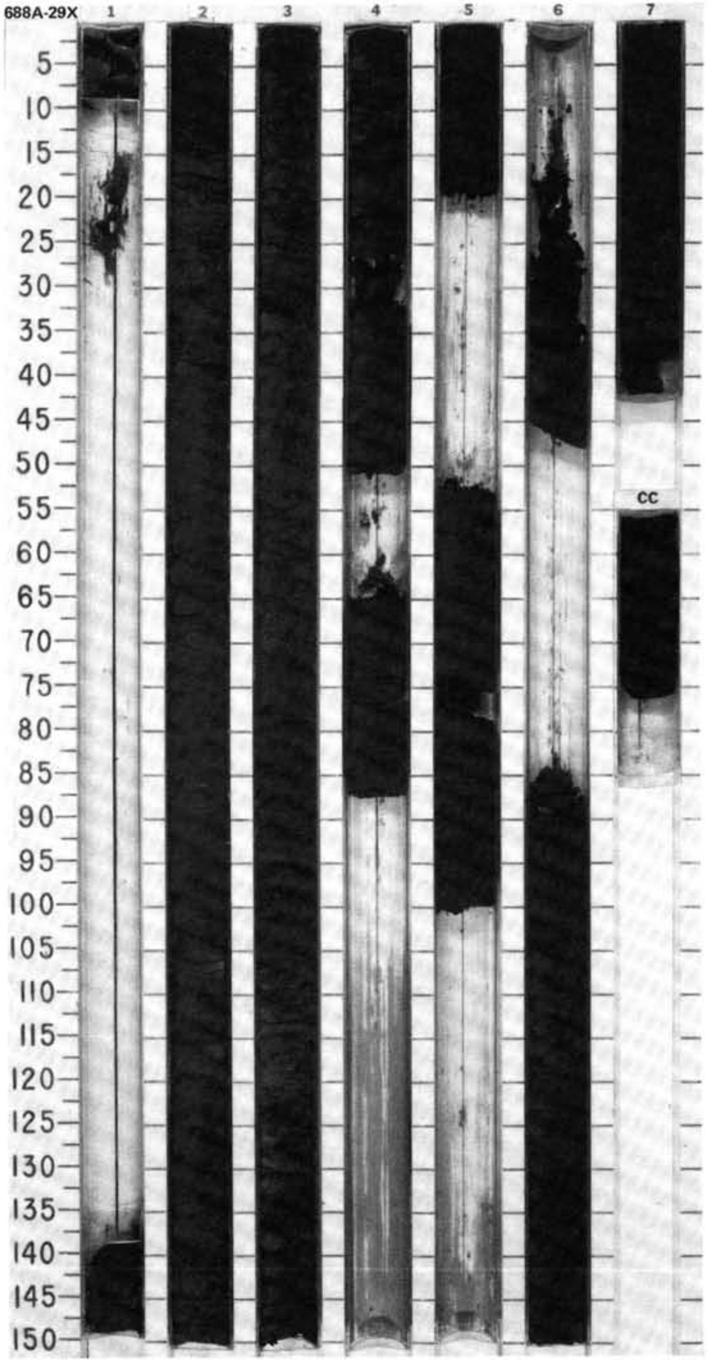

SITE 688 HOLE A CORE 30X CORED INTERVAL 4094.1-4103.6 mbsl; 274.3-283.8 mbsf

TIME-ROCK UNIT	BIOSTRAT. ZONE/ FOSSIL CHARACTER FORAMINIFERS	NANNOFOSSILS	RADIOLARIANS	DIATOMS	PALEOMAGNETICS	PHYS. PROPERTIES	CHEMISTRY	SECTION	METERS	GRAPHIC LITHOLOGY	DRILLING DISTURB.	SED. STRUCTURES	SAMPLES
QUATERNARY	B*	B*	Lower Quaternary-Pliocene*	*N. reinholdii* Zone*	?(normal)	γ=1.61 φ=71.39 ●		1 CC	0.5 1.0	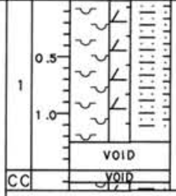			* IW

LITHOLOGIC DESCRIPTION

DIATOMACEOUS MUD

Major lithology: diatomaceous mud, black (2.5Y 2/0). Pyrite and iron monosulfide-rich (5 to 10%), oxidizing to dark gray (5Y 3/1) and very dark greenish gray (5GY 3/1). Intensely to moderately burrowed; burrows are filled with black iron monosulfides.

SMEAR SLIDE SUMMARY (%):

	1, 30 D
TEXTURE:	
Sand	2
Silt	38
Clay	60
COMPOSITION:	
Quartz	5
Feldspar	3
Mica	Tr
Clay	30
Calcite/dolomite	3
Accessory minerals	
Pyrite	4
Iron sulfides	15
Diatoms	40
Radiolarians	Tr
Sponge spicules	Tr

SITE 688 HOLE A CORE 31X CORED INTERVAL 4103.6-4113.1 mbsl; 288.8-293.3 mbsf

TIME-ROCK UNIT	BIOSTRAT. ZONE/ FOSSIL CHARACTER FORAMINIFERS	NANNOFOSSILS	RADIOLARIANS	DIATOMS	PALEOMAGNETICS	PHYS. PROPERTIES	CHEMISTRY	SECTION	METERS	GRAPHIC LITHOLOGY	DRILLING DISTURB.	SED. STRUCTURES	SAMPLES
QUATERNARY	B*	B*	Lower Quaternary-Pliocene*	*N. reinholdii* Zone*	?(normal)	γ=1.57 φ=70.64 ●		1 CC	0.5	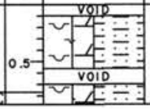			*

LITHOLOGIC DESCRIPTION

DIATOMACEOUS MUD

Major lithology: diatomaceous mud, black (2.5Y 2/0). Pyrite and iron monosulfide-rich (5 to 10%), oxidizing to dark gray (5Y 3/1) and very dark greenish gray (5GY 3/1). Intensely to moderately burrowed; burrows are filled with black iron monosulfides.

SMEAR SLIDE SUMMARY (%):

	1, 27 D
TEXTURE:	
Sand	8
Silt	47
Clay	45
COMPOSITION:	
Quartz	5
Feldspar	5
Rock fragments	5
Clay	35
Calcite/dolomite	2
Accessory minerals	
Pyrite	5
Iron sulfides	10
Nannofossils	Tr
Diatoms	30
Radiolarians	3
Sponge spicules	Tr

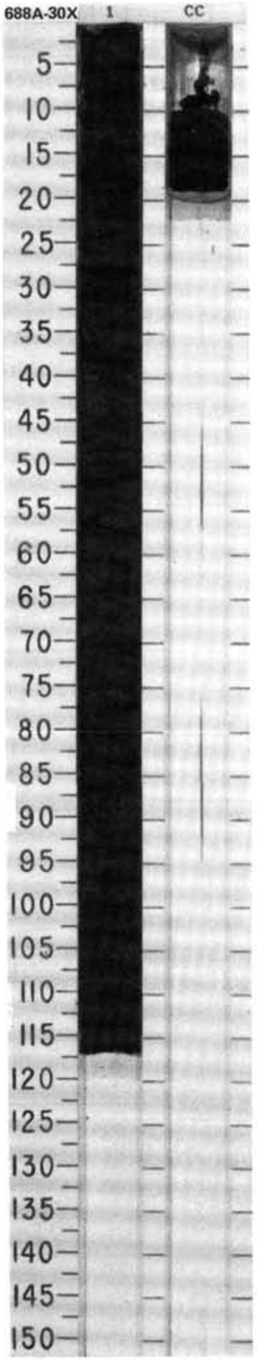

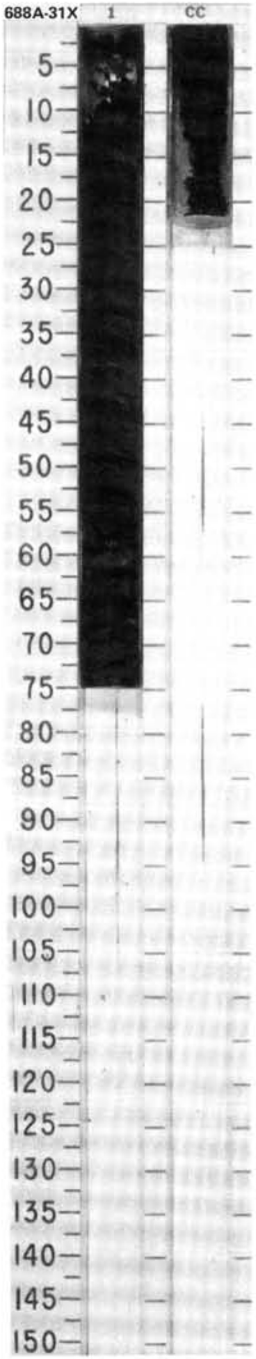

SITE 688 HOLE A CORE 32X CORED INTERVAL 4113.1-4122.6 mbsl; 293.3-302.8 mbsf

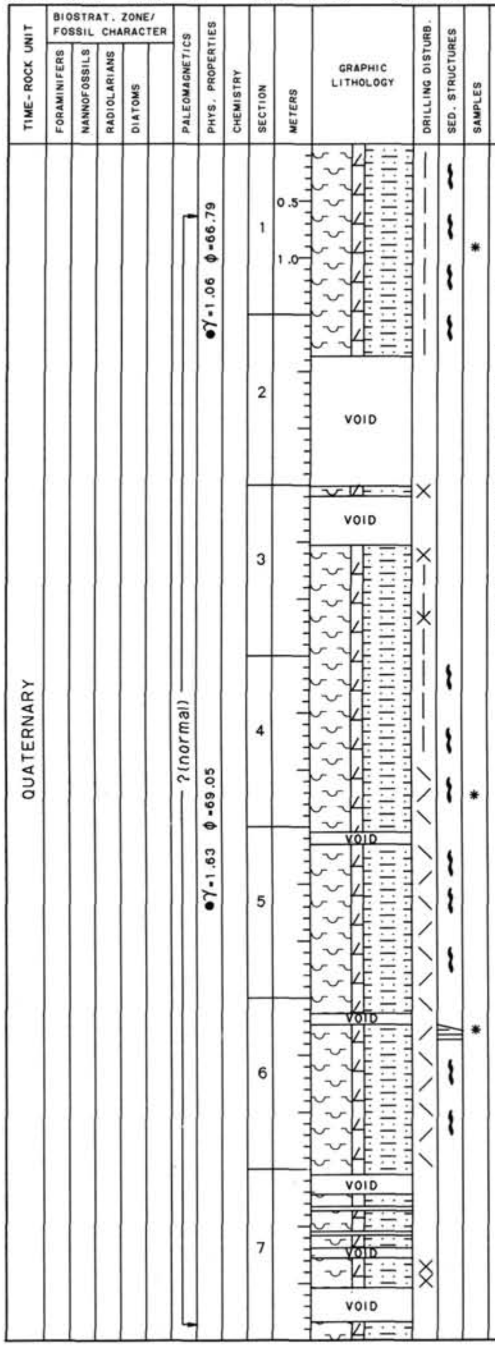

LITHOLOGIC DESCRIPTION

DIATOMACEOUS MUD

Major lithology: diatomaceous mud, black (2.5Y 2/0). Pyrite and iron monosulfide-rich (5 to 10%), oxidizing to dark gray (5Y 3/1) and very dark greenish gray (5GY 3/1). Intensely to moderately burrowed; burrows are filled with black iron monosulfides.

Minor lithology: small sponge spicule nests, 1 to 5–6 mm, throughout. Gastropod shell at Section 4, 138 cm.

SMEAR SLIDE SUMMARY (%):

	1, 100 D	4, 137 M	6, 32 M
TEXTURE:			
Sand	6	10	5
Silt	49	40	25
Clay	45	50	60
COMPOSITION:			
Quartz	5	6	5
Feldspar	5	5	5
Rock fragments	Tr	4	Tr
Mica	Tr	—	—
Clay	35	35	20
Calcite/dolomite	3	2	Tr
Accessory minerals			
Pyrite	5	6	7
Iron sulfides	5	—	—
Foraminifers	Tr	5	3
Nannofossils	2	Tr	40
Diatoms	40	35	20
Sponge spicules	Tr	2	—

(con't.)

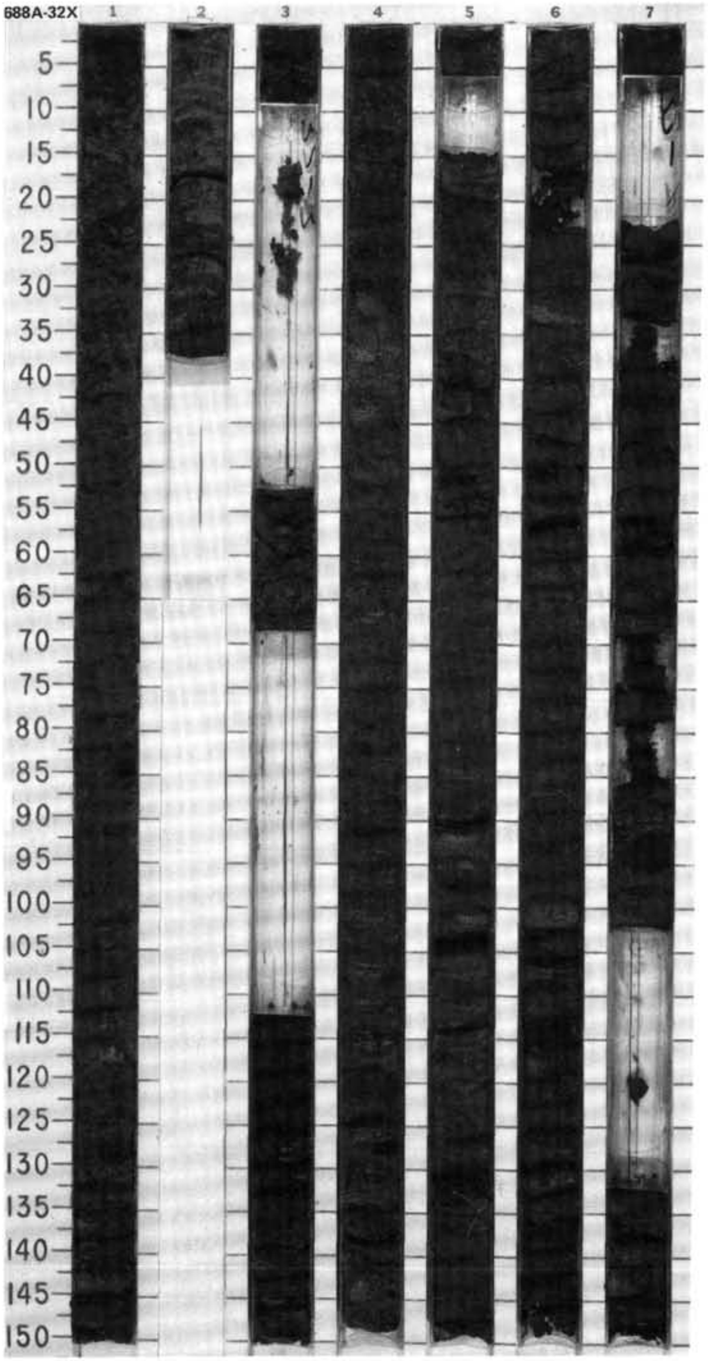

SITE 688 HOLE A CORE 32X CORED INTERVAL 4113.1-4122.6 mbsl; 293.3-302.8 mbsf

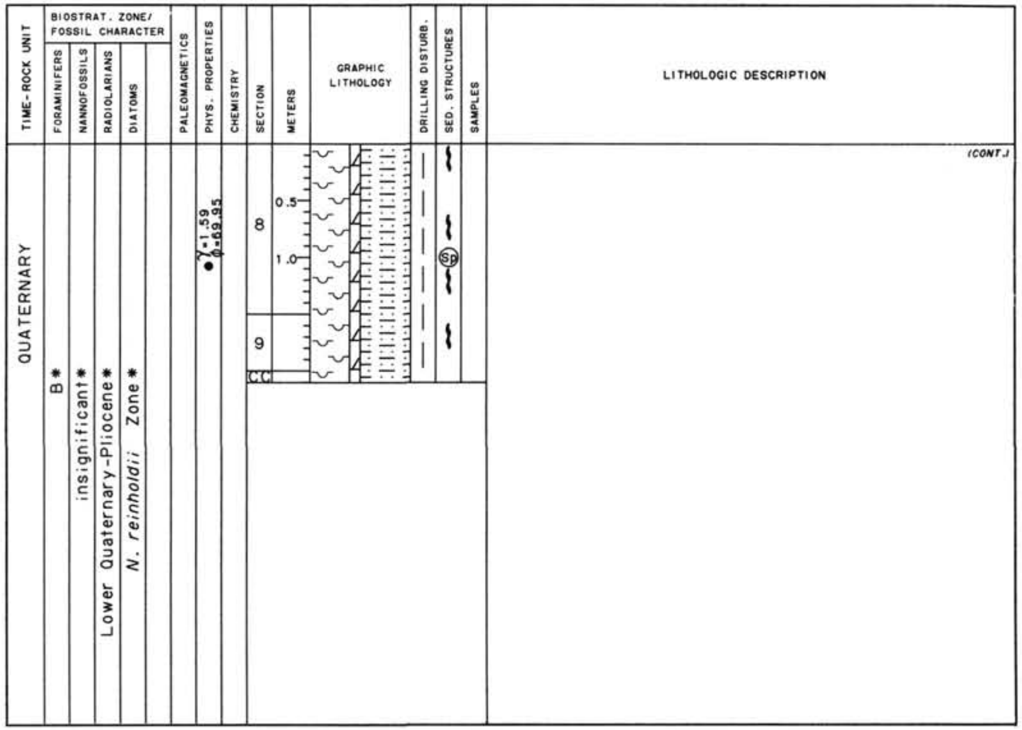

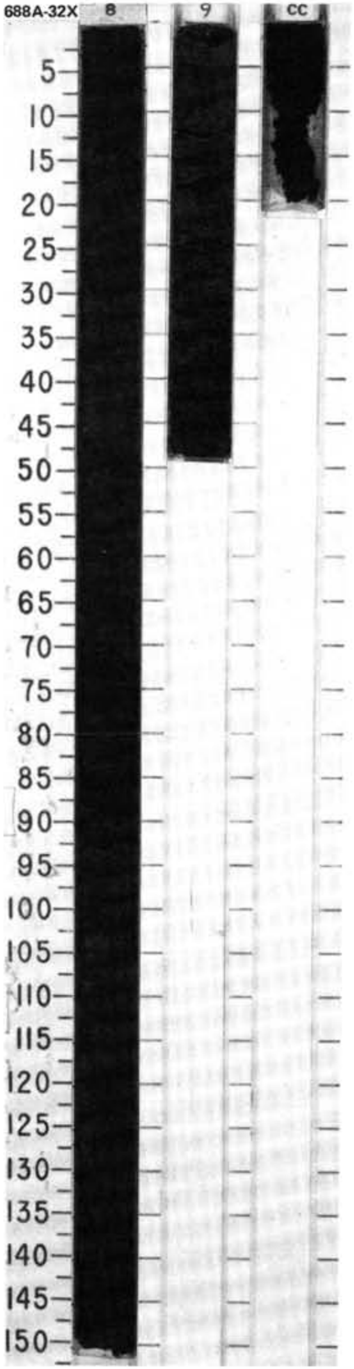

SITE 688 HOLE A CORE 33X CORED INTERVAL 4122.6-4132.1 mbsl; 302.8-312.3 mbsf

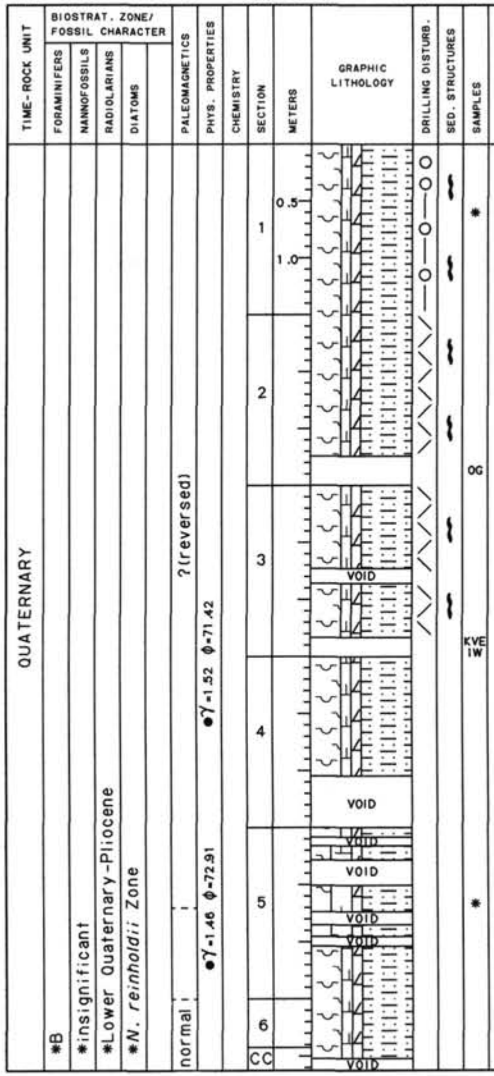

LITHOLOGIC DESCRIPTION

DIATOMACEOUS MUD

Major lithology: foraminifer-bearing diatomaceous mud, black (2.5Y 2/0) to olive black (5Y 2.5/1). Pyrite and iron monosulfide-rich (10%), oxidizing to dark gray (5Y 3/1) and very dark greenish gray (5GY 3/1). Intensely to moderately bioturbated.

Minor lithology: rare sponge spicule nests, 1 to 5–6 mm.

SMEAR SLIDE SUMMARY (%):

	1, 66 D	5, 66 D
TEXTURE:		
Sand	15	15
Silt	45	35
Clay	40	50
COMPOSITION:		
Quartz	8	5
Feldspar	1	5
Rock fragments	3	2
Clay	36	30
Calcite/dolomite	5	10
Accessory minerals		
Pyrite	6	6
Iron sulfides	4	4
Foraminifers	7	15
Nannofossils	—	3
Diatoms	30	20
Sponge spicules	—	Tr

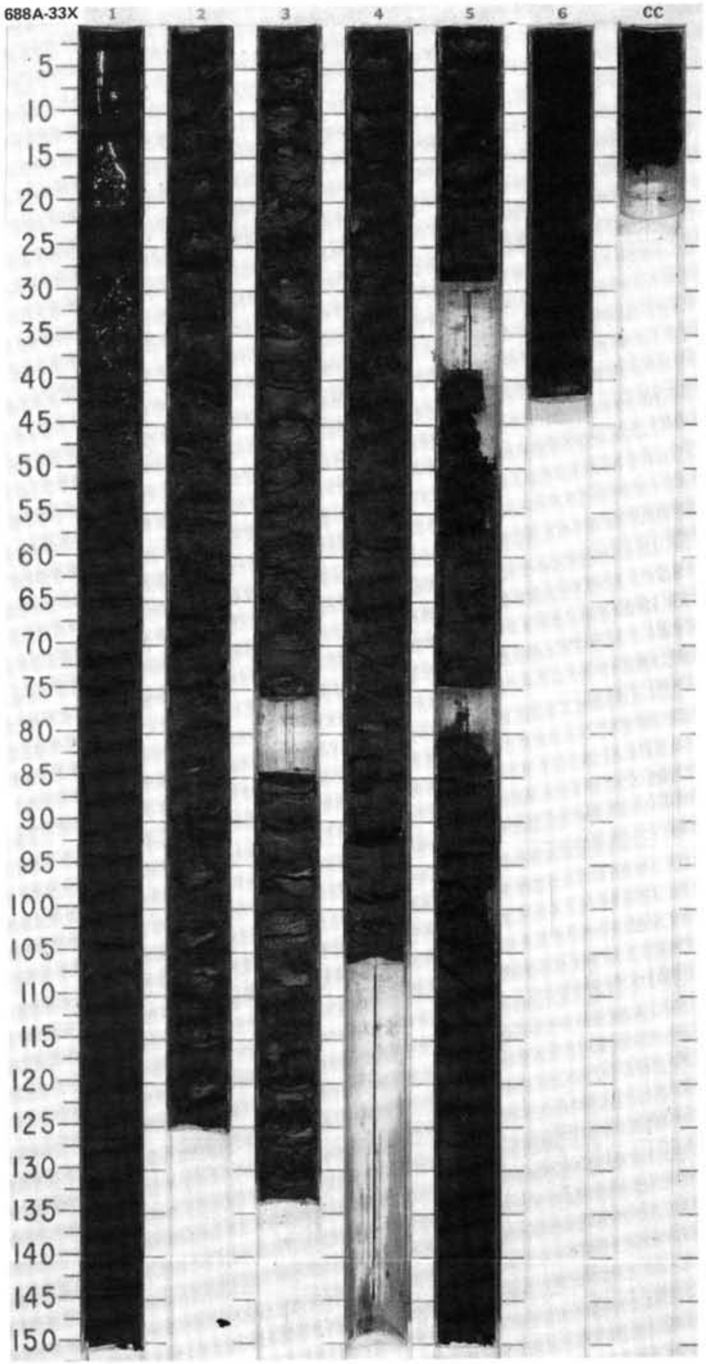

SITE 688 HOLE A CORE 34X CORED INTERVAL 4132.1-4141.6 mbsl; 312.3-321.8 mbsf

TIME-ROCK UNIT	BIOSTRAT. ZONE/ FOSSIL CHARACTER					PALEOMAGNETICS	PHYS. PROPERTIES	CHEMISTRY	SECTION	METERS	GRAPHIC LITHOLOGY	DRILLING DISTURB.	SED. STRUCTURES	SAMPLES	LITHOLOGIC DESCRIPTION
	FORAMINIFERS	NANNOFOSSILS	RADIOLARIANS	DIATOMS											
QUATERNARY	* non diagnostic	* insignificant	* Lower Quaternary-Pliocene	* *N. reinholdii* Zone					1 2 3 4 5 6 7 CC	0.5 1.0		○ ○ ○ ○ ○ ○ ○ ○ ○ ○ ○ ○ ○ ○ ○ ○ ○ ○			WASH CORE Green (5Y 3/2) mud in black (5Y 2.5/1) slurry and black mud soup.

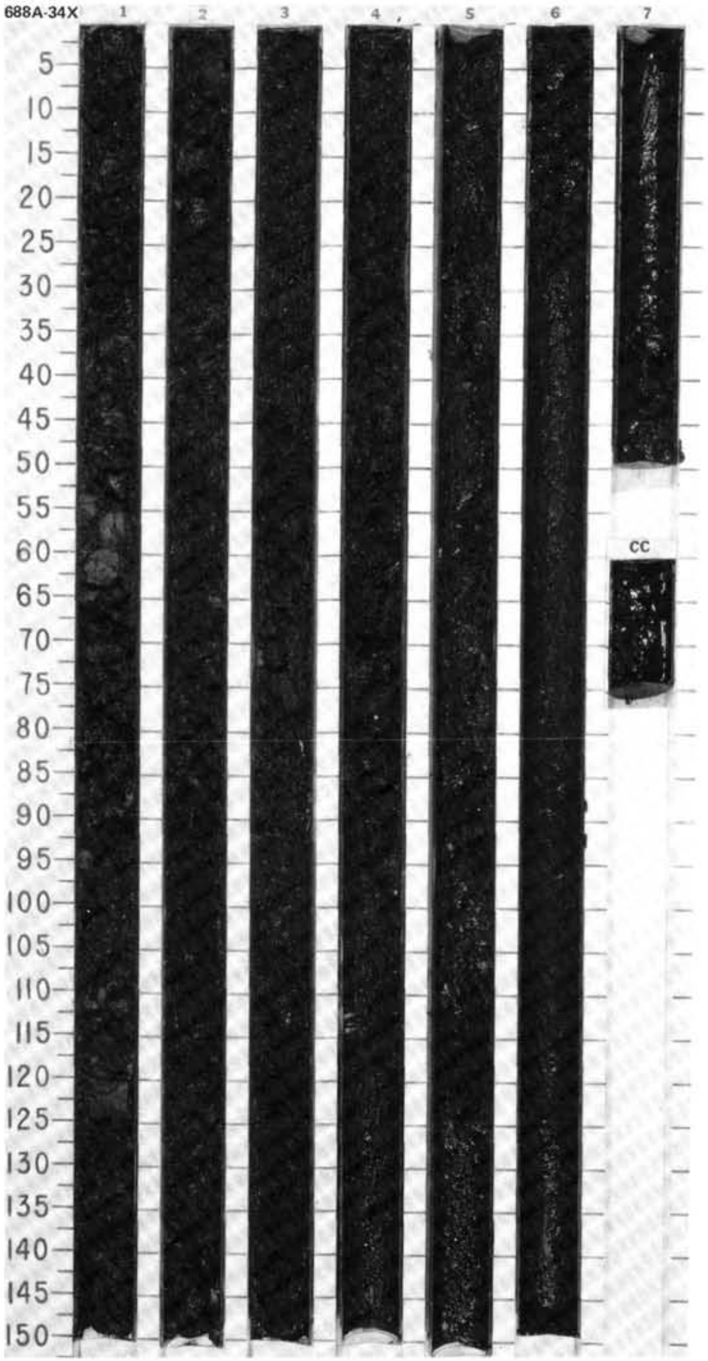

SITE 688 HOLE A CORE 35X CORED INTERVAL 4141.6-4151.1 mbsl; 321.8-331.3 mbsf

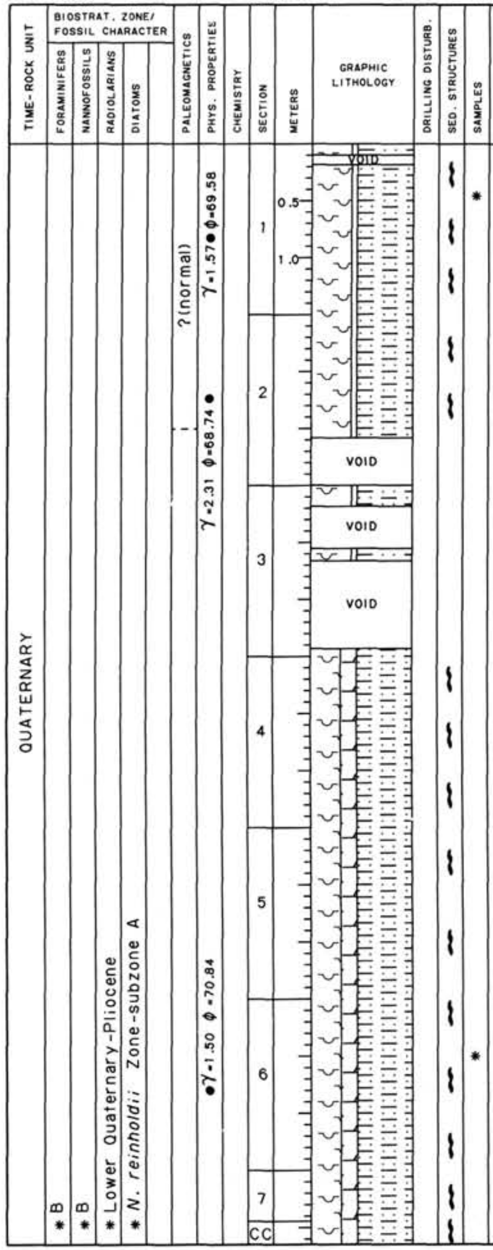

LITHOLOGIC DESCRIPTION

DIATOMACEOUS MUD

Major lithology: diatomaceous mud, black (2.5Y 2/0). Pyrite and iron monosulfide-rich (5 to 10%), oxidizing to dark gray (5Y 3/1) and very dark greenish gray (5GY 3/1). Intensely to moderately burrowed; burrows are filled with black iron monosulfides.

Minor lithology: small sponge spicule nests, 1 to 5–6 mm, throughout.

SMEAR SLIDE SUMMARY (%):

	1, 50 D	6, 50 D
TEXTURE:		
Sand	—	1
Silt	35	45
Clay	65	54
COMPOSITION:		
Quartz	—	10
Feldspar	—	10
Mica	—	Tr
Clay	57	39
Volcanic glass	Tr	Tr
Calcite/dolomite	Tr	1
Accessory minerals		
Giauconite	Tr	—
Pyrite	2	10
Aµatite	—	Tr
Diatoms	40	30
Radiolarians	Tr	Tr
Sponge spicules	1	Tr

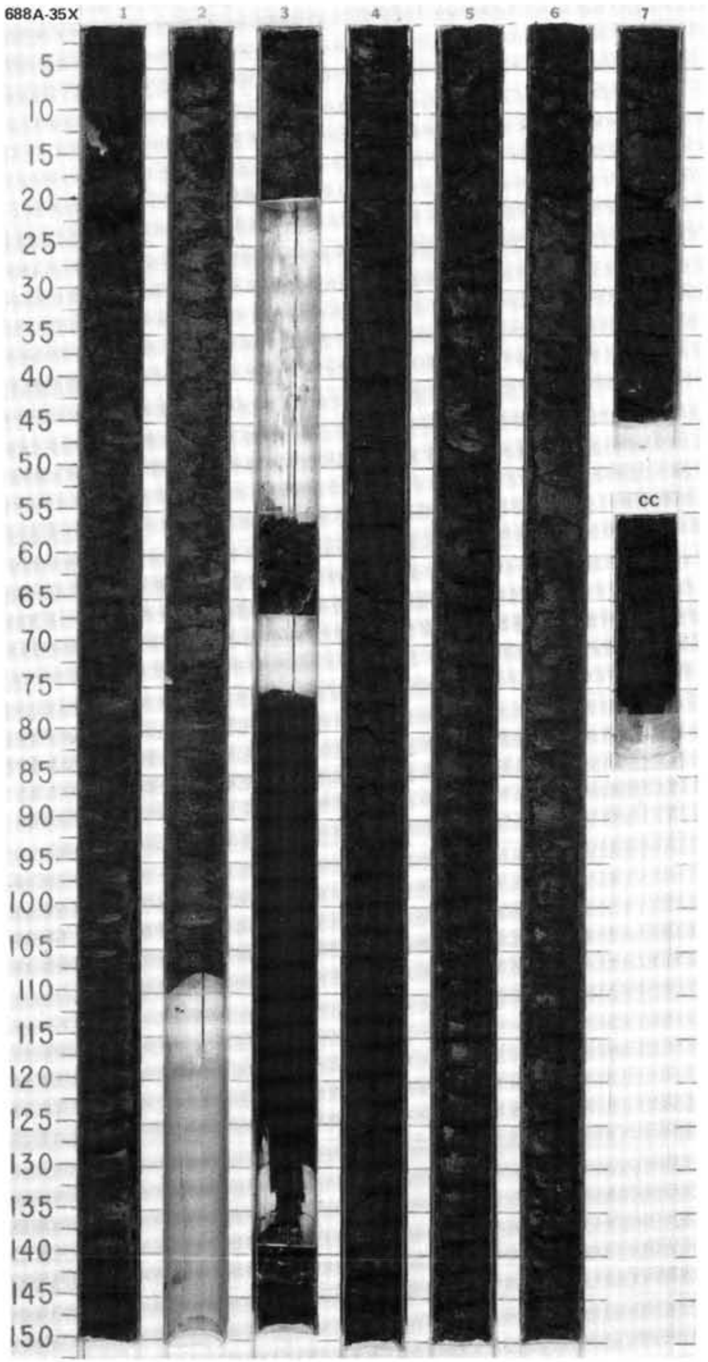

SITE 688 HOLE A CORE 36X CORED INTERVAL 4151.1-4160.6 mbsl; 331.3-340.8 mbsf

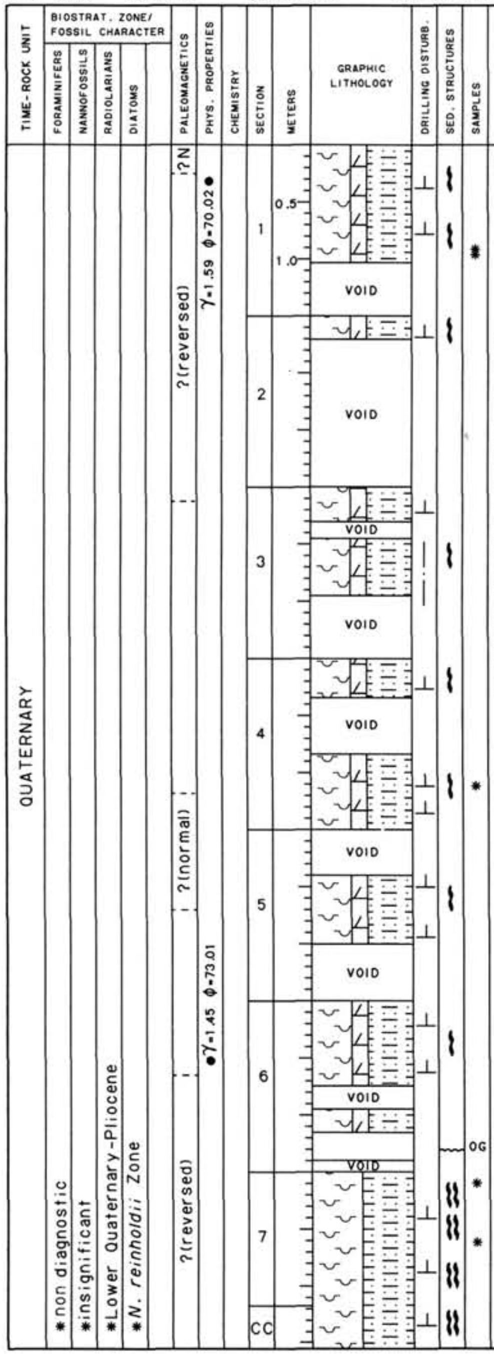

LITHOLOGIC DESCRIPTION

DIATOMACEOUS MUD and DIATOMACEOUS MUDSTONE

Major lithology: sandstone and pebbly sandstone, dark gray (N 4. N 5), very fine to fine grained, rarely coarse grained, including graded conglomeratic units containing rounded clasts of quartz, sedimentary rocks, mud rip-up clasts, and volcanics. Section 1, 0–8 and 110–140 cm, Section 2, 0–16 and 105–126 cm, and Section 4, 21–45 cm. Section 7 and CC: diatomaceous mudstone, very dark gray (5Y 3/1). burrows are filled with coarse grain, sandy silt, and large clast (0.5 to 1 mm), some of which are anguiar. Horizontal fissility is well developed.

Minor lithology: sponge spicule patches throughout Sections 1–6.

SMEAR SLIDE SUMMARY (%):

	1, 87 M	1, 89 D	4, 110 M	7, 7 M	7, 58 M
TEXTURE:					
Sand	1	—	—	—	—
Silt	35	45	40	60	40
Clay	64	55	60	40	60
COMPOSITION:					
Quartz	5	5	5	10	—
Feldspar	10	5	—	9	—
Clay	39	35	30	30	48
Volcanic glass	Tr	Tr	—	Tr	Tr
Calcite/dolomite	1	5	1	Tr	Tr
Accessory minerals					
Pyrite	10	10	2	1	1
Foraminifers	—	Tr	—	—	—
Diatoms	35	40	61	50	50
Radiolarians	—	—	1	Tr	—
Sponge spicules	—	Tr	Tr	—	Tr
Fish remains	—	Tr	—	—	—
Organic material	—	—	—	—	1

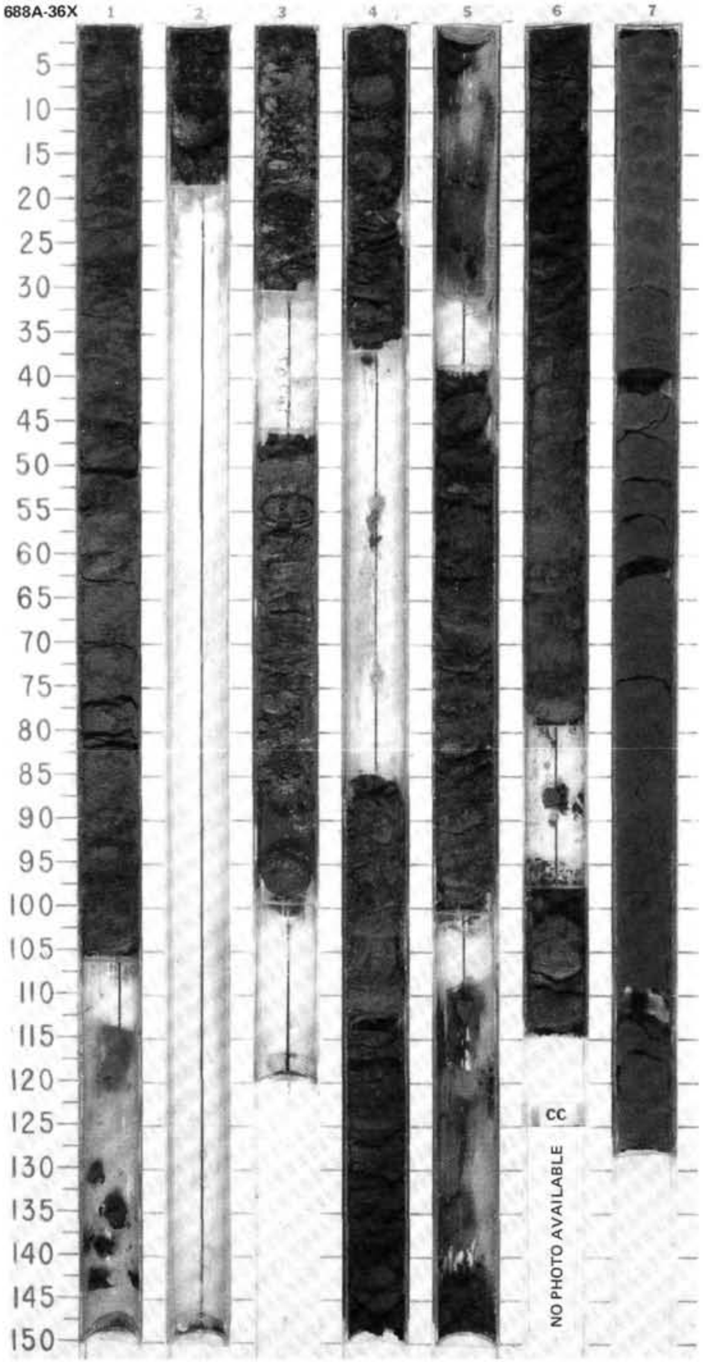

SITE 688 HOLE A CORE 37X CORED INTERVAL 4160.6-4170.1 mbsl; 340.8-350.3 mbsf

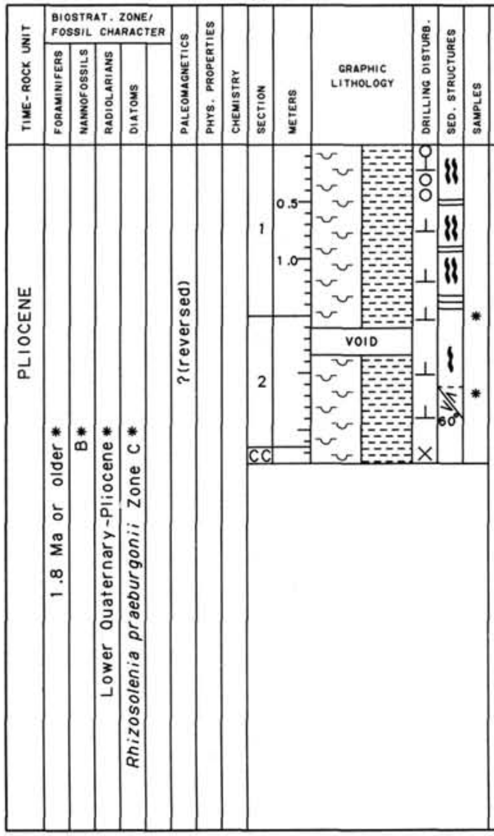

LITHOLOGIC DESCRIPTION

DIATOMACEOUS MUDSTONE

Major lithology: diatomaceous mudstone, very dark gray (5Y 3/1), extensively burrowed. Horizontal fissility is well developed. Reverse fault strikes roughly 297° and dips 60° landward.

SMEAR SLIDE SUMMARY (%):

	2, 4 D	2, 74 D
TEXTURE:		
Silt	52	54
Clay	48	46
COMPOSITION:		
Quartz	—	2
Feldspar	—	1
Clay	48	46
Calcite/dolomite	1	—
Accessory minerals		
Pyrite	1	1
Diatoms	50	50
Radiolarians	Tr	—

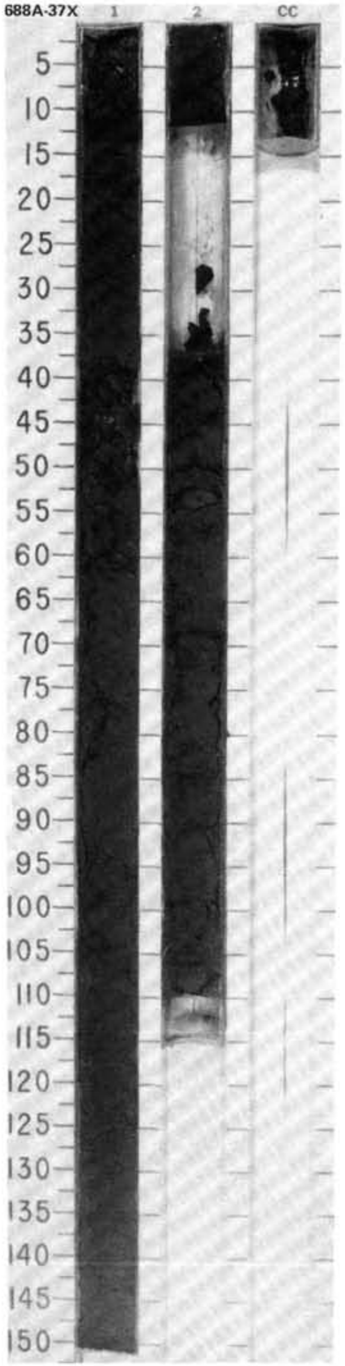

SITE 688 HOLE C CORE 1R CORED INTERVAL 3819.8-3829.3 mbsl; 350.3-359.8 mbsf

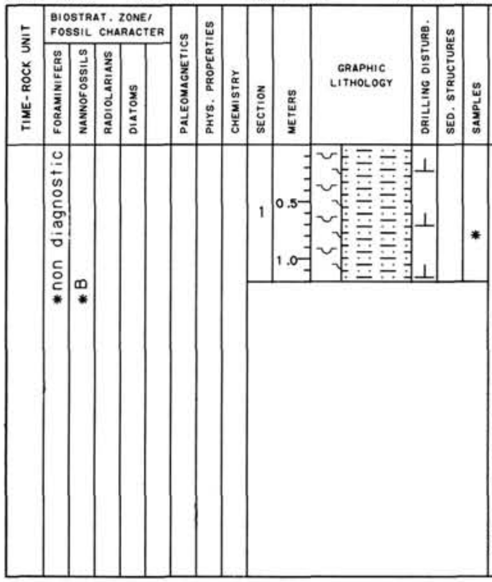

LITHOLOGIC DESCRIPTION

DIATOMACEOUS MUDSTONE

Major lithology: diatomaceous mudstone, very dark gray (5Y 3/1) Moderately burrowed, fissility well developed, occurrence of some silty beds.

SMEAR SLIDE SUMMARY (%):

	1, 81 D
TEXTURE:	
Sand	2
Silt	38
Clay	60
COMPOSITION:	
Quartz	5
Feldspar	5
Clay	54
Volcanic glass	Tr
Calcite/dolomite	1
Accessory minerals	
Pyrite	5
Glauconite	Tr
Diatoms	30
Sponge spicules	Tr
Silicoflagellates	Tr

SITE 688 HOLE E CORE 1R CORED INTERVAL 4175.8-4181.3 mbsl; 350.0-355.5 mbsf

TIME-ROCK UNIT	BIOSTRAT. ZONE/ FOSSIL CHARACTER FORAMINIFERS	NANNOFOSSILS	RADIOLARIANS	DIATOMS	PALEOMAGNETICS	PHYS. PROPERTIES	CHEMISTRY
LOWER QUATERNARY - PLIOCENE	*B	*B	*Lower Quaternary-Pliocene	*N. reinholdii Zone 'B'	? (Reversed)		

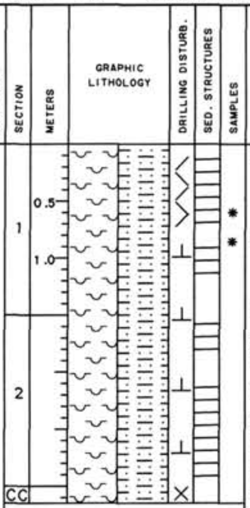

LITHOLOGIC DESCRIPTION

DIATOMACEOUS MUDSTONE

Major lithology: diatomaceous mudstone, very dark gray (5Y 3/1) to black (5Y 2.5/1). Locally bedded or laminated, mainly massive. Occurrence of some silty beds Fissility is well developed.

SMEAR SLIDE SUMMARY (%):

	1, 77.5 D	1, 84 M
TEXTURE:		
Sand	10	—
Silt	35	55
Clay	55	45
COMPOSITION:		
Quartz	5	10
Feldspar	4	5
Rock fragments	1	3
Clay	40	45
Calcite/dolomite	2	2
Accessory minerals		
Pyrite	8	5
Glauconite	—	Tr
Foraminifers	5	Tr
Diatoms	35	30
Sponge spicules	Tr	—
Silicoflagellates	Tr	Tr

SITE 688 HOLE E CORE 2R CORED INTERVAL 4181.3-4190.8 mbsl; 355.5-365.0 mbsf

TIME-ROCK UNIT	BIOSTRAT. ZONE/ FOSSIL CHARACTER FORAMINIFERS	NANNOFOSSILS	RADIOLARIANS	DIATOMS	PALEOMAGNETICS	PHYS. PROPERTIES	CHEMISTRY
	B*	B*	D. kamtschatica Zone B *		? (Reversed)		

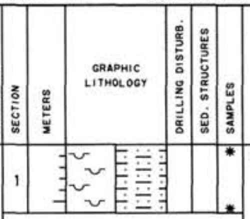

LITHOLOGIC DESCRIPTION

DIATOMACEOUS MUDSTONE

Major lithology: *diatomaceous mudstone, dark olive gray (5Y 3/2)*. Fissility is well developed. Small blue (5Y 5/3) blebs rich in diatoms.

Minor lithologies:
a. brecciated dolomicrite, olive gray (5Y 5/2)
b. micritic diatom ooze

SMEAR SLIDE SUMMARY (%):

	1, 9 D	1, 58 D
TEXTURE:		
Silt	68	60
Clay	32	40
COMPOSITION:		
Quartz	4	3
Feldspar	5	5
Rock fragments	3	1
Mica	1	Tr
Clay	35	35
Calcite/dolomite	3	—
Accessory minerals		
Pyrite	4	4
Phosphate	2	2
Glauconite	Tr	Tr
Micrite	—	5
Diatoms	43	45
Radiolarians	—	Tr
Sponge spicules	Tr	—
Silicoflagellates	Tr	—

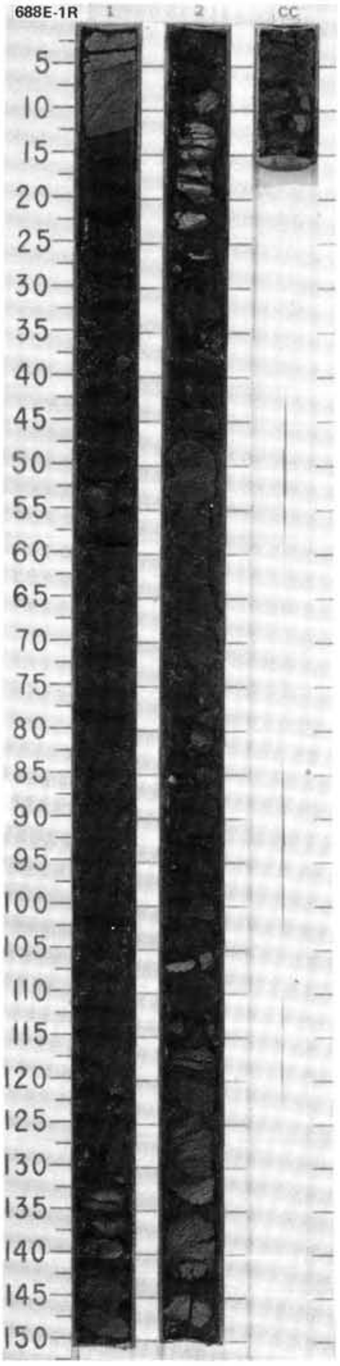

SITE 688 HOLE E CORE 3R CORED INTERVAL 4190.8-4200.3 mbsl; 365.0-374.5 mbsf

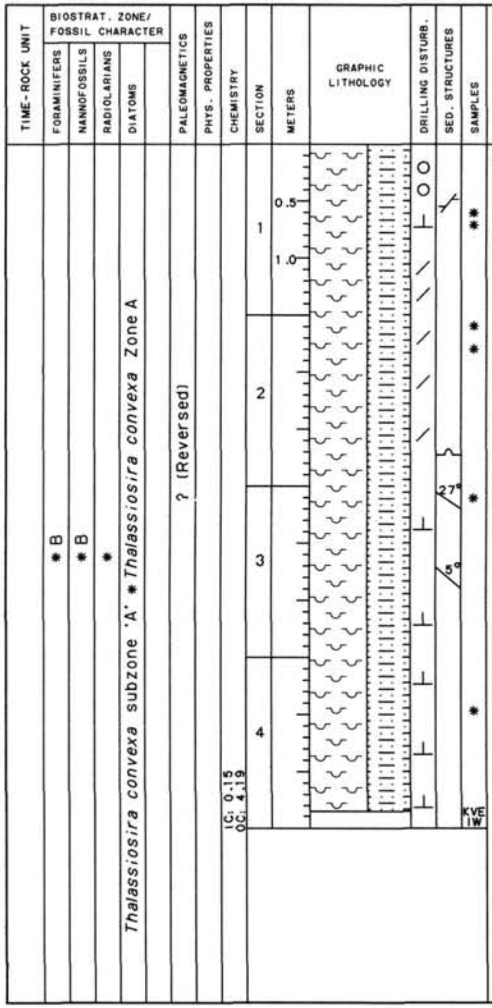

LITHOLOGIC DESCRIPTION

DIATOMITE

Major lithology: diatomite, dark olive gray (5Y 3/2), finely laminated, interbedded micritic diatomite and muddy dolomite. Extensive normal faulting, soft brecciation and disaggregation fracturing. Rock has an anastomosing fabric.

SMEAR SLIDE SUMMARY (%):

	1, 60 D	1, 71 D	2, 2 D	2, 13 D	3, 48 D	4, 47 D
TEXTURE:						
Sand	—	—	10	—	10	10
Silt	75	80	70	70	60	60
Clay	25	20	20	30	30	30
COMPOSITION:						
Quartz	—	8	5	5	5	5
Feldspar	—	6	—	3	—	—
Rock fragments	10	3	Tr	2	Tr	5
Mica	Tr	Tr	5	—	—	—
Clay	10	15	20	25	10	20
Volcanic glass	—	1	—	—	—	—
Calcite/dolomite	5	4	10	5	10	10
Accessory minerals						
Pyrite	3	2	3	3	5	3
Phosphate	1	2	5	1	—	2
Opaques	—	—	2	—	—	—
Micrite	15	5	—	5	—	—
Diatoms	55	54	50	51	70	55
Sponge spicules	—	Tr	Tr	Tr	Tr	Tr
Silicoflagellates	1	—	—	Tr	Tr	—

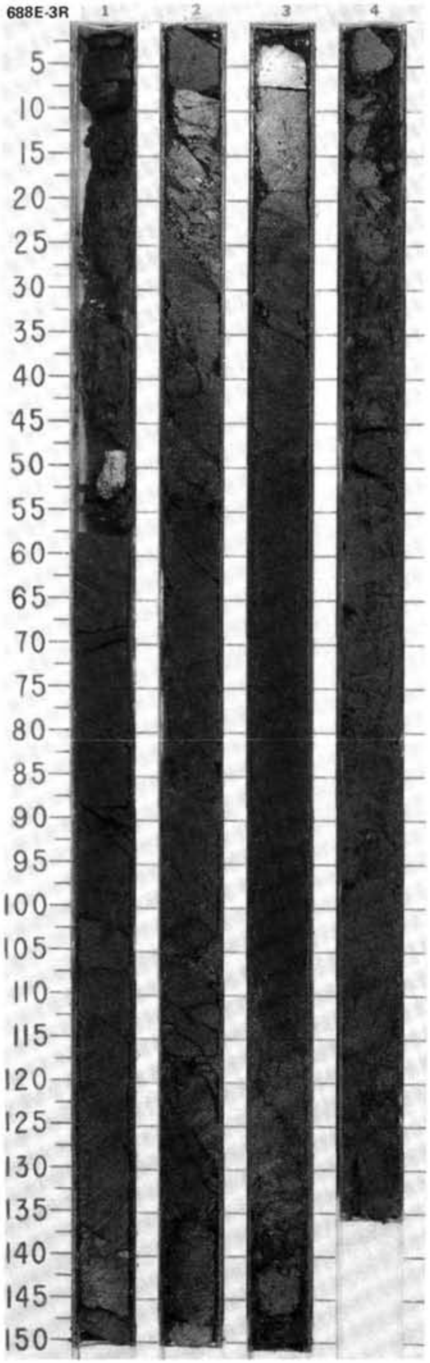

SITE 688 HOLE E CORE 4R CORED INTERVAL 4200.3-4209.8 mbsl; 374.5-384.0 mbsf

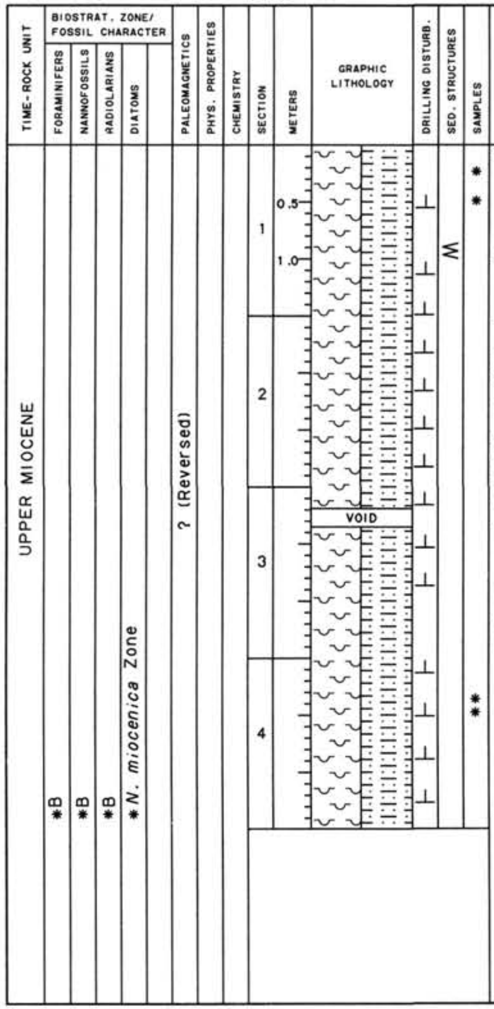

LITHOLOGIC DESCRIPTION

DIATOMITE

Major lithology: diatomite, finely laminated. 90–95% of "pale" laminae dark olive gray (5Y 3/2) in color and 5–10% of dark laminae very dark gray (5Y 3 1) in color. pervasively disrupted and disaggregated. Anastomosing fabric with tensional and compressional tectonic features.

SMEAR SLIDE SUMMARY (%):

	1, 25 M	1, 45 D	4, 31 D	4, 47 M
TEXTURE:				
Sand	—	—	10	—
Silt	30	92	50	97
Clay	70	8	40	3
COMPOSITION:				
Quartz	—	3	—	3
Feldspar	—	3	—	—
Rock fragments	—	2	—	—
Mica	20	—	10	—
Clay	50	7	40	3
Calcite/dolomite	10	3	5	3
Accessory minerals				
Opaques				
Pyrite	10	4	5	1
Dolomite				
Phosphate	—	2	5	1
Diatoms	10	76	35	89
Radiolarians	Tr	—	—	—
Sponge spicules	Tr	Tr	Tr	—
Silicoflagellates	—	Tr	—	Tr
Fish remains	—	—	Tr	—

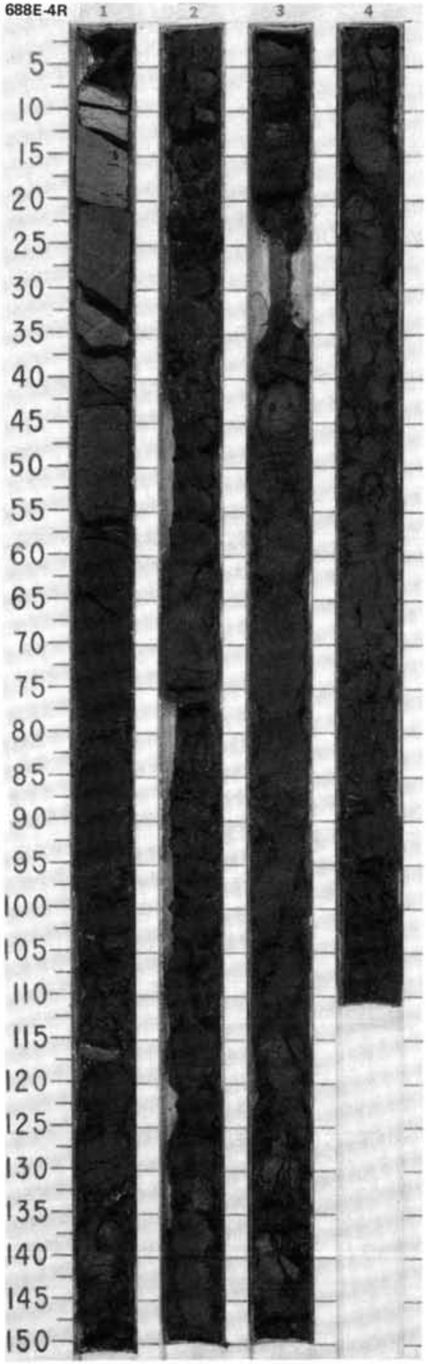

SITE 688 HOLE E CORE 5R CORED INTERVAL 4209.8-4219.3 mbsl; 384.0-393.5 mbsf

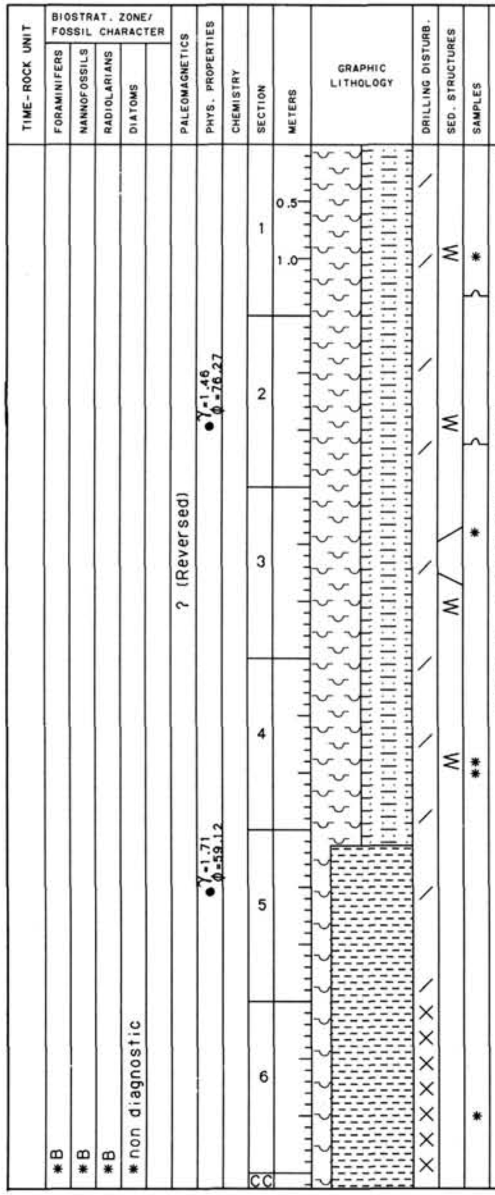

LITHOLOGIC DESCRIPTION

DIATOMITE and DIATOM-BEARING CLAYSTONE

Major lithology: diatomite, finely laminated. Dark olive gray (5Y 2.5/2) to olive gray (5Y 4/2) laminae, light and dark laminae interbedded, light laminae are more diatom-rich. Pervasively disrupted and disaggregated, anastomosing fabric. Sections 1 to 5, 15 cm.

Major lithology: diatom-bearing claystone, black (5Y 2.5/2). Beds are typically 1 to 3–4 cm thick. Less indurated than the diatomite, fissility well developed. Section 5, 15 cm, to CC.

SMEAR SLIDE SUMMARY (%):

	1, 89 D	3, 36 M	4, 85 M	4, 90 D	5, 21 D	6, 91 D
TEXTURE:						
Sand	20	50	10	20	5	—
Silt	40	40	50	50	30	60
Clay	40	10	40	30	65	40
COMPOSITION:						
Quartz	5	5	2	Tr	5	7
Feldspar	—	—	—	—	—	8
Rock fragments	Tr	—	—	—	Tr	3
Mica	Tr	5	Tr	Tr	5	—
Clay	30	10	40	15	55	33
Volcanic glass	—	80	—	30	—	—
Calcite/dolomite	5	Tr	10	—	Tr	1
Accessory minerals						
Pyrite	5	—	5	5	10	4
Phosphorite	5	—	3	3	5	4
Diatoms	30	—	30	47	10	20
Radiolarians	Tr	—	—	—	—	—
Sponge spicules	Tr	—	—	—	Tr	—
Fish remains	—	—	Tr	—	—	—
Plant debris	20	—	10	—	10	10
Organic?	—	—	—	—	—	10

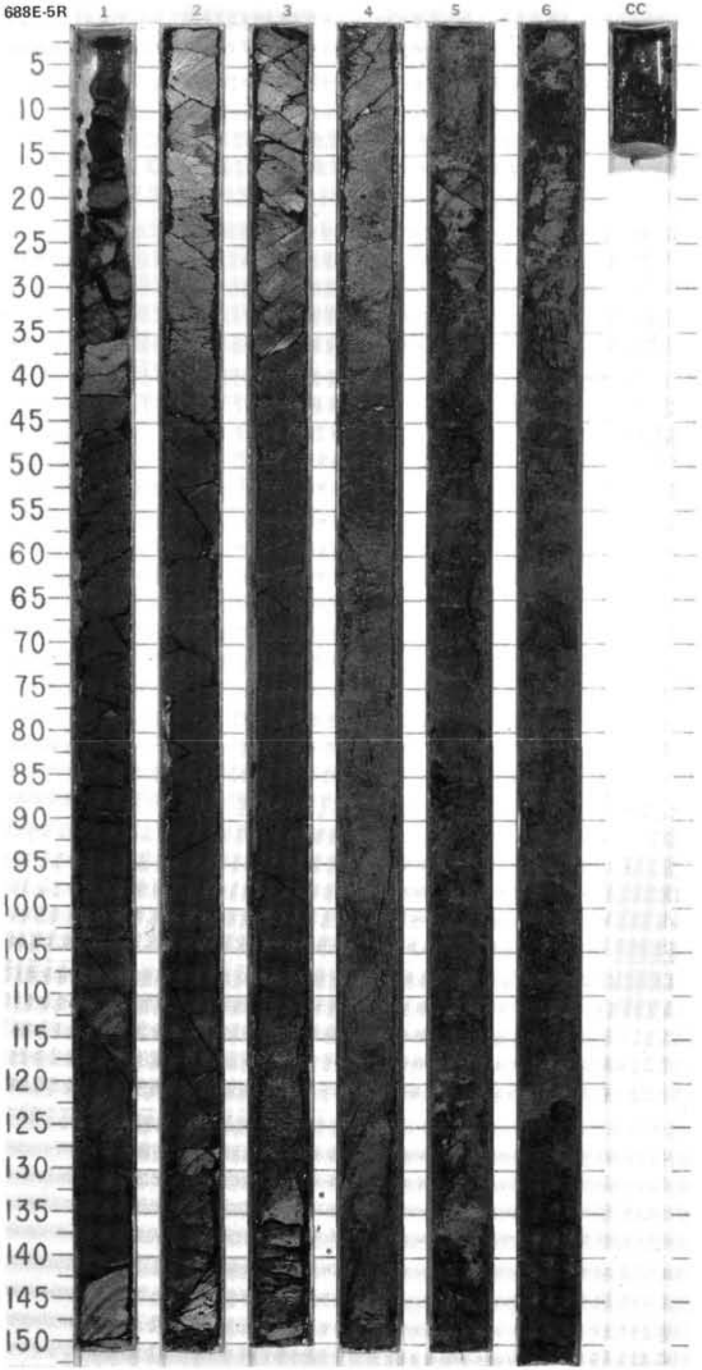

SITE 688 HOLE E CORE 6R CORED INTERVAL 4219.3-4228.8 mbsl; 393.5-403.0 mbsf

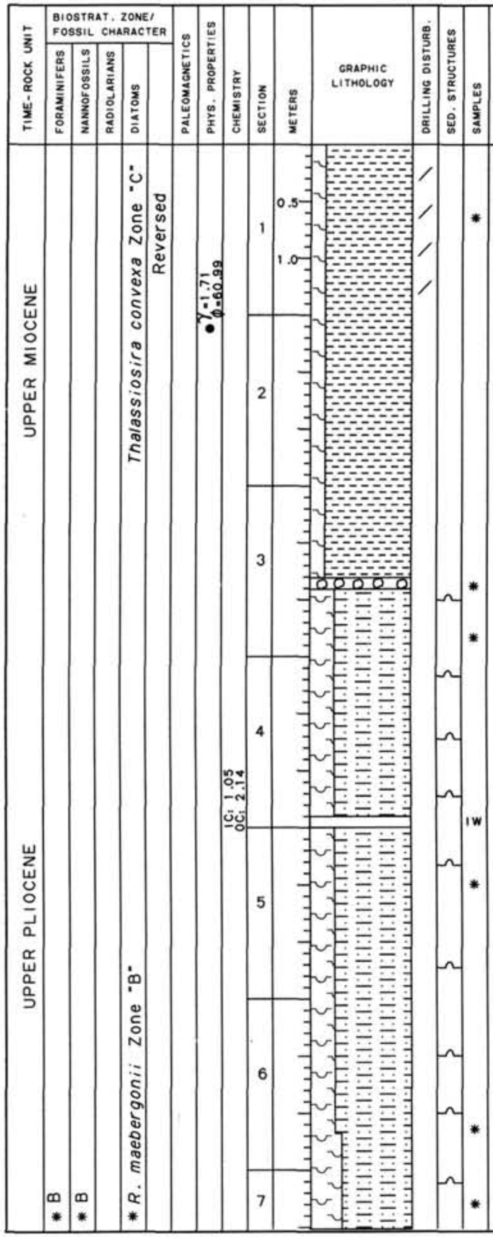

LITHOLOGIC DESCRIPTION

DIATOM-BEARING CLAYSTONE and DIATOM-BEARING MUDSTONE

Major lithology: diatom-bearing claystone, black (5Y 2.5/2). Mainly massive Pervasively disrupted at a microscopic scale. Section 1 to Section 3, 90 cm

Diatom-bearing mudstone, dark olive gray (5Y 3/2), well laminated with laminae of olive (5Y 4/4) diatomite and black (5Y 2.5/2) mudstone. Pale and black laminae are interbedded. Extensively deformed by slumping. Section 3, 90 cm, to Section 7.

SMEAR SLIDE SUMMARY (%):

	1, 65 D	3, 90 M	3, 131 D	5, 44 M	6, 60 D	7, 27 D
TEXTURE:						
Sand	—	—	10	—	—	—
Silt	30	40	40	95	65	55
Clay	70	60	50	5	35	45
COMPOSITION:						
Quartz	5	5	20	3	8	3
Feldspar	—	—	10	2	10	3
Rock fragments	—	5	Tr	—	5	—
Mica	5	10	—	—	Tr	—
Clay	70	55	45	4	35	45
Calcite/dolomite	—	5	3	1	10	2
Accessory minerals						
Pyrite	5	3	5	Tr	—	—
Glauconite	Tr	—	—	—	—	—
Phosphorite	5	2	7	—	—	—
Foraminifers	—	—	—	—	2	2
Diatoms	10	15	10	90	30	45
Radiolarians	—	—	—	—	—	Tr
Sponge spicules	Tr	Tr	—	—	Tr	—
Silicoflagellates	—	Tr	—	—	—	—

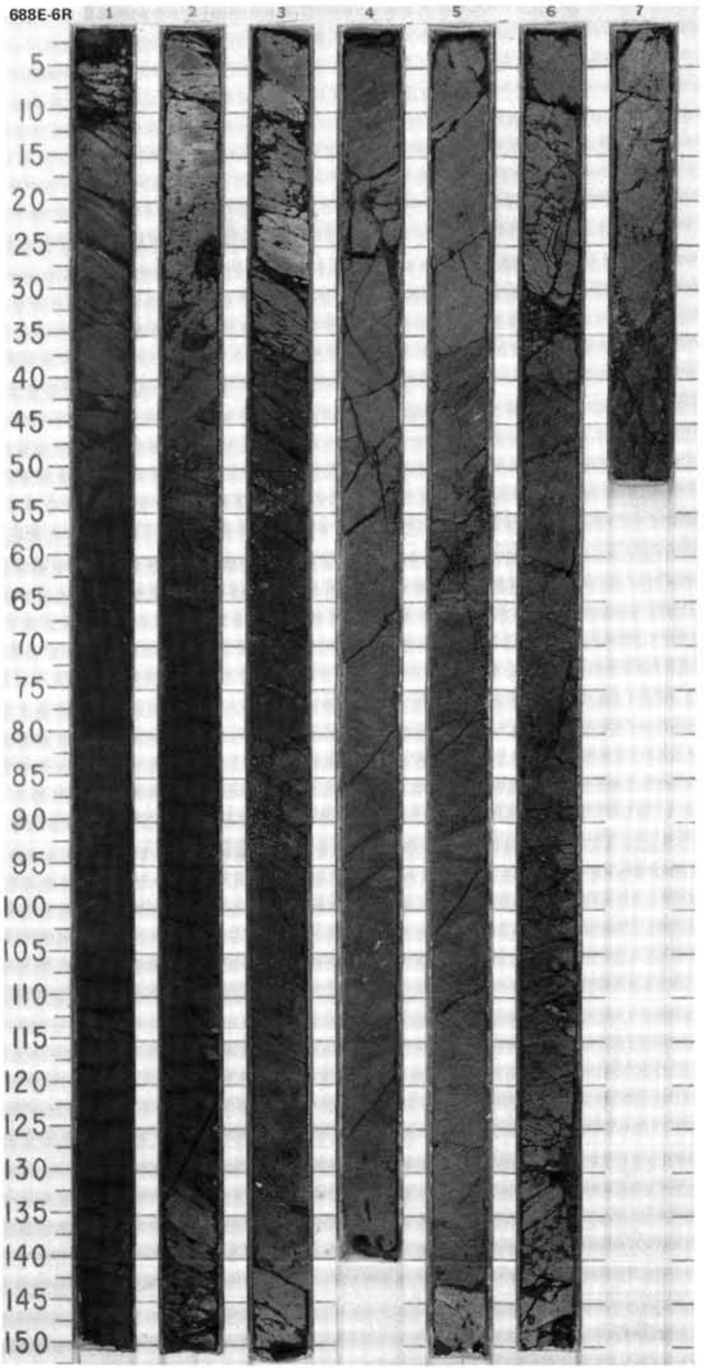

SITE 688 HOLE E CORE 7R CORED INTERVAL 4228.8-4238.3 mbsl; 403.0-412.5 mbsf

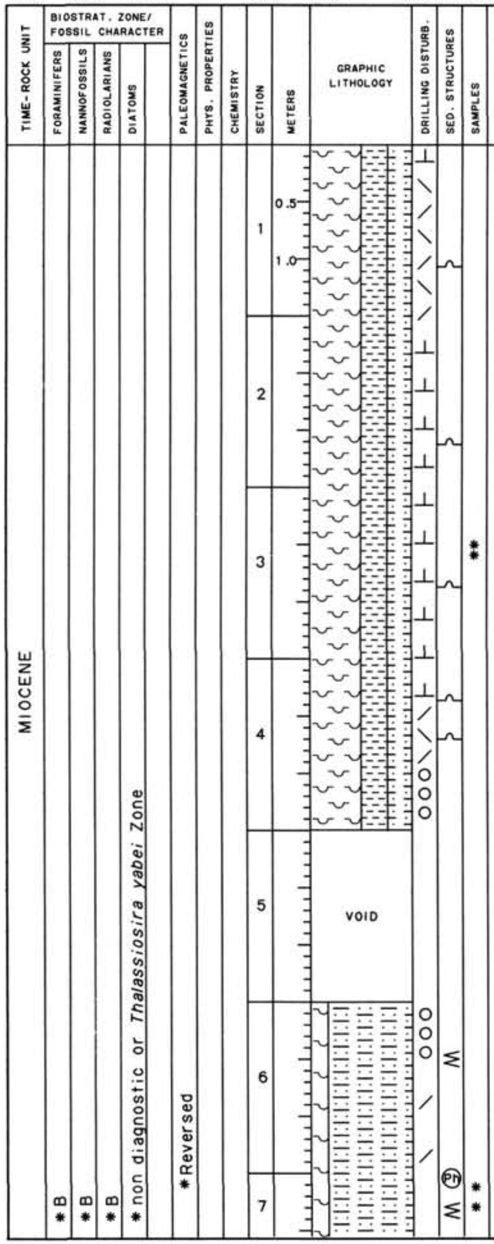

LITHOLOGIC DESCRIPTION

DIATOM-BEARING MUDSTONE TO DIATOMITE and DIATOM-BEARING CLAYSTONE

Major lithology: diatom-bearing mudstone to diatomite, dark olive gray (5Y 3/2). Well laminated with laminae of olive (5Y 4/4) diatomite and black (5Y 2.5/2) mudstone. Pale and black laminae are interbedded. Extensively deformed by slumping. Sections 1 to 4.

Major lithology: diatom-bearing claystone. Dark olive gray (5Y 3/2) to black (5Y 2.5/2). Mainly massive, fissility well developed. Slumping structure. Sections 6 and 7.

SMEAR SLIDE SUMMARY (%):

	3, 54 D	3, 55 D	7, 7 M	7, 17 M	7, 21 D
TEXTURE:					
Sand	—	—	2	—	—
Silt	30	90	7	45	55
Clay	70	10	91	65	45
COMPOSITION:					
Quartz	—	3	2	5	10
Feldspar	—	—	5	5	15
Rock fragments	—	—	2	—	5
Mica	10	10	—	Tr	Tr
Clay	60	—	—	65	45
Calcite/dolomite	5	10	5	5	5
Accessory minerals					
Pyrite	2	2	1	—	—
Opaques	3	—	—	5	5
Apatite	—	—	85	—	—
Foraminifers	—	—	—	Tr	Tr
Diatoms	20	75	—	15	15
Radiolarians	—	—	—	Tr	—
Silicoflagellates	Tr	Tr	—	—	—

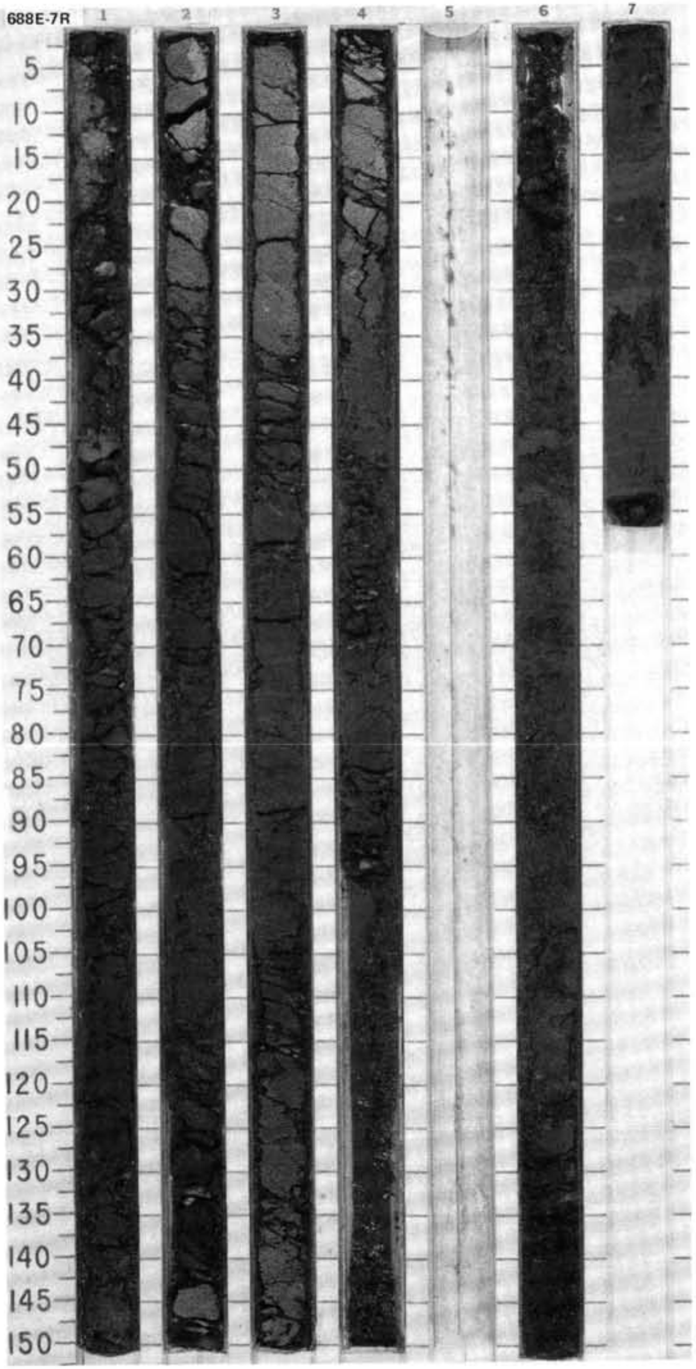

SITE 688 HOLE E CORE 8R CORED INTERVAL 4238.3-4247.8 mbsl; 412.5-422.0 mbsf

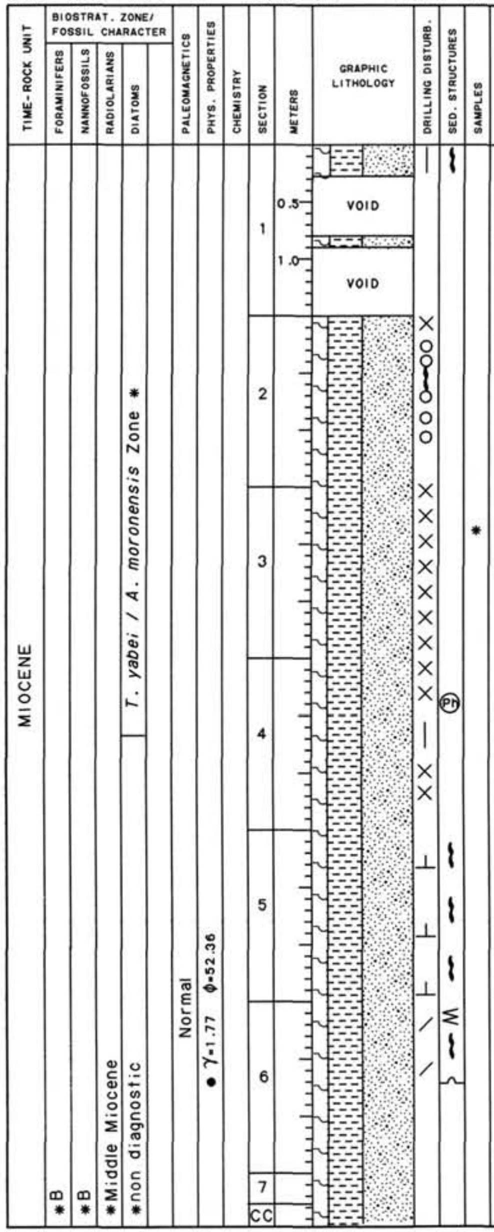

LITHOLOGIC DESCRIPTION

DIATOM-BEARING SILTSTONE

Major lithology: diatom-bearing siltstone, dark olive gray (5Y 3/2) to olive gray (5Y 4/2) and very dark gray (5Y 3/1). Moderately burrowed. Slump evidences in Section 6.

Minor lithology: phosphatic nodule.

SMEAR SLIDE SUMMARY (%):

	3, 38 D	6, 88 D
TEXTURE:		
Sand	20	15
Silt	50	45
Clay	30	40
COMPOSITION:		
Quartz	35	25
Feldspar	20	15
Rock fragments	10	10
Clay	20	30
Calcite/dolomite	—	5
Accessory minerals		
Pyrite	4	—
Glauconite	Tr	—
Foraminifers	Tr	—
Diatoms	15	10
Sponge spicules	5	5

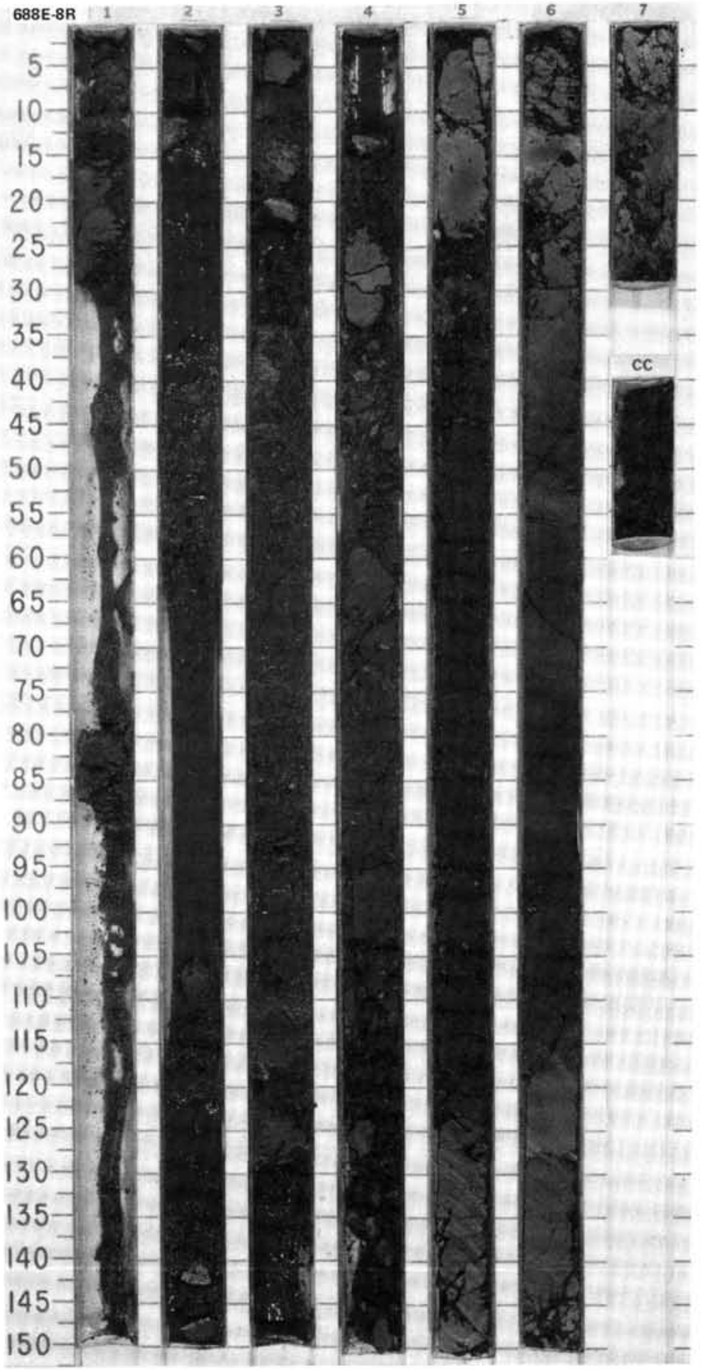

SITE 688 HOLE E CORE 9R CORED INTERVAL 4247.8-4257.3 mbsl; 422.0-431.5 mbsf

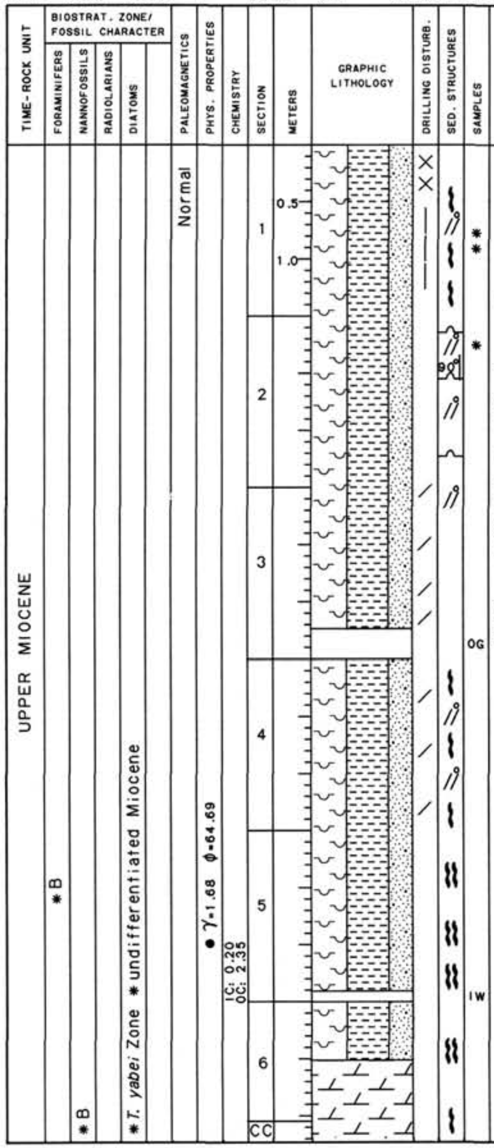

LITHOLOGIC DESCRIPTION

DIATOM-BEARING SILTSTONE

Major lithology: diatom-bearing siltstone, dark olive gray (5Y 3/2) to black (5Y 2.5/2) and olive gray (5Y 4/2). Extensively bioturbated. Dewatering veins of two generations: 1) Horizontal veins are older than 2) vertical veins, which cross out the horizontal one. Bedding is vertical in Section 3.

Minor lithology: dolomitic siltstone, olive gray (5Y 3/2) fractured. Veins filled with light olive gray (5Y 6/2) calcite.

SMEAR SLIDE SUMMARY (%):

	1, 75 M	1, 85 M	2, 25 D
TEXTURE:			
Sand	20	15	10
Silt	35	35	40
Clay	45	50	50
COMPOSITION:			
Quartz	15	10	10
Feldspar	10	10	10
Rock fragments	10	10	5
Clay	40	40	35
Calcite/dolomite	3	10	4
Accessory minerals			
Pyrite	2	5	8
Green amphibolite	Tr	—	—
Glauconite	Tr	—	—
Foraminifers	—	—	Tr
Diatoms	15	10	25
Sponge spicules	5	5	3

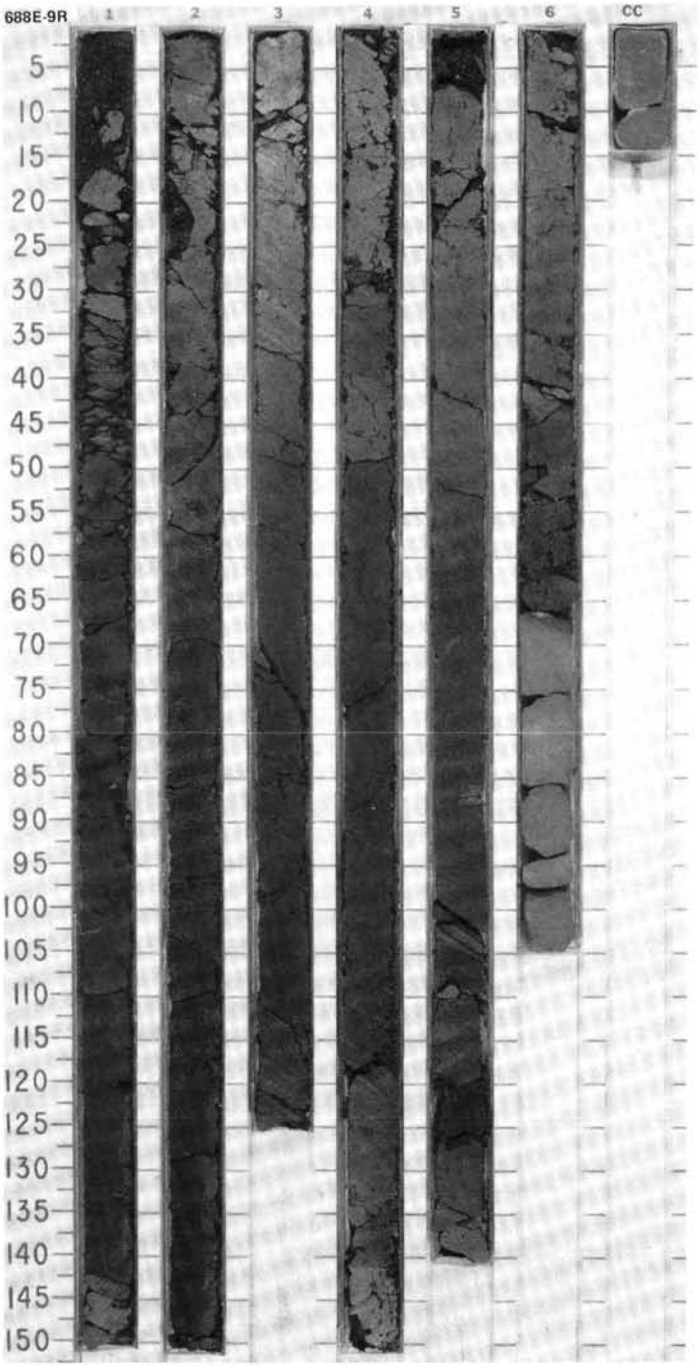

SITE 688 HOLE E CORE 10R CORED INTERVAL 4257.3-4266.8 mbsl; 431.5-441.0 mbsf

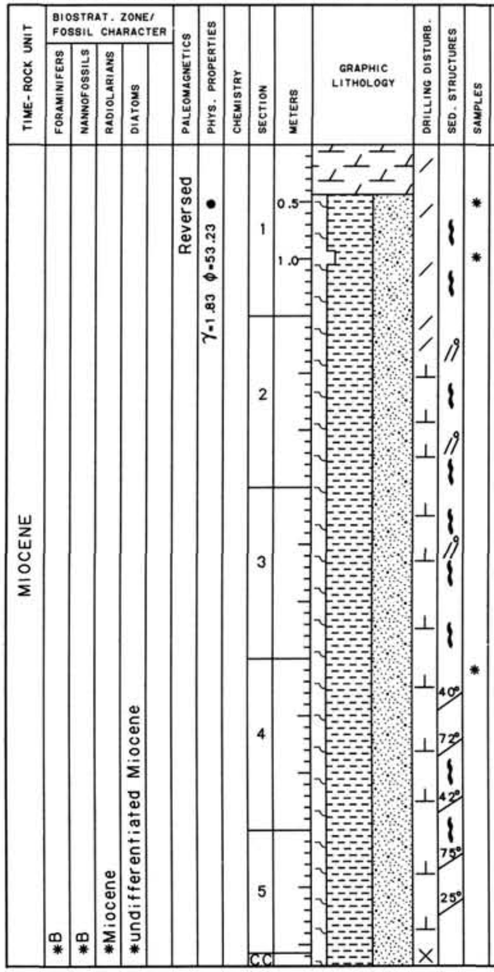

LITHOLOGIC DESCRIPTION

DIATOM-BEARING SILTSTONE

Major lithology: diatom-bearing siltstone, black (5Y 2.5/2) to very dark gray (5Y 3/1). Moderately to extensively bioturbated. Dewatering veins throughout.

Minor lithology: dolomitic siltstone, olive gray (5Y 3/2) brecciated. Veins filled with calcite. At least two ages of veins.

SMEAR SLIDE SUMMARY (%):

	1, 49 D	1, 91 D	4, 18 D
TEXTURE:			
Sand	5	30	5
Silt	40	25	40
Clay	55	45	55
COMPOSITION:			
Quartz	20	15	20
Feldspar	20	10	15
Rock fragments	5	5	5
Mica	—	Tr	Tr
Clay	55	30	58
Calcite/dolomite	Tr	7	Tr
Accessory minerals			
Pyrite	—	8	—
Phosphate	—	Tr	—
Brown amphibole	—	Tr	—
Diatoms	Tr	25	2
Sponge spicules	—	Tr	—

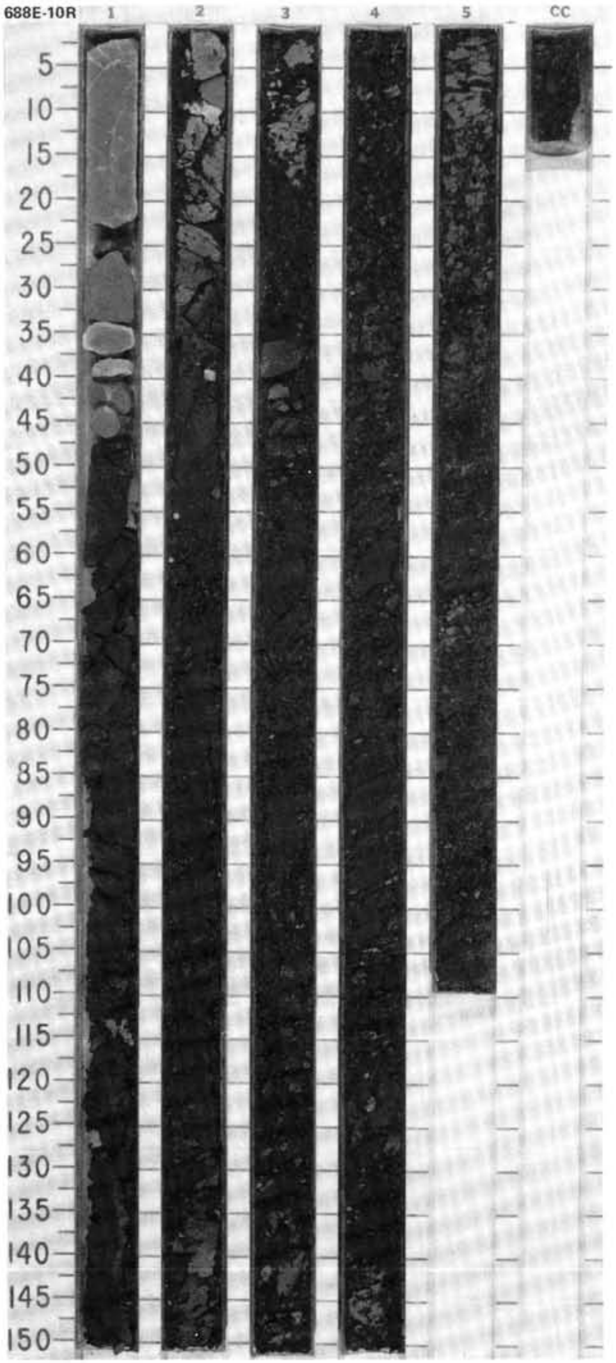

SITE 688 HOLE E CORE 11R CORED INTERVAL 4266.8-4276.3 mbsl; 441.0-450.5 mbsf

TIME-ROCK UNIT	BIOSTRAT. ZONE/ FOSSIL CHARACTER					PALEOMAGNETICS	PHYS. PROPERTIES	CHEMISTRY	SECTION	METERS	GRAPHIC LITHOLOGY	DRILLING DISTURB.	SED. STRUCTURES	SAMPLES	LITHOLOGIC DESCRIPTION
	FORAMINIFERS	NANNOFOSSILS	RADIOLARIANS	DIATOMS											
MIDDLE MIOCENE	B*	B*	Middle Miocene (base *D. pettersoni* to *C. costata*) *	undifferentiated *					CC			X		*	DIATOM-BEARING SILTSTONE

DIATOM-BEARING SILTSTONE

Major lithology: diatom-bearing siltstone, black (5Y 2.5/2).

SMEAR SLIDE SUMMARY (%):

	CC, 10 D
COMPOSITION:	
Quartz	20
Feldspar	20
Clay	43
Accessory minerals	
Pyrite	2
Apatite	Tr
Diatoms	15
Sponge spicules	Tr

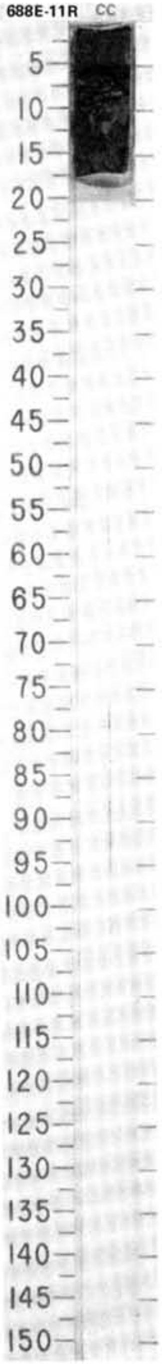

SITE 688 HOLE E CORE 12R CORED INTERVAL 4276.3-4285.8 mbsl; 450.5-460.0 mbsf

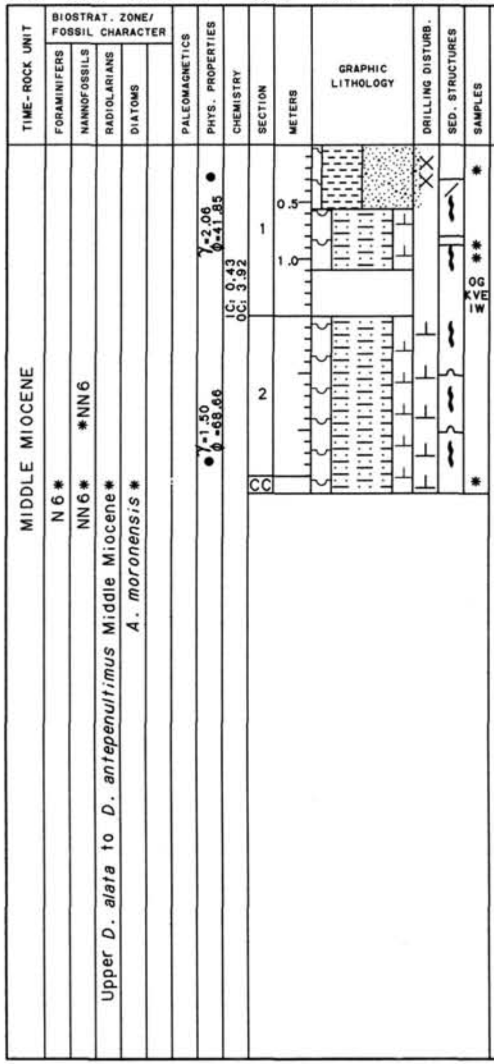

LITHOLOGIC DESCRIPTION

DIATOM-BEARING SILTSTONE and NANNOFOSSIL-FORAMINIFER-BEARING DIATOMACEOUS MUDSTONE

Major lithology: Section 1, 0–55 cm: diatom-bearing siltstone, dark greenish gray (5GY 4/1); Section 1, 55 cm, to CC: nannofossil-foraminifer-bearing diatomaceous mudstone, dark olive gray (5Y 3/2). Extensively burrowed.

Minor lithology: calcidolomite pebble, olive (5Y 5/3) in CC.

SMEAR SLIDE SUMMARY (%):

	1, 30 D	1, 90 D	1, 98 D	CC, 11 D
TEXTURE:				
Sand	20	10	2	—
Silt	60	15	28	50
Clay	20	75	70	50
COMPOSITION:				
Quartz	15	5	5	5
Feldspar	40	5	3	5
Rock fragments	Tr	5	Tr	Tr
Clay	20	65	45	37
Volcanic glass	10	—	—	—
Calcite/dolomite	Tr	5	—	8
Accessory minerals				
Pyrite	5	5	5	5
Foraminifers	—	Tr	2	—
Nannofossils	—	—	20	10
Diatoms	10	10	20	30

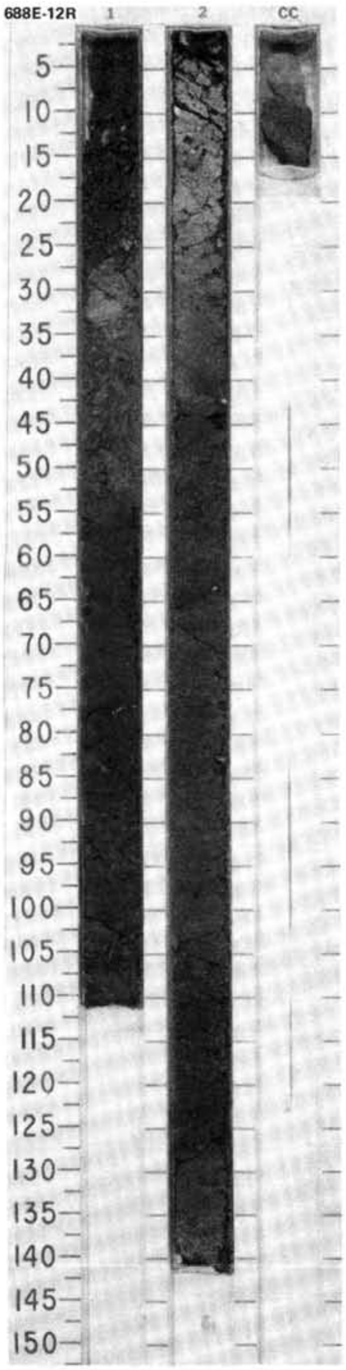

SITE 688 HOLE E CORE 13R CORED INTERVAL 4285.8-4295.3 mbsl; 460.0-469.5 mbsf

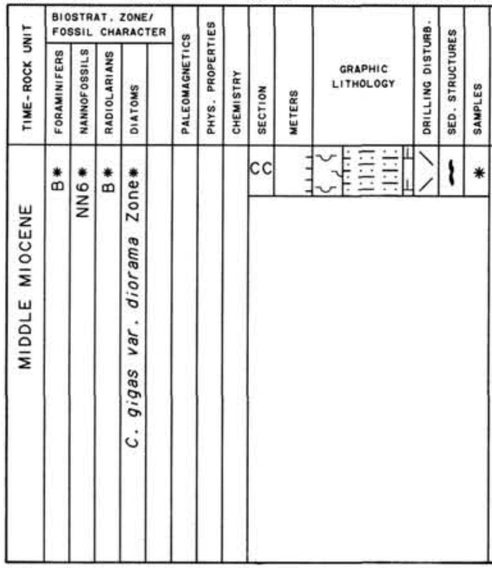

LITHOLOGIC DESCRIPTION

NANNOFOSSIL-BEARING DIATOMACEOUS MUDSTONE

Major lithology: nannofossil-bearing diatomaceous mudstone, black (5Y 2.5/2). Mainly massive, moderately bioturbated.

SMEAR SLIDE SUMMARY (%):

	CC, 22 D
TEXTURE:	
Silt	30
Clay	70
COMPOSITION:	
Quartz	5
Feldspar	5
Clay	47
Calcite/dolomite	5
Accessory minerals	
Pyrite	3
Glauconite	Tr
Apatite	Tr
Nannofossils	5
Diatoms	30
Sponge spicules	Tr

SITE 688 HOLE E CORE 14R CORED INTERVAL 4295.3-4304.8 mbsl; 469.5-479.0 mbsf

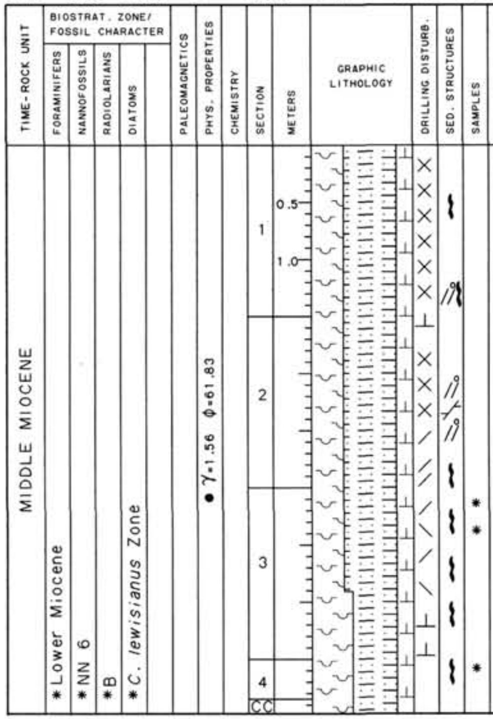

LITHOLOGIC DESCRIPTION

NANNOFOSSIL-FORAMINIFER-BEARING DIATOMACEOUS MUDSTONE

Major lithology: nannofossil-foraminifer-bearing diatomaceous mudstone, black (5Y 2.5/2) to dark olive gray (5Y 3/2). Moderately burrowed, dewatering veins, moderately to highly fractured in Sections 3 and 4.

Minor lithology: volcanic ash layer disrupted by tectonics in Section 4, 8–25 cm.

SMEAR SLIDE SUMMARY (%):

	3, 13 M	3, 39 D	4, 85 M	CC, 7 D
TEXTURE:				
Sand	5	—	10	5
Silt	30	40	85	50
Clay	65	60	5	45
COMPOSITION:				
Quartz	5	2	5	3
Feldspar	3	2	5	2
Rock fragments	2	—	—	2
Clay	25	52	—	25
Volcanic glass	—	10	85	—
Calcite/dolomite	2	1	Tr	7
Accessory minerals				
Pyrite	10	1	—	8
Foraminifers	3	—	—	3
Nannofossils	20	2	Tr	10
Diatoms	30	30	5	40
Sponge spicules	Tr	Tr	—	—
Fish remains	—	Tr	—	—

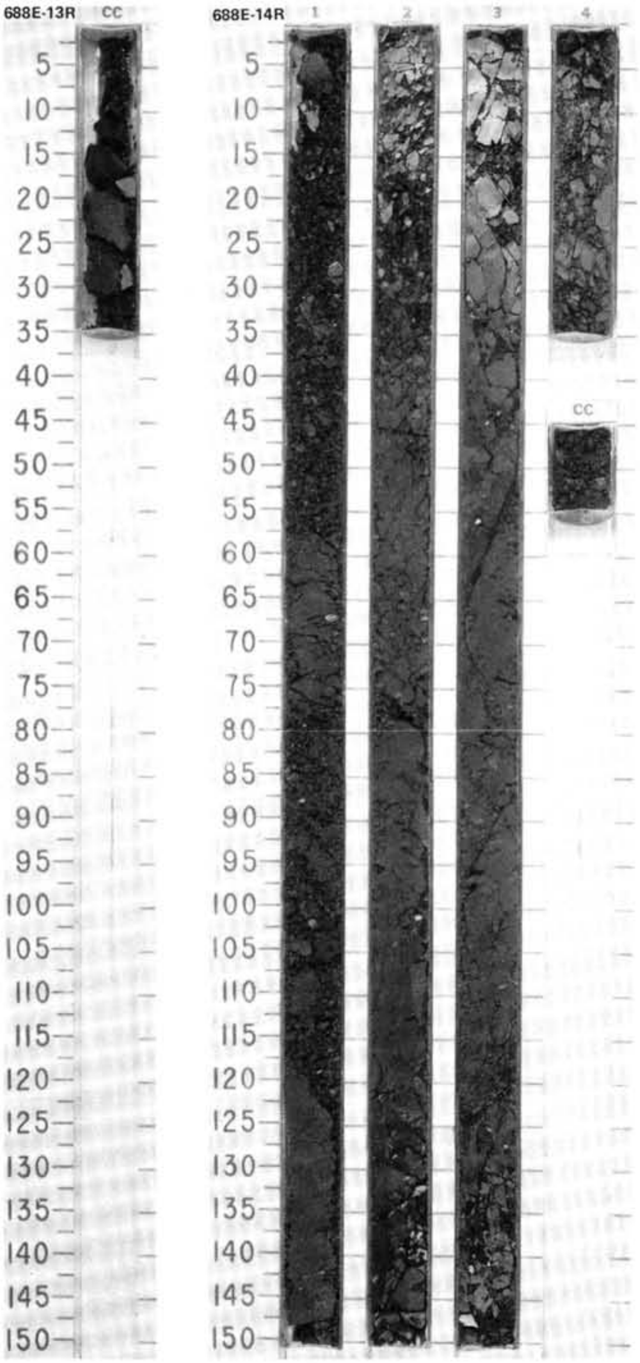

SITE 688 HOLE E CORE 15R CORED INTERVAL 4304.8-4314.3 mbsl; 479.0-488.5 mbsf

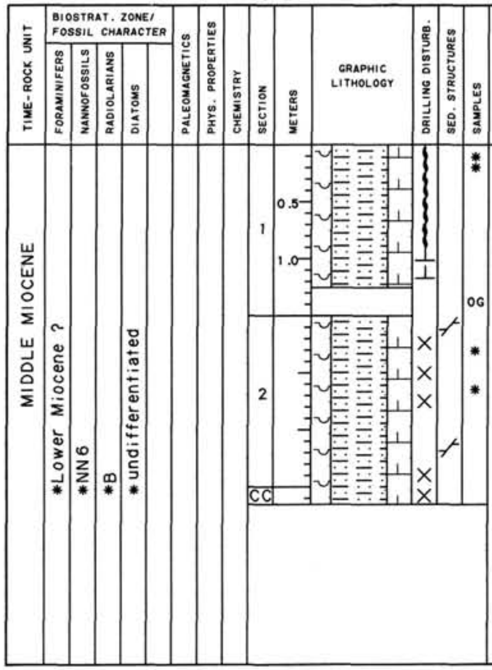

LITHOLOGIC DESCRIPTION

NANNOFOSSIL-FORAMINIFER-BEARING DIATOMACEOUS MUDSTONE

Major lithology: nannofossil-foraminifer-bearing diatomaceous mudstone, black (5Y 2.5/2) to olive gray (5Y 3/2). Evidence of soft sediment deformation.

Minor lithology: volcanic ash particle in Section 2, 62 cm.

SMEAR SLIDE SUMMARY (%):

	1, 12 D	1, 18 D	2, 31 M	2, 62 M
TEXTURE:				
Silt	32	25	25	95
Clay	68	75	75	5
COMPOSITION:				
Quartz	2	Tr	2	10
Feldspar	3	Tr	3	10
Mica, biotite	—	—	Tr	Tr
Clay	60	50	—	5
Volcanic glass	—	—	—	75
Calcite/dolomite	5	Tr	5	—
Accessory minerals				
Opaques	5	—	—	—
Micrite	—	5	—	—
Hornblende	—	—	—	Tr
Foraminifers	2	5	5	—
Nannofossils	8	20	75	—
Diatoms	15	20	10	—
Radiolarians	—	Tr	Tr	—
Sponge spicules	—	Tr	Tr	—
Echinoid spine?	Tr	—	—	—

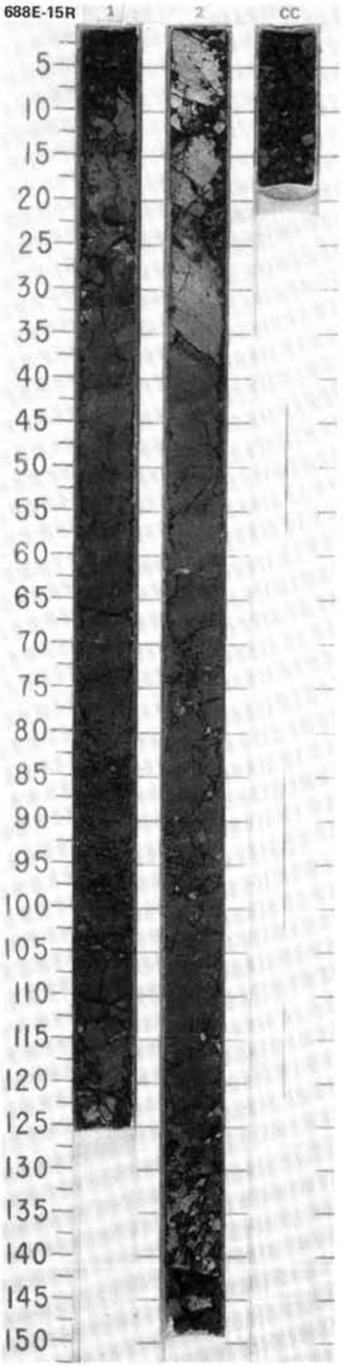

SITE 688 HOLE E CORE 16R CORED INTERVAL 4314.3-4323.8 mbsl; 488.5-498.0 mbsf

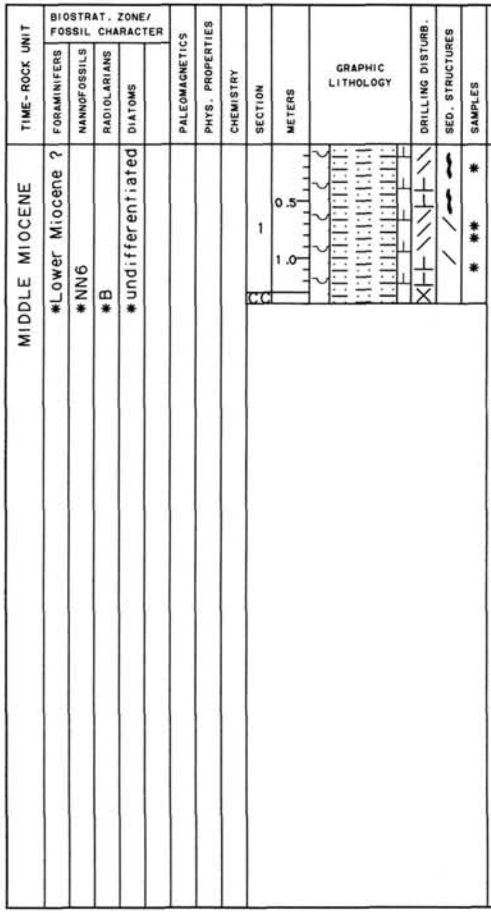

LITHOLOGIC DESCRIPTION

FORAMINIFER-BEARING DIATOMACEOUS MUDSTONE

Major lithology: foraminifer-bearing diatomaceous mudstone, very dark gray (3Y 3/1). General appearance is one of disaggregation of sliding origin. Sub-round to sub-angular clasts.

Minor lithologies:
a. nannofossil-bearing mudstone, very dark gray (3Y 3.5/2) block floating in the matrix. Section 1, 80 cm.
b. diatomite as a small bleb in the matrix.

SMEAR SLIDE SUMMARY (%):

	1, 23 D	1, 77 D	1, 80 M	1, 101 M
TEXTURE:				
Sand	—	—	—	1
Silt	40	50	63	79
Clay	60	50	37	20
COMPOSITION:				
Quartz	5	5	2	6
Feldspar	8	5	3	10
Rock fragments	—	—	—	6
Mica	Tr	Tr	—	—
Clay	60	50	55	15
Calcite/dolomite	2	2	2	4
Accessory minerals				
Opaque/pyrite	5	5	—	2
Chlorite	—	—	—	Tr
Glauconite	Tr	—	—	—
Foraminifers	5	8	5	—
Nannofossils	Tr	Tr	8	1
Diatoms	15	25	25	55
Radiolarians	Tr	Tr	—	—
Sponge spicules	Tr	Tr	—	1
Silicoflagellates	—	—	—	Tr

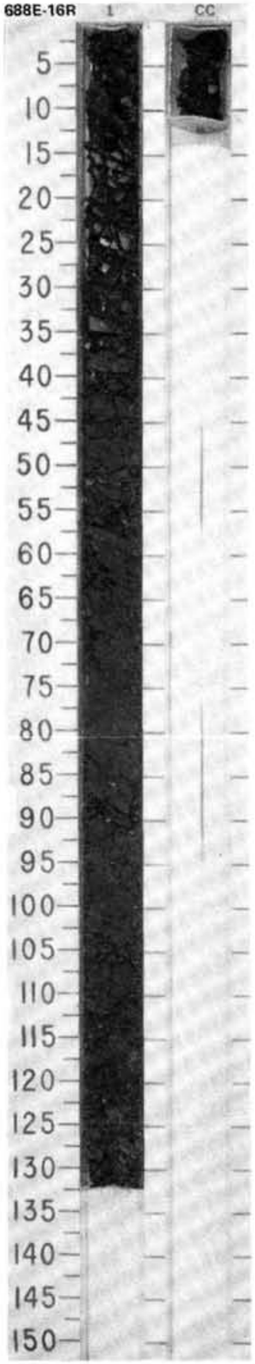

SITE 688 HOLE E CORE 17R CORED INTERVAL 4323.8-4333.3 mbsl; 498.0-507.5 mbsf

TIME-ROCK UNIT	BIOSTRAT. ZONE/ FOSSIL CHARACTER					PALEOMAGNETICS	PHYS. PROPERTIES	CHEMISTRY	SECTION	METERS	GRAPHIC LITHOLOGY	DRILLING DISTURB.	SED. STRUCTURES	SAMPLES	LITHOLOGIC DESCRIPTION
	FORAMINIFERS	NANNOFOSSILS	RADIOLARIANS	DIATOMS											
MIDDLE MIOCENE	Lower Miocene ? *	caved in NN6 *	top *D. alata* to bottom *C. petterson*i Middle Miocene *	undifferentiated [*Macrora stella*] *										*	*DIATOMACEOUS MUDSTONE and DIATOMITE*

Major lithology: diatomaceous mudstone, very dark gray (5Y 3/2) and olive gray (5Y 4/2) diatomite as drilling chips in CC.

SMEAR SLIDE SUMMARY (%):

	CC D
TEXTURE:	
Silt	95
Clay	5
COMPOSITION:	
Quartz	Tr
Feldspar	—
Rock fragments	—
Clay	Tr
Calcite/dolomite	1
Accessory minerals	
Pyrite	2
Phosphate	2
Foraminifers	—
Nannofossils	10
Diatoms	85
Radiolarians	Tr
Silicoflagellates	—
Fish remains	—

CORE 112-688E-17R NO PHOTO AVAILABLE

SITE 688 HOLE E CORE 18R CORED INTERVAL 4333.3-4342.8 mbsl; 507.5-517.0 mbsf

TIME-ROCK UNIT	BIOSTRAT. ZONE/ FOSSIL CHARACTER					PALEOMAGNETICS	PHYS. PROPERTIES	CHEMISTRY	SECTION	METERS	GRAPHIC LITHOLOGY	DRILLING DISTURB.	SED. STRUCTURES	SAMPLES	LITHOLOGIC DESCRIPTION
	FORAMINIFERS	NANNOFOSSILS	RADIOLARIANS	DIATOMS											
MIDDLE MIOCENE	Lower Miocene*	caved in NN6*	*C. costata* (to *S. wolffii*) Upper Lower Miocene to Lowermost Middle Miocene*	undifferentiated*											MUDSTONE Major lithology: olive gray (5Y 4/2) mudstone, only drilling chips in CC.

CORE 112-688E-18R NO PHOTO AVAILABLE

SITE 688 HOLE E CORE 19R CORED INTERVAL 4342.8-4352.3 mbsl; 517.0-526.5 mbsf

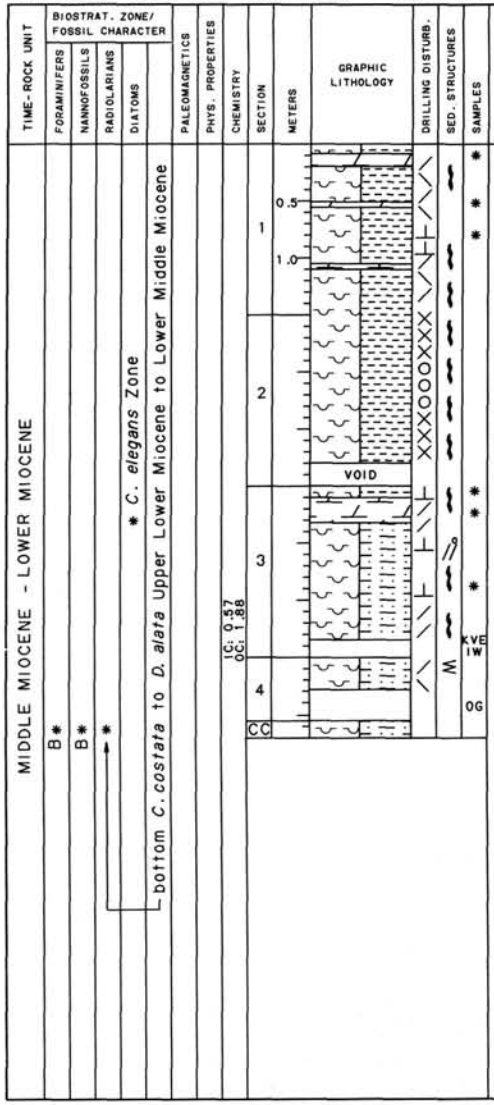

LITHOLOGIC DESCRIPTION

DIATOMACEOUS MUD

Major lithology: diatomaceous mud, black (5Y 2.5/1) to dark olive gray (5Y 3/2). Microfaulting throughout, moderately burrowed.

Minor lithology: dolomicrite beds, olive gray (5Y 4/2) 3–4 to 25 cm thick. Beds are in *Section 1 (10, 50 and 105 cm)* and Section 3 (10 and 100 cm), dolomitization is located in more porous beds (silt- or diatom-rich).

SMEAR SLIDE SUMMARY (%):

	1, 11 M	1, 44 M	1, 80 D	3, 10 D	3, 23 M	3, 89 M
TEXTURE:						
Sand	—	—	—	10	—	10
Silt	90	55	55	60	95	80
Clay	10	45	45	30	5	10
COMPOSITION:						
Quartz	Tr	5	5	Tr	—	10
Clay	7	45	45	25	—	5
Volcanic glass	—	Tr	—	Tr	—	80
Calcite/dolomite	90	5	5	10	95	Tr
Accessory minerals						
Opaques	Tr	—	5	—	2	2
Pyrite	—	25	—	3	—	—
Phosphatic blebs	—	—	—	2	—	—
Foraminifers	—	5	—	—	—	—
Diatoms	3	15	40	50	3	3
Sponge spicules	Tr	Tr	Tr	—	—	—
Silicoflagellates	—	—	Tr	—	—	—
Plant org. matter	—	—	—	10	—	—

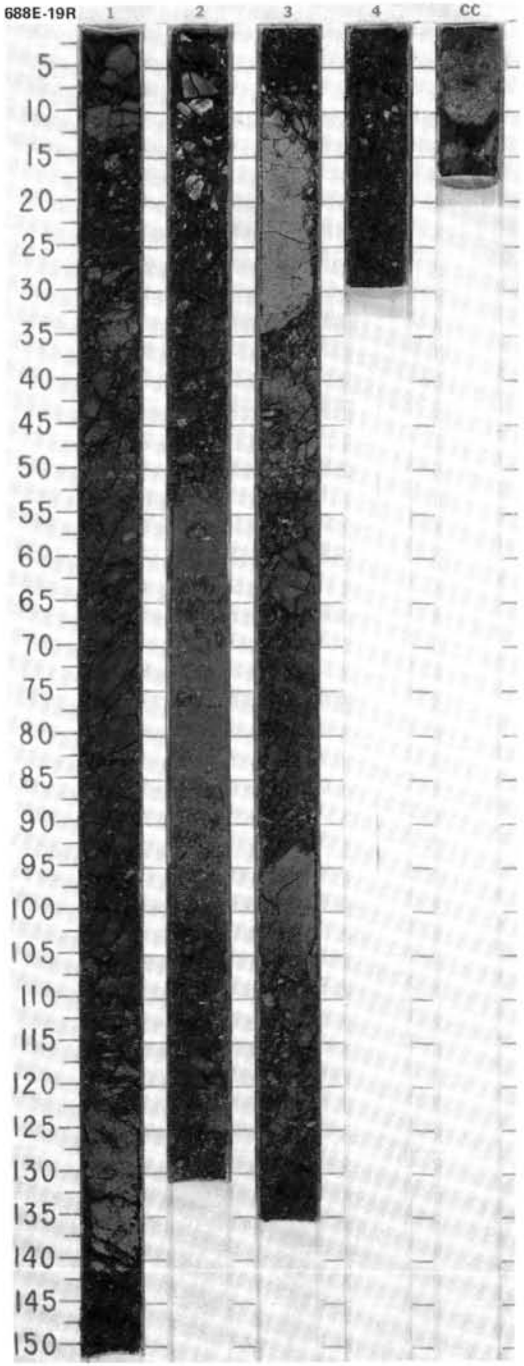

SITE 688 HOLE E CORE 20R CORED INTERVAL 4352.3-4361.8 mbsl; 526.5-536.0 mbsf

TIME-ROCK UNIT	BIOSTRAT. ZONE/ FOSSIL CHARACTER					PALEOMAGNETICS	PHYS. PROPERTIES	CHEMISTRY	SECTION	METERS	GRAPHIC LITHOLOGY	DRILLING DISTURB.	SED. STRUCTURES	SAMPLES
	FORAMINIFERS	NANNOFOSSILS	RADIOLARIANS	DIATOMS										
MIDDLE MIOCENE - LOWER MIOCENE	B*	NN6*	Upper Lower Miocene-Lower Middle Miocene*	*C. elegans* Zone*					1 2 CC	0.5 1.0	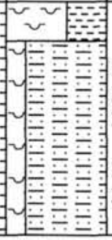	× × × × ×		** * *

LITHOLOGIC DESCRIPTION

DIATOMACEOUS MUDSTONE

Major lithology: diatomaceous mudstone, dark olive gray (5Y 3/2). Fissility well developed. Brecciation and microfaulting throughout (sliding features).

Minor lithology: diatomaceous ooze and diatomaceous mud interbedded, finely laminated, this packet (Section 1, 0–35 cm) is a possible block in the diatomaceous mudstone. Ash layer in Section 1, 140–142 cm.

SMEAR SLIDE SUMMARY (%):

	1, 13 D	1, 15 M	1, 60 D	1, 142 M
TEXTURE:				
Sand	—	10	1	20
Silt	80	20	19	70
Clay	20	70	80	10
COMPOSITION:				
Quartz	—	2	3	1
Feldspar	—	3	7	4
Rock fragments	—	1	2	—
Mica	—	2	1	—
Clay	20	45	60	5
Volcanic glass	—	Tr	—	88
Calcite/dolomite	5	1	2	—
Accessory minerals				
Pyrite	—	3	2	2
Glauconite	—	Tr	1	—
Collophane	—	—	Tr	—
Nannofossils	Tr	1	1	—
Diatoms	75	40	18	Tr
Radiolarians	—	Tr	2	—
Sponge spicules	—	1	1	—
Fish remains	—	1	—	—

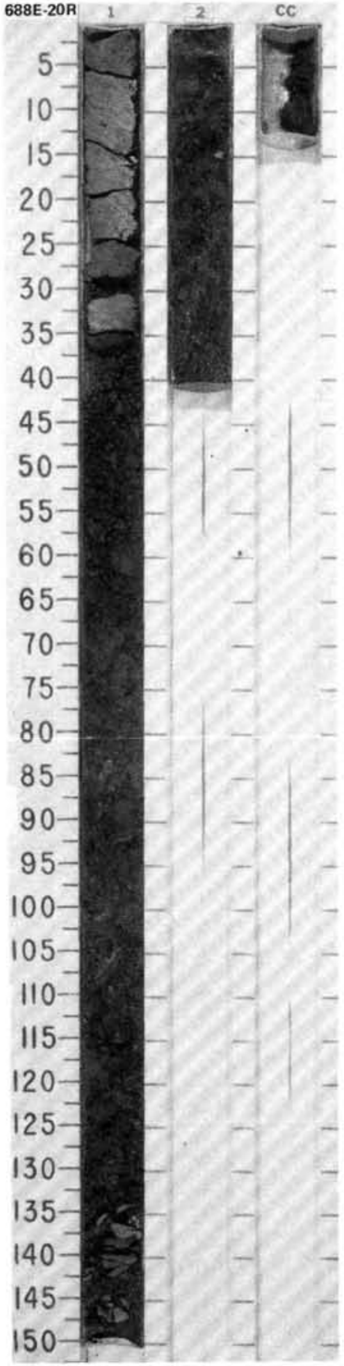

SITE 688 HOLE E CORE 21R CORED INTERVAL 4361.8-4371.3 mbsl; 536.0-545.5 mbsf

TIME-ROCK UNIT	BIOSTRAT. ZONE/ FOSSIL CHARACTER FORAMINIFERS	NANNOFOSSILS	RADIOLARIANS	DIATOMS		PALEOMAGNETICS	PHYS. PROPERTIES	CHEMISTRY	SECTION	METERS	GRAPHIC LITHOLOGY	DRILLING DISTURB.	SED. STRUCTURES	SAMPLES	LITHOLOGIC DESCRIPTION
MIDDLE MIOCENE	B *	caved-in NN6 *		*C. gigas* / *C. coscinodiscus* Zone *										*	DIATOMACEOUS MUDSTONE

DIATOMACEOUS MUDSTONE

Major lithology: diatomaceous mudstone, very dark gray (5Y 3/1). Only two pieces, approximately 2 cm in diameter.

SMEAR SLIDE SUMMARY (%):

	CC D
TEXTURE:	
Silt	50
Clay	50
COMPOSITION:	
Quartz	5
Clay	50
Calcite/dolomite	7
Accessory minerals	
Pyrite	5
Glauconite	Tr
Foraminifers	3
Diatoms	30
Radiolarians	Tr

SITE 688 HOLE E CORE 22R CORED INTERVAL 4371.3-4380.8 mbsl; 545.5-555.0 mbsf

TIME-ROCK UNIT	BIOSTRAT. ZONE/ FOSSIL CHARACTER FORAMINIFERS	NANNOFOSSILS	RADIOLARIANS	DIATOMS		PALEOMAGNETICS	PHYS. PROPERTIES	CHEMISTRY	SECTION	METERS	GRAPHIC LITHOLOGY	DRILLING DISTURB.	SED. STRUCTURES	SAMPLES	LITHOLOGIC DESCRIPTION
LOWER MIOCENE	B *	NN1/2 *	MIOCENE *	undifferentiated *					1 CC		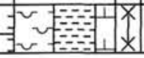	X X		* *	NANNOFOSSIL-BEARING DIATOMACEOUS MUDSTONE

NANNOFOSSIL-BEARING DIATOMACEOUS MUDSTONE

Major lithology: nannofossil-bearing diatomaceous mudstone, black (5Y 3/1) to olive gray (5Y 4/1).

SMEAR SLIDE SUMMARY (%):

	1, 9 D	1, 17 D
TEXTURE:		
Sand	—	5
Silt	30	50
Clay	70	45
COMPOSITION:		
Feldspar	—	5
Clay	20	20
Volcanic glass	5	—
Calcite/dolomite	2	5
Accessory minerals		
Pyrite	1	15
Foraminifers	—	Tr
Nannofossils	10	30
Diatoms	62	25

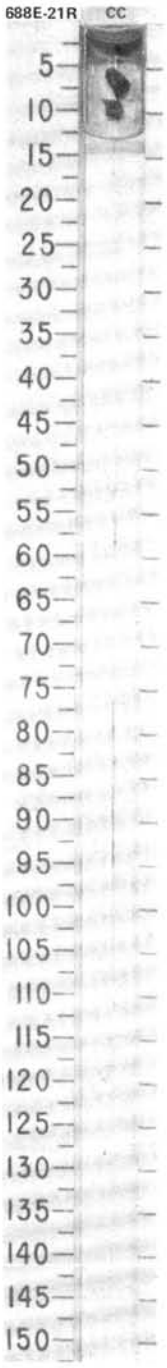

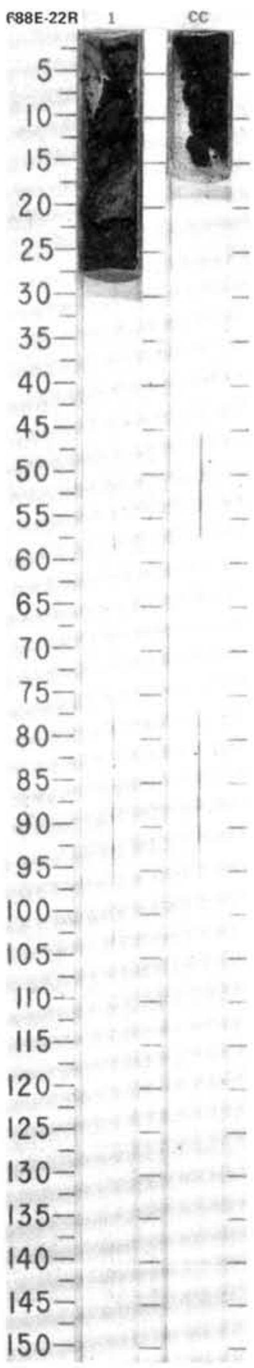

SITE 688 HOLE E CORE 23R CORED INTERVAL 4380.8-4390.3 mbsl; 555.0-564.5 mbsf

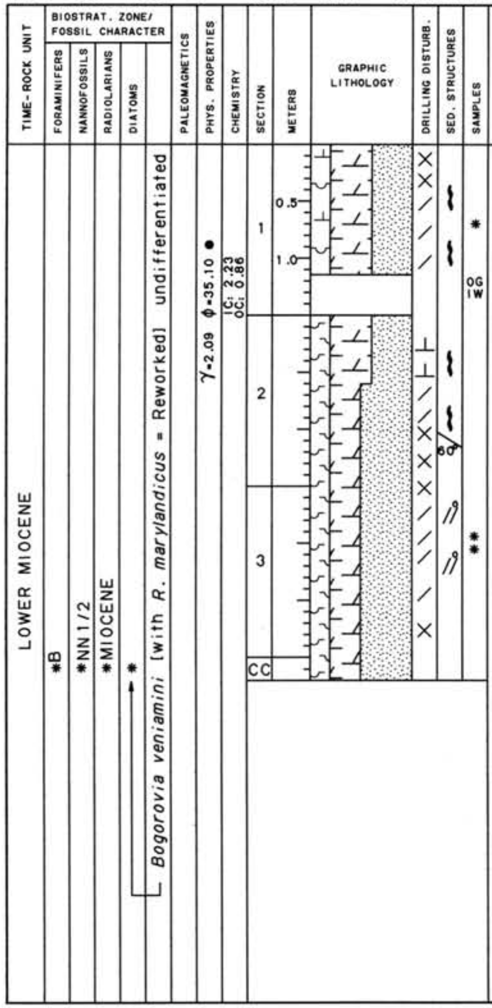

LITHOLOGIC DESCRIPTION

DIATOM-AND NANNOFOSSIL-BEARING SANDY SILTSTONE

Major lithology: diatom- and nannofossil-bearing sandy siltstone. Dark olive gray (5Y 3/1), rare burrows. Locally bearing sponge spicules, dolomitized throughout.

SMEAR SLIDE SUMMARY (%):

	1, 70 D	3, 42 M	3, 49 D
TEXTURE:			
Sand	25	55	45
Silt	45	30	25
Clay	30	15	30
COMPOSITION:			
Quartz	15	15	25
Feldspar	15	10	15
Rock fragments	10	10	—
Mica	—	—	Tr
Clay	5	5	8
Volcanic glass	5	—	—
Calcite/dolomite	33	15	20
Accessory minerals	—	2	—
Pyrite	5	3	14
Glauconite	2	5	3
Phosphate	—	—	5
Foraminifers	2	10	5
Nannofossils	Tr	—	1
Diatoms	3	—	2
Radiolarians	Tr	—	Tr
Sponge spicules	5	25	10
Fish remains	—	Tr	—

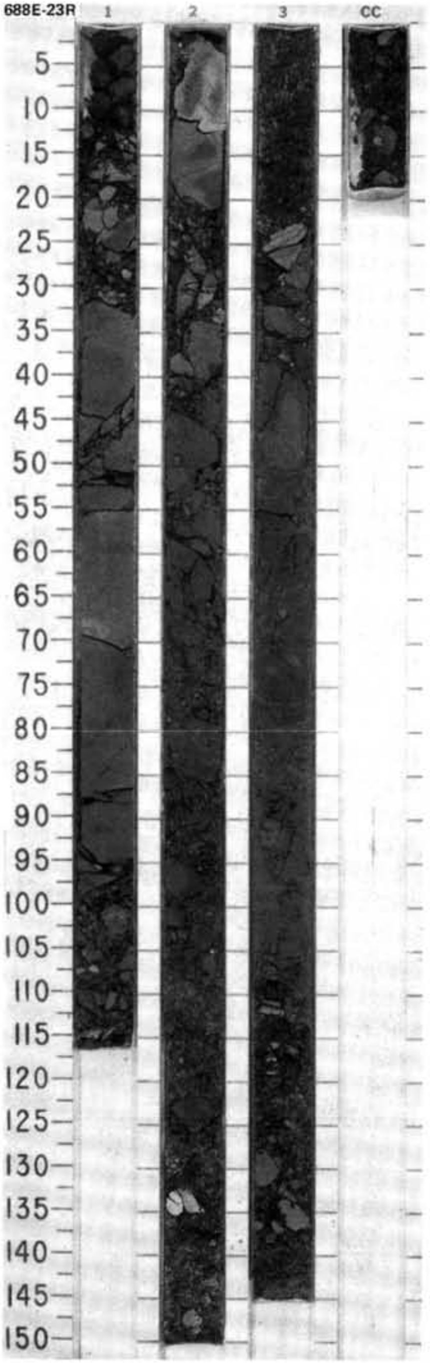

SITE 688 HOLE E CORE 24R CORED INTERVAL 4390.3-4399.8 mbsl; 564.5-574.0 mbsf

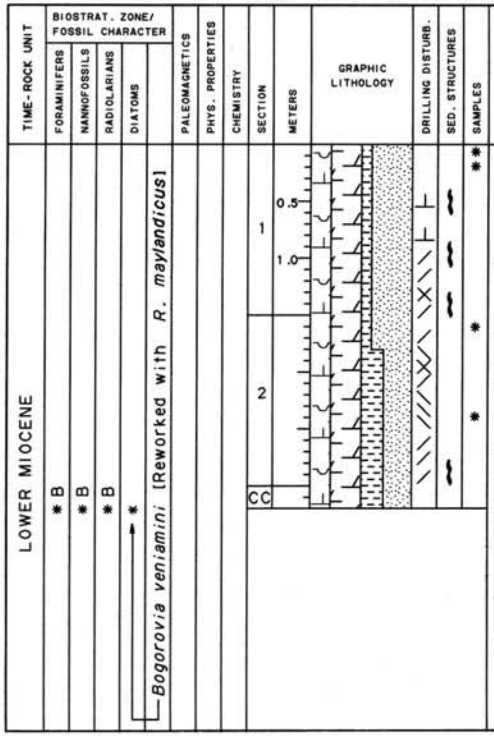

LITHOLOGIC DESCRIPTION

DIATOM-BEARING SANDY MUDDY SILTSTONE and FORAMINIFER-BEARING MUDDY SILTY SAND

Major lithology: Section 1 to Section 2, 64 cm: diatom-bearing, sandy muddy siltstone, very dark gray (5Y 3/1 to 5Y 3.5/1). Moderate bioturbation throughout. Variably calcareous and dolomitic. Section 2, 64 cm, to CC: foraminifer-bearing, muddy silty sand. Rare burrowing.

SMEAR SLIDE SUMMARY (%):

	1, 8 M	1, 20 D	2, 4 M	2, 87 D
TEXTURE:				
Sand	40	30	30	35
Silt	25	45	50	35
Clay	35	25	20	30
COMPOSITION:				
Quartz	20	15	15	15
Feldspar	15	10	10	10
Rock fragments	5	10	10	5
Mica	Tr	Tr	—	—
Clay	23	5	15	25
Volcanic glass	—	—	5	—
Calcite/dolomite	5	15	24	10
Accessory minerals				
Pyrite	7	15	7	5
Glauconite	15	3	1	10
Phosphate	—	5	—	—
Foraminifers	5	10	—	10
Nannofossils	—	2	—	3
Diatoms	—	5	10	2
Sponge spicules	5	5	3	5
Fish remains	—	—	—	Tr

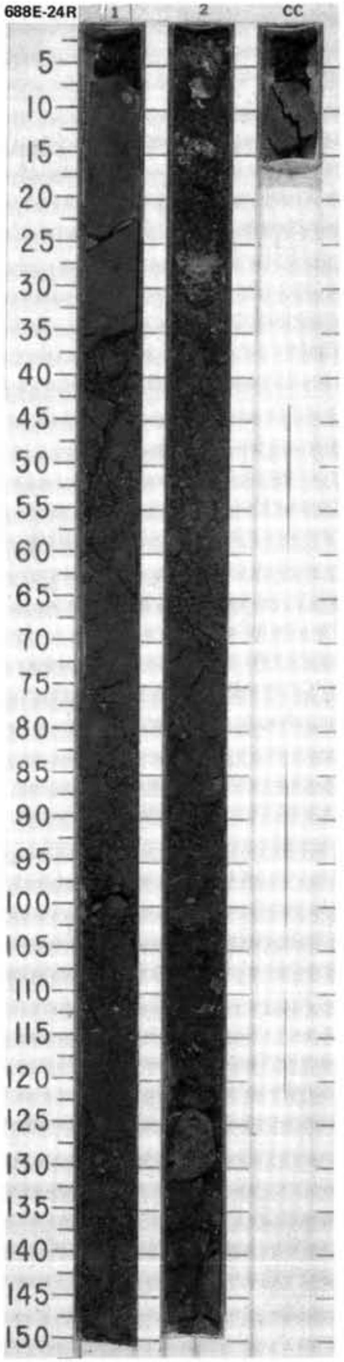

SITE 688 HOLE E CORE 25R CORED INTERVAL 4399.8-4409.3 mbsl; 574.0-583.5 mbsf

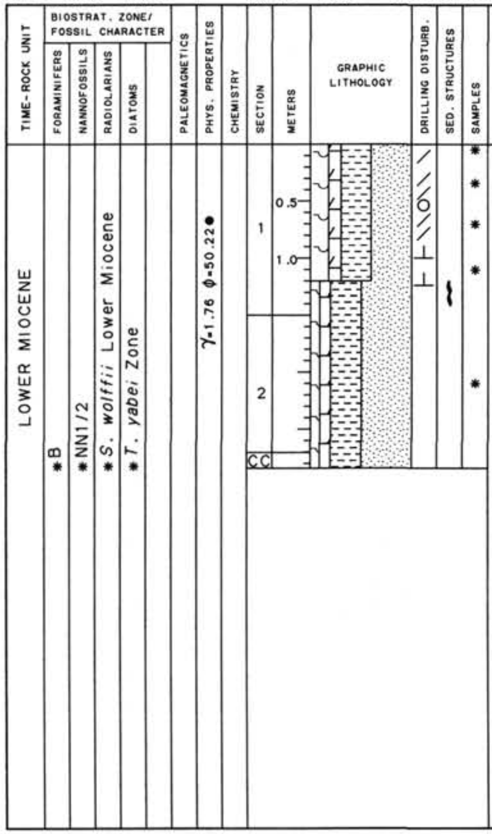

LITHOLOGIC DESCRIPTION

DIATOM-BEARING MUDDY SILTSTONE

Major lithology: diatom-bearing muddy siltstone, very dark gray (5Y 3/1), massive, bioturbation in places.

Minor lithology: diatomite as rare clasts throughout, olive (5Y 5/2), 0.5–3 mm rounded to subangular grains.

SMEAR SLIDE SUMMARY (%):

	1, 2 M	1, 32 D	1, 67 M	1, 107 M	2, 65 D
TEXTURE:					
Sand	—	10	10	—	10
Silt	30	75	50	80	50
Clay	70	15	40	20	40
COMPOSITION:					
Quartz	—	15	10	3	15
Feldspar	—	20	15	1	20
Rock fragments	—	5	5	2	5
Mica	—	1	—	Tr	—
Clay	—	32	40	13	40
Volcanic glass	—	1	6	—	—
Calcite/dolomite	—	—	2	—	5
Accessory minerals					
Micrite	100	1	—	—	—
Pyrite	—	7	5	1	5
Glauconite	—	2	2	—	Tr
Foraminifers	—	—	Tr	—	Tr
Nannofossils	—	—	—	Tr	Tr
Diatoms	—	13	15	80	10
Radiolarians	—	Tr	—	Tr	—
Sponge spicules	—	3	Tr	Tr	—

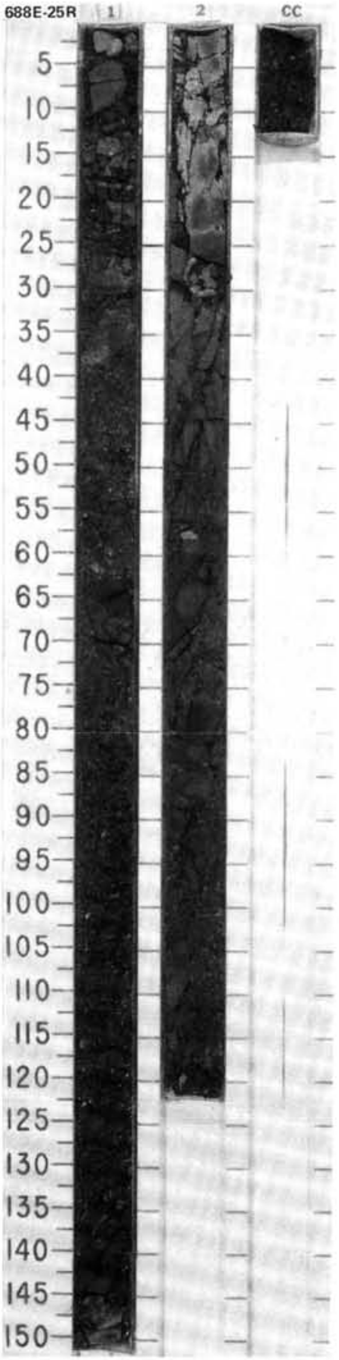

SITE 688 HOLE E CORE 26R CORED INTERVAL 4409.3-4418.3 mbsl; 583.5-593.0 mbsf

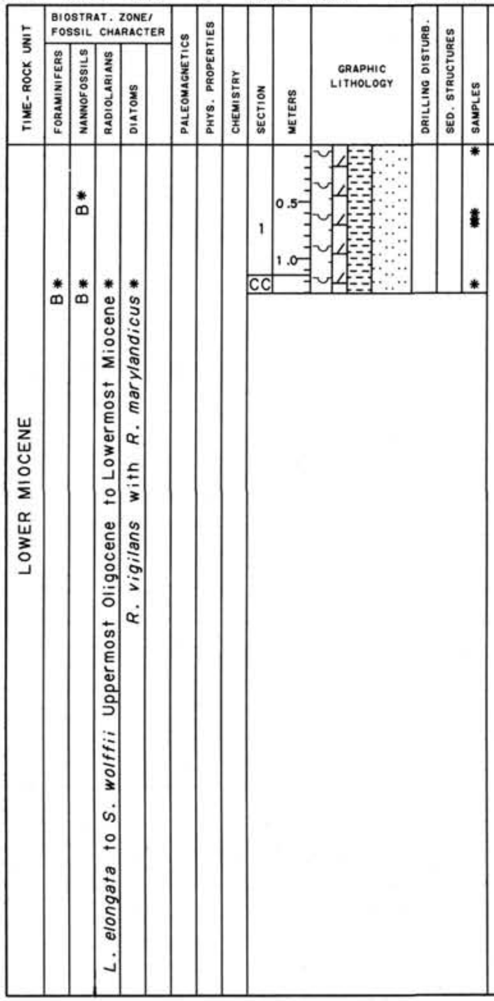

LITHOLOGIC DESCRIPTION

DIATOMACEOUS MUDDY SILTSTONE

Major lithology: diatomaceous muddy siltstone, very dark gray (5Y 3/1), massive. Bioturbation locally evident.

Minor lithology:
a. very dark grayish brown (2.5Y 4/2) diatomaceous mudstone as clasts or pellets throughout.
b. olive (5Y 5/3) muddy diatomite.

SMEAR SLIDE SUMMARY (%):

	1, 1 M	1, 65 M	1, 67 M	1, 68 D	CC, 6 D
TEXTURE:					
Sand	—	—	—	—	10
Silt	90	30	65	70	60
Clay	10	70	35	30	30
COMPOSITION:					
Quartz	2	5	5	10	10
Feldspar	1	—	—	16	20
Rock fragments	1	—	—	4	2
Mica	Tr	—	—	1	1
Clay	10	70	35	28	30
Volcanic glass	—	—	Tr	1	3
Calcite/dolomite	80	—	—	2	1
Accessory minerals					
Pyrite	1	—	—	5	3
Collophane	Tr	—	—	3	—
Glauconite	—	—	—	2	4
Micrite	—	—	—	—	1
Diatoms	5	25	60	25	22
Radiolarians	—	Tr	—	1	1
Sponge spicules	—	Tr	—	2	2

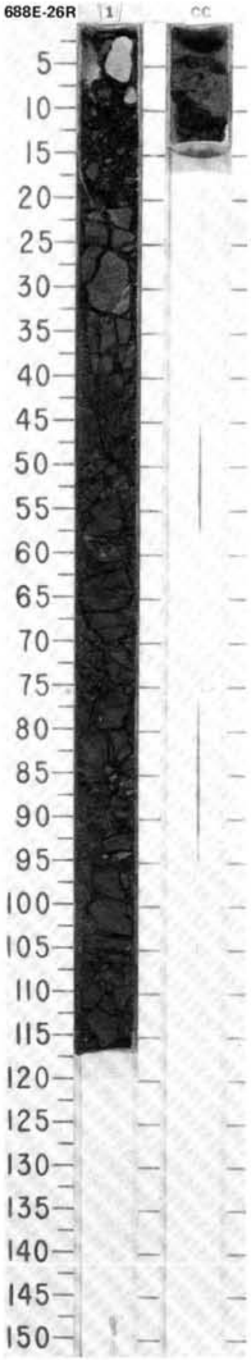

SITE 688 HOLE E CORE 27R CORED INTERVAL 4418.8-4428.3 mbsl; 593.0-602.5 mbsf

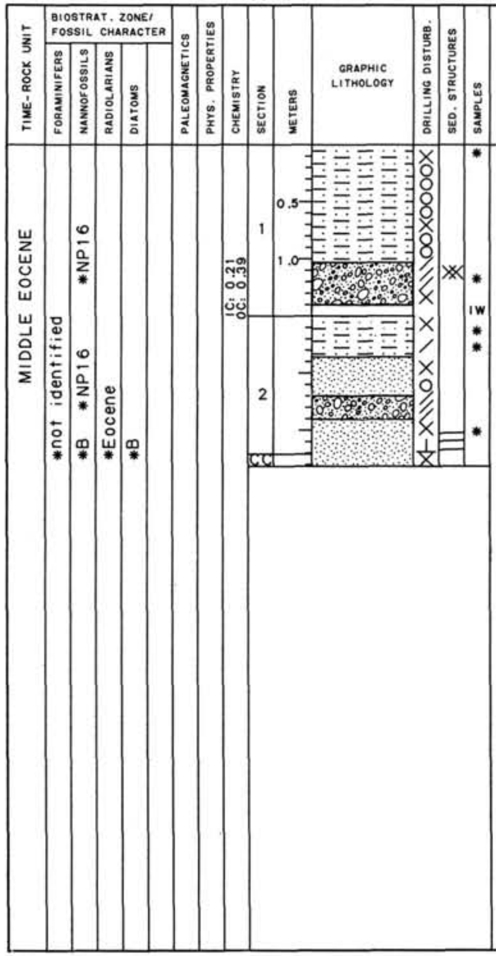

LITHOLOGIC DESCRIPTION

MUDSTONE, SANDSTONE, SILTSTONE, and CALCAREOUS SILTSTONE

Major lithology: Section 1, 0–80 cm: mudstone, black (N 1/), clay-rich as broken fragments in drilling slurry: 60–64 cm: large 4 × 3 × 3 cm fragment of dark-gray (N 3/), brecciated, calcareous siltstone. Section 1, 80–106 cm: mudstone, black (N 1/), and sandstone, dark bluish gray (5B 4/1), as fragments in drilling slurry. Section 1, 106–140 cm: calcareous siltstone, dark gray (N 3/), as cataclastic breccia. Section 2, 0 cm to CC: mudstone, dark gray (N 3/), and calcareous siltstone, mainly fragments but intact cataclastic zone at Section 2, 67–90 cm.

Minor lithology: very fine to fine sandstone, dolomite cemented, dark blue gray (5B 4/1), and poorly sorted, as fragments and interlaminated with dark gray mudstone from Section 2, 108–122 cm.

SMEAR SLIDE SUMMARY (%):

	1, 5 M	1, 120 D	2, 12 M	2, 31 M	2, 104 D
TEXTURE:					
Sand	—	—	—	40	—
Silt	10	65	20	30	35
Clay	90	35	80	30	65
COMPOSITION:					
Quartz	2	10	5	20	8
Feldspar	2	15	5	25	20
Rock fragments	2	5	—	10	10
Mica	—	Tr	—	—	1
Clay	88	23	—	15	64
Volcanic glass	1	—	—	—	—
Calcite/dolomite	1	15	—	15	2
Accessory minerals					
Pyrite/opaques	3	10	10	—	3
Red-brown isotrophic collophane	—	10	—	—	1
Micrite	—	10	80	15	—
Meta rock fragments	—	Tr	—	—	—
Chalcedony	—	—	—	Tr	
Needles (rutile? in quartz)	—	—	—	Tr	—
Metaquartzite	—	—	—	Tr	—
Foraminifers	—	Tr	—	—	—
Nannofossils	—	2	—	—	—
Diatoms	1	—	—	—	1
Radiolarians	Tr	—	—	—	—
Sponge spicules	Tr	—	—	—	—

CORE 112-688E-28R NO RECOVERY

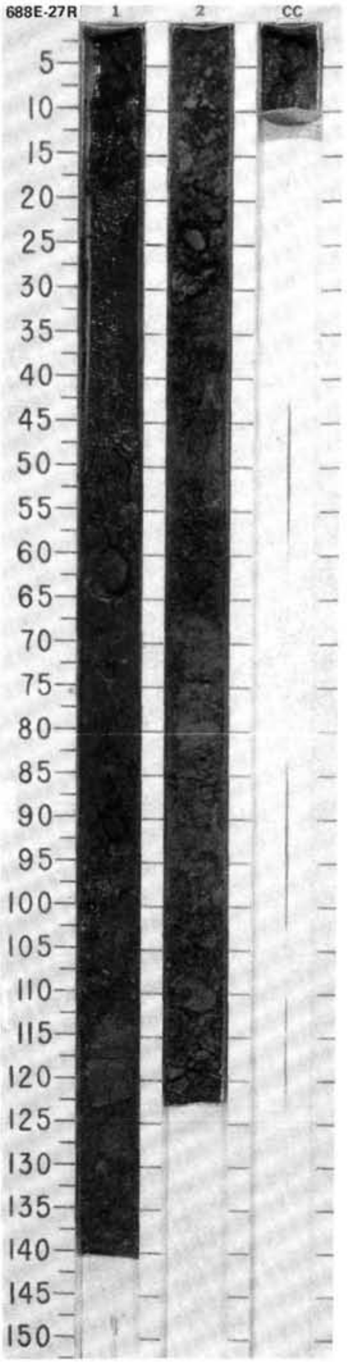

SITE 688 HOLE E CORE 29R CORED INTERVAL 4437.8-4447.3 mbsl; 612.0-621.5 mbsf

TIME-ROCK UNIT	FORAMINIFERS	NANNOFOSSILS	RADIOLARIANS	DIATOMS		PALEOMAGNETICS	PHYS. PROPERTIES	CHEMISTRY	SECTION	METERS	GRAPHIC LITHOLOGY	DRILLING DISTURB.	SED. STRUCTURES	SAMPLES
(LOWER MIOCENE ?)	B *	B *	B *	R. vigilans with R. marylandicus *					CC					*

BIOSTRAT. ZONE/ FOSSIL CHARACTER

LITHOLOGIC DESCRIPTION

CALCAREOUS SILICEOUS MUDSTONE, CHERT, QUARTZ, and PHOSPHORITE

Major lithology: a tectonic breccia which includes calcareous siliceous mudstone, *chert, quartz and phosphatic material as one piece of 5 cm length.*

SMEAR SLIDE SUMMARY (%):

	CC D
COMPOSITION:	
Quartz	5
Feldspar	5
Clay	75
Calcite/dolomite	Tr
Accessory minerals	
Micrite	10
Foraminifers	Tr
Nannofossils	5

SITE 688 HOLE E CORE 30R CORED INTERVAL 4447.3-4456.8 mbsl; 621.5-631.0 mbsf

TIME-ROCK UNIT	FORAMINIFERS	NANNOFOSSILS	RADIOLARIANS	DIATOMS		PALEOMAGNETICS	PHYS. PROPERTIES	CHEMISTRY	SECTION	METERS	GRAPHIC LITHOLOGY	DRILLING DISTURB.	SED. STRUCTURES	SAMPLES
MIDDLE EOCENE	*B	*NP16	*Eocene ?	*B				IC: 0.38 OC: 0.25	1 2 CC	0.5 1.0				* * KVE *** *

BIOSTRAT. ZONE/ FOSSIL CHARACTER

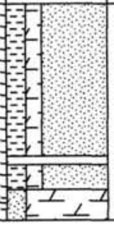

LITHOLOGIC DESCRIPTION

SAND, SANDY SILTSTONE, and MUDSTONE

Major lithology: sand, sandy siltstone, and mudstone, greenish gray (5GY 5/1) to dark greenish gray (5GY 4/1) and cemented by dolomite.

Minor lithologies:
a. black (5Y 2.5/1) to reddish brown (5YR 4/2) phosphate nodule, brecciated.
b. dolomitic muddy mudstone and dolomitic sandy siltstone.

SMEAR SLIDE SUMMARY (%):

	1, 10 D	1, 97 D	2, 4 D	2, 7 M	2, 20 M	CC, 14 M
TEXTURE:						
Sand	5	40	65	35	5	25
Silt	5	30	20	50	40	40
Clay	90	30	15	15	55	35
COMPOSITION:						
Quartz	10	20	30	20	10	10
Feldspar	5	20	15	10	10	5
Rock fragments	—	20	25	15	—	5
Mica	—	3	Tr	—	—	—
Clay	—	20	5	10	—	—
Volcanic glass	—	—	5	3	—	—
Calcite/dolomite	7	5	15	35	75	80
Accessory minerals						
Apatite	78	—	—	—	—	—
Pyrite	—	2	3	5	5	—
Glauco–phosphate	—	10	2	1	—	—
Nannofossils	—	—	Tr	1	—	—
Diatoms	—	—	—	Tr	—	—
Sponge spicules	—	—	—	Tr	—	—
Fish remains	—	—	Tr	Tr	—	—

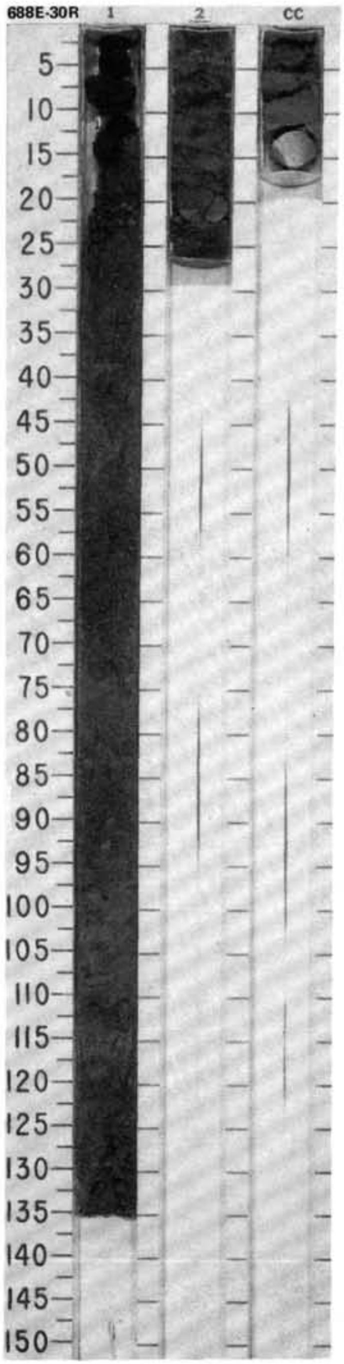

SITE 688 HOLE E CORE 31R CORED INTERVAL 4456.8-4466.3 mbsl; 631.0-640.5 mbsf

TIME-ROCK UNIT	BIOSTRAT. ZONE/ FOSSIL CHARACTER				PALEOMAGNETICS	PHYS. PROPERTIES	CHEMISTRY	SECTION	METERS	GRAPHIC LITHOLOGY	DRILLING DISTURB.	SED. STRUCTURES	SAMPLES
	FORAMINIFERS	NANNOFOSSILS	RADIOLARIANS	DIATOMS									
MIDDLE EOCENE	B *	NP16 *	Eocene ? *	B *				CC					**

LITHOLOGIC DESCRIPTION

SILTY MUDSTONE

Major lithology: silty mudstone, dark gray (5Y 4/1), with minor burrows, finely laminated and gray (N 5/) calcirudite or silty calcareous sandstone consisting of angular to subangular fine-grained quartz, feldspar, and rock fragments that include metamorphic rocks.

SMEAR SLIDE SUMMARY (%):

	CC, 7 D	CC, 11 D
TEXTURE:		
Sand	45	25
Silt	35	25
Clay	20	50
COMPOSITION:		
Quartz	30	20
Feldspar	25	15
Rock fragments	23	10
Clay	5	30
Volcanic glass	Tr	—
Calcite/dolomite	10	20
Accessory minerals		
Phosphate	5	—
Glauconite	1	—
Pyrite	1	5
Radiolarians	Tr	Tr

SITE 688 HOLE E CORE 32R CORED INTERVAL 4466.3-4475.8 mbsl; 640.5-650.0 mbsf

TIME-ROCK UNIT	BIOSTRAT. ZONE/ FOSSIL CHARACTER				PALEOMAGNETICS	PHYS. PROPERTIES	CHEMISTRY	SECTION	METERS	GRAPHIC LITHOLOGY	DRILLING DISTURB.	SED. STRUCTURES	SAMPLES
	FORAMINIFERS	NANNOFOSSILS	RADIOLARIANS	DIATOMS									
MIDDLE EOCENE	* B	* B	* B	* B				1 2 CC	0.5 1.0	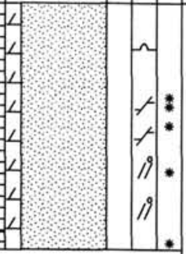			

LITHOLOGIC DESCRIPTION

SANDSTONE and SILTY SAND

Major lithology: fine sandstone or silty sand, gray (N 5.5/) to dark gray (N 5.3/), to massive gray (N 5.5/) coarse sandstone. Cemented by carbonate. Veins of calcidolomite and large fracture zone appear as dewatering veins.

Minor lithologies:
a. plant debris and organic matter in thin bands (<1 mm).
b. phosphatic nodule as grains in the coarse-grained sand.

SMEAR SLIDE SUMMARY (%):

	1, 83 M	1, 87 M	1, 106 D	1, 143 M	CC, 15 M
TEXTURE:					
Sand	5	5	90	20	—
Silt	75	80	10	65	—
Clay	20	15	—	15	100
COMPOSITION:					
Quartz	5	2	40	10	—
Feldspar	15	15	15	12	—
Rock fragments	20	20	30	35	—
Clay	15	10	—	10	—
Volcanic glass	5	5	Tr	8	—
Calcite/dolomite	30	40	5	15	—
Accessory minerals	3	—	—	5	—
Pyrite	3	2	—	—	—
Glauconite	3	5	—	5	—
Phosphate peloids	—	—	10	—	—
Hornblende	—	—	Tr	—	—
Pyroxene	—	—	Tr	—	—
Olivine	—	—	Tr	—	—
Foraminifers	Tr	—	—	—	—
Nannofossils	1	1	—	Tr	—
Radiolarians	Tr	Tr	—	—	—
Organic matter	—	—	—	—	100

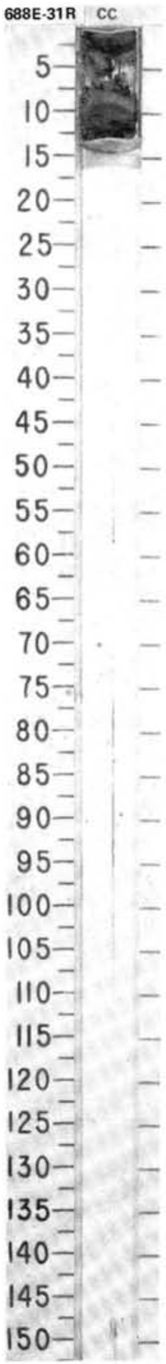

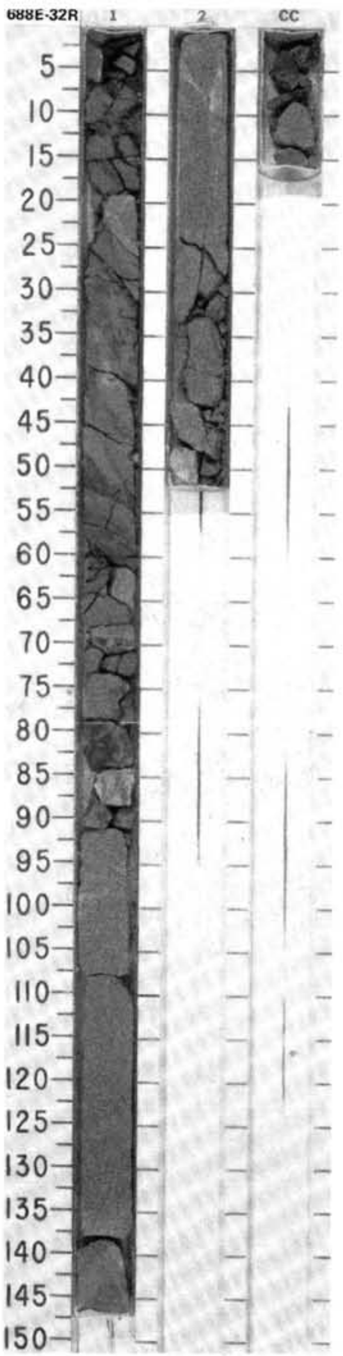

SITE 688 HOLE E CORE 33R CORED INTERVAL 4475.8-4485.3 mbsl; 650.0-659.5 mbsf

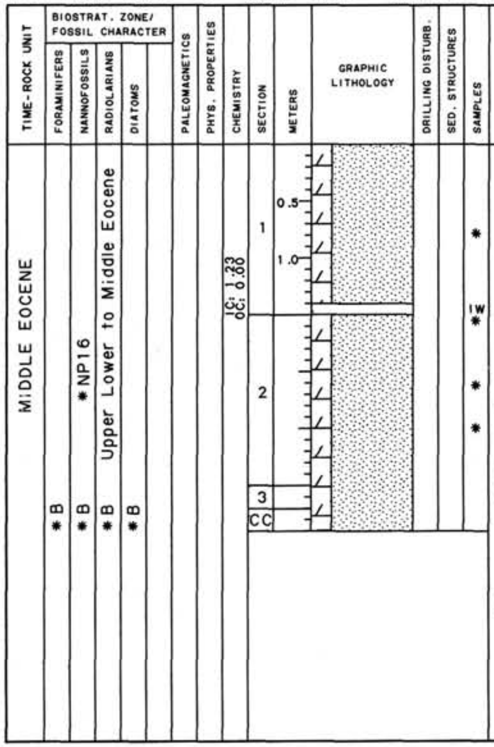

LITHOLOGIC DESCRIPTION

SANDSTONE, SAND, and MUDSTONE

Major lithology: fine sandstone and medium to coarse-grained sand, gray (N 5.5/) to dark gray (N 5.3/). Black (5Y 2.5/1) mudstone. Cemented by dolomite.

Minor lithology: phosphatic nodules.

SMEAR SLIDE SUMMARY (%):

	1, 80 M	2, 3 M	2, 65 M	2, 99 D
TEXTURE:				
Sand	—	—	1	70
Silt	—	30	30	30
Clay	—	70	69	—
COMPOSITION:				
Quartz	2	—	10	25
Feldspar	2	Tr	5	20
Rock fragments	—	—	—	10
Clay	—	—	80	—
Volcanic glass	—	—	Tr	—
Calcite/dolomite	60	30	2	20
Accessory minerals				
Chlorite	36	70	—	—
Glauconite	—	—	Tr	—
Opaques	—	—	3	—
Phosphate peloids	—	—	—	20
Horr.blende	—	—	—	5
Radiolarians	—	—	Tr	—
Sponge spicules	Tr	—	—	—

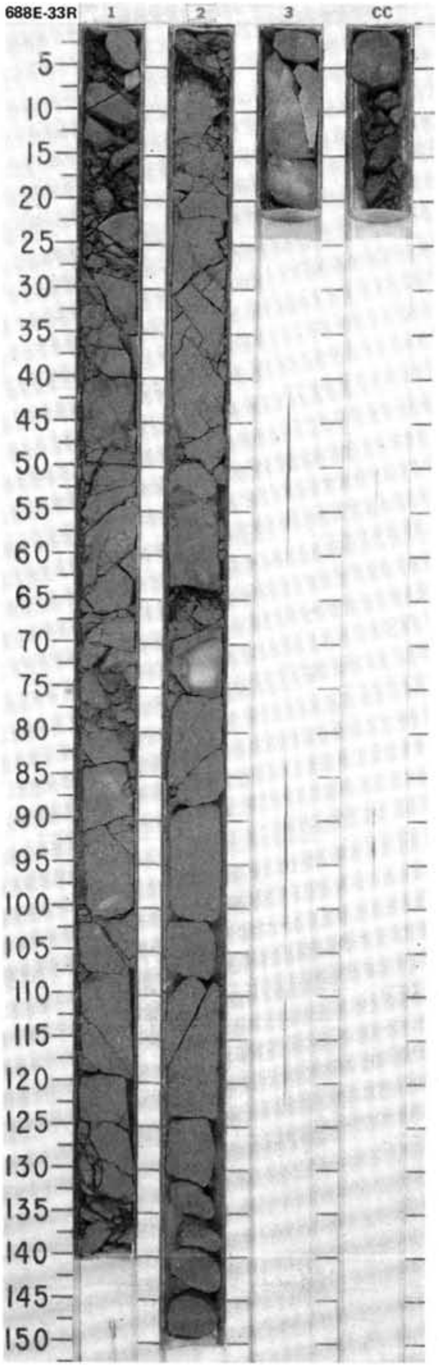

SITE 688 HOLE E CORE 34R CORED INTERVAL 4485.3-4494.8 mbsl; 659.5-669.0 mbsf

TIME-ROCK UNIT	BIOSTRAT. ZONE/ FOSSIL CHARACTER: FORAMINIFERS	NANNOFOSSILS	RADIOLARIANS	DIATOMS		PALEOMAGNETICS	PHYS. PROPERTIES	CHEMISTRY	SECTION	METERS	GRAPHIC LITHOLOGY	DRILLING DISTURB.	SED. STRUCTURES	SAMPLES
MIDDLE EOCENE	*B	*NP16 *NP16	Lower Middle Eocene* *Eocene ?	*B					1 2 CC	0.5 1.0				* **

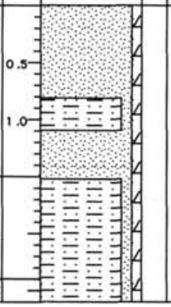

LITHOLOGIC DESCRIPTION

SAND and MUDSTONE

Major lithology: sand, coarse to medium grained and poorly sorted, gray (N 5/). Calcite veins and dewatering fractures. Black (5Y 2.5/1) massive to mottled mudstone, highly fractured.

SMEAR SLIDE SUMMARY (%):

	2, 20 D	2, 78 M	2, 83 M
TEXTURE:			
Sand	5	5	2
Silt	20	50	30
Clay	75	45	68
COMPOSITION:			
Quartz	10	20	20
Feldspar	5	25	5
Clay	68	48	68
Volcanic glass	Tr	2	—
Calcite/dolomite	10	5	2
Accessory minerals			
Opaque pyrite	5	—	3
Nannofossils	2	—	2

SITE 688 HOLE E CORE 35R CORED INTERVAL 4494.8-4504.3 mbsl; 669.0-678.5 mbsf

TIME-ROCK UNIT	BIOSTRAT. ZONE/ FOSSIL CHARACTER: FORAMINIFERS	NANNOFOSSILS	RADIOLARIANS	DIATOMS		PALEOMAGNETICS	PHYS. PROPERTIES	CHEMISTRY	SECTION	METERS	GRAPHIC LITHOLOGY	DRILLING DISTURB.	SED. STRUCTURES	SAMPLES
MIDDLE EOCENE	*B	*NP16 NP16*	*Eocene ?	*B				IC: 0.45 OC: 0.65	1 CC	0.5 1.0				* * * IW

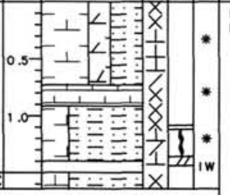

LITHOLOGIC DESCRIPTION

NANNOFOSSIL MARL, NANNOFOSSIL CHALK, and CALCAREOUS SILTY MUDSTONE and MUDDY SILTSTONE

Major lithology: Section 1, 0–75 cm: nannofossil marl, black (5Y 2.5/1), pyritic and phosphatic, massive. Section 1, 75–94 cm: nannofossil chalk, greenish gray (5G 5/1), silty, highly fragmented. Section 1, 94 cm, to CC: calcareous silty mudstone and muddy siltstone, dark greenish gray (5GY 3/1), rare sand laminae, possible ripple cross-lamination. Bioturbation.

SMEAR SLIDE SUMMARY (%):

	1, 30 D	1, 80 (D)	1, 125 D
TEXTURE:			
Sand	—	5	5
Silt	75	55	50
Clay	25	40	45
COMPOSITION:			
Quartz	6	8	9
Feldspar	10	12	18
Rock fragments	5	—	8
Mica	1	—	—
Clay	6	—	36
Volcanic glass	2	1	—
Calcite/dolomite	15	9	15
Accessory minerals			
Pyrite	10	7	3
Phosphatics	10	—	1
Micrite	5	10	5
Foraminifers	Tr	—	Tr
Nannofossils	30	53	5
Radiolarians	Tr	—	—

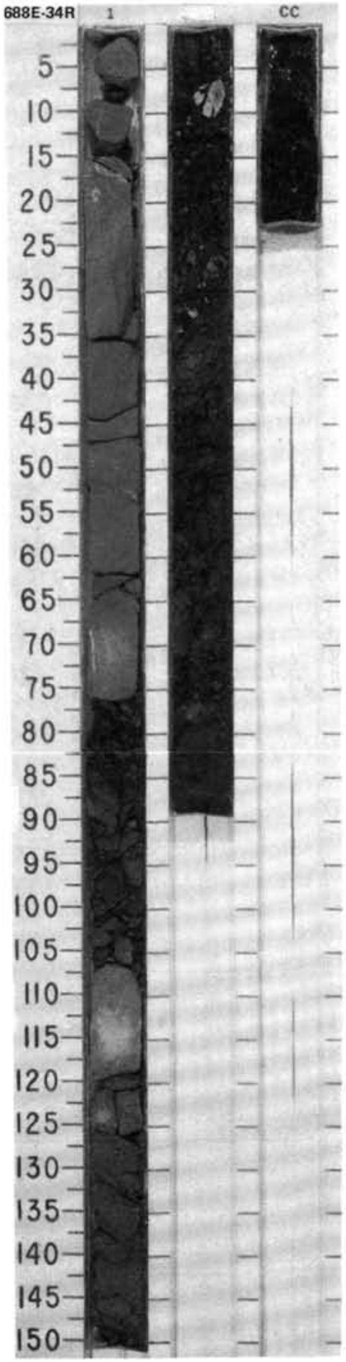

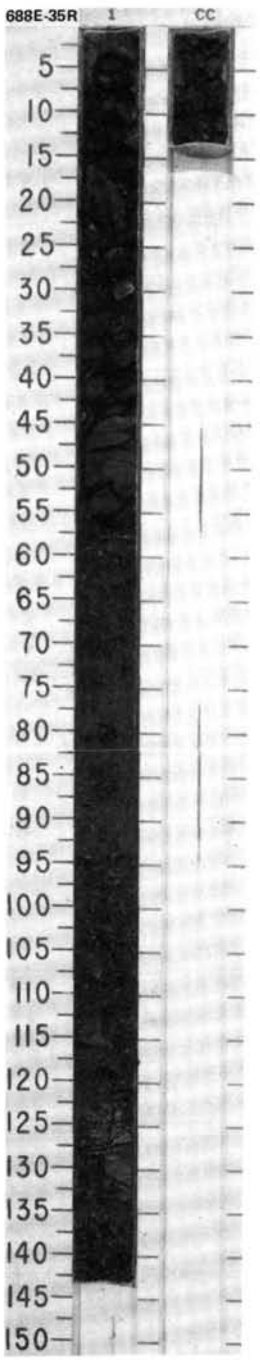

SITE 688 HOLE E CORE 36R CORED INTERVAL 4504.3-4513.8 mbsl; 678.5-688.0 mbsf

TIME-ROCK UNIT: MIDDLE EOCENE

BIOSTRAT. ZONE/FOSSIL CHARACTER

FORAMINIFERS: *B

NANNOFOSSILS: *NP16, *NP14, *NP13, NP13 * *NP13

RADIOLARIANS: *B

DIATOMS: *B

PALEOMAGNETICS

PHYS. PROPERTIES

CHEMISTRY

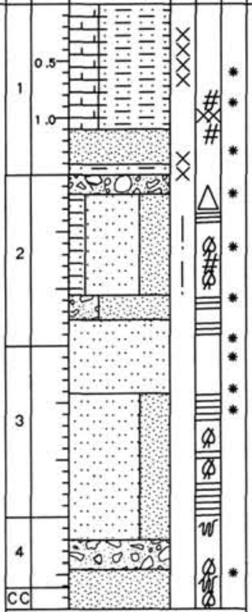

LITHOLOGIC DESCRIPTION

SANDSTONE and PEBBLY SANDSTONE, SILTY NANNOFOSSIL MARL, and SILTSTONE

Major lithology: sandstone and pebbly sandstone, dark gray (N 4, N 5), very fine to fine-grained, rarely coarse grained, including graded conglomeratic units containing rounded clasts of quartz, sedimentary rocks, mud rip-up clasts, and volcanics. Section 1, 0–8 and 110–140 cm, Section 2, 0–16 and 105–126 cm, and Section 4, 21–45 cm.

Silty nannofossil marl, black (N 1), less calcareous from 140–150 cm. Section 1, 8–110 and 140–150 cm, Section 2, 16–105 cm, Section 3, 42 cm.

Siltstone, dark gray (N 4); sandstone, dark gray (N 5, N 4), and mudstone, dark gray (N 4) (subordinate); interlaminated plant-debris concentrated along individual laminae. Rare cross-lamination. Section 4, 21 cm, and CC, 0–20 cm.

Siltstone, dark gray (N 4), quartzose with parallel lamination throughout. Plant debris concentrated along individual laminae. Section 2, 126 *cm*, Section 3, 42 *cm*, and Section 4, 45–62 cm.

SMEAR SLIDE SUMMARY (%):

	1, 60 D	1, 131 D	2, 13 M	2, 65 M	2, 130 M	3, 10 M
TEXTURE:						
Sand	10	60	15	20	30	—
Silt	60	35	80	70	70	100
Clay	30	5	5	10	—	—
COMPOSITION:						
Quartz	15	25	20	20	15	—
Feldspar	20	30	15	10	10	—
Rock fragments	—	12	10	10	15	—
Mica	—	—	1	2	—	—
Clay	5	—	5	5	—	—
Volcanic glass	3	—	1	2	—	—
Calcite/dolomite	7	5	30	1	6	—
Accessory minerals	—	1	—	—	—	—
Pyrite	4	—	1	2	—	—
Opaques	—	5	—	—	—	—
Zircon	Tr	Tr	—	—	—	—
Altered grains	—	20	—	—	—	—
Micrite	—	—	15	2	—	—
Chlorite	—	—	—	1	—	—
Foraminifers	3	—	Tr	—	3	—
Nannofossils	30	2	—	—	1	—
Radiolarians	—	—	—	Tr	—	—
Plant debris	—	—	—	45	50	100
Organic matter	13	—	2	—	—	—

	3, 37 D	3, 50 M	4, 58 D
TEXTURE:			
Sand	—	35	5
Silt	70	45	93
Clay	30	20	2
COMPOSITION:			
Quartz	20	40	35
Feldspar	15	25	25
Rock fragments	10	10	5
Mica	2	—	—
Clay	29	15	2
Volcanic glass	5	2	5
Calcite/dolomite	2	Tr	10
Cement	—	1	—
Pyrite	2	2	—
Opaques	—	—	5
Acicular crystals	—	2	Tr
Altered grains	—	—	10
Micrite	3	1	—
Chlorite	1	—	—
Collophane	3	—	—
Foraminifers	Tr	Tr	Tr
Nannofossils	3	—	1
Plant debris	—	2	2
Organic matter	5	—	—

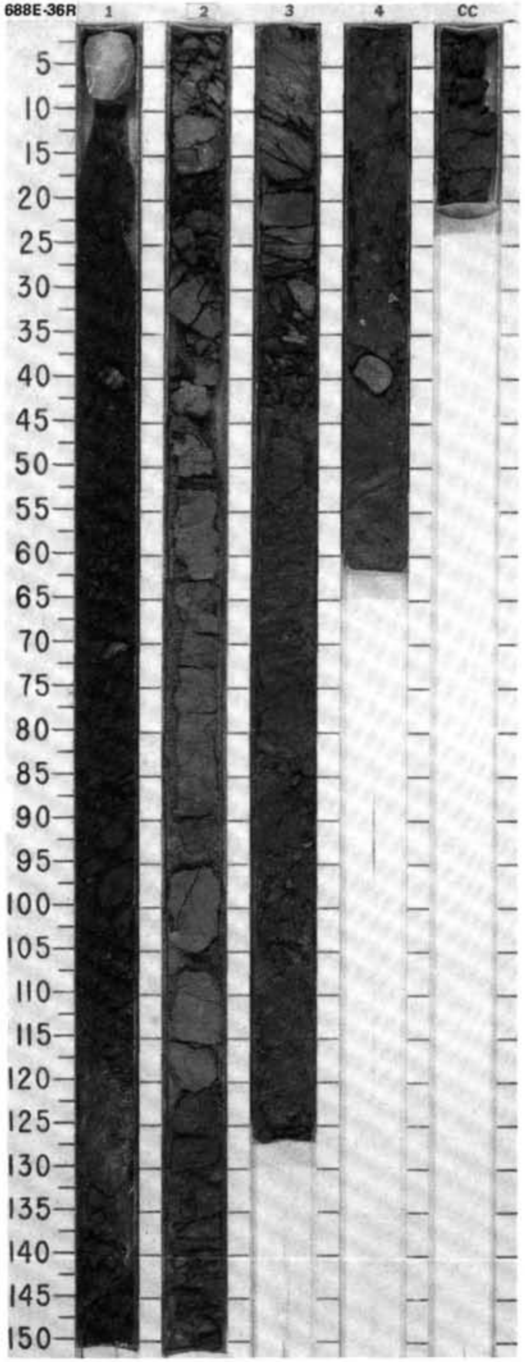

SITE 688 HOLE E CORE 37R CORED INTERVAL 4513.8-4523.3 mbsl; 688.0-697.5 mbsf

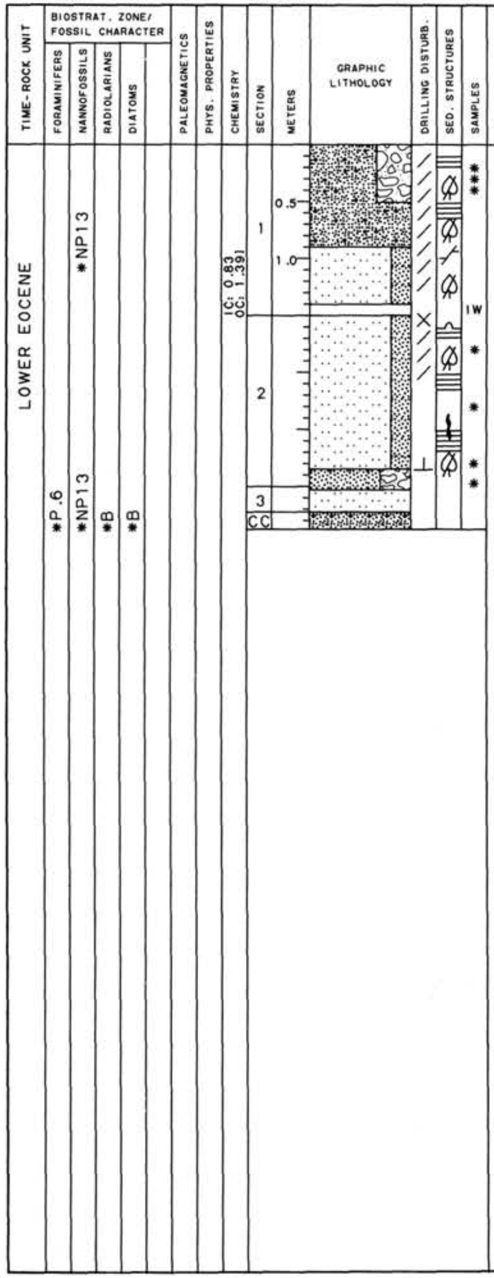

LITHOLOGIC DESCRIPTION

SILTY SANDSTONE and SILTSTONE

Major lithology: silty sandstone, dark gray (5Y 4/1, N 4/), pebbly in places, quartzose, locally calcareous. Containing rip-up clasts of interbedded siltstone and pebbles of milky quartz (common), chert, micritic limestone. Section 1, 0–90 cm; Section 2, 135 cm, to Section 3, 2 cm; and CC, 0–14 cm.

Siltstone, dark gray (N 4/–5GY 4/1), calcareous in places, contains plant debris. Parallel laminated and interlaminated with dark blue-gray sandstone. Nannofossil-bearing, especially finer grained parts. Section 1, 90 cm to Section 2, 135 cm; and Section 3, 2–18 cm.

SMEAR SLIDE SUMMARY (%):

	1, 26 M	1, 33 D	1, 39 M	2, 34 D	2, 84 D	2, 128 M
TEXTURE:						
Sand	10	60	—	15	5	25
Silt	80	30	4	65	75	60
Clay	10	10	96	20	20	15
COMPOSITION:						
Quartz	5	58	2	25	25	20
Feldspar	2	10	—	10	10	10
Rock fragments	1	15	—	10	10	7
Mica	—	—	—	Tr	Tr	1
Clay	2	5	—	15	13	15
Volcanic glass	Tr	—	—	2	1	2
Calcite	1	3	2	15	5	25
Accessory minerals	—	1	—	—	—	—
Glauconite	Tr	—	—	1	—	—
Cryptocrysatlline silica (chert)	88	—	—	—	—	—
Micrite	1	—	96	5	3	5
Acicular crystals	—	Tr	—	—	1	—
Pyrite	—	—	—	1	—	—
Needles	—	Tr	—	—	—	—
Foraminifers	Tr	Tr	—	—	2	5
Nannofossils	—	—	—	1	15	—
Diatoms	—	—	—	—	—	Tr
Radiolarians	—	—	—	Tr	Tr	—
Plant debris	—	8	—	15	15	—
Organic matter	—	—	—	—	—	10

	2, 147 D
TEXTURE:	
Sand	30
Silt	60
Clay	10
COMPOSITION:	
Quartz	20
Feldspar	3
Rock fragments	5
Mica	1
Clay	10
Volcanic glass	2
Calcite/dolomite	37
Accessory minerals	
Glauconite	1
Micrite	5
Acicular crystals	—
Pyrite	1
Chlorite	1
Foraminifers	1
Nannofossils	2
Radiolarians	—
Fish remains	1
Plant debris	—
Organic matter	10

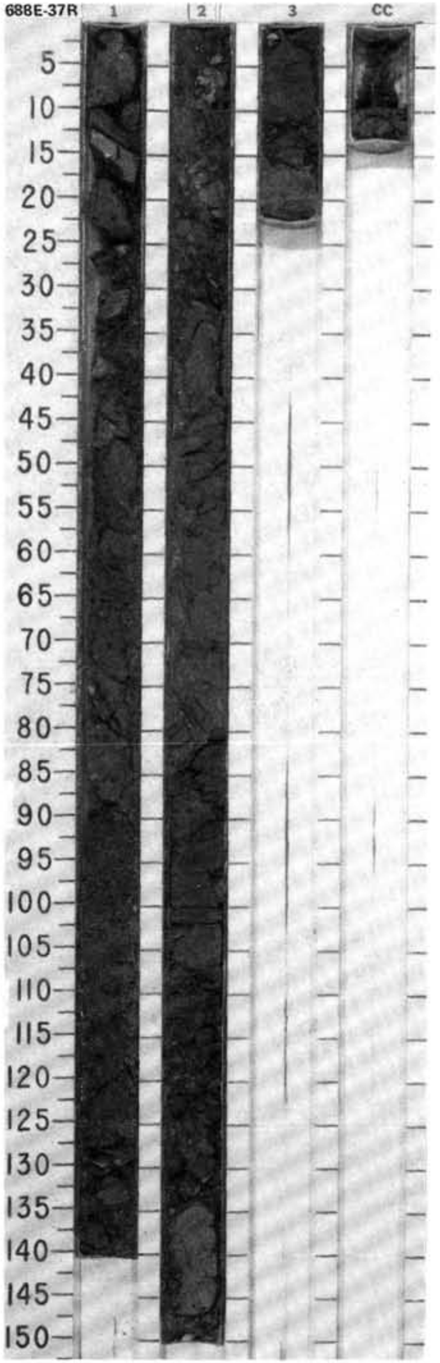

SITE 688 HOLE E CORE 38R CORED INTERVAL 4523.3-4532.8 mbsl; 697.5-707.0 mbsf

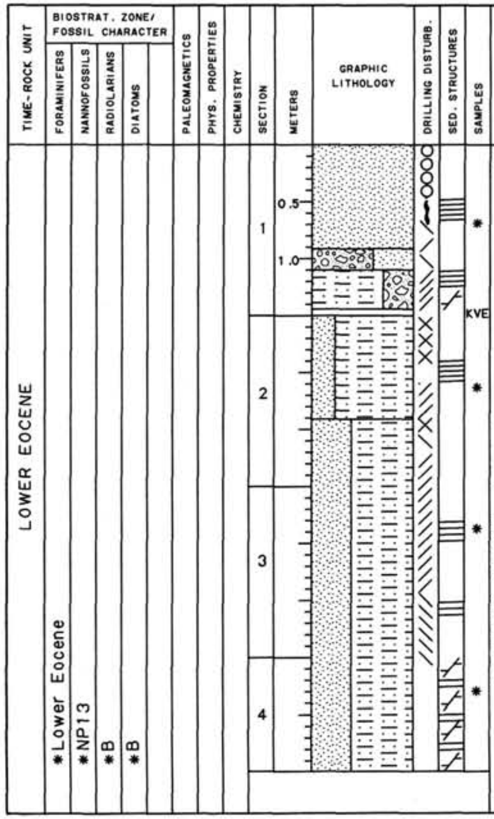

LITHOLOGIC DESCRIPTION

SANDSTONE, SANDY MUDSTONE, CONGLOMERATE, PEBBLY MUDSTONE, SILTY MUDSTONE, and MUDSTONE

Major lithology: sandstone and sandy mudstone, very dark gray to black (5Y 4/1, 5Y 2.5/2), fine to coarse-grained, moderately well sorted, locally containing glauconite and phosphate peloids. Section 1, *0–92* cm.

Granule pebble conglomerate, gray (N 5/), with yellow brown, dark brown, black and white, angular to subangular clasts of chert, vein quartz, shell fragments, and mudstone. Section 1, 92–109 cm.

Pebbly mudstone, dark gray (5Y 4/1), mainly intraformational clasts of sandstone and mudstone. Section 1, 109–145 cm.

Silty mudstone and mudstone, dark gray, black, dark olive gray (5Y 4/1, 5Y 2.5/1, N 4/) with sandstone, silty, lithic. Common fine parallel laminations, some with carbonaceous material. Rare pebbles of white quartz in Section 4. Section 2, 0 cm, to Section 4, 96 cm.

SMEAR SLIDE SUMMARY (%):

	1, 69 D	2, 69 D	3, 36 D	4, 40 D
TEXTURE:				
Sand	30	40	70	40
Silt	40	30	20	35
Clay	30	30	10	25
COMPOSITION:				
Quartz	25	20	20	40
Feldspar	20	10	15	20
Rock fragments	30	40	65	15
Mica	—	—	—	Tr
Clay	20	10	—	10
Accessory minerals				
Pyrite framboids	5	—	—	5
Carbonaceous matter	—	20	—	10
Glauconite	—	—	Tr	—

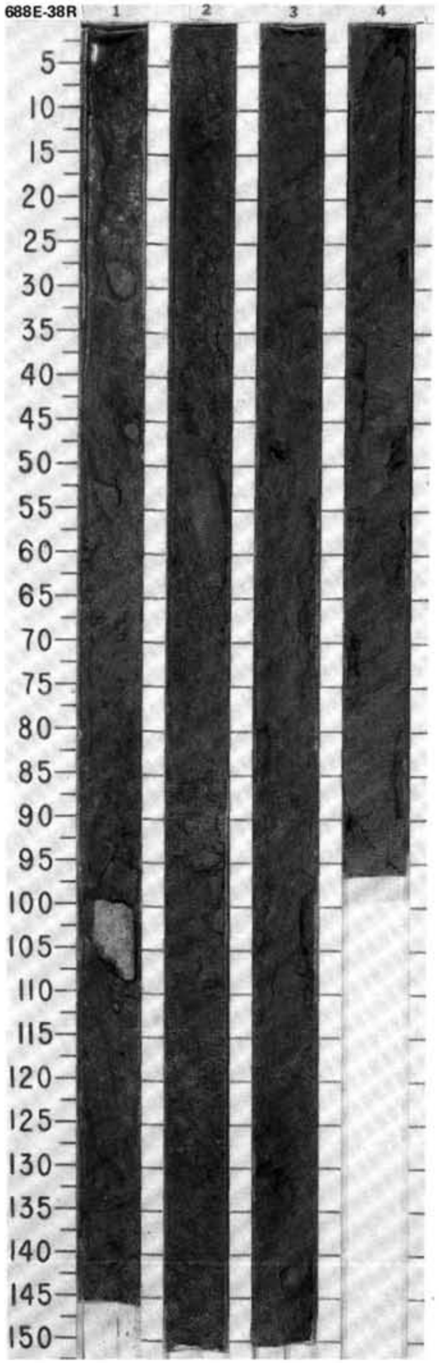

SITE 688 HOLE E CORE 39R CORED INTERVAL 4532.8-4542.3 mbsl; 707.0-716.5 mbsf

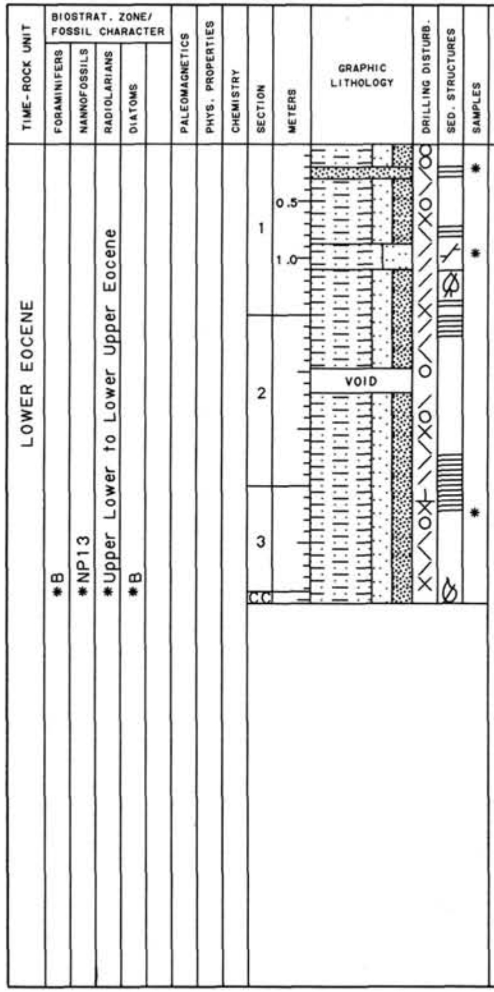

LITHOLOGIC DESCRIPTION

SILTSTONE, SILTY MUDSTONE, and SANDY MUDSTONE

Major lithology: siltstone, silty mudstone, sandy mudstone, dark gray (N 4, 5Y 4/1), calcareous, with laminae of sandstone, dark bluish gray (5B 4/1), in parallel laminated intervals of 1 mm to 5 cm. Local concentrations of plant material along laminae and in one small scour.

Section 1, 18–30 cm: sandstone, dark gray (N 4, 5Y 4/1), quartzo-feldspathic, lithic, finely laminated, calcareous.

Section 1, 86–110 cm: silty mudstone, dark gray (N 4), massive, calcareous.

Section 3, 88–92 cm, CC, 0–10 cm: calcareous phosphatic sandstone, gray (N 5), bioclastic (including oysters), very fine-grained phosphatic peloids and apatite cement, sparry calcite cement and vein infill.

SMEAR SLIDE SUMMARY (%):

	1, 23 D	1, 96 D	2, 13 M	3, 30 D	
TEXTURE:					
Sand	45	30	5	40	—
Silt	30	25	67	30	—
Clay	25	45	28	30	—
COMPOSITION:					
Quartz	35	20	30	15	30
Feldspar	20	15	15	15	—
Rock fragments	20	15	10	18	—
Clay	5	35	17	20	—
Volcanic glass	—	—	Tr	—	—
Calcite/dolomite	15	—	6	30	—
Cement	—	—	—	—	—
Accessory minerals					
Pyrite framboids	1	6	—	2	—
Acicular crystals	1	—	Tr	—	—
Glauconite	—	Tr	Tr	—	—
Calcispherefl—	Tr	—	—	—	—
Micrite	—	—	10	—	—
Phosphate	—	—	—	—	—
Foraminifers	—	2	Tr	—	—
Nannofossils	—	2	4	—	—
Fish remains	—	—	—	—	—
Plant debris	—	—	3	—	70
Organic matter	3	5	5	—	—
Bioclasts	—	—	—	—	—

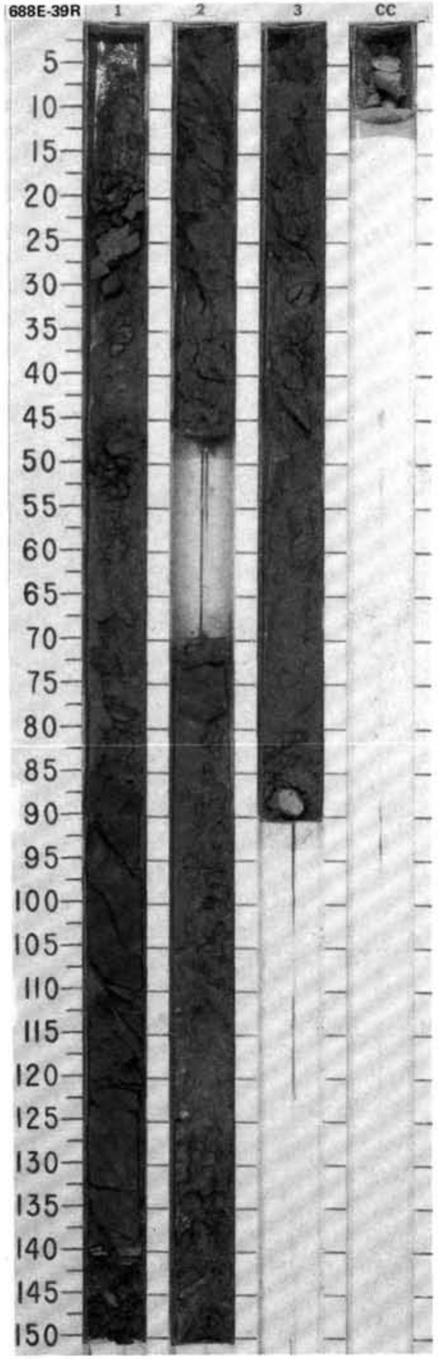

SITE 688 HOLE E CORE 40R CORED INTERVAL 4542.3-4551.8 mbsl; 716.5-726.0 mbsf

TIME-ROCK UNIT	BIOSTRAT. ZONE/ FOSSIL CHARACTER: FORAMINIFERS	NANNOFOSSILS	RADIOLARIANS	DIATOMS	PALEOMAGNETICS	PHYS. PROPERTIES	CHEMISTRY	SECTION	METERS	GRAPHIC LITHOLOGY	DRILLING DISTURB.	SED. STRUCTURES	SAMPLES
LOWER EOCENE	B *	B *	B *	B *				CC			X		*

LITHOLOGIC DESCRIPTION

BIOCLASTIC LIMESTONE

Major lithology: bioclastic limestone, gray (N 5/, N 4/), silty, foraminifer-rich. Mollusk shells, in several concentrated shell layers; some shells still articulated.

SMEAR SLIDE SUMMARY (%):

	CC, 10 *D*
TEXTURE:	
Sand	55
Silt	20
Clay	25
COMPOSITION:	
Quartz	10
Feldspar	3
Rock fragments	2
Calcite/dolomite	20
Cement	10
Accessory minerals	
Pyrite framboids	2
Phosphate peloids	1
Foraminifers	30
Fish remains	2
Organic matter	10
Bioclasts	10

SITE 688 HOLE E CORE 41R CORED INTERVAL 4551.8-4561.3 mbsl; 726.0-735.5 mbsf

TIME-ROCK UNIT	BIOSTRAT. ZONE/ FOSSIL CHARACTER: FORAMINIFERS	NANNOFOSSILS	RADIOLARIANS	DIATOMS	PALEOMAGNETICS	PHYS. PROPERTIES	CHEMISTRY	SECTION	METERS	GRAPHIC LITHOLOGY	DRILLING DISTURB.	SED. STRUCTURES	SAMPLES
LOWER EOCENE	*B	*B	*B	*B				1 2 CC					*

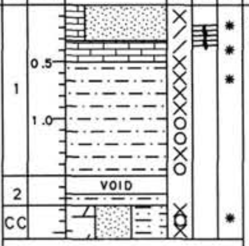

LITHOLOGIC DESCRIPTION

QUARTZ ARENITE, MUDDY MICRITIC LIMESTONE, SANDY MUDSTONE, SILTSTONE, MUDSTONE, and DRILLING BRECCIA

Major lithology: quartz arenite, dark gray (N 4/), slightly calcareous, faintly laminated; with dark brown burrow fills (0.5–2 cm). Section 1, 0–32 cm.

Muddy micritic limestone, dark brown (2.5Y 3/2), rare burrows, white blebs of calcareous material, calcareous cement. Section 1, 32–50 cm.

Sandy mudstone, siltstone and mudstone, black to dark gray (5Y 2.5/1; N 3/), as *broken fragments in soup. Section 1, 50–150 cm and Section 2, 0–27 cm.*

Fragments in drilling breccia of calcareous quartz arenite, dark gray (5Y 3/1); dolomicrite, dark brownish gray (10YR 5/1); dominantly small pieces of black (N 2/–N 1/) silty mudstone. CC, 0–28 cm.

SMEAR SLIDE SUMMARY (%):

	1, 18 D	1, 40 M	1, 65 D	CC, 10 M
TEXTURE:				
Sand	65	—	25	—
Silt	25	30	25	20
Clay	10	70	50	80
COMPOSITION:				
Quartz	35	10	15	3
Feldspar	15	—	10	Tr
Rock fragments	20	—	10	—
Clay	8	35	40	10
Calcite/dolomite	10	20	15	15
Accessory minerals				
Pyrite	2	2	5	3
Opaques	10	—	—	—
Organic matter	—	3	5	—
Micrite	—	30	—	69

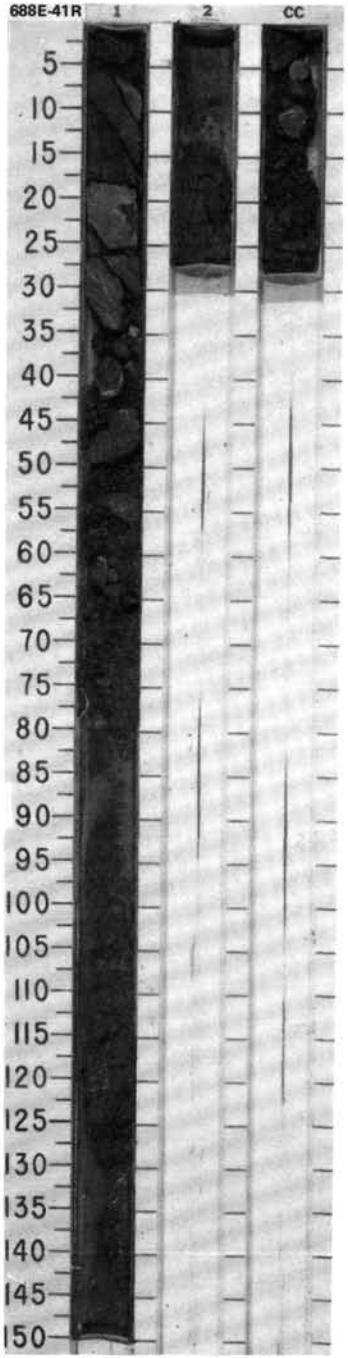

SITE 688 HOLE E CORE 42R CORED INTERVAL 4561.3-4570.8 mbsl; 735.5-745.0 mbsf

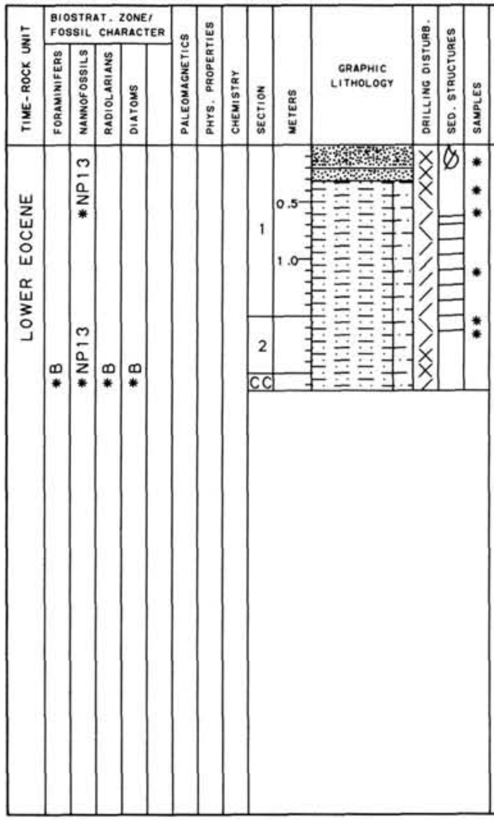

LITHOLOGIC DESCRIPTION

MUDSTONE and SANDSTONE

Major lithology: mudstone, dark olive gray (5Y 3/2), with frequent thin-very thin interbeds of sandy mudstone, dark gray (N 4/). Mudstone occasionally calcareous.

Minor lithologies: sandy siltstone, dark olive gray (5Y 3/2), with mollusk shell fragments and mudstone rip up clasts, Section 1, 0–18 cm; sandstone, dark gray (N 4), lithic, fine to medium grained, Section 1, 18–32 cm. .

SMEAR SLIDE SUMMARY (%):

	1, 18 D	1, 40 M	1, 65 D	CC, 10 M
TEXTURE:				
Sand	65	50	25	–
Silt	25	30	25	20
Clay	10	20	50	80
COMPOSITION:				
Quartz	35	10	15	3
Feldspar	15	–	10	–
Rock fragments	20	–	10	–
Clay	8	35	40	10
Calcite/dolomite	10	20	15	15
Accessory minerals				
Pyrite framboids	2	2	5	3
Opaques	10	–	–	–
Micrite	–	30	–	69
Plant debris	–	3	5	–

SITE 688 HOLE E CORE 43R CORED INTERVAL 4570.8-4580.3 mbsl; 745.0-754.5 mbsf

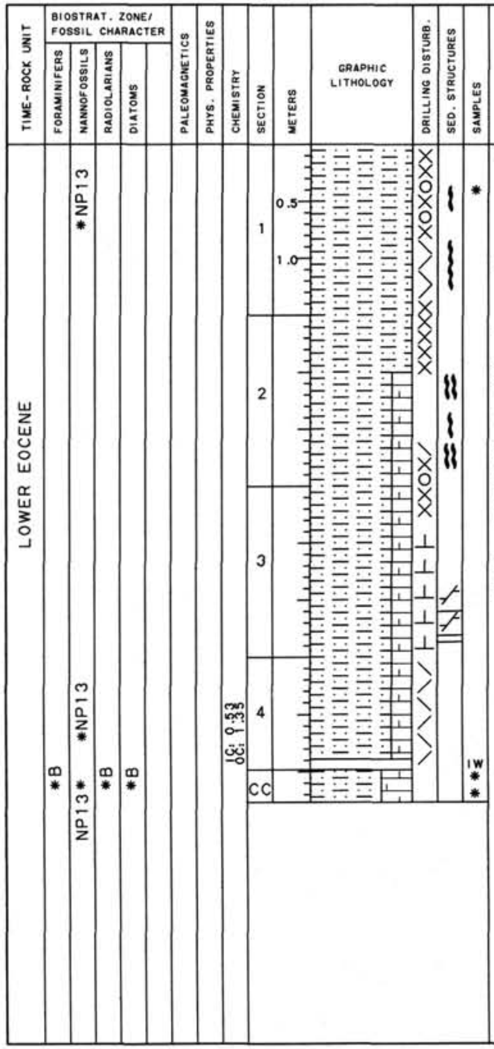

LITHOLOGIC DESCRIPTION

MUDSTONE

Major lithology: mudstone, dark olive gray (5Y 3/2), massive, moderate bioturbation in places.

Minor lithology: dark gray (5Y 4/1) nannofossil chalk, muddy chalk as thin (5–10 mm) interbeds, abundant in CC.

SMEAR SLIDE SUMMARY (%):

	1, 46 D	CC, 12 D	CC, 13 D
TEXTURE:			
Sand	1	—	—
Silt	40	20	15
Clay	59	80	85
COMPOSITION:			
Quartz	35	Tr	5
Feldspar	5	—	2
Clay	46	10	48
Volcanic glass	5	—	Tr
Calcite/dolomite	3	—	—
Accessory minerals	—	—	Tr
Pyrite framboids	5	5	5
Hornblende	Tr	—	—
Foraminifers	—	Tr	—
Nannofossils	1	85	40
Plant debris	—	Tr	—

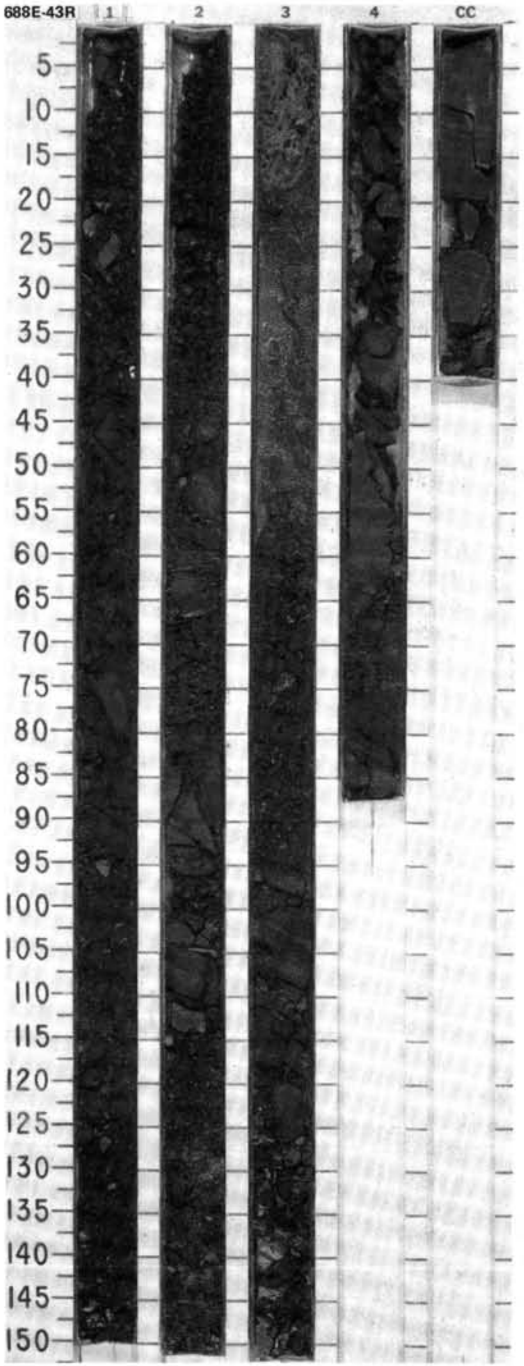

SITE 688 HOLE E CORE 44R CORED INTERVAL 4580.3-4589.8 mbsl; 754.5-764.0 mbsf

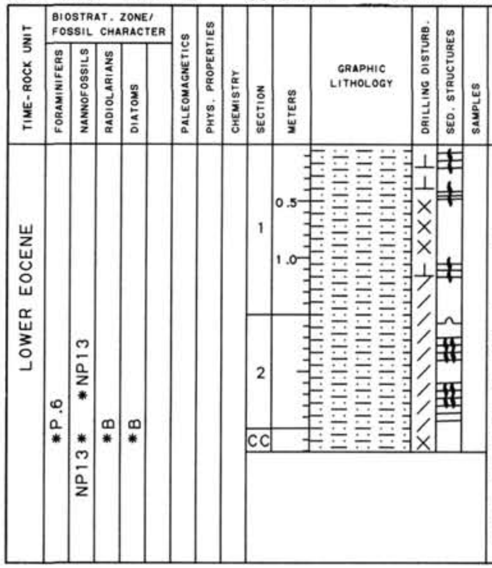

LITHOLOGIC DESCRIPTION

MUDSTONE

Major lithology: mudstone, dark olive gray (5Y 3/2), nannofossil-bearing with some paler layers of nannofossil-rich mudstone. Common bioturbation. Parallel lamination in places, scattered foraminifers.

SMEAR SLIDE SUMMARY (%):

	2, 36 D	2, 40 M	2, 65 M
TEXTURE:			
Silt	30	20	70
Clay	70	80	30
COMPOSITION:			
Quartz	15	10	60
Feldspar	5	8	10
Clay	55	30	—
Volcanic glass	—	5	—
Calcite/dolomite	Tr	—	—
Accessory minerals			
Pyrite framboids	5	2	5
Nannofossils	20	45	Tr
Radiolarians	Tr	—	—
Plant debris	—	—	25

SITE 688 HOLE E CORE 45R CORED INTERVAL 4589.8-4595.3 mbsl; 764.0-769.5 mbsf

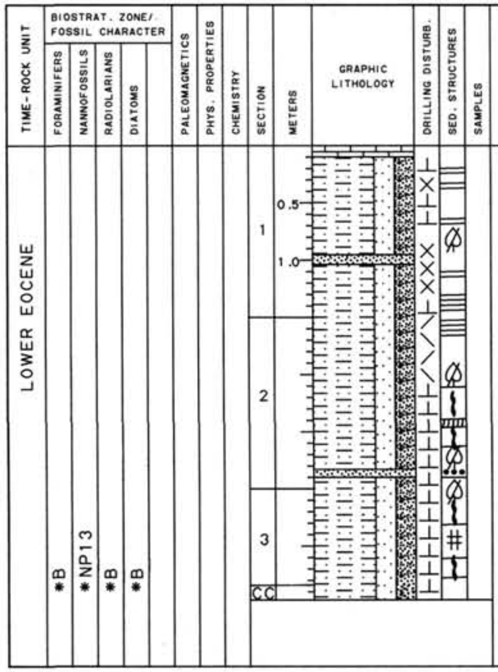

LITHOLOGIC DESCRIPTION

SILTY MUDSTONE

Major lithology: silty mudstone, dark gray (5Y 4/1; N 4/), calcareous with very fine sandstone as laminae in parallel laminated intervals, and as common thin beds throughout. Frequent small-scale ripples, starved ripples and low-angle climbing ripples. Several laminae rich in plant material.

Minor lithology: olive (5Y 4/3) micrite in Section 1, 0–10 cm.

SMEAR SLIDE SUMMARY (%):

	2, 108 M	2, 142 M	3, 56 D	3, 57 M
TEXTURE:				
Sand	65	90	80	—
Silt	35	10	15	46
Clay	—	—	5	54
COMPOSITION:				
Quartz	60	60	—	30
Feldspar	2	—	—	5
Rock fragments	30	20	—	5
Clay	—	—	—	42
Calcite/dolomite	3	10	—	2
Accessory minerals	—	5	—	—
Opaques	5	5	—	—
Pyrite	—	—	5	3
Micrite	—	—	—	8
Acicular minerals	—	—	—	Tr
Nannofossils	—	—	—	4
Plant debris	—	—	95	1

CORE 112-688E-46R NO RECOVERY